THE UNIVERSITY
OF MICHIGAN
AUG 9 - 1960
ENGINEERING
LIBRARY

JOURNAL OF FLUID MECHANICS

VOLUME 8 PART 3

JULY 1960

PUBLISHED BY

CAMBRIDGE UNIVERSITY PRESS

BENTLEY HOUSE, 200 EUSTON ROAD, LONDON, N.W. 1

AMERICAN BRANCH: 32 EAST 57TH STREET, NEW YORK 22, N.Y.

Price 30*s.* (*U.S.A.* $5.00)

The JOURNAL OF FLUID MECHANICS exists for the publication of theoretical and experimental investigations of all aspects of the mechanics of fluids, and is issued in four parts per volume.

EDITOR

DR G. K. BATCHELOR

Department of Applied Mathematics and Theoretical Physics, University of Cambridge, Free School Lane, Cambridge, England

ASSISTANT EDITORS

DR T. B. BENJAMIN, DR I. PROUDMAN, DR P. G. SAFFMAN

Department of Applied Mathematics and Theoretical Physics, University of Cambridge, Free School Lane, Cambridge, England

ASSOCIATE EDITORS

PROF. G. F. CARRIER

Pierce Hall, Harvard University, Cambridge 38, *Massachusetts, U.S.A.*

DR W. C. GRIFFITH

Research and Development Laboratory, Missile Systems Division, Lockheed Aircraft Corporation, Palo Alto, California, U.S.A.

M. J. LIGHTHILL

Royal Aircraft Establishment, Farnborough, Hampshire, England

PROF. R. R. LONG

School of Engineering, The Johns Hopkins University, Baltimore 18, *Maryland, U.S.A.*

Authors wishing to have papers published in the JOURNAL should communicate them to any one of the persons named above, choosing one in their own country where possible.

Authors are urged to ensure that their papers are written clearly and attractively, in order that their work will be readily accessible to readers.

Manuscripts should be typed in double spacing on one side of the paper only, with references listed at the end in alphabetical order of authors. Drawings should be done on a large scale in Indian ink on tracing cloth or drawing paper, the lettering being shown clearly in pencil for reproduction by the printer; the list of captions should be typed at the end of the manuscript. Proofs of papers from overseas will usually be despatched to authors by airmail. There is no charge for publication. Authors are entitled to receive 50 offprints of a paper in the JOURNAL free of charge, and additional offprints can be purchased if ordered in advance.

SUBSCRIPTIONS

The subscription price for a volume of four parts is £5. 10*s*. net, post free, payable in advance; separate parts 30*s*. net, plus postage. Subscriptions may be sent to any bookseller, or to the Cambridge University Press, Bentley House, 200 Euston Road, London, N.W. 1.

Subscribers in the United States should send their orders to the Cambridge University Press, American Branch, 32 East 57th Street, New York 22. The subscription price per volume is $18.50, post free, payable in advance; separate parts $5.00, plus postage.

Quotations for available back volumes and parts may be obtained on application to the Cambridge University Press.

The stability of a stratified flow

By WILLIAM PAUL GRAEBEL
Department of Engineering Mechanics, University of Michigan, Ann Arbor, Michigan

(Received 20 November 1959)

This paper deals theoretically with the problem of the hydrodynamic stability of a stratified flow of a viscous fluid. The primary flow consists of two laminar streams of viscous fluids of different densities flowing in opposite directions between two parallel inclined planes under the action of gravity. The effect of surface tension at the interface of the two fluids is included in the formulation of the problem.

Since instability can be expected to occur at low Reynolds numbers when the inclination is nearly vertical, the solution of the Orr–Sommerfeld equations is developed as a power series in the transverse space co-ordinate. It is shown that for the vertical case, the flow is unstable for all values of the Reynolds number. Surface tension is found to influence both the direction and celerity of the disturbance. Results are also given for inclinations slightly away from the vertical, where small critical Reynolds numbers do exist.

1. Introduction

For most parallel flows past fixed boundaries whose stability has been investigated so far, instability occurs at rather large Reynolds numbers. The Orr–Sommerfeld equation (see Lin 1955) governing the stability of such flows must therefore be solved for large values of the Reynolds number, which appears as a parameter in these equations. The asymptotic solutions of the Orr–Sommerfeld equation, appropriate for large Reynolds numbers, have singularities at the critical points where the wave velocity of the disturbance is equal to the velocity of the mean flow. Great care must therefore be exercised in the evaluation of these solutions as a critical point is crossed. These singularities of the solutions are, however, not inherent in the Orr–Sommerfeld equation, and are introduced entirely by the method of solution. For flows which can be expected to be unstable at low Reynolds numbers, the appropriate solutions can be expressed in ascending powers of the Reynolds number or of one of the co-ordinates. Since asymptotic solutions are not needed, the aforementioned singularities do not occur. The study of the stability of flows which can be expected to become unstable at low Reynolds numbers can therefore be carried out by conventional methods. In view of this, it is perhaps somewhat surprising that until recent years problems of hydrodynamic instability at low Reynolds numbers have been neglected by research workers.

The flow whose stability is studied here is a stratified flow of two fluids of equal viscosity but different densities. It is entirely motivated by gravity and

its velocity distribution is antisymmetric, with the lighter fluid flowing in a direction opposite to that of the heavier fluid, with a point of inflexion of the velocity profile at the interface. Since a point of inflexion is known to have a destabilizing effect, and since the work of Yih (1954) and of Benjamin (1957) has shown that a free surface also has a destabilizing effect, it can be expected to be unstable at low Reynolds numbers, especially if the slope of the mean flow is steep. The Orr–Sommerfeld equation will therefore be solved for small Reynolds numbers.

The type of flow investigated here is encountered in extraction columns in chemical engineering, and can also be found in closed channels such as tunnels and mine shafts. It can also be expected that the results have some bearing on stratified flows occurring in the oceans and the atmosphere, where layers of warm water or air flow over and counter to colder water or air (i.e. the flow of air after cold fronts).

2. The primary flow

The present investigation concerns the stability of a steady laminar stratified flow of an incompressible viscous fluid between two parallel fixed planes. The spacing of the planes is denoted by $2b$. The origin of the co-ordinate system is taken half-way between the planes, with the X-axis parallel to the planes. The planes are inclined at an angle θ with the horizontal (see figure 1).

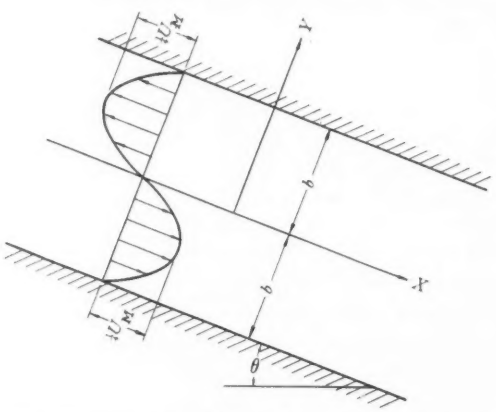

FIGURE 1. Diagram of the primary flow, showing the co-ordinate axes and the velocity profile.

The fluid occupying the region $0 \leqslant Y \leqslant b$, with density ρ_1, flows up the inclined plane in the direction of negative X. The fluid occupying the region $-b \leqslant Y \leqslant 0$, with density ρ_2 greater than ρ_1, flows down the plane under the action of gravity. The viscosity μ of the two fluids are considered equal. Gravity is the sole motivating force for the flow, with the heavier fluid displacing the lighter fluid in a reservoir at $X = +\infty$. The volumetric discharge across the channel is therefore zero.

The Navier–Stokes equations which govern the primary flow are

$$\left.\begin{aligned} 0 &= -P_{1,X}+\rho_1 g\sin\theta+\mu\overline{U}_{1,YY}, \\ 0 &= -P_{1,Y}-\rho_1 g\cos\theta \quad \text{for} \quad 0\leqslant Y\leqslant b, \end{aligned}\right\} \tag{1}$$

and

$$\left.\begin{aligned} 0 &= -P_{2,X}+\rho_2 g\sin\theta+\mu\overline{U}_{2,YY}, \\ 0 &= -P_{2,Y}-\rho_2 g\cos\theta \quad \text{for} \quad -b\leqslant Y\leqslant 0, \end{aligned}\right\} \tag{2}$$

where $\overline{U}_1$ and $\overline{U}_2$, the components of velocity of the two fluids in the X-direction, are functions of Y only, and letter subscripts following commas denote partial differentiation with respect to that quantity. The components of velocity in the Y- and Z-directions are zero. The condition of continuity is thus automatically satisfied. Pressure is indicated by P and the gravitational acceleration by g.

These equations are easily solved for $\overline{U}_1$ and $\overline{U}_2$. It can easily be verified that

$$\overline{U}_1 = U_M\left[-\frac{Y}{b}+\left(\frac{Y}{b}\right)^2\right] \quad (0\leqslant Y\leqslant b), \tag{3}$$

and

$$\overline{U}_2 = -U_M\left[+\frac{Y}{b}+\left(\frac{Y}{b}\right)^2\right] \quad (-b\leqslant Y\leqslant 0), \tag{4}$$

where

$$U_M = \frac{(\rho_2-\rho_1)}{4\mu}b^2 g\sin\theta \tag{5}$$

is four times the maximum velocity. The boundary conditions corresponding to (3) and (4) are conditions of no slipping at the fixed boundaries. The condition of zero volumetric discharge is also satisfied by (3) and (4). The pressure gradient in the X-direction is

$$P_{1,X} = P_{2,X} = \tfrac{1}{2}(\rho_2+\rho_1)g\sin\theta.$$

Thus, the X-variation of pressure is the same as that of the hydrostatic pressure in a fluid of density $\frac{1}{2}(\rho_2+\rho_1)$, while the Y-variation corresponds to a hydrostatic pressure in the fluids at present under consideration.

3. Formulation of the stability problem

A. *Differential equations*

The basic equations to be satisfied are the Navier–Stokes equations and the continuity equations. Following the usual approach to stability problems, it is assumed that the perturbed velocity and pressure fields are expressible in power series expansions in terms of an amplitude parameter ϵ, assumed small and constant (see Lin 1955, § 1.2). Upon substituting these expansions into the field equations and setting coefficients of powers of ϵ to zero, it is noted that the equations in ϵ^0 are those already described as governing the primary flow. The equations in ϵ^1 are

$$u^*_{i,T}+\overline{U}_i u^*_{i,X}+\overline{U}_{i,Y}v^* = -\frac{1}{\rho_i}P^*_{i,X}+\frac{\mu}{\rho_i}\nabla^2 u^*_i, \tag{6}$$

$$v^*_{i,T}+\overline{U}_i v^*_{i,X} = -\frac{1}{\rho_i}P^*_{i,Y}+\frac{\mu}{\rho_i}\nabla^2 v^*_i, \tag{7}$$

$$u^*_{i,X}+v^*_{i,Y} = 0, \tag{8}$$

where the disturbance is assumed to be a two-dimensional one. The convention has been adopted that capital letters refer to the primary flow and small letters with an asterisk in the upper right-hand corner refer to the first-order disturbance flow. The equations hold in the upper region when $i = 1$ and in the lower region when $i = 2$. As is customary in stability analyses, attention will be confined solely to the first-order equations, with the assumption that for sufficiently small disturbances the linearized equations can be used without appreciable error.

To facilitate the solution of (6), (7) and (8), it is convenient to put them in dimensionless form. The following dimensionless parameters are introduced

$$\left.\begin{aligned} u_i &= \frac{u_i^*}{U_M}, \quad v_i = \frac{v_i^*}{U_M}, \quad p_i = \frac{p_i^*}{\rho_i U_M^2}, \quad x = \frac{X}{b}, \quad y = \frac{Y}{b}, \\ t &= T\frac{U_M}{b}, \quad U_i = \frac{\overline{U}_i}{U_M}, \quad R_i = \frac{bU_M\rho_i}{\mu}, \quad r = \frac{\rho_2}{\rho_1}. \end{aligned}\right\} \tag{9}$$

Formulating (6), (7) and (8) in terms of these parameters, the following dimensionless equations are obtained

$$u_{i,t} + U_i u_{i,x} + U_{i,y} v_i = -p_{i,x} - \frac{1}{R_i}\nabla^2 u_i, \tag{10}$$

$$v_{i,t} + U_i v_{i,x} = -p_{i,y} + \frac{1}{R_i}\nabla^2 v_i, \tag{11}$$

$$u_{i,x} + v_{i,y} = 0, \tag{12}$$

in which R_i is the Reynolds number based on the half-spacing b and U_M. Since the flow is motivated by gravity, it is expected that the Reynolds number and the Froude number F are not independent of one another. Such is indeed the case, for if F is defined by $F^2 = U_M^2/gb$, then from the primary flow (5) provides the relationship

$$F^2 = \tfrac{1}{4}(r-1)\,R_1 \sin\theta. \tag{13}$$

To reduce the number of equations which are to be solved, it is convenient to introduce stream functions. To simplify solution of (10), (11) and (12), the solutions will be assumed to have exponential time factors. Further, to reduce the partial differential equations to ordinary differential equations, it is assumed that the disturbance may be resolved into Fourier components, which are thus periodic in x. A general disturbance then would consist of either a Fourier series or a Fourier integral of such components. To determine the stability of the flow it is sufficient to consider the effect of a single Fourier component of general period.

Only two-dimensional disturbances are considered, since the work of Squire (1933), Yih (1955) and others has shown that the stability or instability of a three-dimensional disturbance can be determined from that of a two-dimensional disturbance at a higher Reynolds number.

The velocity components and the pressure can thus be assumed to have the following forms, in which $f(y)$ and $h(y)$ are introduced as 'stream functions' to satisfy (12) automatically

$$\left.\begin{aligned} u_1 &= f'(y)\,e^{i\alpha(x-ct)}, \\ v_1 &= -i\alpha f(y)\,e^{i\alpha(x-ct)}, \\ p_1 &= q_1(y)\,e^{i\alpha(x-ct)}, \end{aligned}\right\} \tag{14}$$

in $0 \leqslant y \leqslant 1$, and

$$\left.\begin{aligned} u_2 &= h'(y)\, e^{i\alpha(x-ct)}, \\ v_2 &= -i\alpha h(y)\, e^{i\alpha(x-ct)}, \\ p_2 &= q_2(y)\, e^{i\alpha(x-ct)} \end{aligned}\right\} \tag{15}$$

in $-1 \leqslant y \leqslant 0$, where primes denote differentiation with respect to y. The dimensionless wave number α is related to the wave length λ of the disturbance by $\alpha = 2\pi b/\lambda$. The real part of c represents the dimensionless disturbance celerity, and α times the imaginary part of c gives the dimensionless growth rate of the disturbance.

Upon solving (10), (11), (14) and (15) for the pressure terms, the following are obtained

$$\left.\begin{aligned} q_1 &= \frac{1}{i\alpha R_1}(f''' - \alpha^2 f') + (c - U_1) f' + U_1' f, \\ q_1' &= \frac{1}{i\alpha R_1}(\alpha^2 f'' - \alpha^4 f) + \alpha^2 (c - U_1) f \end{aligned}\right\} \tag{16}$$

in $0 \leqslant y \leqslant 1$, and

$$\left.\begin{aligned} q_2 &= \frac{1}{i\alpha R_2}(h''' - \alpha^2 h') + (c - U_2) h' + U_2' h, \\ q_2' &= \frac{1}{i\alpha R_2}(\alpha^2 h'' - \alpha^4 h) + \alpha^2 (c - U_2) h \end{aligned}\right\} \tag{17}$$

in $-1 \leqslant y \leqslant 0$. The pressure terms can now be eliminated to obtain

$$f^{\mathrm{IV}} + [-2\alpha^2 + i\alpha R_1 (c - U_1)] f'' + [\alpha^4 + i\alpha R_1 U_1'' + i\alpha^3 R_1 (U_1 - c)] f = 0 \tag{18}$$

in $0 \leqslant y \leqslant 1$, and

$$h^{\mathrm{IV}} + [-2\alpha^2 + i\alpha R_2 (c - U_2)] h'' + [\alpha^4 + i\alpha R_2 U_2'' + i\alpha^3 R_2 (U_2 - c)] h = 0 \tag{19}$$

in $-1 \leqslant y \leqslant 0$. These equations are the Orr–Sommerfeld equations. From (3), (4) and (9) the functions U_1 and U_2 are

$$U_1 = -y + y^2, \quad U_2 = -y - y^2. \tag{20}$$

B. *Boundary conditions*

Since the differential equations (18) and (19) are two in number and each is of the fourth order, there must be eight boundary conditions imposed to specify the mathematical problem completely. Two conditions are imposed at each of the fixed boundaries, and a total of four are imposed at the interface.

Since the fluids are considered viscous, there must be no slip at the fixed boundaries. Hence, in terms of the stream functions,

$$f(1) = 0, \quad f'(1) = 0, \quad h(-1) = 0, \quad h'(-1) = 0. \tag{21}$$

The interface is assumed to be displaced from the x-axis by a small amount which in dimensional form is denoted by $b\eta$. This introduces a further unknown into the problem, which, however, may be readily determined from the kinematical condition that the component of velocity at the interface must equal the time derivative of η. In what follows, quantities evaluated at the interface are

expanded in a Taylors series about $y = 0$, and η is considered to be of the same order as the velocity disturbances. In keeping with the previous linearization, only first-order disturbance terms are retained.

At the interface, the velocity components must be continuous; hence

$$f(0) = h(0), \quad f'(0) = h'(0). \tag{22}$$

The kinematic condition at the interface is, in dimensionless terms,

$$v = \eta_{,t} \tag{23}$$

at $y = 0$. Then $\eta_{,t} = -i\alpha f(0)\, e^{i\alpha(x-ct)}$

and upon solving for η

$$\eta = \frac{1}{c} f(0)\, e^{i\alpha(x-ct)}. \tag{24}$$

The shear stress must also be continuous across the interface. To the first order, the dimensionless shear stress at the interface is given by

$$\tau_{xy} = \frac{1}{R}(U' + u' + v_{,x} + U''\eta). \tag{25}$$

Therefore the boundary condition imposed is, after some simplification,

$$4f(0) + cf''(0) - ch''(0) = 0. \tag{26}$$

The dimensionless normal stress at the interface is

$$\tau_{yy} = -\frac{1}{\rho U_M^2}(P + P_{,Y} b\eta + 2\mu U_M v') - p, \tag{27}$$

where P is the pressure in the primary flow. The condition imposed is that the difference in normal stresses must be equal to the curvature of the interface times γ, the surface tension. Since P must already be continuous, and since

$$P_{,Y} = -g\rho\cos\theta,$$

the boundary condition becomes

$$q_1(0) - rq_2(0) + \frac{1}{c}\left[\frac{(r-1)\, bg\cos\theta}{U_M^2} + \frac{\alpha^2}{W}\right] f(0) = 0, \tag{28}$$

where W is the Weber number defined by $W = \rho_1 b U_M^2/\gamma$. This can be written entirely in terms of the stream functions by using (16) and (17). The resulting equation is, after further simplification,

$$c[f'''(0) - h'''(0)] + (r-1)\, i\alpha R_1 c[f(0) - cf'(0)] + i\alpha[4\cot\theta + \alpha^2 S] f(0) = 0. \tag{29}$$

The parameter S is defined by

$$S = \frac{R_1}{W} = \frac{\gamma}{\mu U_M}, \tag{30}$$

and represents the ratio of surface tension to viscous forces.

4. Solution of the stability problem

A. *General*

For the purpose of solving (18) and (19), much labour can be saved by employing the following notation:

$$\left.\begin{aligned} \phi(y) &= \begin{cases} f(y) & \text{in } 0 \leqslant y \leqslant 1, \\ h(y) & \text{in } -1 \leqslant y \leqslant 0, \end{cases} \\ B &= \alpha^2, \\ A &= \begin{cases} A_1 = i\alpha R_1 & \text{in } 0 \leqslant y \leqslant 1, \\ A_2 = i\alpha R_2 & \text{in } -1 \leqslant y \leqslant 0, \end{cases} \\ \delta &= \begin{cases} +1 & \text{in } 0 \leqslant y \leqslant 1, \\ -i & \text{in } -1 \leqslant y \leqslant 0. \end{cases} \end{aligned}\right\} \tag{31}$$

Then (18) and (19) can both be solved simultaneously by solving

$$\phi^{\mathrm{iv}} + [-2B + A(c + y - \delta y^2)]\phi'' + [B^2 + 2A\delta + AB(-c - y + \delta y^2)]\phi = 0. \tag{32}$$

As discussed in the Introduction, instability can be expected to occur at low Reynolds numbers when the inclination θ approaches 90°. Two techniques at once are suggested as alternate methods of solution. The first, expansion of ϕ in ascending powers of the Reynolds number, is certainly the more typical of stability problems and was used by Yih (1954). The alternate approach, expansion of ϕ in powers of the co-ordinate y, has, to the best of the author's knowledge, been previously employed successfully only by Benjamin (1957) in spite of its early recognition by Kelvin (1887) and others. This method seems more useful in carrying out the solution for ϕ to higher powers of the Reynolds number, and conclusions are drawn on the basis of these calculations. Of course, the validity of approximations based on either method can be determined only *a posteriori*.

B. *Expansion in powers of the co-ordinate y*

Following Benjamin (1957), a solution of the form

$$\phi(y) = \sum_{n=0}^{\infty} a_n y^n \tag{33}$$

can be assumed. It is most convenient to expand around the origin since four of the boundary conditions must be satisfied there. Upon substituting (33) into (32) and setting coefficients of y^n to zero, the following recurrence relation is obtained:

$$\begin{aligned} a_n = \frac{(n-4)!}{n!}\{&(n-2)(n-3)(2B - Ac)a_{n-2} - (n-4)(n-3)Aa_{n-3} \\ &+ [A\delta(n-4)(n-5) - B^2 - 2A\delta + ABc]a_{n-4} + ABa_{n-5} - AB\delta a_{n-6}\}. \end{aligned} \tag{34}$$

All of the a_n for $n \geqslant 4$ can now be found from (34) in terms of a_0, a_1, a_2 and a_3. Since these four coefficients are arbitrary, four independent solutions of the

fourth-order equation are thus obtained. They are (where a_0, a_1, a_2 and a_3 have been set equal to 1, 1, 1 and 1/3!, respectively)

$$\begin{aligned}\phi_1(y) = 1 &+ (1/4!)(ABc - B^2 - 2A\delta)y^4 + (1/5!)AB y^5 \\ &+ (1/6!)(2A^2c\delta - 6AB\delta + 3AB^2c - A^2Bc - 2B^3)y^6 \\ &+ (1/7!)(6A^2\delta + 5AB^2 - 4A^2Bc^2)y^7 \\ &+ (1/8!)(-20A^2 - 3B^4 + 6AB^3c - 4A^2B^2c^2 - 20AB^2\delta + 18A^2Bc\delta \\ &\quad - 2A^3c^2\delta + A^3Bc^3 - 4A^2B)y^8 \\ &+ (1/9!)(14AB^3 + 50A^2B\delta + 9A^3Bc^2 - 22A^2B^2c - 16A^3c\delta)y^9 + \ldots, \end{aligned} \tag{35}$$

$$\begin{aligned}\phi_2(y) = y &+ (1/5!)(ABc - B^2 - 2A\delta)y^5 + (1/6!)2AB y^6 \\ &+ (1/7!)(2A^2c\delta - 10AB\delta + 3AB^2c - A^2Bc^2 - 2B^3)y^7 \\ &+ (1/8!)(8A^2\delta + 8AB^2 - 6A^2Bc)y^8 \\ &+ (1/9!)(-36A^2 - 3B^4 + 6AB^3c - 36AB^2\delta + 30A^2Bc\delta - 4A^2B^2c^2 \\ &\quad - 2A^3c^2\delta - 10A^2B + A^3Bc^3)y^9 \\ &+ (1/10!)(20AB^3 + 122A^2B\delta + 12A^3Bc^2 - 30A^2B^2c - 20A^3c\delta)y^{10} + \ldots, \end{aligned} \tag{36}$$

$$\begin{aligned}\phi_3(y) = y^2 &+ (1/4!)(4B - 2Ac)y^4 - (1/5!)2A y^5 \\ &+ (1/6!)(6B^2 - 6ABc + 2A^2c^2)y^6 + (1/7!)(8A^2c - 10AB)y^7 \\ &+ (1/8!)(8A^2 + 16AB\delta - 20A^2c\delta + 8B^3 - 12AB^2c + 8A^2Bc^2 - 2A^3c^3)y^8 \\ &+ (1/9!)(-36A^2\delta - 28AB^2 + 44A^2Bc - 18A^3c^2)y^9 \\ &+ (1/10!)(10B^4 - 20AB^3c + 80AB^2\delta + 20A^2B^2c^2 - 164A^2Bc\delta \\ &\quad + 64A^2B + 76A^3c^2\delta - 10A^3Bc^3 - 56A^3c + 2A^4c^4)y^{10} + \ldots, \end{aligned} \tag{37}$$

$$\begin{aligned}\phi_4(y) = (1/3!)y^3 &+ (1/5!)(2B - Ac)y^5 - (1/6!)2Ay^6 \\ &+ (1/7!)(3B^2 - 3ABc + A^2c^2 + 4A\delta)y^7 + (1/8!)(6A^2c - 8AB)y^8 \\ &+ (1/9!)(24AB\delta - 22A^2c\delta + 10A^2 + 4B^3 - 6AB^2c + 4A^2Bc^2 - A^3c^3)y^9 \\ &+ (1/10!)(-80A^2\delta - 20AB^2 + 30A^2Bc - 12A^3c^2)y^{10} \\ &+ (1/11!)(160A^2 + 5B^4 - 10AB^3c + 60AB^2\delta + 10A^2B^2c^2 + 62A^2B \\ &\quad - 142A^2Bc\delta + A^4c^4 - 52A^3c - 5A^3Bc^3 + 62A^3c^2\delta)y^{11} \\ &+ (1/12!)(580A^3c\delta - 72A^3Bc^2 + 90A^2B^2c - 80A^3 - 40AB^3 \\ &\quad - 64A^2B\delta + 20A^4c^3)y^{12} + \ldots. \end{aligned} \tag{38}$$

The solutions must converge for all finite A, B, c and y because of the absence of singularities in the differential equation. An inspection of (35), (36), (37) and (38) indicates that for the range of the parameters considered, the solutions converge rather rapidly. For convenience, a further function ϕ_5, defined by

$$\phi_5(y) = c\phi_1(y) + \phi_2(y) - \delta\phi_3(y), \tag{39}$$

is also introduced. It is found convenient in later work to use the set of four solutions ϕ_2, ϕ_3, ϕ_4 and ϕ_5.

The solutions of (18) and (19) are given by linear combinations of the $f_i(y)$ and $h_i(y)$, these being the values of $\phi_i(y)$ when A and δ are assigned the values A_1, 1 and A_2, -1, respectively.

Satisfaction of boundary conditions (22) and (26) is insured by writing

$$f(y) = a_2 f_2(y) + a_3 f_3(y) + a_4 f_4(y) + a_5 f_5(y), \tag{40}$$

$$h(y) = a_2 h_2(y) + a_3 h_3(y) + a_5 h_5(y) + a_6 h_4(y). \tag{41}$$

To satisfy the remainder of the boundary conditions, it is necessary that

$$\left.\begin{aligned}
0 &= a_2 c(A_1 - A_2) && + a_4 i\alpha(4\cot\theta + \alpha^2 S) - a_6, \\
0 &= a_2 f_2(1) + a_3 f_3(1) && + a_4 f_4(1) + a_5 f_5(1), \\
0 &= a_2 f_2'(1) + a_3 f_3'(1) && + a_4 f_4'(1) + a_5 f_5'(1), \\
0 &= a_2 h_2(-1) + a_3 h_3(-1) && + a_5 h_5(-1) + a_6 h_4(-1), \\
0 &= a_2 h_2'(-1) + a_3 h_3'(-1) && + a_5 h_5'(-1) + a_6 h_4'(-1).
\end{aligned}\right\} \tag{42}$$

In order for a non-trivial solution of these algebraic equations to exist, the determinant of the coefficients must vanish. Therefore we have

$$0 = \begin{vmatrix}
c(A_1 - A_2) & 0 & 1 & i\alpha(4\cot\theta + \alpha^2 S) & -1 \\
f_2(1) & f_3(1) & f_4(1) & f_5(1) & 0 \\
f_2'(1) & f_3'(1) & f_4'(1) & f_5'(1) & 0 \\
h_2(-1) & h_3(-1) & 0 & h_5(-1) & h_4(-1) \\
h_2'(-1) & h_3'(-1) & 0 & h_5'(-1) & h_4'(-1)
\end{vmatrix}. \tag{43}$$

This determinant may be expanded into a number of two-by-two determinants by a method such as Laplace's expansion. This yields the result

$$\begin{aligned}
0 = {} & H_1 F_4 + F_1 H_4 - H_2 F_6 - F_2 H_6 + H_3 F_5 + F_3 H_5 \\
& + i\alpha(4\cot\theta + \alpha^2 S)(H_2 F_3 - F_2 H_3) + c(A_2 - A_1)(F_1 H_3 - H_1 F_3),
\end{aligned} \tag{44}$$

where the following notation has been introduced:

$$\left.\begin{aligned}
F_1 &= \begin{vmatrix} f_4(1) & f_5(1) \\ f_4'(1) & f_5'(1) \end{vmatrix}, & H_1 &= \begin{vmatrix} h_4(-1) & h_5(-1) \\ h_4'(-1) & h_5'(-1) \end{vmatrix}, \\
F_2 &= \begin{vmatrix} f_2(1) & f_4(1) \\ f_2'(1) & f_4'(1) \end{vmatrix}, & H_2 &= \begin{vmatrix} h_2(-1) & h_4(-1) \\ h_2'(-1) & h_4'(-1) \end{vmatrix}, \\
F_3 &= \begin{vmatrix} f_3(1) & f_4(1) \\ f_3'(1) & f_4'(1) \end{vmatrix}, & H_3 &= \begin{vmatrix} h_3(-1) & h_4(-1) \\ h_3'(-1) & h_4'(-1) \end{vmatrix}, \\
F_4 &= \begin{vmatrix} f_2(1) & f_3(1) \\ f_2'(1) & f_3'(1) \end{vmatrix}, & H_4 &= \begin{vmatrix} h_2(-1) & h_3(-1) \\ h_2'(-1) & h_3'(-1) \end{vmatrix}, \\
F_5 &= \begin{vmatrix} f_2(1) & f_5(1) \\ f_2'(1) & f_5'(1) \end{vmatrix}, & H_5 &= \begin{vmatrix} h_2(-1) & h_5(-1) \\ h_2'(-1) & h_5'(-1) \end{vmatrix}, \\
F_6 &= \begin{vmatrix} f_3(1) & f_5(1) \\ f_3'(1) & f_5'(1) \end{vmatrix}, & H_6 &= \begin{vmatrix} h_3(-1) & h_5(-1) \\ h_3'(-1) & h_5'(-1) \end{vmatrix}.
\end{aligned}\right\} \tag{45}$$

To complete the determination of the eigenvalue c it becomes necessary now to approximate the ϕ's, as obviously the infinite series form for the ϕ's must be terminated. It was decided to consider α and R to be of the same order, and to limit the calculation to fifth powers of α and R (and combinations of them). The odd power is introduced by the boundary condition on the normal stresses. No special assumption is made concerning c, although it is considered to be of the order of one. Computations based on such an approximation prove straightforward but lengthy. To carry out the next-higher approximation (to the sixth power) would triple or quadruple the amount of work necessary, which is already considerable.

Treating α and R to be of the same order gives results which are valid in a small circle around the origin in the (α, R)-plane. Calculations based on expansions to the first order in the Reynolds number as made by Yih (1954) would give results valid in a narrow strip along the α-axis in the (α, T)-plane. Since the results of most stability analyses (including this one, as will be seen) indicate the onset of instability with small wave-number, it would seem that an approximation valid for a wider range of R is more desirable. This was the main factor in choosing an analysis based on expansion in terms of powers of the co-ordinate y.

It is desirable to state the range of α and R for which the approximation is valid. Certainly if α and R are both much less than one, the results are very good. For α and R of the order of one or slightly larger, it is felt that the conclusions are still qualitatively true, since the denominators of the terms in the series increase in a factorial manner while the numerators increase only gradually. However, the prohibitive amount of calculations necessary make any definite statements on the range of validity impossible.

Since the calculations are straightforward, they are not included here. Because in several calculations it was necessary to take the difference between two small numbers of almost equal magnitude, it was considered useful to leave the numbers in fractional form. This also facilitated checking of the results.

When all calculations are carried out, an algebraic equation in integral powers of c is obtained. This is

$$
\begin{aligned}
0 = &-320i\alpha\cot\theta+\tfrac{12}{7}(r+1)\,i\alpha R_1-\tfrac{320}{3}i\alpha^3\cot\theta+\tfrac{68}{21}(r-1)\,\alpha^2R_1\cot\theta\\
&-80i\alpha^3S-\tfrac{17}{1155}(r^2-1)\,\alpha^2R_1^2+\tfrac{86}{105}(r+1)\,i\alpha^3R_1+\tfrac{142}{10395}(r^2+1)\,i\alpha^3R_1^2\cot\theta\\
&-\tfrac{8}{245}ri\alpha^3R_1^2\cot\theta+\tfrac{388}{315}(r-1)\,\alpha^4R_1\cot\theta-\tfrac{1856}{105}i\alpha^5\cot\theta\\
&-\tfrac{80}{3}i\alpha^5S+\tfrac{17}{21}\alpha^4R_1S(r-1)\\
&+c\{-1920-\tfrac{380}{7}i\alpha R_1(r-1)-1024\alpha^2-\tfrac{80}{3}(r+1)\,\alpha^2R_1\cot\theta\\
&\quad+\tfrac{13190}{231}(r^2+1)\,\alpha^2R_1^2-\tfrac{62}{105}\alpha^2R_1^2r-\tfrac{608}{21}(r-1)\,i\alpha^3R_1-\tfrac{2048}{7}\alpha^4\\
&\quad-\tfrac{85}{378}(r^2-1)\,i\alpha^3R_1^2\cot\theta-\tfrac{928}{105}(r+1)\,\alpha^4R_1\cot\theta-\tfrac{20}{3}\alpha^4R_1S(r+1)\}\\
&+c^2\{256(r+1)\,i\alpha R_1-\tfrac{323}{63}(r^2-1)\,\alpha^2R_1^2+\tfrac{1024}{7}i\alpha^3R_1(r+1)\\
&\quad+\tfrac{6}{7}(r^2+1)\,i\alpha^3R_1^2\cot\theta+\tfrac{32}{15}i\alpha^3R_1^2r\cot\theta\}\\
&+c^3\alpha^2R_1^2[(r^2+1)\tfrac{181}{14}+29r]. \qquad (46)
\end{aligned}
$$

The root of interest can be computed by assuming $c = c_0 + c_1\alpha + c_2 R + c_3\alpha^2 + \ldots$, and substituting this into (46). After this is done, upon separation into real and imaginary parts, the result is

$$c_r = \frac{\alpha^2 R_1(r-1)}{1920}\left\{\frac{2183}{64{,}680}(r+1)R_1 - \tfrac{61}{42}\alpha^2 S - \cot\theta\left[\tfrac{122}{21} - \tfrac{46}{35}\alpha^2\right]\right\}, \tag{47}$$

$$\begin{aligned} c_i = \frac{\alpha}{1920}\Bigg\{&\frac{(r+1)R_1}{7}(12 - 2/3\alpha^2) - 16\alpha^2 S(5-\alpha^2) \\ &- \cot\theta\left[64\left(5 - \alpha^2 + \frac{\alpha^4}{21}\right) - \frac{443{,}683}{1{,}164{,}240}(r^2+1)\alpha^2 R_1^2\right. \\ &\left. + \frac{2787}{17{,}640}r\alpha^2 R_1^2\right] - \cot^2\theta[8/3(r+1)\alpha^2 R_1]\Bigg\}. \end{aligned} \tag{48}$$

The growth rate σ is given by

$$\sigma = \alpha c_i. \tag{49}$$

It can be argued (see, for instance, Schubauer & Skramstad 1947) that the most likely wave-number to occur is the one with the highest growth rate. This value of α can be determined by setting to zero the derivative of σ with respect to α. The relation obtained by this is

$$\begin{aligned} 0 = \frac{\alpha}{1920}\Bigg\{&\frac{8(r+1)R_1}{7}(3 - \tfrac{1}{3}\alpha^2) - 32S\alpha^2(10 - 3\alpha^2) - \cot\theta\left[64\left(10 - 4\alpha^2 + \frac{6\alpha^4}{21}\right)\right. \\ &\left. - \frac{443{,}683}{291{,}060}(r^2+1)\alpha^2 R_1^2 + \frac{2787}{4410}r\alpha^2 R_1^2\right] - \cot^2\theta[\tfrac{32}{3}(r+1)\alpha^2 R_1]\Bigg\}. \end{aligned} \tag{50}$$

For the case of vertical inclination, the possible roots of (50) are, besides $\alpha = 0$,

$$\alpha_{\mathrm{cr}}^2 = \tfrac{1}{6}[10 + \beta \pm (100 - 88\beta + \beta^2)^{\frac{1}{2}}], \tag{51}$$

where

$$\beta = \frac{(r+1)R_1}{84S}. \tag{52}$$

(In the case of $S = 0$, the roots reduce to 0, 3.) For small β, (51) may be expanded using the binomial theorem to obtain

$$\alpha_{\mathrm{cr}}^2 = \tfrac{10}{6}\{1 + 0{\cdot}1\beta \pm (1 - 0{\cdot}44\beta - 0{\cdot}092\beta^2)\}, \tag{53}$$

or, for the root of interest,

$$\alpha_{\mathrm{cr}}^2 = \beta\{0{\cdot}9 + 0{\cdot}15\beta\}. \tag{54}$$

5. Discussion of results

A. *The special case of infinite slope*

An inspection of (48) and the corresponding figures 2, 3 and 4 reveals that for the case of vertical inclination and zero surface tension, every value of α makes c_i zero for zero Reynolds number. Hence the α-axis is the neutral stability curve. (The analysis does not hold true for large values of α, however, it can be argued on physical grounds that in the absence of surface tension there is no restoring force when the slope is infinite.) Surface tension has a stabilizing effect (figures 2, 4) and reduces the range of α for which instability occurs at zero Reynolds

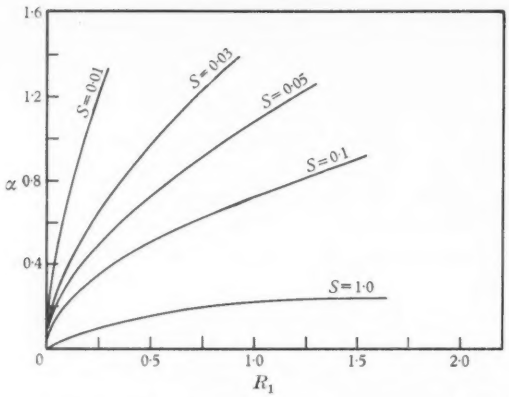

FIGURE 2. Curves of neutral stability for flow between vertical walls with various values of the surface tension parameter S. $\sigma = 0$, $r = 1{\cdot}2$, $\theta = 90°$.

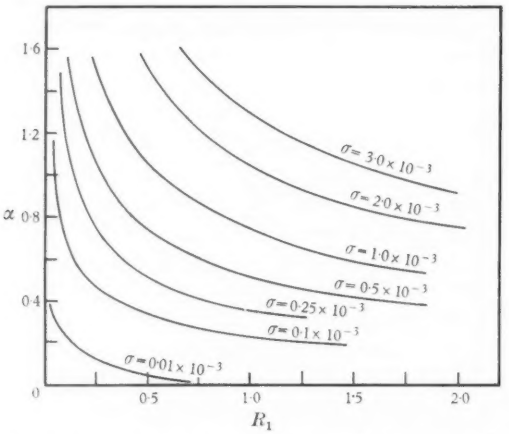

FIGURE 3. The rate of amplification of waves of various wave-numbers for the vertical case. $S = 0$, $r = 1{\cdot}2$, $\theta = 90°$.

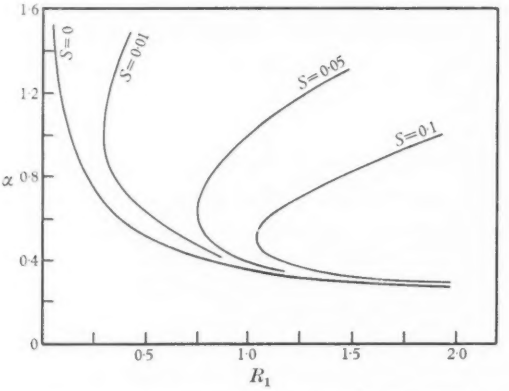

FIGURE 4. The effect of surface tension on growth rate for the vertical case. $\sigma = 0{\cdot}25 \times 10^{-3}$, $r = 1{\cdot}2$, $\theta = 90°$.

number to the point $\alpha = 0$, hence it can never completely prevent instability. From a physical point of view, the effect of surface tension decreases with curvature. From a mathematical point of view, S is always accompanied by a curvature term (α^2), so for very small wave-numbers the stabilizing force would be small.

The shape of the growth rate curves of figure 4 is very similar to the neutral stability curve shown by Yih (1954). It might be speculated that the disagreement between Yih's and Benjamin's (1957) results could be due to the difference

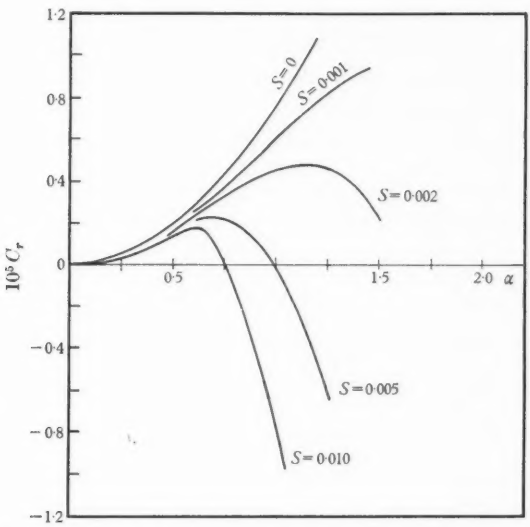

FIGURE 5. The effect of surface tension on the celerity of the disturbance for the vertical case. $R = 1{\cdot}0$, $r = 1{\cdot}2$, $\theta = 90°$.

in the approximations which might yield different members of the same family of curves. Benjamin's result would be the true neutral stability curve, while Yih's would be a curve of constant (small) growth rate.

It is noted from (9) and (47) that the dimensional celerity of the disturbance is directly dependent on the difference in densities of the two fluids and the velocity of the primary flow. A small Reynolds number implies either large viscosity or small difference in densities, hence the speed of propagation of the disturbance is small for the approximation considered. The celerity is also small for the case of small wave-numbers. The disturbance anticipated by the analysis is then in effect almost a standing wave, in the sense that it does not propagate, at least not very quickly.

It is seen from (47) and figure 5 that the surface tension could make the celerity negative, hence disturbances would travel uphill. This effect is perhaps unexpected, but not unreasonable. Such results have in fact been noted in experiments conducted by William M. Sangster of the University of Iowa, for layers of different thicknesses.

If (47) is contrasted with the corresponding results of the stability analyses of Yih and Benjamin, it is seen that the celerities represented in their analyses have values of the same order as the primary flow for very small Reynolds and wave-numbers, while the celerities presented here are many orders smaller than the velocity of the primary flow.

The direct dependence of the disturbance celerity on the difference in densities of the two fluids may seem surprising when compared with previous results (Lamb 1932, p. 370) for gravity waves. The reason for this difference is that the present waves are predominantly influenced by viscosity rather than gravity.

The fact that the primary flow velocity is zero at the interface may explain some aspects of the disturbance celerity. Although a free surface is generally regarded as a destabilizing agent, this effect is somewhat diminished in the present problem due to the counterflow. If the free surface were replaced by a rigid boundary, the problem would be the familiar one of plane Poiseuille flow, for which instability is known to occur for Reynolds numbers many orders higher than contemplated in the present analysis (see, for example, Lin 1955, p. 28).

Another interesting feature is that (24) shows that the disturbance amplitude is inversely proportional to c. For small c then, even if the y velocity component is small, the amplitude of the disturbance may be considerably larger in comparison.

Naturally, the onset of instability at such low Reynolds numbers does not mean the onset of turbulence, but only the onset of waves at the free surface. The analysis performed here is, of course, based on the assumption that the two fluids do not mix across the interface.

B. *Other slopes*

The results are not as informative for values of θ other than 90°. As the inclination becomes even slightly less steep, the θ terms in (48) predominate and exert a strong stabilizing influence. For θ more than a degree of two away from vertical, the results probably are not sufficiently accurate to predict instability, and higher-order approximations are necessitated. Neutral stability curves are shown in figure 6 for various values of the parameter S for the case $\theta = 89{\cdot}5°$. The curve for $S = 0$ bends towards the α-axis and predicts instability again for all small Reynolds numbers. It is believed, however, that this is not a reliable result, and that if higher-order terms were present the curve would be almost vertical for small α, and then would go in the positive R_1 direction, as do the curves for non-zero values of S. This same effect is shown in figure 7. The results shown in figure 8, with a non-zero value of S, are more reliable in regard to the shape of the curve, and show that for inclinations other than the vertical, critical Reynolds numbers do exist. It seems reasonable that the critical Reynolds number should occur at $\alpha = 0$. The greater surface tension effect and greater dissipation of the disturbance energy at higher wave-numbers would both tend to stabilize the flow. Such tendencies were shown for the case of vertical inclination. A definite mathematical answer to this matter would require a higher-order approximation.

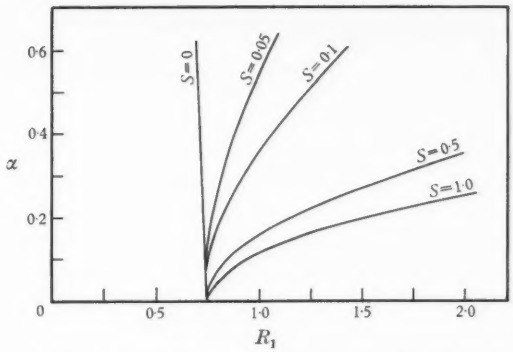

FIGURE 6. Neutral stability curves for the case $\theta = 89{\cdot}5°$, for various values of the surface tension parameter S. $\sigma = 0$, $r = 1{\cdot}2$.

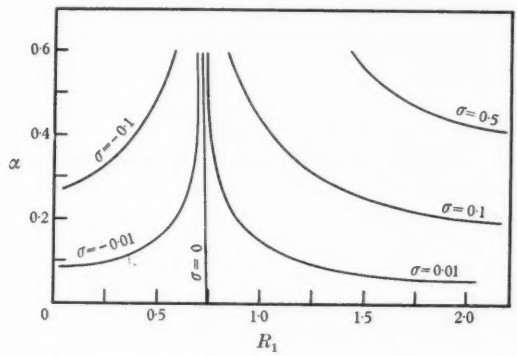

FIGURE 7. The rate of amplification of waves of various wave-numbers for the case $\theta = 89{\cdot}5°$, $S = 0$, $r = 1{\cdot}2$.

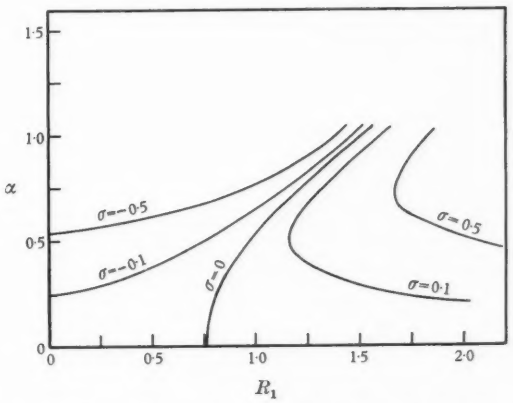

FIGURE 8. The rate of amplification of waves of various wave-numbers for the case $\theta = 89{\cdot}5°$, $S = 0{\cdot}05$, $r = 1{\cdot}2$.

6. Conclusions

From the results presented, the following conclusions can be drawn:

(*a*) For the case of vertical inclination, there are values of α for which the flow is unstable at all values of the Reynolds number. The celerity of such disturbances is small, but the effect on the interface can be large.

(*b*) The stabilizing effect of surface tension is shown, although surface tension can never induce complete stability, since it has no effect at zero wave-number.

(*c*) For slopes other than the vertical, a critical Reynolds number exists. The value of the critical Reynolds number probably is the value of R_1 which occurs at $\alpha = 0$, although a more thorough investigation is needed in order that a definite statement can be made in this regard.

(*d*) The presence of the interface is responsible for instability at low Reynolds numbers at steep slopes. However, the layer in counterflow does contribute a stabilizing influence.

(*e*) The critical wave number has been found and is given in equation (54). Specific results for the (complex) phase velocity are given in equations (47) and (48).

The author wishes to express his appreciation to Dr C. S. Yih for suggesting the present problem and for his advice during the course of its solution. The partial support of this work by the Office of Ordnance Research of the U.S. Army is also gratefully acknowledged.

REFERENCES

Benjamin, T. Brooke 1957 *J. Fluid Mech.* **2**, 554.

Kelvin, Lord 1887 *Math. Phys. Pap.* **4**, 321. Cambridge University Press.

Lamb, H. 1932 *Hydrodynamics*, 6th ed. New York: Dover.

Lin, C. C. 1955 *The Theory of Hydrodynamic Stability.* Cambridge University Press.

Schubauer, G. B. & Skramstad, H. K. 1947 *J. Res. Nat. Bur. Stand., Wash.*, **38**, 251.

Squire, H. B. 1933 *Proc. Roy. Soc.* A, **142**, 621.

Yih, C. S. 1954 *Proc. of the Second U.S. Nat. Congr. of Appl. Mech.*, p. 623.

Yih, C. S. 1955 *Quart. J. Mech. Appl. Math.* **12**, 434.

Calculations of the motion of non-uniform shock waves

By JAN ROŚCISZEWSKI
Pierce Hall, Harvard University

(Received 31 March 1959 and in revised form 30 January 1960)

Problems of the propagation of shock waves and strong detonation waves through ducts of variable cross-section and ducts with porous walls, and the interaction of a rarefaction wave with a shock and a contact surface in one-dimensional unsteady, or two-dimensional steady, flow are solved using a simple rule. Tables enclosed in this paper permit efficient calculation of several problems of non-uniform shock motion.

1. Introduction

The aim of this paper is to give a simple method of analysing various situations involving the motion of non-uniform shock waves. The method is a modified form of the characteristic rule given by Whitham (1958), or the methods given by Chisnell (1957) and the author (1958). The rule developed in this paper enables one to treat many cases of the motion of non-uniform shock waves with different boundary conditions. Whitham's characteristic rule is a special case of this method when a particular kind of boundary condition obtains.

The problems treated represent boundary-value problems for a system of partial differential equations, in which one boundary condition is given on one line, and on another unknown line (the shock locus) a second boundary condition is defined by compatibility equations. The rule of this paper enables the behaviour of the shock wave to be calculated without solving the system of partial differential equations governing the flow.

Some of the problems discussed below have been solved by the use of methods differing from the present one. Some very practicable step-by-step methods for difference equations are discussed by Courant & Friedrichs (1948). The problem of the propagation of shock waves through a duct of variable cross-section was solved by Chisnell (1957), for the case when the gas in front of the shock is at rest. Another method of solving this problem was given by the author (1958). In the present paper, shock-wave propagation through ducts of variable cross-section, when a given non-uniform steady flow exists ahead of the shock wave, is discussed.

The interaction of a simple wave and a shock wave was solved in a closed form by Friedrichs (1948) for the case of weak shocks where the entropy changes may be neglected. The influence, of a slow perturbation of the otherwise uniform piston motion on a shock wave, was discussed by Gundersen (1958). The present

method gives good results for arbitrary shock strength and arbitrary piston motion.

A similar procedure applied to the case of plane hypersonic flow around a profile gives better results than the shock expansion method.*

2. General relations for unsteady non-isentropic flow in ducts

The system of equations governing unsteady non-isentropic flow behind a shock wave in a duct can be written in the characteristic form

$$\frac{\partial r}{\partial \alpha} \equiv \frac{\partial r}{\partial t} + (V+a)\frac{\partial r}{\partial x} = \frac{a}{2c_p(k-1)}\frac{\partial S}{\partial \alpha} - \frac{a}{2}\frac{D\ln A}{Dt} + F(a, V, x, t), \tag{2.1}$$

$$\frac{\partial s}{\partial \beta} \equiv \frac{\partial s}{\partial t} + (V-a)\frac{\partial s}{\partial x} = \frac{a}{2c_p(k-1)}\frac{\partial S}{\partial \beta} - \frac{a}{2}\frac{D\ln A}{Dt} + G(a, V, x, t), \tag{2.2}$$

where

$$r = \frac{a}{k-1} + \frac{V}{2}, \quad s = \frac{a}{k-1} - \frac{V}{2},$$

a denotes the velocity of sound, V the velocity of flow, α and β the curvilinear characteristic co-ordinates, S the specific entropy, and A the cross-section area

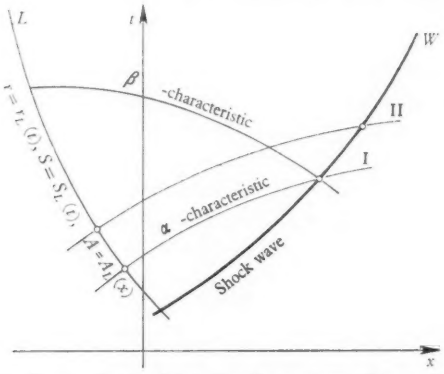

FIGURE 1. The boundary-value problem for the system of equations (2.1) and (2.2).

measured along plane, cylindrical or spherical surfaces for the cases of approximately cylindrical, wedge-shaped or conical ducts, respectively.

$$\frac{D}{Dt} = \frac{\partial}{\partial t} + V\frac{\partial}{\partial x}$$

is the substantial derivative, and F and G are coefficients which express the entropy change of an element of the gas and the cross-outflow influence on the mass and momentum equations.† The boundary-value problem for the above system of differential equations can be set as follows. In the (x, t)-plane, suppose the line L, not a characteristic, is given (see figure 1) and that on this line values

* In an as yet unpublished paper the author has applied similar methods to the calculation of the shock-wave shape and pressure distribution for hypersonic flow around bodies of revolution.

† See §5.

$r = r_L(t)$, $S = S_L(t)$ and $A = A_L(x)$ are known. On the right of a second unknown line (the shock wave) the state of the gas is prescribed by $V_1 = V_1(x)$, $a_1 = a_1(x)$ and $S_1 = S_1(x)$. Along this line compatibility conditions must be fulfilled. These conditions connect the parameters ahead of the shock wave (suffix 1) with parameters on the back of the shock wave (suffix W), and can be written in the form

$$\bar{V}_W = \frac{2}{k+1}\left(\overline{W}_1 - \frac{1}{\overline{W}_1}\right) + \bar{V}_1, \tag{2.3}$$

$$\bar{a}_W = \frac{1}{k+1}\sqrt{\left[2(k-1)\left(k\overline{W}_1^2 - \frac{1}{\overline{W}_1^2}\right) + 6k - k^2 - 1\right]}, \tag{2.4}$$

$$r_W \equiv f(\overline{W}_1, \bar{V}_1, a_1) = \left(\frac{\bar{a}_W}{k-1} + \frac{\bar{V}_W}{2}\right) a_1, \tag{2.5}$$

$$S_W \equiv \phi(\overline{W}_1, S_1) = c_V \ln\left\{\left[\frac{2k}{k+1}\overline{W}_1^2 - \frac{k-1}{k+1}\right]\left[\frac{(k-1)\overline{W}_1^2 + 2}{(k+1)\overline{W}_1^2}\right]^k\right\} - S_1, \tag{2.6}$$

where
$$\overline{W}_1 = \frac{U - V_1}{a_1}, \quad \bar{V}_W = \frac{V_W}{a_1}, \quad \text{etc.}, \tag{2.7}$$

and U is the velocity of propagation of the shock wave.

We suppose that $A = A(x)$. Then equation (2.1) can be written in the form

$$\frac{\partial r}{\partial \alpha} - \frac{a}{2c_p(k-1)}\frac{\partial S}{\partial \alpha} + \frac{aV}{2(V+a)}\frac{\partial \ln A}{\partial \alpha} = F(a, V, \alpha, \beta). \tag{2.8}$$

Integrating equation (2.8) along α-characteristics (see figure 1) and expressing the values on the shock wave by equations (2.5) and (2.6), we obtain*

$$f(\overline{W}_1, V_1, a_1) - r_L - \int_{S_L}^{\phi(\overline{W}_1, S_1)} \frac{a}{2(k-1)c_p}\, dS + \int_{\ln A_L}^{\ln A_W} \frac{aV}{2(V+a)}\, d\ln A = \int_{\alpha_L}^{\alpha_W} F(a, V, x, t)\, d\alpha,$$

where the suffix L refers to values of the parameters on the L-line. We now apply this expression to two neighbouring characteristics I and II (see figure 1). On subtracting these expressions, we obtain in the limit as characteristic I approaches characteristic II,†

$$f'_{\overline{W}_1}(\overline{W}_1, V_1, a_1)\, d\overline{W}_1 + f'_{V_1}(\overline{W}_1, V_1, a_1)\, dV_1 + f'_{a_1}(\overline{W}_1, V_1, a_1)\, da_1 - dr_L - \left[\frac{a}{2(k-1)c_p}\right]_W \times [dS_1 + \phi'_{\overline{W}_1}(\overline{W}_1, S_1)\, d\overline{W}_1] + \left[\frac{a}{2(k-1)c_p}\right]_L dS_L - \left[\frac{1}{2(k-1)c_p}\, da\right]_m [\phi(\overline{W}_1, S_1) - S_L] + \left[\frac{aV}{2(V+a)}\right]_W d\ln A_W - \left[\frac{aV}{2(V+a)}\right]_L d\ln A_L + \frac{1}{2}\left[d\left(\frac{aV}{V+a}\right)\right]_m \ln\frac{A_W}{A_L} = F_W\, d\alpha_W - F_L\, d\alpha_L + [dF]_m(\alpha_W - \alpha_L),$$

where the suffix m refers to the mean value in the interval considered.

* $\int_{\alpha_L}^{\alpha_W} \frac{\partial r}{\partial \beta}\, d\beta = 0$, etc., because $d\beta = 0$ along α-characteristics.

† From equation (2.6) we have $\phi'_{S_1}(\overline{W}_1, S_1) = 1$.

For the case when the variations of the flow behind the shock wave are small (the linearized case), all values can be written as $A = A_L + \epsilon_A$, $a = a_L + \epsilon_a$, etc., where $\epsilon_A \ll A_L$, $\epsilon_a \ll a_L$, etc. We can then omit in the above equation as small quantities of the second order all the terms in which the suffix m appears. Then we obtain

$$f'_{\overline{W}_1}(\overline{W}_1, V_1, a_1)\,d\overline{W}_1 + f'_{V_1}(\overline{W}_1, V_1, a_1)\,dV_1 + f'_{a_1}(\overline{W}_1, V_1, a_1)\,da_1 - \left[\frac{a}{2(k-1)c_p}\right]_W [dS_1 + \phi'_{W_1}(\overline{W}_1, S_1)\,d\overline{W}_1] + \left[\frac{aV}{2(V+a)}\right]_W d\ln A_W - F_W\,d\alpha_W = dr_L - \left[\frac{a}{2(k-1)c_p}\right]_L dS_L + \left[\frac{aV}{2(V+a)}\right]_L d\ln A_L - F_L\,d\alpha_L. \tag{2.9}$$

For the general case we may use the formula (2.9) as an approximation.

The same procedure can be carried out with the formula analogous to (2.8) for the β-characteristics. In this manner we could obtain in addition the value of $s_L = a_L/(k-1) - \frac{1}{2}V_L$ along the L-line. The main difficulty is to find the points of intersection of corresponding characteristics with the W-line and the L-line. For this purpose an additional assumption is necessary (see § 6 B below). Often, instead of $r_L(t)$, the value of $V_L(t)$ (for example, the piston velocity) is given along the L-curve. In this case, the value of $r_L(t)$ depends on $s_L(t)$, which can be found only if the distribution of $r_L(t)$ is known. The situation is now more complicated. This kind of boundary condition occurs in the problem of variable piston motion behind the shock wave, when the reflected wave reaches the piston. This problem was solved by Gundersen (1958), but only in the linearized approximation for small variations of the piston velocity when all the flow field can be found in closed form.*

In the special case of boundary conditions such that $r_L = \text{const.}$, $S_L = \text{const.}$, $A_L = A_0 = \text{const.}$, we obtain from (2.9) Whitham's characteristic rule. In the case of $F = 0$ and constant state ahead of the shock wave, this rule can be written in the form

$$f'_U\,dU - \frac{a_W}{2c_p(k-1)}\,\phi'_U\,dU + \left[\frac{aV}{2(V+a)}\right]_W d\ln\frac{A_W}{A_0} = 0.$$

Whitham obtained this rule in a different way: he made use of the equation (2.1), in which he replaced derivatives in the characteristic direction by derivatives in the shock-wave direction $\{\partial/\partial\gamma = \partial/\partial t + U(\partial/\partial x)\}$. He remarks that the slope of the α-characteristics is close to that of the shock-wave line (in the linearized approximation, they are the same).

The same result can be obtained (see Chisnell 1957 and Rościszewski 1958) by solving first the linearized case for small shock-wave velocity variations, and then, for the case of arbitrarily variable shock-wave velocity, changing the parameter in the linearized solution. The quasi-linearized solution obtained in

* In the general case it is necessary to make use of the expression analogous to (2.9) for β-characteristics. Unknown β-characteristics could be replaced by characteristics taken from the simple wave solution. In the analogous case discussed in the author's unpublished work dealing with hypersonic flow around bodies of revolution, a similar method shows good accuracy.

this way is, in fact, the result of applying a series of local linearized solutions to the case where finite changes in shock-wave velocity takes place.

The formula (2.9) will be applied below to many different cases of non-uniform shock-wave motion. The results will be compared diagrammatically with finite difference calculations obtained from the method of characteristics; these comparisons display the surprisingly good accuracy of the present method.

A similar boundary-value problem will later be formulated for plane steady supersonic flow (see § 8).

3. Shock-wave propagation in a duct of non-uniform cross-section

We shall now apply the rule to the case of shock-wave motion in a tube in which the cross-section is initially constant and then varies, and for which there is a given constant state ahead of the shock wave (see figure 2). In particular, shock-wave propagation in ducts of variable cross-section, when the gas ahead of the shock wave is in steady motion or at rest with a variable temperature field, can be considered.

We suppose that $A = A(x)$ and neglect the heat exchange and surface friction ($F = 0$). In the case considered, along the t-axis we have $r = \text{const.}$ and $A = A_0$ (see figure 2). Taking the t-axis as an L-line, we have $dr_L = 0, dA_L = 0, dS_L = 0$. Now taking a_1, V_1, S_1 as variable, and dividing equation (2.9) by dx, we obtain, using equation (2.7),

$$\frac{dU}{dx} = \left(1 - \frac{1}{2N}\right)\frac{dV_1}{dx} - \left(\overline{V}_1 - \overline{U} + \frac{\bar{r}_W - \frac{1}{2}\overline{V}_1}{N}\right)\frac{da_1}{dx} + \frac{a_W}{2(k-1)c_p N}\frac{dS_1}{dx} - \frac{V_W a_W}{2N(V_W + a_W)}\frac{d\ln(A/A_0)}{dx}, \tag{3.1}$$

where

$$N = R - \frac{\bar{a}_W E}{2(k-1)}, \tag{3.2}$$

$$R = f'_{\overline{W}_1}(\overline{W}_1, V_1, a_1) = \frac{1}{k+1}\left[\frac{2k\overline{W}_1 + (2/\overline{W}_1^3)}{(k+1)\bar{a}_W} + 1 + \frac{1}{\overline{W}_1^2}\right], \tag{3.3}$$

$$E = \varphi'_{\overline{W}_1}(\overline{W}_1, S_1)\frac{1}{c_p} = \frac{4\overline{W}_1}{2k\overline{W}_1^2 - k + 1} - \frac{4}{\overline{W}_1[(k-1)\,\overline{W}_1^2 + 2]}. \tag{3.4}$$

For the given state ahead of the shock wave, dV_1/dx, da_1/dx, and dS_1/dx are known functions of x, and the equation (3.1) is a first-order differential equation for $U = U(x)$. In general this equation can be quite easily solved numerically; then we obtain the unknown shock wave without having to solve the partial differential equations. In the special case of an approximately cylindrical duct and small variations of the values of the flow parameters ahead of the shock wave, all the coefficients of equation (3.1) can be taken, according to the linearized approximation, as constant. Therefore, a closed-form solution can be obtained for the shock-wave velocity change and the entire field on the back of the shock wave. The discussion of this solution was given in the author's previous work (Rościszewski 1958).

In the more general case when the time-dependent field ahead of the shock wave is given $[V_1 = V_1(x,t), a_1 = a_1(x,t), S_1 = S_1(x,t)]$ and, as before, $dr_L = 0$, $dA_L = 0$, $dS_L = 0$, in place of d/dx on the right-hand side of equation (3.1) we must put $\partial/\partial x + (1/U)(\partial/\partial t)$. We then obtain the equation for the shock-wave velocity in the form

$$\frac{dU}{dx} = F(U,x,t) \equiv F\left(U, x, \int_0^x \frac{dx}{U}\right).$$

This equation can also easily be solved numerically.

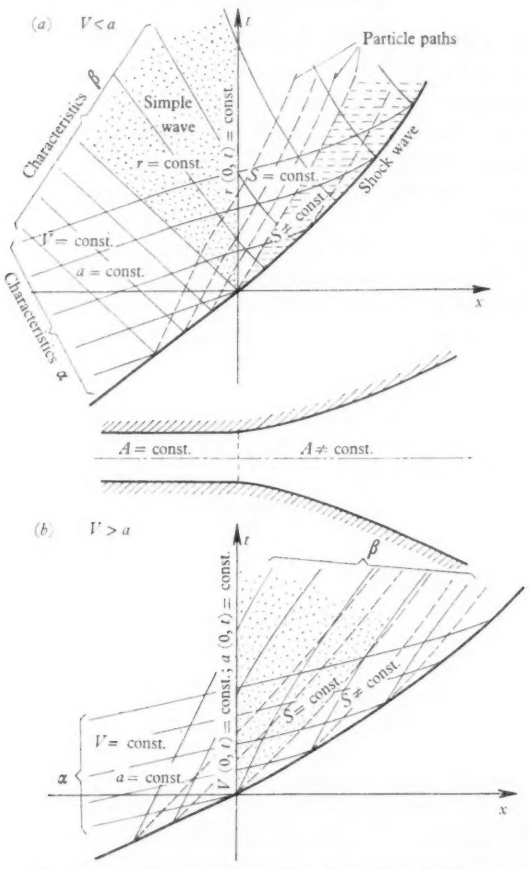

FIGURE 2. Propagation of a shock wave through a duct of variable cross-section, (*a*) subsonic flow behind the shock wave, (*b*) supersonic flow behind the shock wave.

The solution of the problem when time-dependent boundary conditions on curve L are given $[r_L = r_L(t), A_L = A_L(t)]$ is also possible, and it is not very complicated when the curve L lies outside the domain of dependence bounded by the β-characteristic and the shock wave, i.e. when the condition on the L-curve does not depend on the shock-wave motion.

In the special case when $a_1 = a_0 = \text{const.}$, $V_1 = 0$, $S_1 = \text{const.}$, using equations (2.3)–(2.6) we obtain from equation (3.1),

$$\ln \frac{A}{A_0} = -\int_{\bar{U}_*}^{U} \left\{ \frac{2(k+1)}{\sqrt{\{2(k-1)[k\bar{U}^2 - (1/\bar{U}^2)] + 6k - k^2 - 1\}}} + \frac{k+1}{\bar{U} - (1/\bar{U})} \right\} \times \left\{ R - \frac{\bar{a}_W E}{2(k-1)} \right\} d\bar{U}, \quad (3.5)$$

where R and E are functions of $\bar{U}$ given by equations (3.3) and (3.4).

$\bar{U}$	$-\int_2^{\bar{U}} \{\}\, d\bar{U}$	$\bar{U}$	$-\int_2^{\bar{U}} \{\}\, d\bar{U}$	$\bar{U}$	$-\int_2^{\bar{U}} \{\}\, d\bar{U}$
1·2	−4·514	3·5	3·186	5·8	5·817
1·3	−3·563	3·6	3·338	5·9	5·854
1·4	−2·612	3·7	3·481	6·0	5·991
1·5	−1·999	3·8	3·623	6·1	6·076
1·6	−1·490	3·9	3·757	6·2	6·160
1·7	−1·053	4·0	3·891	6·3	6·242
1·8	−0·668	4·1	4·017	6·4	6·323
1·9	−0·322	4·2	4·144	6·5	6·402
2·0	0·000	4·3	4·265	6·6	6·482
2·1	0·294	4·4	4·385	6·7	6·559
2·2	0·587	4·5	4·501	6·8	6·635
2·3	0·845	4·6	4·616	6·9	6·710
2·4	1·102	4·7	4·727	7·0	6·785
2·5	1·330	4·8	4·838	7·1	6·858
2·6	1·559	4·9	4·944	7·2	6·930
2·7	1·767	5·0	5·050	7·3	7·001
2·8	1·974	5·1	5·152	7·4	7·071
2·9	2·160	5·2	5·254	7·5	7·140
3·0	2·356	5·3	5·352	7·6	7·208
3·1	2·537	5·4	5·449	7·7	7·275
3·2	2·707	5·5	5·543	7·8	7·341
3·3	2·870	5·6	5·636	7·9	7·407
3·4	3·033	5·7	5·727	8·0	7·472

TABLE 1

In the limiting case when $\bar{U} \to \infty$ we obtain the asymptotic formula

$$\ln \frac{A}{A_0} = \left(\sqrt{\frac{2k}{k-1}} + 1 + \frac{2}{k} \right) \ln \frac{\bar{U}}{\bar{U}_0}. \quad (3.6)$$

In fact, equation (3.5) is the Chisnell answer presented in another form. Some numerical differences between Chisnell's tables and present formula are, however, found (see the converging cylindrical wave calculation). Values of the integral in (3.5) are given in table 1 for $k = 1{\cdot}4$.

Equation (3.4) enables us to examine the influence of entropy changes on shock-wave motion. The coefficient depends on

$$\frac{1}{c_p} \frac{d(S_W - S_1)}{dW_1} = E,$$

where E given by equation (3.4) expresses the entropy change influence. When $\overline{W}_1 = 1$ (very weak shock wave) and $\overline{W}_1 = \infty$ (very strong shock wave) E vanishes. This means that entropy changes for hypersonic shock motion can be neglected. Table 2 gives values of E as a function of W_1 for $k = 1{\cdot}4$.

The results of calculations by the use of Table 1 are compared with step-by-step calculations* applied to the basic differential equations for various duct shapes and various initial shock strengths (figures 3–10). In special cases these

W	0	1·5	2	3	4	5	6	8	10	15	20	∞
E	0	0·097	0·185	0·246	0·241	0·221	0·198	0·161	0·123	0·092	0·0714	0

TABLE 2

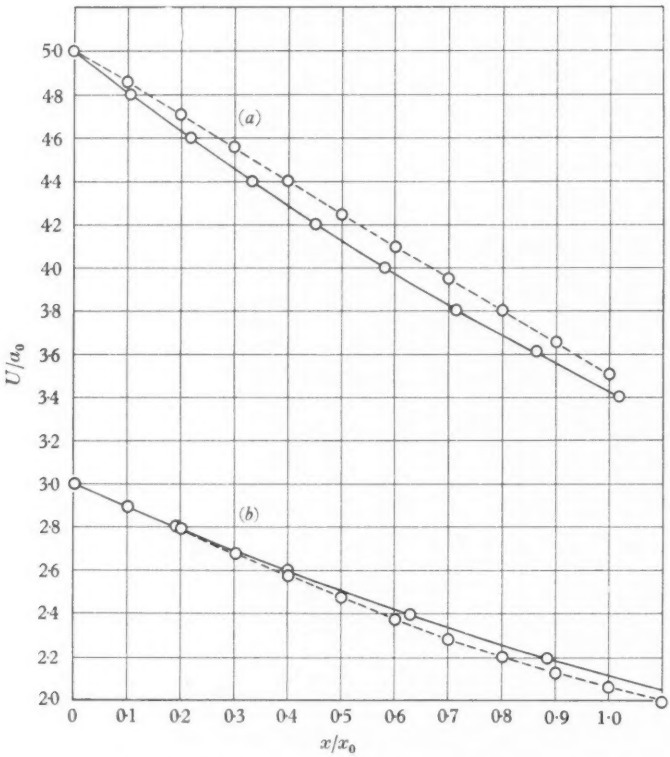

FIGURE 3. Comparison of the present method with step-by-step calculations by the method of characteristics for the case of shock-wave propagation through a duct of varying cross-section area given by $A/A_0 = e^{2(x/x_0)}$ (divergent duct) and initial shock strengths (*a*) $U_0/a_0 = 5$ and (*b*) $U_0/a_0 = 3$. The shock is assumed plane. – – – –, Step-by-step calculation; ——, present method.

* This calculation was based on the method of characteristics. The accuracy was checked by taking some mean characteristics which give the errors lying within the limits of accuracy of the wave diagram calculations.

results are compared (figure 9) with Payne's (1957) calculations for a cylindrical convergent wave. In this case, because of other boundary conditions (in Payne's work $V(1, t) \neq$ const.) Payne's results differ from those given by the present method and from those given by finite difference calculations by the method of

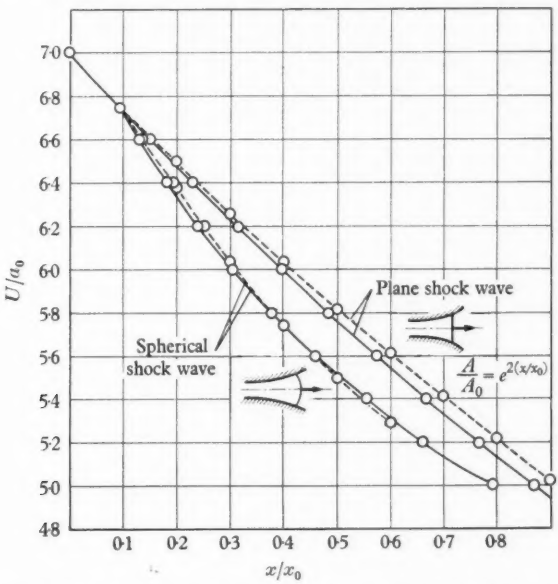

FIGURE 4. Comparison of the present method with calculations by the method of characteristics for the case of shock-wave propagation through a duct varying cross-section area given by $A/A_0 = e^{2(x/x_0)}$ (divergent duct) and initial shock strength $U_0/a_0 = 7$. The comparison is made for both a plane and spherical shock wave, originating at $x = 0$, for $x/x_0 > 0{\cdot}1$. ----, Step-by-step calculations; ——, present method.

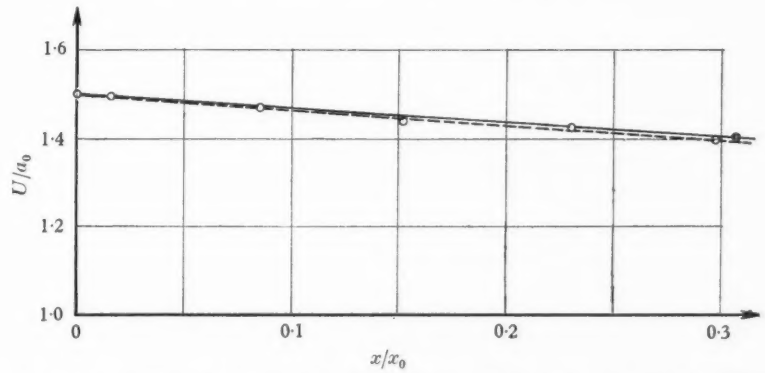

FIGURE 5. Comparison of the present method with calculations by the method of characteristics for the case of shock-wave propagation through a duct with $A/A_0 = e^{(x/x_0)}$ (divergent duct) and initial shock strength $U_0/a_0 = 1{\cdot}5$. ----, Step-by-step calculations; ——, present theory.

characteristics. The results are not strictly insensitive to the initial conditions, see Whitham (1958). Chisnell's tables show some disagreement with the present tables, and they give results very close to Payne's calculations for different

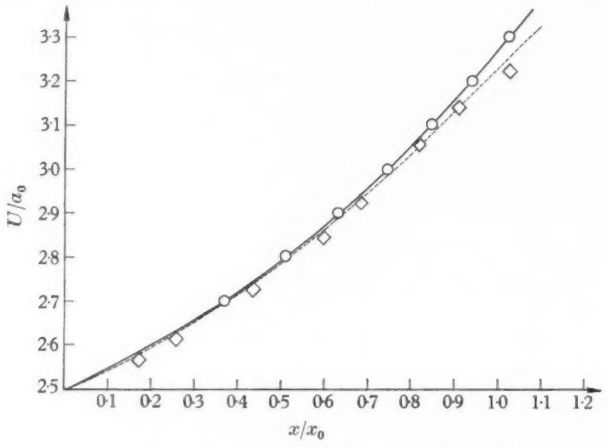

FIGURE 6. Comparison of the present method with calculations by the method of characteristics for the case of shock wave propagation through a duct with $\frac{A}{A_0} = \exp\left[-\left(\frac{x}{x_0} + \frac{x^2}{2x_0^2}\right)\right]$ (convergent duct) and initial shock strength $U_0/a_0 = 2{\cdot}5$. ----, Step-by-step calculations; ——, present method.

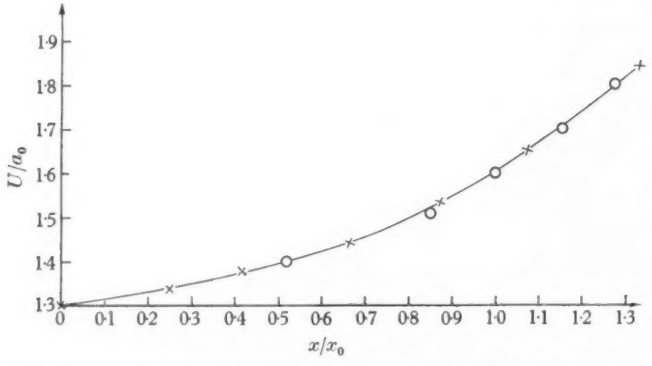

FIGURE 7. Comparison of the present method with calculations by the method of characteristics for the case of shock-wave propagation through a duct with $\frac{A}{A_0} = \exp\left[-\left(\frac{x}{x_0} + \frac{x^2}{2x_0^2}\right)\right]$ (convergent duct) and initial shock strength $U_0/a_0 = 1{\cdot}3$. ○, Step-by-step calculations; ×, present theory.

boundary conditions. For other cases calculated in this paper, Chisnell's tables also show some deviations. Results of the comparison of the present method with experimental results and calculations by Hertzberg & Kantrowitz (1950) are given in figure 10.

4. Propagation of strong detonation wave through ducts of non-uniform cross-section

Here we shall be concerned with the propagation of a strong detonation wave, i.e. the detonation wave described by the points on the Hugoniot curve lying above the Chapman–Jouguet point (see Courant & Friedrichs 1948). Such a detonation wave can be obtained by additional compression behind the detonation wave, for example, by piston motion or by the propagation of the Chapman–

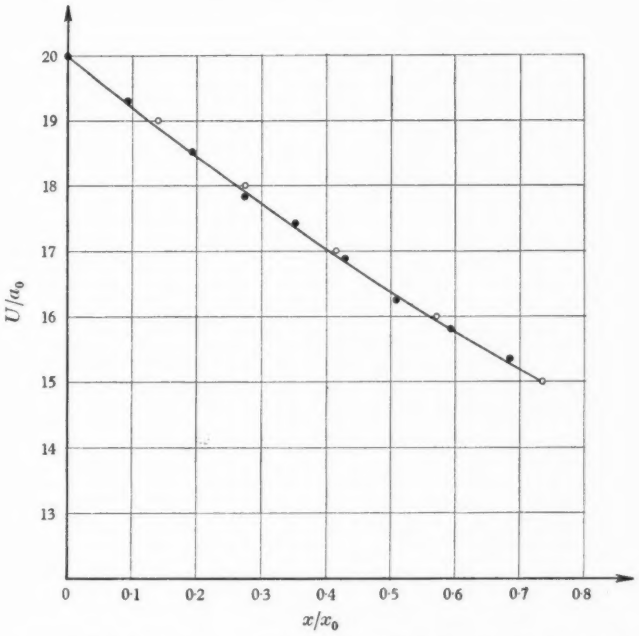

FIGURE 8. Comparison of the present method with calculations by the method of characteristics for the case of a very strong shock wave ($U_0/a_0 = 20$) propagating through a duct of variable cross-section $A/A_0 = e^{2(x/x_0)}$. The gas is treated as ideal with $k = 1{\cdot}4$. ●, Step-by-step calculations; ○, present method.

Jouguet detonation wave through a duct of suddenly convergent cross-section. We assume the strong detonation wave to be propagated through a duct of initially constant cross-section, which at some point changes into a duct with variable cross-section. The gas ahead of the detonation wave is assumed to be at rest with a constant velocity of sound.

In a divergent duct the velocity of a detonation wave can be decreased only to that corresponding to the Chapman–Jouguet wave. The only difference between the solution of the previous case and the present one is in the different compatibility equations for shock and detonation waves.

We assume different values of $k = c_p/c_v$ in front (suffix 1) and at the back (suffix W) of the detonation wave.

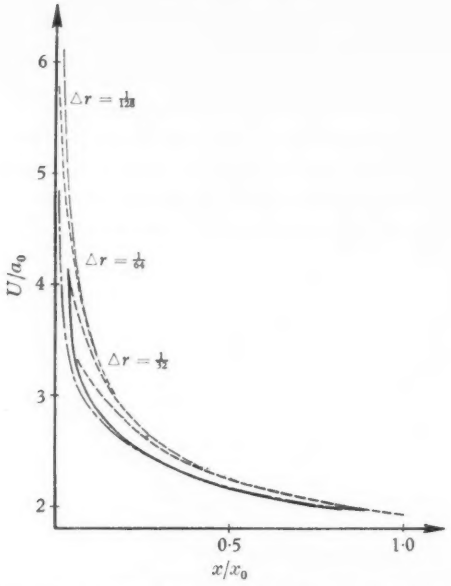

FIGURE 9. Comparison of the present method with calculations by the method of characteristics (assuming $V(1, t) = \text{const.}$) and Payne's calculations with different boundary conditions ($V(1, t) \neq \text{const.}$). ——·——, Step-by-step calculations with boundary condition $V(1, t) = \text{const.}$; – – – –, finite difference calculations by Payne $V(1, t) \neq \text{const.}$; ——, present method; ——, Chisnell (published in Payne's work).

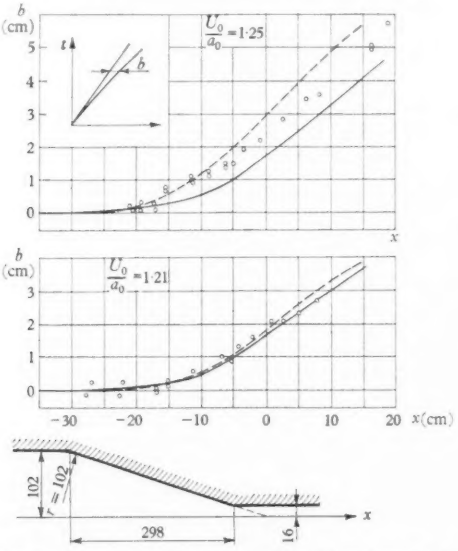

FIGURE 10. Comparison of the present method with Hertzberg & Kantrowitz's experimental curve and their calculations by the method of characteristics. ○, Experimental points (Hertzberg–Kantrowitz); – – – –, finite difference calculations (Hertzberg–Kantrowitz); ——, present method.

The equations of conservation of mass, momentum and energy (see Courant & Friedrichs 1948) give

$$\overline{V} = \frac{1}{k_2+1}\left(\overline{U} - \frac{k_2}{k_1}\frac{1}{\overline{U}}\right) + \sqrt{\left\{\left(\overline{U} - \frac{k_2}{k_1}\frac{1}{\overline{U}}\right)\frac{1}{(k_2+1)^2} + \frac{2(k_2-1)Q}{(k_2+1)a_0^2} + \frac{2(k_1-k_2)}{k_1(k_1-1)(k_2+1)}\right\}}, \tag{4.1}$$

where $\overline{U} = U/a_0$ and $V = V_W/a_0$; Q is the heat released by the combustion process. Also,

$$\bar{a} = \sqrt{\left\{k_2(\overline{U}-\overline{V})\left(\overline{V} + \frac{1}{k_1\overline{U}}\right)\right\}}, \tag{4.2}$$

$$\frac{\Delta S}{c_p} = \frac{1}{k_2}\ln\bar{a} - \frac{k_2-1}{k_2}\ln\frac{\overline{U}}{\overline{U}-\overline{V}}, \tag{4.3}$$

where $\bar{a} = a_W/a_0$.

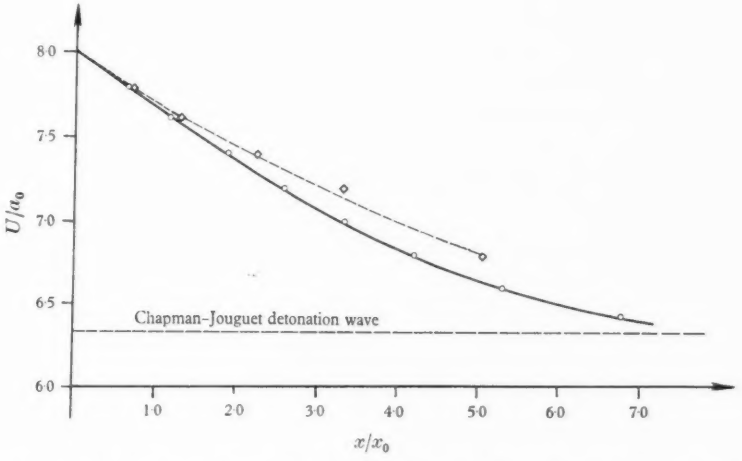

FIGURE 11. Comparison of the present method with calculations by the method of characteristics for the case of propagation of a strong detonation wave in a duct of cross-section given by $A/A_0 = e^{2(x/x_0)}$, with $k_1 = 1{\cdot}4$, $k_1 = 1{\cdot}3$ and $Q/a_0^2 = 28{\cdot}3$. ○, Present method; ◇, step-by-step calculations.

From equation (2.9) ($dV_1 = da_1 = dS_1 = 0$) we obtain

$$\ln\frac{A}{A_0} = \int_{\overline{U}_0}^{\overline{U}} \frac{2(\overline{V}+\bar{a})}{\overline{V}\bar{a}}\left\{\frac{1}{2}\frac{d\overline{V}}{d\overline{U}} + \frac{1}{k_2-1}\left(\frac{\partial\bar{a}}{\partial\overline{U}} + \frac{\partial\bar{a}}{\partial\overline{V}}\frac{d\overline{V}}{d\overline{U}}\right)\right.$$
$$\left. - \frac{\bar{a}}{2(k_2-1)c_p}\left[\frac{\partial S}{\partial\overline{U}} + \frac{\partial S}{\partial\overline{V}}\frac{d\overline{V}}{d\overline{U}} + \frac{\partial S}{\partial\bar{a}}\left(\frac{\partial\bar{a}}{\partial\overline{U}} + \frac{\partial\bar{a}}{\partial\overline{V}}\frac{d\overline{V}}{d\overline{U}}\right)\right]\right\} d\overline{U}, \tag{4.4}$$

where the derivatives in equation (4.4) can be calculated by the use of equations (4.1), (4.2) and (4.3).

Comparison of the calculations by the use of the present method and step-by-step calculations are given in figure 11 for $k_1 = 1{\cdot}4$, $k_2 = 1{\cdot}3$ and $Q/a_0^2 = 28{\cdot}9$.

5. Shock-wave propagation through a duct with porous walls

In this section we consider the shock-wave attenuation due to the cross-outflow through porous walls of the duct. We take a cylindrical duct and we assume the cross mass flow $\pi d_0 l \rho \bar{v}$ to be small in comparison with $\rho V A$, where v is the cross-flow velocity, η is the ratio of the area of the pores to the area of the wall, and $\bar{v} = v\eta$.

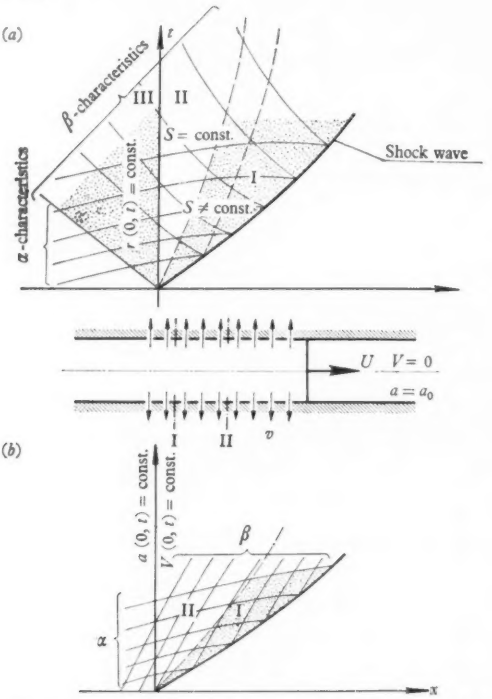

FIGURE 12. Flow induced by shock-wave propagation through a duct with porous walls ($\eta \ll 1$). (*a*) The case $V^0 < a^0$; (*b*) the case $V^0 > a^0$.

We apply the basic mechanical equations to the ideal flow through the duct with the porous wall (figure 12). We assume all parameters to be constant in the given cross-section. The continuity equation is

$$\rho_{\mathrm{I}} V_{\mathrm{I}} A_0 - \rho_{\mathrm{II}} V_{\mathrm{II}} A_0 - \pi d_0 \int_{x_{\mathrm{I}}}^{x_{\mathrm{II}}} \rho \bar{v}\, dx = \frac{\partial}{\partial t} \int_{x_{\mathrm{I}}}^{x_{\mathrm{II}}} \rho A_0\, dx,$$

or for $x_{\mathrm{I}} \to x_{\mathrm{II}}$

$$\frac{D\rho}{Dt} + \rho \frac{\partial V}{\partial x} = -\frac{4\rho\bar{v}}{d_0}. \tag{5.1}$$

For the momentum equation, we assume that the cross-stream has no momentum in the direction of the axis of the tube. Then we have

$$(p_{\mathrm{I}} - p_{\mathrm{II}}) A_0 + \rho_{\mathrm{I}} V_{\mathrm{I}}^2 A_0 - \rho_{\mathrm{II}} V_{\mathrm{II}}^2 A_0 = \frac{\partial}{\partial t} \int_{x_{\mathrm{I}}}^{x_{\mathrm{II}}} \rho V A_0\, dx,$$

or, using equation (5.1) for $x_{\mathrm{I}} \to x_{\mathrm{II}}$, we obtain

$$\frac{DV}{Dt}+\frac{1}{\rho}\frac{\partial p}{\partial x}=\frac{4V\bar{v}}{d_0}. \tag{5.2}$$

The energy equation is

$$\rho_1 V_{\mathrm{II}}\left(\frac{V_{\mathrm{I}}^2}{2}+\frac{k}{k-1}\frac{p_{\mathrm{I}}}{\rho_{\mathrm{I}}}\right)A_0-\rho_{\mathrm{II}}V_{\mathrm{II}}\left(\frac{V_{\mathrm{II}}^2}{2}+\frac{k}{k-1}\frac{p_{\mathrm{II}}}{\rho_{\mathrm{II}}}\right)A_0-\pi d_0\int_{x_{\mathrm{I}}}^{x_{\mathrm{II}}}\rho\bar{v}\left(\frac{v^2}{2}+\frac{k}{k-1}\frac{p}{\rho}\right)dx$$

$$=\frac{\partial}{\partial t}\left[A_0\int_{x_{\mathrm{I}}}^{x_{\mathrm{II}}}\rho\left(\frac{V^2}{2}+\frac{1}{k-1}\frac{p}{\rho}\right)dx\right],$$

or, using equations (5.1) and (5.2) for $x_{\mathrm{II}} \to x_{\mathrm{I}}$, we get

$$\frac{1}{c_p}\frac{DS}{Dt}=-\frac{2\bar{v}}{d}\left[(k-1)M^2+\frac{k-1}{a^2}\bar{v}^2\right]. \tag{5.3}$$

We shall calculate the velocity of the cross-flow by assuming quasi-steady flow. This is based on the fact that due to a sudden change in the cross-section the local derivatives (in the equation of motion), are small in comparison with the convective terms. Then we apply the Bernoulli equation and assume the cross-flow to be isentropic

$$v=\zeta\sqrt{\left\{\frac{2k}{k-1}\frac{p}{\rho}\left[1-\left(\frac{p_a}{p}\right)^{(k-1)/k}\right]\right\}}=\zeta\sqrt{\left\{\frac{2a^2}{k-1}\left[1-\left(\frac{p_a}{p}\right)^{(k-1)/k}\right]\right\}}, \tag{5.4}$$

where $p_a = \text{const.}$ is the outside pressure, $p = p(x,t)$ is the pressure in the duct, and ζ is the loss coefficient.

The pressure in this formula can be calculated from

$$\frac{p}{p_2^0}=\left(\frac{a}{a_2^0}\right)^{2k/(k-1)}\exp\left(\frac{S_2^0-S}{c_p-c_v}\right). \tag{5.5}$$

Taking into account the three equations of motion (5.1), (5.2), (5.3) and equation (5.4) we find the coefficients in equations (2.1) and (2.2) which express the entropy change and the cross-mass flow influence

$$F=-\frac{2a^2\eta\zeta}{d_0}\sqrt{\left\{\frac{2}{k-1}\left[1-\left(\frac{p_a}{p}\right)^{(k-1)/k}\right]\right\}}\left\{1-M+\frac{k-1}{2}M^2+\zeta^2\left[1-\left(\frac{p_a}{p}\right)^{(k-1)/k}\right]\right\}, \tag{5.6}$$

$$G=-\frac{2a^2\eta\zeta}{d_0}\sqrt{\left\{\frac{2}{k-1}\left[1-\left(\frac{p_a}{p}\right)^{(k-1)/k}\right]\right\}}\left\{1+M+\frac{k-1}{2}M^2+\zeta^2\left[1-\left(\frac{p_a}{p}\right)^{(k-1)/k}\right]\right\}, \tag{5.7}$$

where $M = V/a$.

We obtain from (2.9), where we substitute $d\alpha_L = 0$ (the t-axis is taken as the L-curve) and

$$d\alpha_W-d\alpha_L=\frac{dx}{V_W+a_W},$$

$$\int_{\bar{U}_*}^{\bar{U}}\frac{d\bar{U}}{B(\bar{U})}=\int\eta\,dx, \tag{5.8}$$

where
$$B(\bar{U}) = \frac{F_W}{(V_W + a_W)\left[R - \dfrac{\bar{a}_W E}{2(k-1)}\right]}.$$

E and R are given by (3.3) and (3.4), respectively. The integral of the left-hand side of equation (5.8) is given in table 3 for $k = 1.4$ and $\zeta = 1$.

In figure 13 a comparison of the present method with the numerical method of characteristics is given for $\eta = 0{\cdot}1$ and $\bar{U}_0 = 4$. In this case the numerical method was not very accurate.

$\bar{U}$	$\int_{\bar{U}_0}^{U} \frac{dU}{\overline{B(U)}}$	$\bar{U}$	$\int_{\bar{U}_0}^{\bar{U}} \frac{dU}{\overline{B(U)}}$	$\bar{U}$	$\int_{U_0}^{\bar{U}} \frac{dU}{\overline{B(U)}}$
1·2	−2·775	3·6	0·755	6·0	1·295
1·4	−0·900	3·8	0·814	6·2	1·328
1·6	−0·425	4·0	0·870	6·4	1·360
1·8	−0·172	4·2	0·922	6·6	1·391
2·0	0·000	4·4	0·972	6·8	1·421
2·2	0·144	4·6	1·019	7·0	1·450
2·4	0·264	4·8	1·064	7·2	1·478
2·6	0·367	5·0	1·107	7·4	1·506
2·8	0·460	5·2	1·148	7·6	1·532
3·0	0·544	5·4	1·187	7·8	1·558
3·2	0·621	5·6	1·224	8·0	1·584
3·4	0·691	5·8	1·260		

TABLE 3

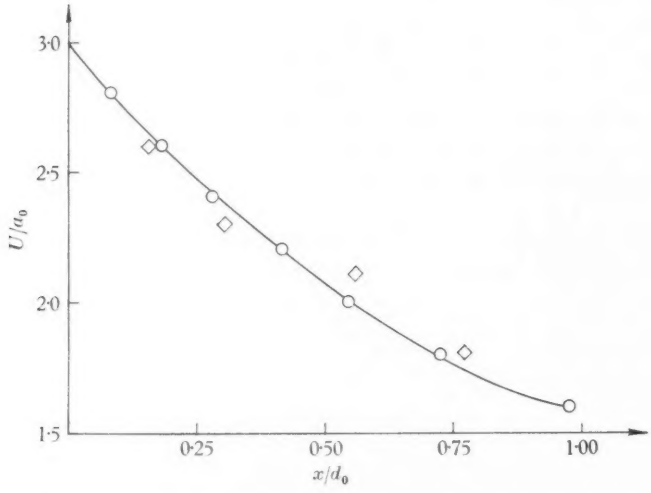

FIGURE 13. Comparison of the present method with the calculation by the method of characteristics for the case of shock-wave propagation through a duct with porous walls. The ratio of pore area to wall area $\eta = 0{\cdot}1$. Initial shock strength $U_0/a_0 = 4$. ◇, Step-by-step calculations; ○, present method.

6. Interaction of a rarefaction wave and a shock wave in one-dimensional unsteady flow

A. *Case of head-on collision*

Until now, these problems for arbitrary waves were solved by the use of finite difference methods. A discussion of these methods is given by Geiringer (1948).* We discuss the case of interaction of a simple wave and a shock wave of arbitrary strength (figure 14) in a duct of constant cross-section.† The flow behind the shock wave is governed by the unsteady non-isentropic flow equations.

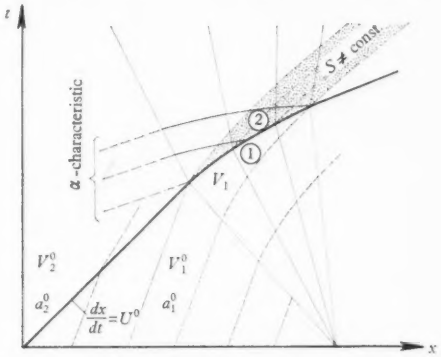

FIGURE 14. Head-on collision of a shock wave and simple rarefaction wave.

Introducing a simple wave relation ahead of the shock wave

$$da_1 = -\tfrac{1}{2}(k-1)\,dV_1, \tag{6.1}$$

and taking into account the fact that α-characteristics cross the uniform flow region behind the shock wave (see figure 13) ($dr_L = 0$), we get from equations (2.9) the first-order linear ordinary differential equation

$$\left[1 - \frac{\chi(\overline{W}_1) + \tfrac{1}{2}(k-1)\,\overline{V}_1}{1 + \tfrac{1}{2}(k-1)\,\overline{V}_1}\right]\frac{d\overline{V}_1}{d\overline{W}_1} = \psi(\overline{W}_1), \tag{6.2}$$

where from equations (2.4)–(2.7)

$$\chi(\overline{W}_1) = \frac{k-1}{k+1}\left(\overline{W}_1 - \frac{1}{\overline{W}_1}\right) + \bar{a}_W, \tag{6.3}$$

$$\psi(\overline{W}_1) = \frac{\bar{a}_W}{k-1}E - \frac{2}{k+1}\left(1 + \frac{1}{\overline{W}_1^2}\right) - \frac{4\left(k\overline{W}_1 + \dfrac{1}{\overline{W}_1^3}\right)}{(k+1)^2\,\bar{a}_W}, \tag{6.4}$$

where $\bar{a}_W$ and E are given by (2.4) and (3.4) as a function of $\overline{W}_1$. Table 4 contains the values of $\chi(\overline{W}_1)$ and $\psi(\overline{W}_1)$ for $k = 1{\cdot}4$.

* The numerical example in this paper is incorrect. The principal equations of motion are not satisfied for the shock wave before interaction.

† This case is a special case of §3 when A = const. and $V_1 = V_1(x, t)$, etc., but we solve this here in a simpler manner.

The results for the special case of $V_1 = 0$ and $\overline{W}_1^0 = 4$ are compared in figure 15 with a step-by-step method of calculation (method of characteristics) applied to the basic non-linear partial differential equations. In this case the accuracy of the present method is excellent. The numerical calculations are very difficult because of the slow convergence of the finite difference method. Five iterations

$\overline{W}_1$	$\chi(\overline{W}_1)$	$\psi(\overline{W}_1)$	$\overline{W}_1$	$\chi(\overline{W}_1)$	$\psi(\overline{W}_1)$
1·0	1·00	3·32	4·6	2·92	1·58
1·2	1·11	2·82	4·8	3·10	1·58
1·4	1·21	2·50	5·0	3·22	1·57
1·6	1·32	2·28	5·2	3·33	1·56
1·8	1·43	2·12	5·4	3·44	1·55
2·0	1·54	2·00	5·6	3·56	1·54
2·2	1·65	1·90	5·8	3·68	1·54
2·4	1·76	1·84	6·0	3·80	1·53
2·6	1·86	1·77	6·2	3·92	1·53
2·8	1·98	1·72	6·4	4·03	1·52
3·0	2·08	1·69	6·6	4·15	1·52
3·2	2·19	1·66	6·8	4·27	1·51
3·4	2·30	1·64	7·0	4·38	1·51
3·6	2·41	1·63	7·2	4·51	1·50
3·8	2·52	1·62	7·4	4·63	1·50
4·0	2·64	1·61	7·6	4·74	1·49
4·2	2·76	1·60	7·8	4·86	1·49
4·4	2·88	1·59	8·0	4·98	1·48

TABLE 4

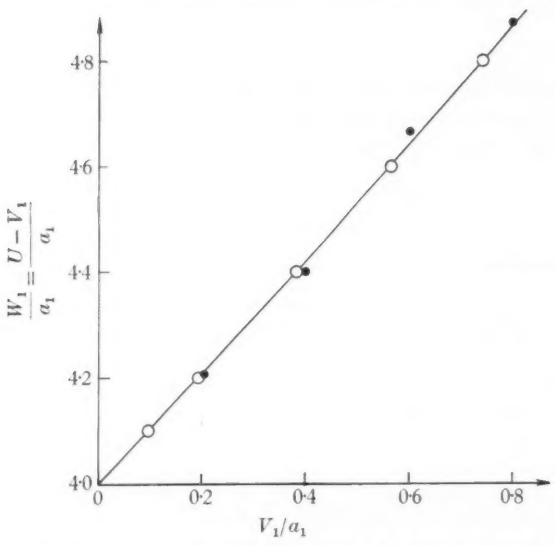

FIGURE 15. Comparison of the computation by use of the present method with the computation by the method of characteristics for the case of head-on collision of a shock wave of initial strength $W_1^c/a_1^0 = 4$ and a simple rarefaction wave. ●, Step-by-step calculations; ○, present method.

were made in each step for obtaining points of intersection of the characteristics α and the shock wave in the wave diagram; calculations in this case were then accurate.

B. *Case of the merging of a rarefaction and shock wave*

We consider the interaction of a rarefaction wave and a shock wave propagating in a duct of constant cross-section with a constant state ahead of the shock. Behind the shock wave is a piston which initially has a constant velocity (see figure 16).

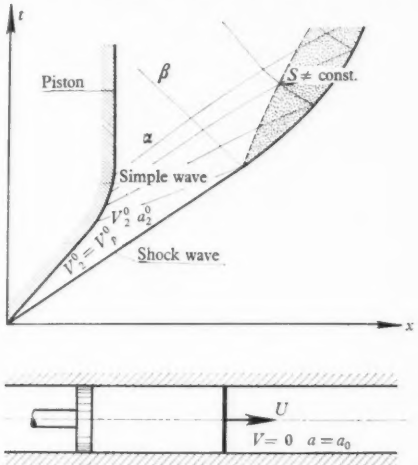

FIGURE 16. Merging of a shock wave and a rarefaction wave caused by non-uniform piston motion.

In the present case we have variable boundary conditions given on the arbitrary L-curve lying near the piston path. We assume that no reflexion wave going back from the shock wave reaches this curve.

Along the given curve we have the simple wave relation

$$s_L = \frac{a_L}{k-1} - \frac{V_L}{2} = \text{const.};$$

therefore

$$dr_L = dV_L = dV_p, \tag{6.5}$$

where V_p is the variable velocity in the simple wave prescribed by the piston motion.

Using equation (2.9) we obtain

$$d\bar{U}\left[R - \frac{\bar{a}_W E}{2(k-1)}\right] \equiv -\tfrac{1}{2}\psi(\bar{U})\,d\bar{U} = d\bar{V}_p, \tag{6.6}$$

where R and E are the functions of $\bar{U}$ given by equations (3.3) and (3.4).

After integrating we obtain the following equation

$$\frac{1}{2}\int_{\bar{U}^0}^{\bar{U}} \psi(\bar{U})\,d\bar{U} = \bar{V}_{p_2} - \bar{V}_{p_1}. \tag{6.7}$$

Table 5 contains values of the integral in equation (6.7) for $k = 1{\cdot}4$.

In this case the entropy change plays an essential role; and the shock expansion method does not give a good approximation. Equation (6.7) only enables the calculation of a change in the shock-wave velocity caused by the piston-velocity variation. To obtain the history of the shock-wave motion it is necessary to find the shape of the characteristics α.

$\bar{U}$	$\frac{1}{2}\int_{\bar{U}_0}^{\bar{U}} \psi(\bar{U})\, d\bar{U}$	$\bar{U}$	$\frac{1}{2}\int_{\bar{U}_0}^{\bar{U}} \psi(\bar{U})\, d\bar{U}$	$\bar{U}$	$\frac{1}{2}\int_{\bar{U}_0}^{\bar{U}} \psi(\bar{U})\, d\bar{U}$
1·2	−0·949	3·2	1·190	5·2	2·795
1·3	−0·806	3·3	1·274	5·3	2·872
1·4	−0·663	3·4	1·358	5·4	2·950
1·5	−0·543	3·5	1·441	5·5	3·027
1·6	−0·424	3·6	1·523	5·6	3·104
1·7	−0·314	3·7	1·605	5·7	3·181
1·8	−0·205	3·8	1·686	5·8	3·258
1·9	−0·102	3·9	1·767	5·9	3·335
2·0	0·000	4·0	1·848	6·0	3·412
2·1	0·098	4·1	1·928	6·1	3·488
2·2	0·196	4·2	2·008	6·2	3·565
2·3	0·290	4·3	2·088	6·3	3·641
2·4	0·385	4·4	2·167	6·4	3·718
2·5	0·477	4·5	2·246	6·5	3·794
2·6	0·568	4·6	2·325	6·6	3·870
2·7	0·707	4·7	2·404	6·7	3·947
2·8	0·847	4·8	2·483	6·8	4·023
2·9	0·923	4·9	2·561	6·9	4·069
3·0	1·020	5·0	2·639	7·0	4·115
3·1	1·105	5·1	2·717		

TABLE 5

On the basis of the step-by-step calculations it is observed that the α-characteristics are not very different from straight-lines.

Using these results we can calculate the change of the shock strength along the tube axis. Comparisons of the calculations by the present method and the finite difference method are given in figures 17–19 for various initial shock strengths and various modes of piston motion.

7. Interaction of a rarefaction wave and a contact surface in one-dimensional unsteady flow

The present method enables us to obtain in closed form the solution for the interaction of a rarefaction wave and a contact surface in an unsteady one-dimensional flow. In a similar way, the analogous problem in plane steady flow can be solved. Until now, the closed form solution only enabled the calculation of the finite value of the contact surface velocity (after interaction) to be done (see Billington 1956). The full history of the contact surface motion was obtained by step-by-step calculations (see Courant & Friedrichs 1948).

We assume the flow to be isentropic on the two sides of the contact surface (figure 20). The compatibility equations on the contact surface are

$$\left.\begin{aligned} V_{1c} &= V_{2c} = V_c, \\ p_{1c} &= p_{2c} = p_c \end{aligned}\right\} \tag{7.1}$$

(no velocity and pressure jump take place on the contact surface).

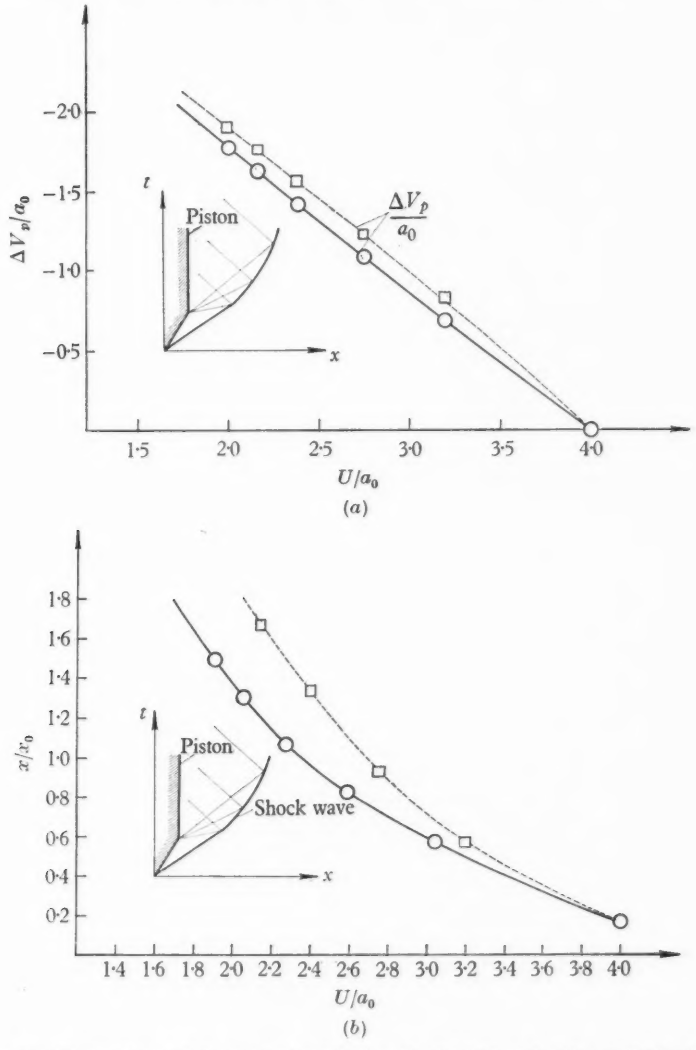

FIGURE 17. Comparison of the present method and calculations by the method of characteristics for the case of a shock wave of initial strength $U_0/a_0 = 4$ merging with a rarefaction wave caused by a suddenly stopped piston. (*a*) Shock-wave velocity versus piston velocity. (*b*) Change of the shock-wave propagation velocity, straight line α-characteristics being assumed. ----, Step-by-step method; ——, present method.

From the second relation (7.1) and the equation of isentropic flow, we get

$$\left(\frac{a_{1c}}{a_1^0}\right)^{2k_1/(k_1-1)} = \left(\frac{a_{2c}}{a_2^0}\right)^{2k_2/(k_2-1)}, \tag{7.2}$$

where a_1^0, a_2^0 are the initial values of the velocity of sound on the right and left side of the contact surface.

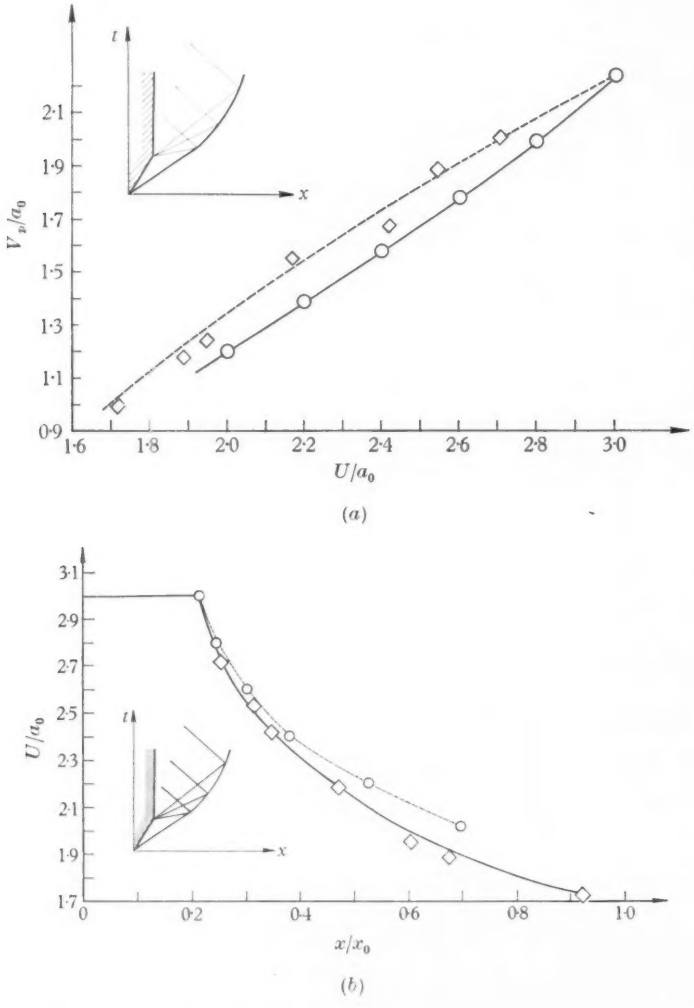

FIGURE 18. Comparison of the present method and calculations by the method of characteristics for the case of a shock wave of initial strength $U_0/a_0 = 3$ merging with a rarefaction wave caused by suddenly stopped piston. (*a*) Shock velocity versus piston velocity. (*b*) Change of the shock-wave propagation velocity, straight line α-characteristics being assumed. – – – –, Step-by-step method; ——, present method.

We have $ds_1 = 0$ for the transmitted wave (simple wave) and therefore along the contact surface

$$\frac{a_{1c}}{k_1-1}-\frac{V_c}{2}=\frac{a_{1c}^0}{k_1-1}-\frac{V_c^0}{2}. \tag{7.3}$$

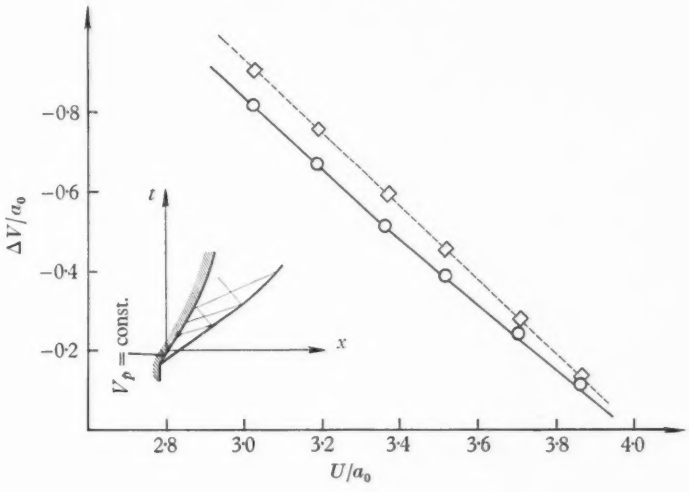

(*a*)

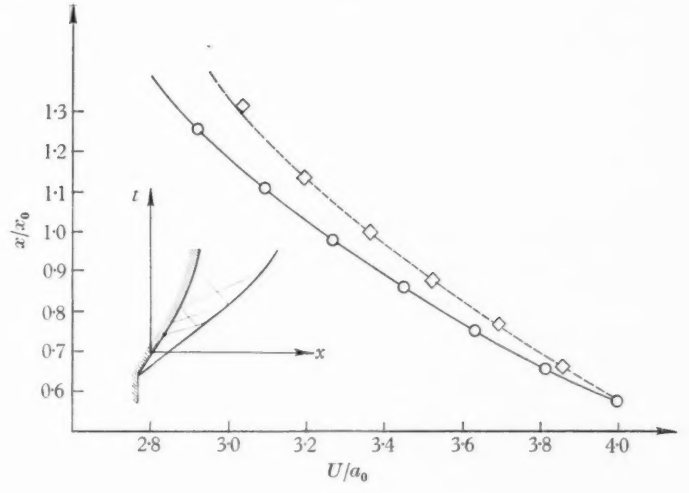

(*b*)

FIGURE 19. Comparison of the present method and calculations by the method of characteristics for the case of a shock wave of initial strength $U_0/a_0 = 4$ merging with a rarefaction wave caused by the retarded piston motion $dV_p/dt = W_p = -30(a_0/t_0)$. (*a*) Shock velocity versus piston velocity. (*b*) Change of the shock-wave propagation velocity, straight α-characteristics being assumed. – – –, Step-by-step method; ——, present method.

For this case, in an analogous way to that leading to equation (2.9), we can write the following equation

$$dr_{2c} \equiv \frac{dV_c}{2} + \frac{da_{2c}}{k_2 - 1} = dr_L = dV_p. \tag{7.4}$$

Using equations (7.2) and (7.3) and integrating, we obtain the following expression

$$\frac{V_c - V_c^0}{2} + \frac{a_2^0}{k_2 - 1}\left[\frac{V_c - V_c^0}{2a_1^0}(k_1 - 1)\right]^{(k_2-1)/(k_1-1)(k_1/k_2)} = V_p - V_p^0. \tag{7.5}$$

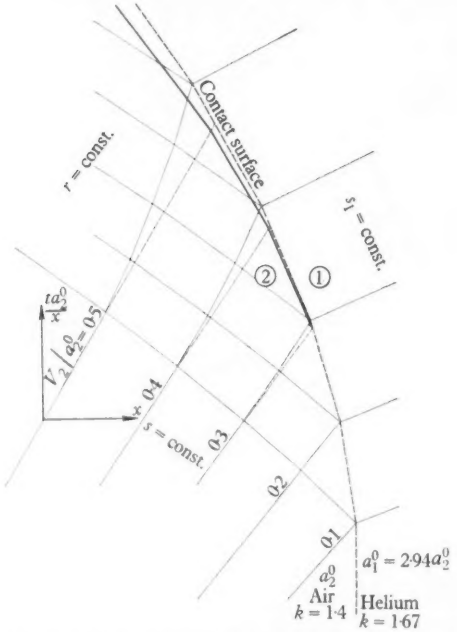

FIGURE 20. Time history of the interaction of a rarefaction wave with an air-helium contact surface, computed by the present method with the assumption of straight α-characteristics and by the method of characteristics. – – –, Step-by-step calculations; ——, present method.

This equation enables one to calculate the velocity of the contact surface for a given change in the simple wave velocity $V_p \equiv V_p(x/t)$. Assuming, as before in the case of the interaction of a rarefaction wave and a shock wave (see § 6 B), that the α-characteristics are straight lines, we get the history of the contact surface motion. The results of the calculation are compared with the results of the method of characteristics and presented in figure 20 for an air-helium contact surface.

8. Wave interactions in plane steady supersonic flow. The basic expression for plane flow

In a way similar to that used for unsteady one-dimensional flow, we introduce the analogous expression for plane flow. We make use of the equation in the

characteristic direction by assuming that the curvature of the characteristics is small (see Howarth 1953, p. 75):

$$\frac{\partial v_\alpha}{\partial \alpha} - \frac{v_\alpha}{v_\beta}\frac{\partial v_\beta}{\partial \alpha} + \frac{v_\alpha}{\rho v_\beta^2}\frac{\partial p}{\partial \alpha} = 0. \tag{8.1}$$

Here, α and β are the characteristic and the orthogonal curvilinear co-ordinates, respectively, p is the pressure, and v_α, v_β are the velocity components in the α

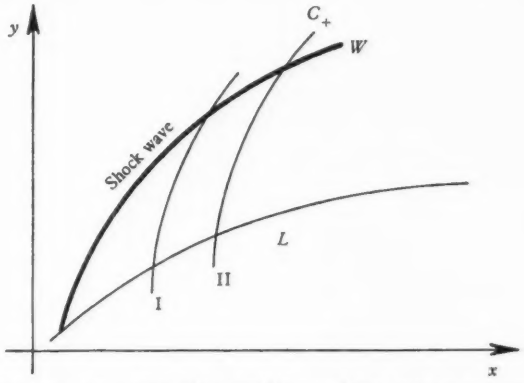

FIGURE 21. The boundary-value problem in plane steady supersonic flow.

and β directions, respectively. We take the α-co-ordinate along the C_+ characteristic. The compatibility equations for an oblique shock wave can be written in the form (see Stanjukovitch 1955)

$$V_W = V_1 \frac{\cos\gamma}{\cos(\gamma-\theta)}, \tag{8.2}$$

where γ, θ are defined in figure 22,

$$\frac{p_W}{p_1} = \frac{2k}{k+1} M_1^2 \sin^2\gamma - \frac{k-1}{k+1}, \tag{8.3}$$

$$\frac{2}{k-1} = M_1^2 \sin^2\gamma \left[\frac{k-1}{k+1}\frac{\tan(\gamma-\theta)}{\tan\gamma} - 1\right]. \tag{8.4}$$

From these equations we obtain

$$v_{\alpha W} = V_W \cos\mu_2 = V_1 \frac{\cos\gamma\cos\mu_2}{\cos(\gamma-\theta)} \equiv f(\gamma, V_1), \tag{8.5}$$

$$v_{\beta W} = V_W \sin\mu_2 \equiv \phi(\gamma, V_1), \tag{8.6}$$

$$p_W = \psi(\gamma, V_1), \tag{8.7}$$

where the Mach angle $\mu_2 = \sin^{-1} 1/M_2$. We assume that we can express all the parameters of the flow in terms of the velocity V_1 in front of the shock wave. The boundary-value problem can then be presented in a similar way as in § 2. We assume that we are given an arbitrary curve L which is not a characteristic (it can be the surface of a body, see figure 21), and that on this curve the boundary conditions $V = V_L(x)$, $p = p_L(x)$ are given.

As before in § 2, we integrate the expression (8.1) along a C_+ characteristic between the L-line and the shock wave. Expressing the values on the shock wave by equations (8.5), (8.6) and (8.7), we obtain

$$f(\gamma, V_1) - v_{x_L} - \int_{v_{\beta L}}^{\phi(\gamma, V_1)} \frac{v_x}{v_\beta} dv_\beta + \int_{p_L}^{\psi(\gamma, V_1)} \frac{v_x}{\rho v_\beta^2} dp = 0.$$

Applying the above equation to two neighbouring characteristics $C_{+\mathrm{I}}$ and $C_{+\mathrm{II}}$ (see figure 21), and subtracting one of these relations from the other, we obtain in the limit as $C_{+\mathrm{I}} \to C_{+\mathrm{II}}$

$$\begin{aligned} &f'_\gamma(\gamma, V_1)\, d\gamma + f'_{V_1}(\gamma, V_1)\, dV_1 - dv_{x_L} - \left[\frac{v_x}{v_\beta}\right]_W [\phi'_\gamma(\gamma, V_1)\, d\gamma + \phi'_{V_1}(\gamma, V_1)\, dV_1] \\ &+ \left[\frac{v_x}{v_\beta}\right]_L dv_{\beta_L} - \left[d\left(\frac{v_x}{v_\beta}\right)\right]_m [\phi(\gamma, V_1) - v_{\beta_L}] + \left[\frac{v_x}{\rho v_\beta^2}\right]_W [\psi'_\gamma(\gamma, V_1)\, d\gamma + \psi'_{V_1}(\gamma, V_1)\, dV_1] \\ &- \left[\frac{v_x}{\rho v_\beta^2}\right]_L dp_L + \left[d\left(\frac{v_x}{\rho v_\beta^2}\right)\right]_m [\psi(\gamma, V_1) - p_L] = 0. \end{aligned} \tag{8.8}$$

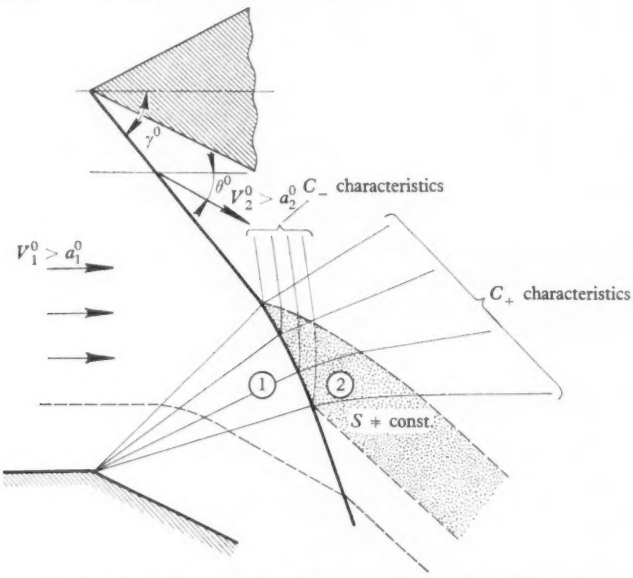

FIGURE 22. Head-on collision of an oblique shock wave and a Prandtl–Meyer expansion in steady plane flow.

Here values with the suffix m are the mean values in the interval of integration. In the linearized case, all the parameters can be written as $V = V_L + \epsilon_v$, etc., where $\epsilon_v \ll V_L$, etc. We see that the terms with mean values are small quantities of the second order. Neglecting these, we obtain

$$\begin{aligned} &f'_\gamma(\gamma, V_1)\, d\gamma + f'_{V_1}(\gamma, V_1)\, dV_1 - \left[\frac{v_x}{v_\beta}\right]_W [\phi'_\gamma(\gamma, V_1)\, d\gamma - \phi'_{V_1}(\gamma, V_1)\, dV_1] \\ &+ \left[\frac{v_x}{\rho v_\beta^2}\right]_W \psi'_\gamma(\gamma, V_1)\, d\gamma + \left[\frac{v_x}{\rho v_\beta^2}\right]_W \psi'_{V_1}(\gamma, V_1)\, dV_1 = dv_x - \left[\frac{v_x}{v_\beta}\right]_L dv_{\beta_L} + \left[\frac{v_x}{\rho v_\beta^2}\right]_L dp_L. \end{aligned} \tag{8.9}$$

We shall henceforth apply equation (8.9) as an approximation for cases in which linearization is not valid. This equation is analogous to equation (2.9) for unsteady flow.

We shall now make use of this expression to solve the problems of the interaction of a Prandtl–Meyer expansion and an oblique shock wave, and plane hypersonic flow around a body.

9. Head-on collision of an oblique shock wave and a Prandtl–Meyer expansion

In a similar way to that for the unsteady wave interaction discussed in § 6, we now apply the relation (8.9) to the head-on collision of a simple rarefaction wave (Prandtl–Meyer flow) and an oblique shock wave (figure 22).

In front of the shock wave, the following equations are satisfied by the Prandtl–Meyer flow

$$\frac{V_1^2}{2}+\frac{a_1^2}{k-1}=\frac{a_0^2}{k-1}, \tag{9.1}$$

$$\frac{p_1}{p_1^0}=\left(\frac{a_1}{a_1^0}\right)^{2k/(k-1)}, \tag{9.2}$$

$$\theta_1=\sqrt{\left(\frac{k+1}{k-1}\right)}\tan^{-1}\sqrt{\left(\frac{k+1}{k-1}(M_1^2-1)\right)}-\tan^{-1}\sqrt{(M_1^2-1)}. \tag{9.3}$$

With these relations, we obtain from equation (8.9) the following expressions:

$$\frac{d\gamma}{dV_1}=\frac{M^2\bar{a}^2\sin\mu_W\left(G-\dfrac{B_1}{B_2}\right)\dfrac{a_0^2}{a_1^2}-\dfrac{\cos\mu_W}{\bar{\rho}k}\left(kM_1P_1-P_2\dfrac{a_0^2}{a_1^2}+P_3\dfrac{B_1}{B_3}\dfrac{a_0^2}{a_1^2}\right)}{\dfrac{B_2}{B_3}\left[M^2\bar{a}^2\sin\mu_W-\dfrac{P_3}{\bar{\rho}k}\right]a_1}, \tag{9.4}$$

where

$$\left.\begin{aligned}
&\bar{a}=\frac{a_W}{a_1},\quad \bar{\rho}=\frac{\rho_W}{\rho_1},\quad M=\frac{V_W}{a_W},\\
&G=\frac{\partial\theta_1}{\partial M_1}=\frac{1}{1-\dfrac{k-1}{k+1}(M_1^2-1)}\frac{M_1}{\sqrt{(M_1^2-1)}}-\frac{1}{M_1\sqrt{(M_1^2-1)}},\\
&B_1=2M_1\sin^2\gamma\left[\frac{k+1}{k-1}\frac{\tan(\gamma-\theta)}{\tan\gamma}-1\right],\\
&B_2=M_1^2\left\{\sin 2\gamma\left[\frac{k+1}{k-1}\frac{\tan(\gamma-\theta)}{\tan\gamma}-1\right]+\frac{k+1}{k-1}\left[\frac{\sin\gamma\cos\gamma}{\cos^2(\gamma-\theta)}-\tan(\gamma-\theta)\right]\right\},\\
&B_3=-M_1^2\sin^2\gamma\frac{k+1}{k-1}\frac{1}{\tan\gamma\cos^2(\gamma-\theta)},\\
&P_1=\frac{\partial p_2}{\partial p_1}=\frac{2k}{k+1}M_1^2\sin^2\gamma-\frac{k-1}{k+1},\\
&P_2=\frac{1}{p_1}\frac{\partial p_2}{\partial M_1}=\frac{4k}{k+1}M_1\sin^2\gamma,\\
&P_3=\frac{1}{p_1}\frac{\partial p_2}{\partial\gamma}=\frac{4k}{k+1}M_1^2\sin\gamma\cos\gamma.
\end{aligned}\right\} \tag{9.5}$$

Using the compatibility equations for the shock wave (8.2), (8.3) and (8.4), and the equations (9.1) and (9.2), we can express all coefficients of equation (9.4) as functions of γ and V_1 alone. We then obtain a first-order ordinary differential equation for γ as a function of V_1. Numerical calculations on the basis of equation

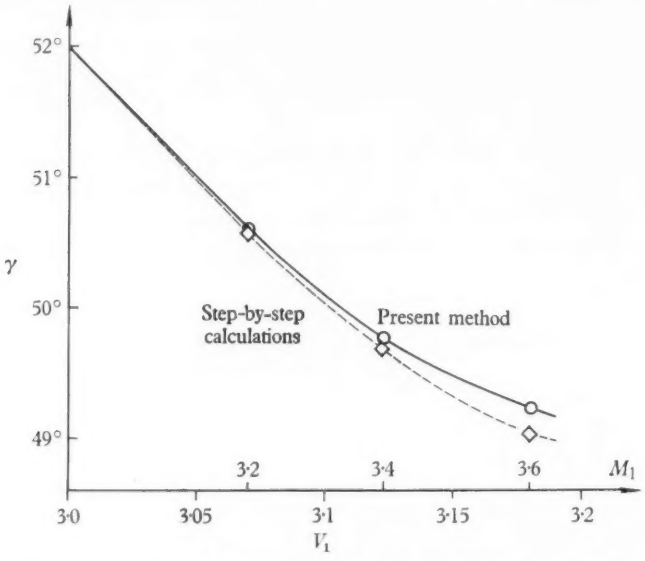

FIGURE 23. Comparison of the present method with the method of characteristics for the case of head-on collision of an oblique shock and a Prandtl–Meyer expansion.

(8.4) enable the computation of the shock-wave path without solving the partial differential equations governing the flow on the back of the shock wave. Equation (9.4) could be used to construct suitable tables.

A comparison of the results obtained with those of finite difference calculations is presented in figure 23 for $M_1^0 = 3$, $\gamma^0 = 52°$.

10. The shock wave in plane flow around a body

We consider the problem of the calculation of the shock-wave shape in plane supersonic flow around a body (see figure 24). We assume the shock wave to be attached (i.e. the nose angle of the body is smaller than the critical one). This problem corresponds to the merging shock and rarefaction wave in one-dimensional unsteady flow considered in § 6B.

Taking the body surface as a curve L and assuming that there is no reflected wave from the shock wave (a small reflexion is observed according to Egger's *et al.* (1955) paper), we can calculate all the parameters on the body surface from the Prandtl–Meyer flow relations. From (8.9) we obtain

$$\frac{d\gamma}{d\theta} = \frac{2V_L^2 \sin\mu_{2L}}{BV_W^2 \sin\mu_W + (p_1/\rho_W) P_3 \cos\mu_W}, \tag{10.1}$$

where B and P_3 are given by equations (9.5).

Expressing all the parameters in the denominator of equation (10.1) in terms of γ and in the numerator in terms of θ, we get the following equation

$$\int_{\gamma^*}^{\gamma} \Phi(\gamma)\, d\gamma = \int_{\theta_L^*}^{\theta_L} \psi(\theta_L)\, d\theta_L, \tag{10.2}$$

where $\Phi(\gamma)$, $\overline{U}(\theta_L)$ are functions given by the denominator and numerator in equation (10.1), respectively.

The equation gives the variation of the shock-wave angle γ as a function of the body shape given by θ_L, taken on the same characteristic.

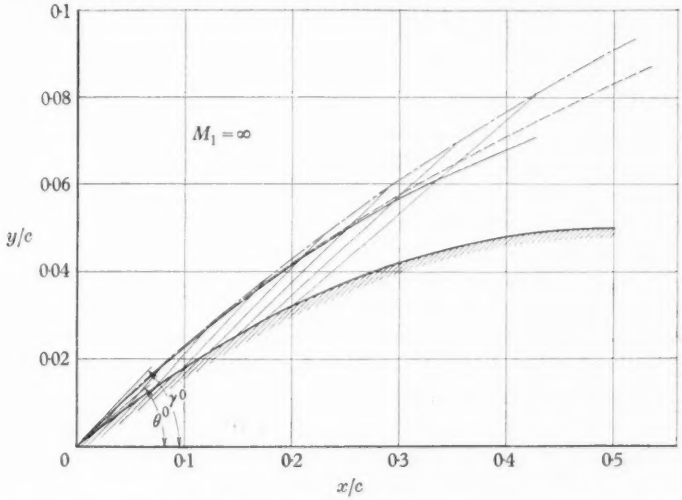

FIGURE 24. Supersonic plane flow around a body (the calculations by the method of characteristics and the shock expansion method are taken from Eggers *et al.* 1955). ——, Present method; – – –, method of characteristics; ——— , shock-expansion method.

This method differs from the shock-expansion method, where all the parameters are assumed to be constant along the C_+ characteristics (i.e. a simple wave). In the present solution θ varies along the characteristics. These solutions are the same only in the linearized case. However, the assumption that the C_+ characteristics are straight lines was made in the calculation of the shock-wave shape.

Figure 24 presents a comparison of the present theory, applied to a 10% thick biconvex airfoil at $M_1 = \infty$, with the results published in Egger's *et al.* paper obtained by the method of characteristics. (This comparison is not very accurate because the figure drawn in their paper is not precise.)

An interesting problem is the influence of the entropy change on the flow behind the shock wave. We obtain for oblique shock waves (in a similar way as in § 3) the following formula

$$\frac{1}{c_p}\frac{dS}{d\gamma} = 4\left\{\frac{M_1 \sin\gamma}{2kM_1^2\sin^2\gamma - k + 1} - \frac{1}{M_1 \sin\gamma[(k-1)M_1^2\sin^2\gamma + 2]}\right\} M_1 \cos\gamma. \tag{10.3}$$

For $M_1 = \infty$

$$\frac{1}{c_p}\frac{dS}{d\gamma} = \frac{2}{k}\cot\gamma. \tag{10.4}$$

We then get for a given curvature of the shock wave a weak entropy gradient behind the shock wave, and hence low vorticity for γ close to $\frac{1}{2}\pi$ (a detached shock wave).

For the given profile, it follows from the above method of shock-shape calculation that the higher the Mach number M_1, the smaller is the curvature of the shock wave. It therefore follows that the entropy change at higher Mach numbers is smaller because of the smaller curvature of the shock wave.

11. Discussion

The results obtained in the present paper seem to be very useful for many cases of non-uniform motion of shocks, detonation waves, and contact surfaces, but the present method enables us to find only the position of the unknown discontinuity line. In the case of small disturbances, when the linearized approximation can be applied, it is possible to find the complete flow field. In the general case, it is necessary for the determination of the flow field to solve the modified Cauchy problem for the basic partial differential equations with the boundary conditions given on the known discontinuity line.

The results obtained in this paper are very close to those obtained by step-by-step calculations based on the method of characteristic, because the neglected expressions containing mean values in equations (2.9) and (8.9) have small contributions. This is because the curvature of the α-characteristics is small in all the problems considered. The assumption of straight characteristics, which was made in some of the cases, gives results which differ little for both methods. This difference depends on the entropy change behind the shock wave.

In this paper the results obtained were compared with step-by-step calculations mainly for shock strengths $\overline{U} = 3, 4, 5$, where the influence of entropy changes is greatest. For weak and strong shocks the results are therefore better than for shocks of medium strength.

The author wishes to express his gratitude to Mr P. Kijkowski and Mr S. Pietrzyk for their help in carrying out the computations necessary for the examination of the present method; and also to the Fluid Mechanics Department of the Institute of Basic Problems of the Polish Academy of Sciences for financing this work.

REFERENCES

Billington, I. J. 1956 *J. Aero. Sci.* **23**, 997.

Chisnell, R. F. 1957 *J. Fluid Mech.* **2**, 286.

Courant, R. & Friedrichs, K. O. 1948 *Supersonic Flow and Shock Waves.* New York: Academic Press.

Eggers, A. J., Savin, R. C. & Syvertson, C. A. 1955. *J. Aero. Sci.* **22**, 231.

Friedrichs, K. O. 1948 *Commun. Pure Appl. Math.* **1**, 211.

Geiringer, H. 1948 *Advances in Applied Mechanics*, vol. I. New York: Academic Press.

GUNDERSEN, R. 1958 *J. Fluid Mech.* **4**, 501.

HERTZBERG, A. & KANTROWITZ, A. 1950 *J. Appl. Phys.* **21**, 874.

HOWARTH, L. 1953 *Modern Development in Fluid Dynamics: High-Speed Flow*, vol. I. Oxford University Press.

PAYNE, R. B. 1957 *J. Fluid Mech.* **2**, 185.

ROŚCISZEWSKI, J. 1958 Ph.D. Thesis. Published in *Archiwum Budowy Maszyn*, no. 1, 1959.

STANJUKOVITCH, K. P. 1955 *Non-Steady Motion of Continuous Media.* Moscow.

WHITHAM, G. B. 1958 *J. Fluid Mech.* **4**, 337.

Velocity and enthalpy distributions in the compressible turbulent boundary layer on a flat plate

By D. A. SPENCE
Royal Aircraft Establishment, Farnborough†

(Received 1 November 1959)

The object of this paper is to present a unified account of the distributions of velocity, shear stress and enthalpy in the compressible turbulent boundary layer on a flat plate. As a start, the set of velocity profiles measured over a range of heat-transfer conditions at Mach numbers between 5 and 8 by Lobb, Winkler & Persh (1955) is examined. It is found that by plotting in terms of the Howarth variable $\eta = \int_0^y (\rho/\rho_0)\,dy$, the outer parts of the profiles for different Mach numbers are brought together on a single curve of the approximate form $u/u_\infty = (\eta/\Delta)^{1/n}$, Δ being the transformed boundary-layer thickness. By evaluating the reference density ρ_0 and kinematic viscosity ν_0 at the so-called 'intermediate' enthalpy (Eckert 1955) the inner parts of the profiles can also be collapsed, although less completely, to fit a 'law of the wall' $u/u_\tau = A\log(\eta u_\tau/\nu_0 - c) + B$. Here $u_\tau = (\tau_w/\rho_0)^{\frac{1}{2}}$, and A, B and c are the same constants as in incompressible flow.

These properties provide a physical starting point from which the remaining features of the mean flow can be calculated. By substitution of appropriate stream functions in the equation of motion the distribution of shear stress τ in inner and outer regions is found; this approximates to the form

$$\tau/\tau_w = 1 - (u/u_\infty)^{n+2}$$

over the whole layer. A relation between the distributions of enthalpy and shear stress is then found from the energy equation, using a turbulent Prandtl number α which is assumed constant across the layer to relate eddy conductivity to eddy viscosity. The final expression is similar in form to Crocco's integral for the laminar boundary layer with α taking the place of the laminar Prandtl number σ, but contains two extra terms proportional respectively to $(\alpha-\sigma)c_f$ and $(\alpha-\sigma)c_f^{\frac{1}{2}}$, which represent the effect of the inner viscous regions.

The enthalpy integral is evaluated using the stated velocity-shear relation, and an expression which agrees well with the available experimental data is found for the heat-transfer coefficient as a function of recovery factor and skin-friction coefficient. It is also found that the usual quadratic enthalpy-velocity relation, exact for $\alpha = \sigma = 1$, remains an acceptable approximation for Prandtl numbers considerably different from unity.

† At Cornell University, Ithaca, New York, 1959–60.

1. Introduction

1.1. *Howarth's transformation*

A number of recent authors on the compressible turbulent boundary layer have noticed that, as in the laminar case, the analysis can be greatly simplified by using instead of the physical co-ordinate y the variable

$$\eta = \int_0^y (\rho/\rho_0)\, dy \tag{1}$$

introduced by Howarth. Here ρ is the density at height y above the surface, and ρ_0 an arbitrarily chosen reference density. For the laminar boundary layer on a flat plate, if the product $\rho\mu$ of density and viscosity is treated as constant, the effect of the transformation is to free the velocity profiles of explicit dependence on Mach number and Prandtl number. They can be written

$$u/u_\infty = f(\eta/\Delta), \tag{2}$$

where f is a universal function, u_∞ is the free-stream velocity at the outer edge of the boundary layer, and Δ is the transformed value of a suitably-defined boundary-layer thickness δ.

It seems natural to ask whether any property like this may also hold for velocity profiles in the turbulent case. In an attempt to answer this question, a set of profiles measured by Lobb *et al.* (1955) is examined in the present paper. These were obtained at Mach numbers between 5 and 8, and momentum-thickness Reynolds numbers R_θ between 5000 and 12,500, with varying amounts of heat transfer. When plotted in the form of u/u_∞ against y/δ as in figure 6 the profiles are widely different, but the transformation (1) almost eliminates the scatter, so that in figure 7 all lie close to a single curve. Except near the inner and outer limits, the power law

$$u/u_\infty = (\eta/\Delta)^{1/n} \tag{3}$$

with $n = 9$ provides a good interpolation to the curve, and from experience of incompressible boundary layers one would expect the index $1/n$ to decrease slowly with increasing R_θ over a wider range.

This particular form of interpolation has of course no special physical significance, but it does make the calculation of the remaining properties of the mean flow fairly straightforward. Most recent workers on the incompressible boundary layer have preferred to express the outer velocity distribution in terms of the 'defect' or 'wake' laws elegantly formulated by Clauser (1956) and Coles (1956). These laws offer more insight into the physical processes at work in transferring turbulent energy through successive eddy scales within the boundary layer, but in the zero-pressure gradient case they have little advantage in accuracy over the simpler type of law used here. Dimensional analysis shows that the incompressible boundary-layer profile on a flat plate can depend on two parameters only; in the outer part one of these must be y/δ, and no generality is lost in using for the second the index $1/n$ of the interpolating power law, which clearly depends on R_θ.

1.2. *Law of the wall*

The form of equation (2) is, however, inappropriate in the sublayer and inner turbulent core, for we know that in incompressible flow the velocity distribution

in these regions is given by the 'law of the wall'. That is, the velocity ratio u/u_τ, where u_τ is the friction velocity $(\tau_w/\rho)^{\frac{1}{2}}$, is a universal function of yu_τ/ν. This could only be strictly true if the boundary-layer thickness were infinite, but its approximate validity at finite Reynolds numbers is established beyond doubt, and one is naturally led to try to generalize the law for compressible flows.

A way of doing this is suggested by the form of the sublayer profile. If the friction velocity is defined for a compressible flow in terms of the reference density by

$$\tau_w = \rho_0 u_\tau^2, \tag{4}$$

then, since the shear stress $\mu(\partial u/\partial y)$ in the sublayer is nearly constant and equal to τ_w, the profile may be written

$$\frac{u}{u_\tau} = \frac{\tau_w}{u_\tau}\int_0^y \frac{dy}{\mu} = \eta u_\tau/\nu_0. \tag{5}$$

Here $\nu_0 = \mu_0/\rho_0$, and it has been assumed as before that $\rho\mu$ is constant. The accuracy of this assumption is discussed in §7. Equation (5) is of the form

$$\frac{u}{u_\tau} = g(\eta u_\tau/\nu_0) \tag{6}$$

and by analogy with the incompressible case one might expect an expression of this form to hold also in the buffer layer and in the turbulent core. To agree with the well-known expression for incompressible flow, g would have to approach the form $A\log(\eta u_\tau/\nu_0)+B$ in the fully turbulent core, i.e. for $\eta u_\tau/\nu_0 > 30$ say. If, in addition, the physically realistic requirement of a continuous derivative, i.e. of continuous viscous shear stress, at the intersection with the sublayer profile (5) is imposed, we are led to the compressible version of an expression derived by Squire (1948), namely

$$\frac{u}{u_\tau} = A\log\left(\frac{\eta u_\tau}{\nu_0} - c\right) + B \tag{7}$$

in which A and B have the accepted values 2·5, 5·5, respectively, and $c = 5{\cdot}3$. With these values the intersection of (5) and (7) is at $\eta u_\tau/\nu_0 = 7{\cdot}8$.

1.3. *Choice of the reference density*

The outer velocity distribution (2) is independent of ρ_0, but that defined by (6) does depend on the particular reference density which is chosen. A way of deciding on the appropriate value is suggested by the 'intermediate enthalpy' method of correlating compressible and incompressible values of the skin fraction. It has been found experimentally—for example, by Matting, Chapman, Nyholm & Thomas (1959)—that the wall shearing stress τ_w a distance x downstream of the virtual origin of turbulence in a compressible boundary layer can be written $\frac{1}{2}\rho_m u_\infty^2 c_f(u_\infty x/\nu_m)$, where c_f is the same function of the Reynolds number as in incompressible flow. The suffix m now denotes evaluation of the physical quantities at a certain intermediate value h_m of the enthalpy, for which Eckert (1955) has given the empirical equation

$$h_m = 0{\cdot}5(h_w + h_\infty) + 0{\cdot}22(h_r - h_\infty), \tag{8}$$

where suffixes w, ∞ and r refer to wall, free stream and recovery (i.e. zero heat transfer) values.

But the velocity distributions (3) and (7) alone contain enough information for the skin friction to be deduced, and it is shown in §2 that if the two laws join with $\partial u/\partial y$ continuous, then

$$\tau_w/\rho_0 u_\infty^2 = C(\rho_\infty u_\infty \theta/\mu_0)^{-2(n+1)} = D(u_\infty x/\nu_0)^{-2(n+3)}, \tag{9}$$

where $C(n)$ and $D(n)$ have almost exactly the values used in the recognized incompressible power-law formulae. The fact that the power-law formulae for skin friction can be derived *a priori* in this way does not seem to be well known: most authors have regarded the formulae, at least for the cases $n = 9$ and $n = 11$, merely as interpolations to more complicated expressions of the Karman–Schoenherr type, which were originally derived by use of a velocity-defect law. But if ρ_0 and μ_0 are the values which apply at Eckert's intermediate enthalpy h_m, then (9) gives precisely the value of skin friction predicted when his law is used to generalize the latter formulae to compressible flow. It follows, therefore, that if we set

$$\rho_0 = \rho_m, \quad \mu_0 = \mu_m, \tag{10}$$

the inner law (6) is consistent with the known variation of skin friction with Mach number. These reference values are therefore used in the remainder of the paper.

1.4. *Distributions of shear stress and enthalpy*

Before comparing the velocity laws (3) and (7) directly with the available experimental profiles, it is useful to calculate the distributions of shear stress and enthalpy across the layer on the assumption that they do in fact hold. The shear stress is found in §3, using the equations of motion in conjunction with appropriate forms of the steam function in inner and outer regions. General expressions involving only the functional forms of the velocity profile are found first, but on inserting the precise distributions (3) and (7) an approximate expression is obtained for τ/τ_w in terms of u/u_∞ alone. This is required in §4, where a turbulent analogue of Crocco's integral relating the enthalpy distribution to those of shear stress and velocity is derived from the energy equation.

The derivation calls for some further knowledge of the turbulent transport mechanism, in addition to that implied by the distribution of velocity (from which those of shear stress and therefore of eddy viscosity followed). For this purpose it is assumed, following van Driest (1955) and Rubesin (1953), that the ratio of diffusivities of momentum and heat due to the turbulent motion is constant across the layer. This ratio defines a turbulent Prandtl number α, different in general from the laminar value σ which corresponds to molecular transport mechanisms. Rubesin and van Driest had recourse to mixing length theories to provide the distribution of shear stress, but we can now use the distribution obtained directly from the velocity profile. Both this and the distribution of enthalpy to which it leads are therefore consistent with the equations of continuity, momentum and energy, and with each other. This was not the case with those obtained by previous authors.

1.5. *Recovery factor and heat-transfer coefficient*

From the enthalpy distribution, expressions are found in §5 for the recovery factor (i.e. the fraction of the kinetic energy of the free stream which is recovered as enthalpy at an adiabatic wall) and for the heat-transfer coefficient. In each, the more important term depends only on α, but correction terms proportional to $(\alpha-\sigma)(\rho_\infty c_f/\rho_m)$ and to $(\alpha-\sigma)(\rho_\infty c_f/\rho_m)^{\frac{1}{2}}$, respectively, appear. The value of α cannot be obtained directly from experiments, but it is possible to infer a value from that of the recovery factor, which can be measured. The value of α so found can then be used to predict the heat-transfer coefficient which corresponds to a particular recovery factor. The resulting heat-transfer coefficients lie well within the range which would have been expected from experiments.

Finally, in §6, the experimental velocity profiles referred to are examined to show their compatibility with the model of the boundary layer which has been elaborated in the paper.

2. Expression for skin friction

As remarked in §1.3, an expression for skin friction can be derived directly from those for the inner and outer velocity profiles, on the assumption that the gradient $\partial u/\partial\eta$ is continuous at their intersection. Using (2), (6) and writing $\eta u_\tau/\nu_0 = \zeta$, we should have at this point

$$\frac{u}{u_\infty} = f\left(\frac{\zeta\nu_0}{u_\tau\Delta}\right) = \frac{u_\tau}{u_\infty}g(\zeta),$$

$$\frac{1}{u_\infty}\frac{\partial u}{\partial\zeta} = \frac{\nu_0}{u_\tau\Delta}f'\left(\frac{\zeta\nu_0}{u_\tau\Delta}\right) = \frac{u_\tau}{u_\infty}g'(\zeta).$$

Eliminating ζ between these two equations clearly yields a relation between u_τ/u_∞ and $u_\tau\Delta/\nu_0$ or, what is the same thing, between $(u_\tau/u_\infty)^2$ and $u_\infty\Delta/\nu_0$. In particular, the power law (3) can be rewritten

$$\frac{u}{u_\tau} = \left(\frac{u_\tau}{u_\infty}\right)^{-(n+1)/n}\left(\frac{u_\infty\Delta}{\nu_0}\right)^{-1/n}\zeta^{1/n} = K\zeta^{1/n} \tag{11}$$

say, whence

$$\frac{\tau_w}{\rho_0 u_\infty^2} = \left(\frac{u_\tau}{u_\infty}\right)^2 = K^{-2n/(n+1)}\left(\frac{u_\infty\Delta}{\nu_0}\right)^{-2/(n+1)}. \tag{12}$$

Applying the second condition that $\partial u/\partial\zeta$ is continuous at the intersection of (11) with the logarithmic law (7) (from which c can be omitted since the join occurs at values of ζ much greater than 5·3), K is found explicitly as

$$K = nA\exp[(B/nA)-1]. \tag{13}$$

The values of K for $n = 7, 9, 11$ are tabulated in table 1, and the corresponding outer curves are plotted against ζ in figure 1. The fact that the power and logarithmic laws in each case lie close together for a fair distance on either side of the point of contact shows the joining condition to have been a realistic one.

The momentum thickness may be evaluated using the power law (3), since integration smooths out errors produced by the departure of the profile from this form at the inner and outer edges; we obtain

$$\theta = \int_0^\delta (\rho u/\rho_\infty u_\infty)(1-u/u_\infty)\,dy = \{n/(n+1)(n+2)\}(\rho_0\Delta/\rho_\infty). \tag{14}$$

n	K	$2/(n+1)$	C	C'	Range of R_θ
7	8·82	$\frac{1}{4}$	0·0124	0·0130	100–5000
9	10·57	$\frac{1}{5}$	0·0087	0·0088	500–50,000
11	12·36	$\frac{1}{6}$	0·00645	0·00655	3000–600,000

TABLE 1. Power laws for incompressible skin friction

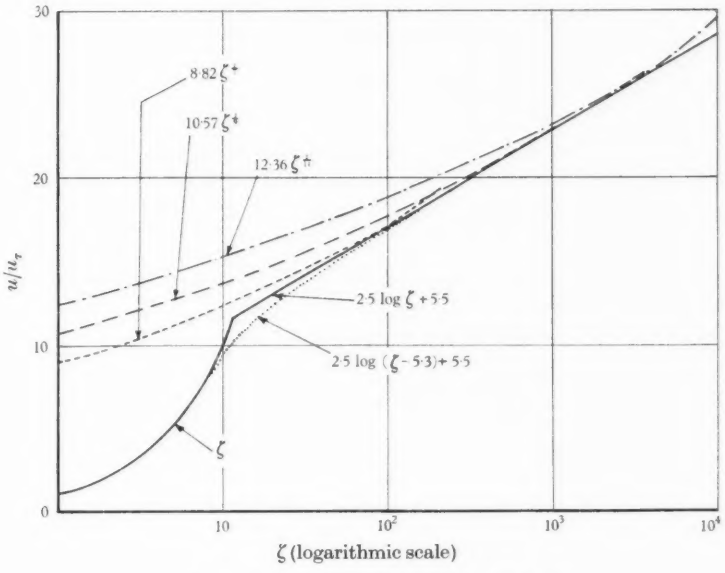

FIGURE 1. Various 'inner' velocity laws.

Replacing Δ in (12) by this value of θ yields the first of the expressions (9) for skin friction. The second, in terms of a Reynolds number based on x, follows it by writing the integral momentum equation as

$$d(\rho_\infty u_\infty \theta/\mu_m)/d(u_\infty x/\nu_m) = (u_\tau/u_\infty)^2$$

and setting $\theta = 0$ when $x = 0$ after integration. The constants C and D are related to K by

$$(n+1)\,C^{\frac{1}{2}(n+1)} = (n+3)\,D^{\frac{1}{2}(n+3)} = n(n+2)^{-1}K^{-n}.$$

The values of C obtained using K from (13) in this relation are listed in table 1, together with values C' corresponding to the accepted incompressible power-law expressions $\frac{1}{2}c_f = C'R_\theta^{-2/(n+1)}$ given in the three cases by von Kármán (1921), Young (1953) and Falkner (1943). The ranges of applicability of the incompressible laws are those suggested by Culick & Hill (1958).

The agreement between the value of C found by the method just described and the accepted value C' is close for the $\frac{1}{5}$th and $\frac{1}{6}$th power-laws, and within 5% for the quarter power-law which holds at the lowest Reynolds number. With slightly different values of K (8·85, 10·50, 12·23, respectively) C could be made to agree exactly with C'. The corresponding power-law velocity curves would still approximate closely to the logarithmic expression over a considerable range of R_θ and might just as well have been chosen in the first place instead of those given by (13).

3. Shear-stress distribution

The equations of continuity and motion are

$$\frac{\partial}{\partial x}(\rho u)+\frac{\partial}{\partial y}(\rho v+\overline{\rho' v'}) = 0, \tag{15}$$

$$\rho u\frac{\partial u}{\partial x}+(\rho v+\overline{\rho' v'})\frac{\partial u}{\partial y} = \frac{\partial \tau}{\partial y}, \tag{16}$$

respectively, where primes denote turbulent fluctuations, bars the time means of their products, and

$$\tau = \mu\frac{\partial u}{\partial y}-\rho\overline{u'v'}$$

is the shear stress. In view of (15) a stream function ψ may be defined by writing

$$\rho_m\frac{\partial \psi}{\partial y} = \rho u, \quad -\rho_m\frac{\partial \psi}{\partial x} = \rho v+\overline{\rho' v'}. \tag{17}$$

Different forms for ψ are appropriate in the inner and outer regions, which we now treat in turn.

3.1. *Inner region*

The stream function may be written

$$\psi = \nu_m G\left(\frac{\eta u_\tau}{\nu_m}\right) = \nu_m G(\zeta) \tag{18}$$

say. Then

$$g(\zeta) = \frac{u}{u_\tau} = G'(\zeta)$$

and (treating ν_m as independent of x, i.e. for a constant temperature wall) the momentum equation (16) becomes

$$-\rho u^2\lambda(x) = \frac{\partial \tau}{\partial y}, \tag{19}$$

where $\lambda(x) = -(d/dx)\log(u_\tau/u_\infty)$. This is the compressible flow version of an expression found in an earlier paper (Spence 1951). On integration

$$\tau/\tau_w = 1-(\nu_m/u_\tau)\lambda(x)\int_0^\zeta [g(\zeta_1)]^2 d\zeta_1. \tag{20}$$

Thus with a knowledge of the universal function g in equation (6) and of the

variation of τ_w with x, the shear stress in the inner part of the layer may be found from (19). The result of integrating the logarithmic expression (7) can be written

$$\int_0^\zeta g^2 d\zeta = \zeta g^2\{1 - Ag^{-1} + O(g^{-2})\}$$

so that for large enough values of $g = u/u_\tau$,

$$\tau/\tau_w \doteqdot 1 - (\nu_m/u_\tau)\lambda(x)\zeta\left(\frac{u}{u_\tau}\right)^2 = 1 - \lambda(x)\eta\left(\frac{u}{u_\tau}\right)^2. \tag{21}$$

3.2. *Outer region*

The velocity law (2) may be written in terms of a stream function

$$\psi = u_\infty \Delta F(\eta/\Delta) = u_\infty \Delta F(\xi) \tag{22}$$

say. In this case $$f(\xi) = \frac{u}{u_\infty} = F'(\xi)$$

and the momentum equation can be written

$$-\Lambda F(\xi)\, F''(\xi) = (\rho_m \Delta/\rho\tau_w)\frac{\partial \tau}{\partial y} = \frac{\partial}{\partial \xi}\left(\frac{\tau}{\tau_w}\right), \tag{23}$$

where $\Lambda = (\rho_m u_\infty^2/\tau_w)(d\Delta/dx)$ may be supposed known. F contains a constant of integration which should strictly be evaluated by equating this value for $\partial\tau/\partial y$ to that given by (20) at the point of contact of the corresponding velocity laws, but as in determining θ/Δ, an adequate approximation is found simply by applying the outer law across the whole layer. Then by (22) $F(0) = 0$ since ψ must be constant on $\xi = 0$, and using the power-law velocity distribution we obtain $F(\xi) = \{n/(n+1)\}\xi^{1+1/n}$. Therefore, integrating (23),

$$1 - \frac{\tau}{\tau_w} = \xi^{1+2/n} = \xi\left(\frac{u}{u_\infty}\right)^2. \tag{24}$$

The coefficient of $\xi^{1+2/n}$ here has been set equal to unity in order to make τ/τ_w vanish at $\xi = 1$. The coefficient is actually $n\Lambda/(n+1)(n+2)$, which equals $(\rho_\infty u_\infty^2/\tau_w)(d\theta/dx)$ by (14), so this is a statement of the integral momentum equation.

The expression (24) is not very different from that which would have been found by using the inner law in the region where it applies, for logarithmic differentiation of (12) shows that

$$\lambda(x) = \{1/(n+1)\Delta\}(d\Delta/dx),$$

whence (21) may be written

$$1 - \frac{\tau}{\tau_w} = \frac{\Lambda}{n+1}\frac{\eta}{\Delta}\left(\frac{u}{u_\infty}\right)^2 = \left(1 + \frac{2}{n}\right)\xi\left(\frac{u}{u_\infty}\right)^2.$$

This is an approximation to (24) if $n \gg 1$.

Finally, (24) may be written in terms of velocity alone as

$$\frac{\tau}{\tau_w} = 1 - \left(\frac{u}{u_\infty}\right)^{n+2}, \tag{25}$$

in which form it will be used in the next section to evaluate the enthalpy distribution

4. Enthalpy distribution in terms of velocity and shear stress

The energy equation may be written

$$\rho u \frac{\partial h}{\partial x} + (\rho v + \overline{\rho' v'}) \frac{\partial h}{\partial y} = \frac{\partial q}{\partial y} + \tau \frac{\partial u}{\partial y}, \tag{26}$$

where h is the static enthalpy, and

$$q = \frac{k}{C_p} \frac{\partial h}{\partial y} - \rho \overline{v' h'}$$

is the heat flux per unit area towards the wall. In forming equation (26) triple products such as $\overline{u'^2 v'}$ have been excluded as is customary. Regarding h and q as functions of u, so that $\partial h/\partial x = (\partial u/\partial x)(dh/du)$, etc., and using the equation of motion (16), the left-hand side of (26) is seen to equal $(\partial \tau/\partial y)(dh/du)$. After dividing through by $\tau(\partial u/\partial y)$ the equation may therefore be written

$$\frac{1}{\tau} \frac{d\tau}{du} \frac{dh}{du} = \frac{1}{\tau} \frac{dq}{du} + 1. \tag{27}$$

An eddy viscosity ϵ and an eddy conductivity κ may now be defined by means of

$$-\rho \overline{u' v'} = \epsilon \frac{\partial u}{\partial y}, \quad -\rho \overline{h' v'} = \frac{\kappa}{C_p} \frac{\partial h}{\partial y}. \tag{28}$$

The laminar and turbulent Prandtl numbers are then

$$\sigma = \mu C_p / k, \quad \alpha = \epsilon C_p / \kappa,$$

respectively. In terms of these the ratio of the molecular contributions to q and τ is, say,

$$q_L / \tau_L = \left(\frac{k}{C_p} \frac{\partial h}{\partial y}\right) \Big/ \left(\mu \frac{\partial u}{\partial y}\right) = \frac{1}{\sigma} \frac{dh}{du},$$

and similarly that of the turbulent contributions (28) is

$$q_T / \tau_T = \frac{1}{\alpha} \frac{dh}{du}.$$

Combining the last two equations,

$$q = q_L + q_T = \left(\frac{\tau_L}{\sigma} + \frac{\tau_T}{\alpha}\right) \frac{dh}{du} = \left\{\frac{\tau}{\alpha} + \left(\frac{1}{\sigma} - \frac{1}{\alpha}\right) \tau_L\right\} \frac{dh}{du}$$

and the energy equation (27) becomes

$$\frac{1}{\tau} \frac{d}{du} \left[\left\{\frac{\tau}{\alpha} + \left(\frac{1}{\sigma} - \frac{1}{\alpha}\right) \tau_L\right\} \frac{dh}{du}\right] - \frac{1}{\tau} \frac{d\tau}{du} \frac{dh}{du} = -1. \tag{29}$$

So far it has not been necessary to make any physical assumptions, and equation (29) is exact. To proceed further we may suppose both σ and α are constant across the layer. The accepted value of σ is about 0·7 for air up to about 1000 °K, and a value of about 0·85 for α will be inferred in §5 from the known values of recovery factor.

4.1. *Integration of the energy equation*

The fact that the viscous contribution to shear stress falls off very rapidly with distance from the wall—in fact exponentially with velocity, decreasing almost to zero in a region of the turbulent core where the total stress is still not much less than τ_w—makes it possible to integrate the last equation in a simple manner. After multiplication through by $\tau^{1-\alpha}$, the equation can be written

$$\frac{d}{du}\left(\tau^{1-\alpha}\frac{dh}{du}\right)+\alpha\tau^{1-\alpha}=-\beta\tau^{-\alpha}\frac{d}{du}\left(\tau_L\frac{dh}{du}\right), \tag{30}$$

where $\beta=(\alpha/\sigma)-1$. In the region where $\tau_L \neq 0$, τ may be treated as constant and equal to τ_w on the right-hand side. Then integrating

$$\left(\frac{\tau}{\tau_w}\right)^{1-\alpha}\frac{dh}{du}-\left(\frac{dh}{du}\right)_w+\alpha\int_0^u\left(\frac{\tau}{\tau_w}\right)^{1-\alpha}du=-\beta\left\{\frac{\tau_L}{\tau_w}\frac{dh}{du}-\left(\frac{dh}{du}\right)_w\right\} \tag{31}$$

and re-arranging,

$$\frac{dh}{du}=\left(\frac{\tau}{\tau_w}\right)^{\alpha-1}\left\{\frac{\alpha}{\sigma}\left(\frac{dh}{du}\right)_w-\int_0^u\left(\frac{\tau}{\tau_w}\right)^{1-\alpha}du\right\}\left\{1-\beta\left(\frac{\tau}{\tau_w}\right)^{\alpha-1}\left(\frac{\tau_L}{\tau_w}\right)+O(\beta^2)\right\}. \tag{32}$$

The result of integrating (32) with respect to u, treating τ again as equal to τ_w in the term involving τ_L, may be written, excluding $O(\beta^2)$, as

$$h(u)-h_w=\frac{u_\infty}{\sigma}\left(\frac{dh}{du}\right)_w\left\{I(f)-(\alpha-\sigma)\frac{u_\tau}{u_\infty}L(g)\right\}-u_\infty^2\left\{K(f)-(\alpha-\sigma)\left(\frac{u_\tau}{u_\infty}\right)^2N(g)\right\}, \tag{33}$$

where for convenience f and g have been written for u/u_∞ and u/u_τ, respectively, and

$$\left.\begin{aligned} I(f)&=\alpha\int_0^f\left(\frac{\tau}{\tau_w}\right)^{\alpha-1}df_1,\\ K(f)&=\alpha\int_0^f\left(\frac{\tau}{\tau_w}\right)^{\alpha-1}df_1\int_0^{f_1}\left(\frac{\tau}{\tau_w}\right)^{1-\alpha}df_2\end{aligned}\right\} \tag{34}$$

and

$$L(g)=\int_0^g\frac{\tau_L}{\tau_w}dg, \quad N(g)=\int_0^g\frac{\tau_L}{\tau_w}g\,dg. \tag{35}$$

On setting $\alpha=\sigma$, we are left in (33) with the well-known Crocco integral for the enthalpy distribution in the laminar boundary layer at zero pressure gradient (which could also have been obtained at once from (32)). To evaluate the last two integrals we may set $\tau_L=\tau_w$ in the sublayer, and obtain the value of $\tau_L=\mu(\partial u/\partial y)$ in the buffer layer by differentiating (7) with $\rho\mu$ constant; this yields

$$\tau_L/\tau_w=1, \quad \exp\left(-\frac{g-\zeta_1}{A}\right),$$

according as $u/u_\tau = g \lesseqgtr \zeta_1 (= 7{\cdot}8)$. Then for $g > \zeta_1$,

$$L = L_0 - \frac{\tau_L}{\tau_w} A, \quad N = N_0 - \frac{\tau_L}{\tau_w} A(g + A), \tag{36}$$

where $$L_0 = \zeta_1 + A = 10{\cdot}3, \quad N_0 = \tfrac{1}{2}L_0^2 + \tfrac{1}{2}A^2 = 56{\cdot}2.$$

Except in the innermost part of the turbulent core we may set $\tau_L/\tau_w = 0$ and simply use the latter values. Values fairly close to these can also be obtained from other recognized interpolations for the buffer-layer profile; for instance, Rannie (1956) has suggested the formula

$$\frac{u}{u_\tau} = (1/\sqrt{\kappa_1}) \tanh (\zeta \sqrt{\kappa_1})$$

with $1/\sqrt{\kappa_1} = 14{\cdot}53$, for incompressible flow in the region $0 < \zeta < 27{\cdot}8$. The corresponding value of τ_L/τ_w is $1 - \kappa_1 (u/u_\tau)^2$, and by integrating up to the point where this vanishes we find $L_0 = 9{\cdot}7$, $N_0 = 52{\cdot}8$. (The less accurate assumption of an abrupt laminar-turbulent interface without a buffer layer at the point where $\zeta = A \log \zeta + B$, i.e. at $\zeta = 11{\cdot}7$, gives $L_0 = 11{\cdot}7$, $N_0 = 68{\cdot}5$.)

4.2. *Recovery factor and heat-transfer coefficient*

Since it gives the enthalpy at the outer edge of the boundary-layer equation (32) provides expressions for the recovery factor, i.e. the fraction of the kinetic energy of the external stream which is recovered as enthalpy at an insulated wall—and for the heat-transfer coefficient. With $u = u_\infty$, and introducing the skin-friction coefficient $c_f = \rho_m u_\tau^2 / \tfrac{1}{2}\rho_\infty u_\infty^2$, (32) becomes

$$h_\infty - h_w = \frac{u_\infty}{\sigma} \left(\frac{dh}{du}\right)_w \left\{ I(1) - (\alpha - \sigma) L_0 \left(\frac{\rho_\infty c_f}{\rho_m 2} \right)^{\frac{1}{2}} \right\} - u_\infty^2 \left\{ K(1) - (\alpha - \sigma) N_0 \frac{\rho_\infty c_f}{\rho_m 2} \right\}. \tag{37}$$

In the case of zero heat transfer $(dh/du)_w = 0$, and h_w equals the recovery enthalpy h_r. The recovery factor is therefore

$$r = (h_r - h_\infty)/\tfrac{1}{2}u_\infty^2 = 2K(1) - \frac{\rho_\infty}{\rho_m} (\alpha - \sigma) N_0 c_f. \tag{38}$$

The inward heat flux at the wall per unit area when $h_w \neq h_r$ is

$$q_w = \left(\frac{k}{C_p} \frac{\partial h}{\partial y} \right)_w = \left(\frac{\mu}{\sigma} \right)_w \left(\frac{\partial u}{\partial y} \right)_w \left(\frac{dh}{du} \right)_w = \frac{\tau_w}{\sigma} \left(\frac{dh}{du} \right)_w.$$

Elimination of h_∞ from (37) and (38) shows that the first term on the right-hand side of (37) is equal to $h_r - h_w$. This value may be used to calculate the Stanton number, defined by

$$1/St = \rho_\infty u_\infty (h_r - h_w)/q_w = (2/c_f) I(1) - (2\rho_\infty/\rho_m c_f)^{\frac{1}{2}} (\alpha - \sigma) L_0. \tag{39}$$

For $\alpha = 1$ we should have $I(1) = 1$, and the right-hand side of (39) reduces for incompressible flow to the form $2/c_f - (2/c_f)^{\frac{1}{2}} \phi(\sigma)$ found by Rannie (1956). If also $\sigma = 1$ the equation becomes simply $St = \tfrac{1}{2}c_f$, which expresses the Reynolds analogy between heat and momentum transfer. In the general case, a Reynolds analogy factor may be defined by the ratio $St/\tfrac{1}{2}c_f$ as calculated from (39).

5. Evaluation of the enthalpy distribution

The distribution of shear stress in terms of velocity as given by (25) may now be used to evaluate the functions $I(f)$, $K(f)$ which occur in the enthalpy-velocity relationship (33). Writing f for u/u_∞, (25) is

$$\tau/\tau_w = 1-f^p,$$

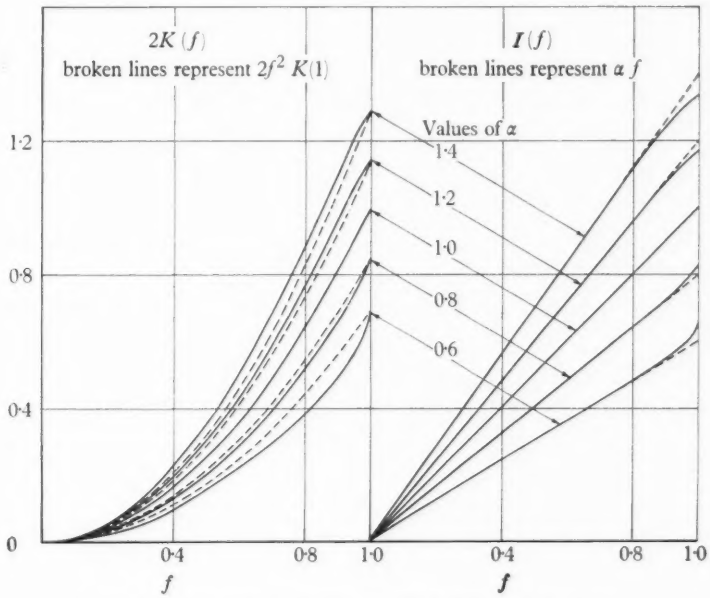

FIGURE 2. $I(f)$ and $2K(f)$ for several values of α ($p = 11$).

where $p = n+2$, and I and K, from (34), are

$$I(f) = \alpha \int_0^f (1-f_1^p)^{\alpha-1}\, df_1,$$

$$K(f) = \alpha \int_0^f (1-f_1^p)^{\alpha-1}\, df_1 \int_0^{f_1} (1-f_2^p)^{1-\alpha}\, df_2.$$

These functions have been computed for $p = 9$, 11 and $\alpha = 0{\cdot}5(0{\cdot}1)1{\cdot}5$. $I(f)$ is an incomplete beta function, but the standard tables do not cover the required range of α and p; the functions were therefore found by quadrature after writing

$$(1-f)^{1-|1-\alpha|} = 1-z, \quad \left(\frac{1-f}{1-f^p}\right)^{|1-\alpha|} = i(z), \quad [(1-f)(1-f^p)]^{|1-\alpha|} = k(z).$$

Then for $\alpha < 1$

$$I(f) = \int_0^{z(f)} i(z_1)\, dz_1, \quad K(f) = \frac{1}{\alpha}\int_0^{z(f)} i(z_1)\, dz_1 \int_0^{z_1} k(z_2)\, dz_2,$$

and for $\alpha > 1$

$$I(f) = \frac{\alpha}{2-\alpha}\int_0^{z(f)} k(z_1)\, dz_1, \quad K(f) = \frac{\alpha}{(2-\alpha)^2}\int_0^{z(f)} k(z_1)\, dz_1 \int_0^{z_1} i(z_2)\, dz_2.$$

A check is provided by the fact that

$$I(1) = \alpha! \left(\frac{1}{p}\right)! \Big/ \left(\alpha + \frac{1}{p} - 1\right)!, \tag{40}$$

which can be found from tables.

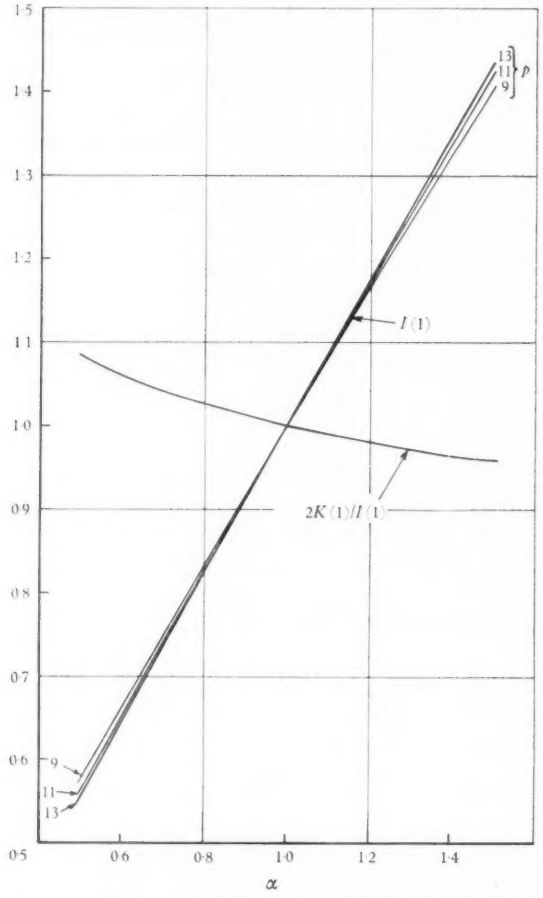

FIGURE 3. The values of $I(1)$ for $p = 9$, 11, 13, and $2K(1)/I(1)$ for $p = 11$.

Figure 2 shows the results for $\alpha = 0{\cdot}6$–$1{\cdot}4$ and $p = 11$ (i.e. for the $\frac{1}{9}$th power velocity profile). The broken lines representing αf and $f^2K(1)$ lie close in all cases to the curves of $I(f)$ and $K(f)$, respectively, and it follows that within the limits imposed by ignoring the terms involving c_f in (33), the enthalpy variation across the boundary layer can be well approximated by a quadratic in velocity, i.e. by

$$h(u) = h_w + (h_r - h_w)\frac{u}{u_\infty} - \tfrac{1}{2}ru^2 \tag{41}$$

over the range of Prandtl numbers (or recovery factors) covered by the computation.

Figure 3 shows the variation with α of $I(1)$. The curves for $p = 9$ and $p = 11$ lie very close together. A curve of $2K(1)/I(1)$ is also shown; in this case the results for $p = 9$ and $p = 11$ were indistinguishable. The variation of $2K(1)/I(1)$ is fairly slow, and its value can be read sufficiently accurately at non-tabular values of α

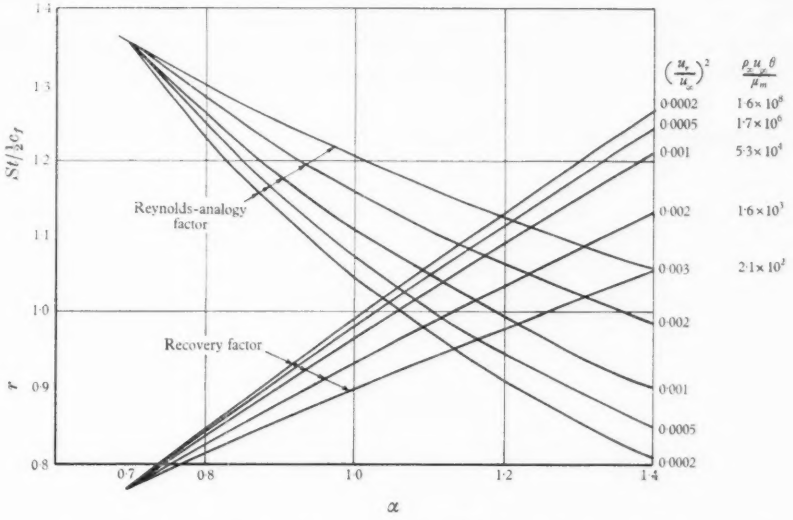

FIGURE 4. Variation of Reynolds analogy factor $St/\frac{1}{2}c_f$ and recovery factor r with α for several values of $(u_\tau/u_\infty)^2$ ($\sigma = 0{\cdot}7$).

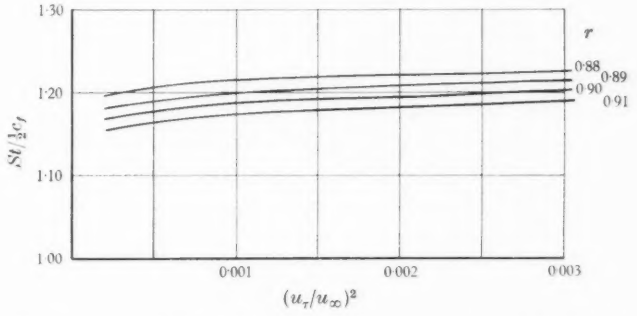

FIGURE 5. Variation of Reynolds analogy factor with $(u_\tau/u_\infty)^2$ for fixed values of recovery factor.

to permit accurate evaluation of $K(1)$, using the exact expression (40) for $I(1)$ at such values. A fairly wide range of Reynolds numbers is probably covered by the case $p = 11$; the values of $I(1)$ and $K(1)$ for this case have therefore been used to express the recovery and Reynolds analogy factors as functions of α for a number of values of $(u_\tau/u_\infty)^2$ (i.e. effectively of boundary layer Reynolds number $\rho_\infty u_\infty \theta/\mu_m$) in figure 4.

As was stated in § 1.5, values of α cannot be found directly from experiment. We do know, however, that for air at Mach numbers up to 8 the recovery factor r lies somewhere between 0·88 and 0·91. The curves of figure 4 have therefore been cross-plotted in figure 5 for constant values of r in this range, to show the variation of the Reynolds analogy factor with $(u_\tau/u_\infty)^2$. The actual magnitude of the factor $St/\frac{1}{2}c_f$ and its decrease when c_f decreases, i.e. when $\rho_\infty u_\infty \theta/\mu_m$ increases, are in good agreement with those found experimentally, which have been reviewed by Seiff (1954). The values of α in the cross-plot are in the range 0·85–0·9.

6. Experimental velocity profiles

6.1. *Outer law*

Figure 6 shows a set of profiles of u/u_∞ against y/δ measured by Lobb *et al.* (1955) at Mach numbers between 4·93 and 8·18 and stagnation temperatures near 300 °K. The $M = 8$ profiles lie near a $\frac{1}{5}$th power law, and those for $M = 5$ near a $\frac{1}{8}$th power law. The effect of the Howarth transformation is illustrated in figure 7 by plotting the profiles with η/Δ as the ordinate. This was found in terms of y/θ by writing

$$y = \int_0^\eta (h/h_m)\, d\eta \tag{42}$$

and using the quadratic enthalpy-velocity relationship (41) with $u/u_\infty = (\eta/\Delta)^{1/n}$. Integrating and inserting θ from (14), the relation

$$\eta/\Delta = (y/\theta)\,[a + b(u/u_\infty) - c(u/u_\infty)^2]^{-1} \tag{43}$$

is obtained, where

$$na = (n+1)\,(n+2)\,(h_w/h_\infty), \quad (n+2)\,b = (h_r - h_w)/h_\infty, \quad (n+1)\,c = (h_r/h_\infty) - 1.$$

The experimental values of y/θ, u/u_∞ and a, b, c (with $n = 9$) were used in (43). As plotted in figure 7 the profiles have collapsed almost entirely to a single curve lying close to the $\frac{1}{9}$th power law. This justifies the use that was made of the law in simplifying the integration with regard to η.

To avoid overcrowding the figure, only five of the profiles measured by Lobb *et al.* are shown. The same collapse to a single curve was, however, obtained with the remaining nine profiles as well.

6.2. *Law of the wall*

The inner parts of the same set of velocity profiles are plotted in the form of u/u_τ against $\eta u_\tau/\nu_m$ in figure 8, which also contains data from tests at the R.A.E. by Monaghan & Cooke (1953). The calculation of η from y by means of (42) is a little more complicated in this case, since it is necessary to take account of the dependence of the enthalpy distribution in the sublayer and buffer layer on τ_L/τ_w, as represented in (33) and (36). The details need not be given here.

The friction velocity was found from the experimental values of $\rho_\infty u_\infty \theta/\mu_m$, using the $\frac{1}{5}$th power-law formula for skin fraction in the form given by (9). The intermediate enthalpy was found from the wall and free-stream values, using Eckert's formula (8) and assuming a recovery factor $r = 0{\cdot}89$.

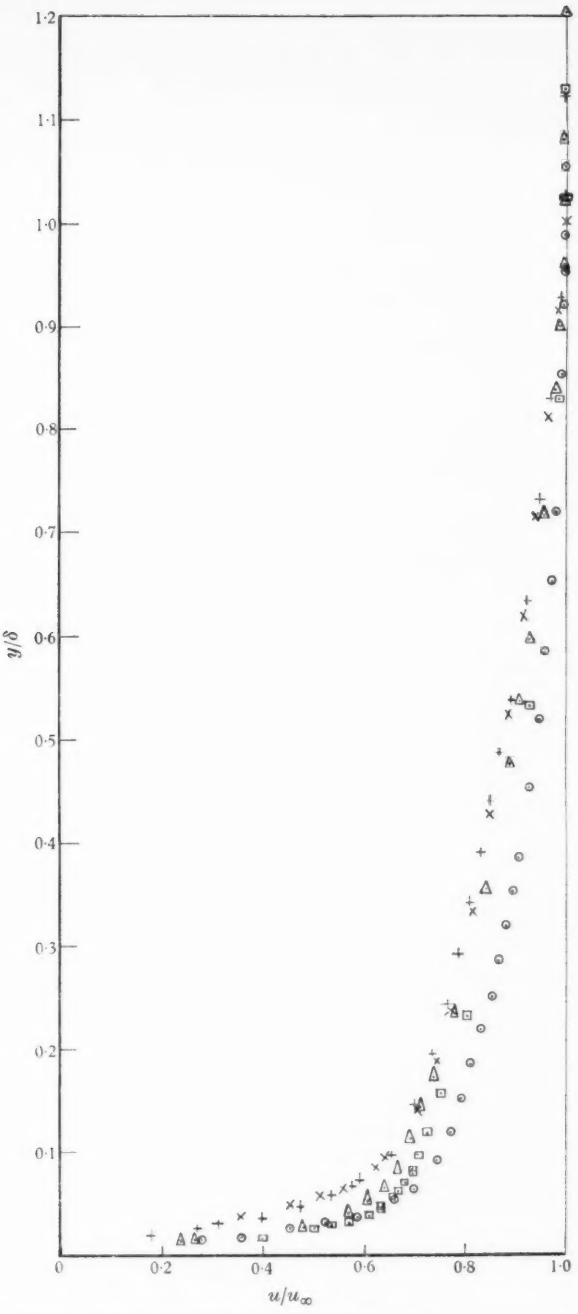

FIGURE 6. N.O.L. velocity profiles in physical co-ordinates. Key:

Symbol	M	$\frac{h_r - h_w}{h_r}$	Symbol	M	$\frac{h_r - h_w}{h_r}$
⊙	4·93	0	+	7·67	0·488
⊡	5·06	0·420	×	8·18	0·495
△	6·83	0·444			

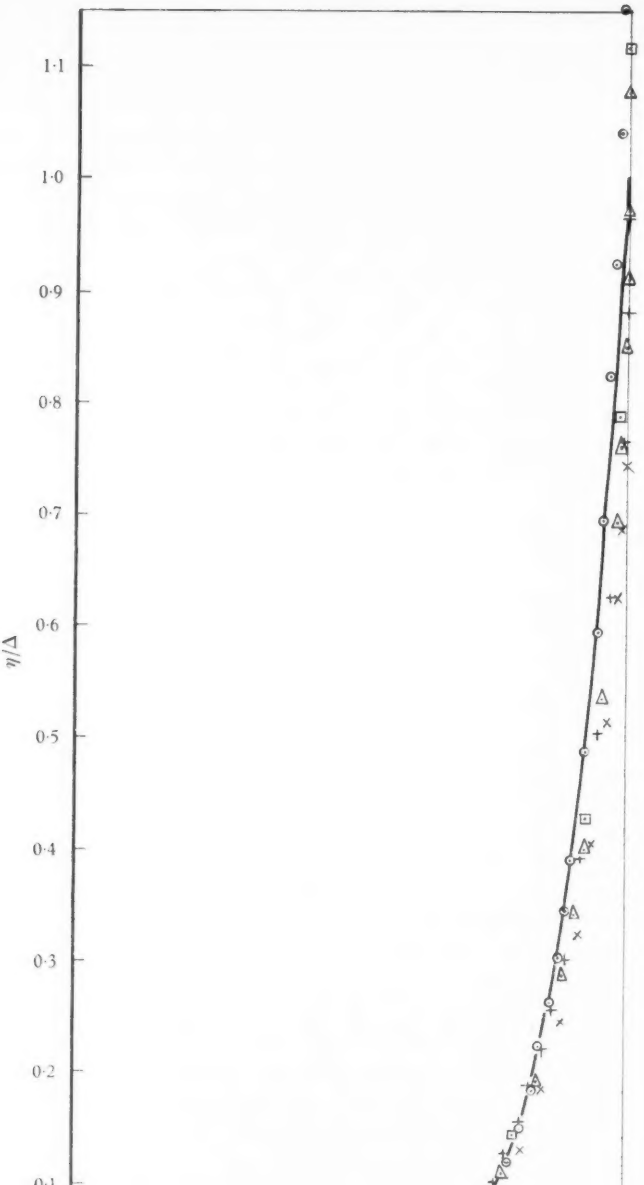

FIGURE 7. N.O.L. velocity profiles in transformed co-ordinates. Symbols as in Figure 6. ——, $u/u_\infty = (n/\Delta)^{\frac{1}{5}}$.

The values of $(u_\tau/u_\infty)^2$ so found agreed well with those published for the R.A.E. data, but with the N.O.L. data there were systematic discrepancies of up to 25 % in the cases with heat transfer. The values of c_f measured by the N.O.L. decrease with wall cooling, which is the opposite tendency to that predicted by the intermediate enthalpy theory. The measured values were obtained (*a*) from the measured heat-transfer rates, assuming the Reynolds analogy factor to be 1·2, and (*b*) from the slopes of the velocity profiles in the sublayer. Neither method is very reliable, and the theoretical values of skin friction corresponding to the

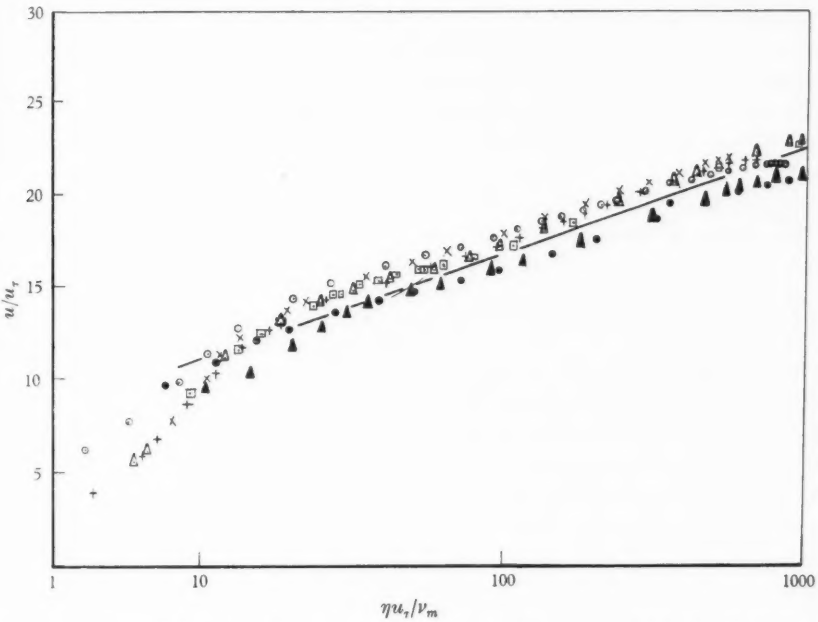

FIGURE 8. Inner behaviour of experimental velocity profiles. ——, $2{\cdot}5 \log (\eta u_\tau/\nu_m) + 5{\cdot}5$. R.A.E. data 13·4 station: ●, with heat transfer; ▲, zero heat transfer. Other symbols as for figures 6 and 7.

observed local Reynolds numbers were preferred in the present analysis to those quoted by Lobb *et al.*, since the bulk of other experimental work tends to support the intermediate enthalpy formula. The collapse to a single profile shown in figure 8 would not have been as complete if u_τ had been based on the quoted values of c_f, although the curves would still lie closer together than when plotted with y, ν_w and a wall-friction velocity $u_{\tau_w} = (\tau_w/\rho_w)^{\frac{1}{2}}$ in place of η, ν_m and u_τ, as in their paper.

There is a small but systematic discrepancy between the data from the two sources as plotted in figure 8, the N.O.L. points all lying a little above the standard curve $u/u_\tau = 2{\cdot}5 \log (\eta u_\tau/\nu_m) + 5{\cdot}5$ and the R.A.E. points somewhat below. This is almost certainly due in part to residual Mach number effects not removed by the transformation, the presence of which would be likely to show since Monaghan

& Cooke worked at about $M = 2$ and Lobb *et al.* at hypersonic speeds. The discrepancy may also reflect the fact that even to-day there is no general agreement among experimental workers on the precise values of the constants A, B in the logarithmic law (see, for example, Table 1.1 of the forthcoming volume *Incompressible Aerodynamics* edited by Thwaites, in which a number of sets of values from the literature are listed). The values $A = 2{\cdot}5$, $B = 5{\cdot}5$ used in this paper are probably the best known. The reason for this measure of disagreement may lie in the fact that some dependence on a Reynolds number such as $u_\infty \delta/\nu_\infty$ should strictly be included in the inner law; but in part no doubt it also arises from the difficulty of measuring skin friction accurately.

In a recent note Yasuhara (1959) has attempted a correlation of some experimental profiles in terms of a defect law of the form $(u_\infty - u)/u_\tau$ as a function of η/Δ. The fact that this was not very successful may also have been due to uncertainty about the skin friction.

7. Concluding remarks

From the evidence of figures 6 and 7 there seems little doubt that the method of collapsing the outer four-fifths or so of the velocity profiles as a function of η/Δ is valid, and this justifies *a posteriori* the calculations of the shear stress and enthalpy distributions in §§3 and 4. Other investigators have remarked on the fact that the index n in the approximating power law $(y/\delta)^{1/n}$ decreases with Mach number—as shown in figure 6—but this change in n is conveniently removed by the present transformation. This result, and the further fact that the enthalpy-velocity relation is approximately quadratic, can be used empirically to treat more complicated boundary-layer flows as well: for instance, the relation between the compressible and incompressible values H and H_i, say, of the form parameter δ^*/θ, is found from (2) and (41) to be

$$H = (h_w/h_\infty)\, H_i + (h_r/h_\infty) - 1, \tag{44}$$

and this equation has been used (Spence 1960) to calculate the growth of the boundary layer in a pressure gradient by an extension of the methods available for incompressible flow.

The uncertainty about the skin friction in the N.O.L. tests make the validity of the inner law (7) less certain than that of the outer law. One can certainly draw the more limited conclusion that if u_τ is defined from the value of τ_w predicted by equation (9), irrespective of whether this is correct, then u/u_τ is somewhere near the standard logarithmic function of $\eta u_\tau/\nu_m$ given by (7). This on its own, however, is not a very tidy result, for if $\rho_m u_\tau^2$ so defined were not in fact equal to the wall shearing stress, the profile in the sublayer could not be written $u/u_\tau = \eta u_\tau/\nu_m$ as in equation (5), and the reasoning leading to the functional form $u/u_\tau = g(\eta u_\tau/\nu_m)$ in the logarithmic region would no longer apply.

It was also assumed in deriving this expression that the density-viscosity law could be approximated for constant pressure by $\rho\mu =$ constant, i.e. excluding effects of dissociation by $\mu \propto T$. This might at first sight seem to rule out hypersonic flows at the extreme stagnation enthalpies typical of re-entry. But the relation can always be taken in this form over a suitably restricted range of

temperatures, and as table 2 shows, the width of the range over which a single constant of proportionality could be used becomes surprisingly wide at high temperatures. The table is constructed from the results for dry air calculated by Hirschfelder *et al.* (1955). The assumption is clearly satisfactory for the temperatures between 100 and 300 °K covered by both sets of data analysed, and

T (°K)	100	200	300	500	1000	2000	3000	5000
$\mu/T \times 10^7$ (g/cm sec °K)	7·02	6·68	6·17	5·36	4·26	3·34	2·90	2·41

TABLE 2

should work moderately well, at least across the sublayer, to which the viscous effects are mainly confined even for wall temperature as high as 1000 °K. Since the viscosity enters the expression for skin friction only to a small power, this will not be greatly in error. But the use of the intermediate enthalpy formula would of course be highly speculative at such temperatures, and departures from the inner law might well become more marked. On the other hand, there is no particular reason to expect the outer law to break down at higher temperatures, since it does not depend on viscosity; but the conclusions drawn from it regarding the enthalpy distribution might be slightly modified by the variation of specific heat and Prandtl number.

REFERENCES

CLAUSER, F. H. 1956 *Advances in Applied Mechanics. IV*, 1. New York: Academic Press.

COLES, D. 1956 *J. Fluid Mech.* **1**, 191.

CULICK, F. E. C. & HILL, J. A. F. 1958 *J. Aero. Sci.* **25**, 259.

ECKERT, E. R. G. 1955 *J. Aero Sci.* **22**, 585.

FALKNER, V. M. 1943 *Aircr. Engr.* **15**, 169.

HIRSCHFELDER, J. O., BIRD, R. B., CURTISS, C. F. & SPOTZ, E. L. 1955 Section D of *Thermodynamics and Physics of Matter* (Table D7*d*) (F. D. Rossini, editor). Princeton University Press.

LOBB, R. K., WINKLER, E. M. & PERSH, J. 1955 *J. Aero. Sci.* **22**, 1.

MATTING, F. W., CHAPMAN, D. R., NYHOLM, J. R. & THOMAS, A. G. 1959 *Proc. Heat Trans. and Fluid Mech. Inst., Los Angeles*, p. 80.

MONAGHAN, R. J. & COOKE, J. R. 1953 *Aero. Res. Coun.* C.P. no. 140.

RANNIE, W. D. 1956 *J. Aero. Sci.* **23**, 485.

RUBESIN, M. W. 1953 *Nat. Adv. Com. Aeron., Tech. Note* 2917.

SEIFF, A. 1954 *Nat. Adv. Com. Aeron., Tech. Note* 3284.

SPENCE, D. A. 1951 *Aero Res. Coun. Rep.* 14162 (see also, *J. Aero. Sci.* 1956, **23**, 3).

SPENCE, D. A. 1960 *R. & M. Aero. Res. Coun., Lond.*, no. 3191.

SQUIRE, H. B. 1948 *Phil. Mag.* (7), **39**, 1.

VAN DRIEST, E. R. 1955 *Proc. Heat Trans. and Fluid Mech. Inst., Los Angeles*, paper XII.

VON KÁRMÁN, TH. 1921 *Z. angew Math. Mech.* **1**, 237.

YOUNG, A. D. 1953 *Rep. Coll. Aero. Cranfield*, no. 73.

YASUHARA, M. 1959 *J. Aero/Space Sci.* **26**, 528.

Flow between torsionally oscillating disks

By S. ROSENBLAT
Department of Mathematics, King's College, London

(Received 4 November 1959)

Two parallel infinite plane disks, between which is contained a viscous fluid, oscillate torsionally about a common axis. Of specific interest are the cases where (i) one disk only is in motion, and (ii) the disks oscillate 180° out of phase, but with the same frequency and amplitude. The basic parameter is found to be the Reynolds number derived from the frequency, the kinematic viscosity and the disk separation. Solutions of the Navier–Stokes equations for both small and large Reynolds numbers are developed and the transverse and radial-axial flows investigated.

1. Introduction

In a recent paper (Rosenblat 1959) the author examined the flows resulting from the small torsional oscillations of an infinite disk in a viscous fluid otherwise unbounded and at rest. It was found that linearizing expansions depending on the smallness of the oscillation amplitude were insufficient to describe one of the velocity components, namely, the mean steady radial-axial component. This was essentially because the method does not allow for the fact that non-linear inertia terms predominate outside a thin boundary layer, though they are negligible within it.

As a sequel, the present paper investigates the analogous problem in which the fluid is now bounded by a second, parallel disk at a given distance. Two cases only are studied: (i) when one disk performs small torsional oscillations and the other is at rest; and (ii) when both disks oscillate with the same amplitude and frequency, though with a phase difference of 180°.

Commencing with the Navier–Stokes equations, we seek solutions on the assumption that certain non-linear inertia terms may be omitted. It is found that, unlike in the above-mentioned problem, such solutions are in fact obtainable with all boundary conditions satisfied. Moreover, it is subsequently shown that the approximate method is valid provided a single condition relating the amplitude of the oscillation with the Reynolds number of the flow holds.

Although exact solutions can be developed throughout they prove cumbersome, and approximations for low and high Reynolds number are more convenient. The former apply for $R < 10$ in case (i) and $R < 40$ in case (ii); the latter for $R > 20$ and $R > 80$, respectively.

Transverse velocities are first calculated and are seen to have a boundary-layer character at large R. The rotational motion of the disks gives rise to centrifugal forces which in turn cause the fluid to be thrown radially outwards. Hence

a radial-axial flow is set up which has a mean steady component as well as a fluctuating component. The behaviour of the steady term is of particular interest and is fully discussed.

In order to balance the fluid expelled by centrifugal action a radial inflow between the disks is required. Hence a radial pressure gradient is induced which maintains this flow. It is found from the equations of motion to act inwards and to be constant. At high Reynolds numbers it is the dominant factor outside the boundary layers so that the flow there has a Poiseuille-type profile.

The case of large amplitude oscillations is not considered here. In the limit as the amplitude becomes infinite the problem becomes that studied by Batchelor (1951) and Stewartson (1953), where two parallel disks rotate steadily about a common axis. Some formal comparison of results may therefore be made.

2. One disk oscillating

Consider a body of fluid bounded by two parallel disks which are represented by the planes $z = 0$ and $z = d$ in a cylindrical polar co-ordinate system. The axis $r = 0$, perpendicular to the disks, is the axis about which they may perform torsional oscillations. If u, v and w be respectively the radial, transverse and axial velocity components, p the pressure, ρ the density and ν the kinematic viscosity, then the Navier–Stokes equations of motion are

$$\frac{\partial u}{\partial t}+u\frac{\partial u}{\partial r}+w\frac{\partial u}{\partial z}-\frac{v^2}{r}=-\frac{1}{\rho}\frac{\partial p}{\partial r}+\nu\left[\frac{\partial^2 u}{\partial r^2}+\frac{1}{r}\frac{\partial u}{\partial r}-\frac{u}{r^2}+\frac{\partial^2 u}{\partial z^2}\right], \tag{1}$$

$$\frac{\partial v}{\partial t}+u\frac{\partial v}{\partial r}+w\frac{\partial v}{\partial z}+\frac{uv}{r}=\nu\left[\frac{\partial^2 v}{\partial r^2}+\frac{1}{r}\frac{\partial v}{\partial r}-\frac{v}{r^2}+\frac{\partial^2 v}{\partial z^2}\right], \tag{2}$$

$$\frac{\partial w}{\partial t}+u\frac{\partial w}{\partial r}+w\frac{\partial w}{\partial z}=-\frac{1}{\rho}\frac{\partial p}{\partial z}+\nu\left[\frac{\partial^2 w}{\partial r^2}+\frac{1}{r}\frac{\partial w}{\partial r}+\frac{\partial^2 w}{\partial z^2}\right], \tag{3}$$

while the equation of continuity is

$$\frac{1}{r}\frac{\partial}{\partial r}(ru)+\frac{\partial w}{\partial z}=0. \tag{4}$$

We take the disk $z = 0$ to perform torsional oscillations of frequency n and angular speed Ω, while the disk $z = d$ remains at rest. The boundary conditions are then

$$\left.\begin{aligned} &u = w = 0, \quad v = r\Omega e^{int} \quad \text{on} \quad z = 0,\\ &u = v = w = 0 \quad \text{on} \quad z = d. \end{aligned}\right\} \tag{5}$$

Equations (1)–(5) can be satisfied by writing

$$\left.\begin{aligned} &v = r\Omega e^{i\tau}g(y), \quad u = \frac{r\Omega^2}{n}\frac{\partial F}{\partial y}(y,\tau), \quad w = -2d\frac{\Omega^2}{n}F(y,\tau),\\ &p/\rho = \Omega^2 d^2 P(y,\tau)+\tfrac{1}{2}\Omega^2 r^2 K(\tau), \quad y = z/d, \quad \tau = nt. \end{aligned}\right\} \tag{6}$$

That is, we seek a solution in which the radial and transverse velocities are linear functions of r. The equations of motion then establish the required form of the pressure, with $P(y,\tau)$ and $K(\tau)$ unknown functions of the variables indicated.

On substitution from (6), equations (1) and (2) become

$$\frac{\partial^2 F}{\partial y\,\partial \tau}+\left(\frac{\Omega}{n}\right)^2\left[\left(\frac{\partial F}{\partial y}\right)^2-2F\frac{\partial^2 F}{\partial y^2}\right]-(g\,e^{i\tau})^2=-K(\tau)+\frac{1}{R}\frac{\partial^3 F}{\partial y^3} \tag{7}$$

and

$$ig+2\left(\frac{\Omega}{n}\right)^2\left[g\frac{\partial F}{\partial y}-F\frac{dg}{dy}\right]=\frac{1}{R}\frac{d^2 g}{dy^2}, \tag{8}$$

where

$$R\equiv nd^2/\nu \tag{9}$$

is the Reynolds number of the flow. The boundary conditions (5) become

$$\left.\begin{aligned} F=\frac{\partial F}{\partial y}=0,\quad g=1\quad \text{on}\quad y=0,\\ F=\frac{\partial F}{\partial y}=g=0\quad \text{on}\quad y=1. \end{aligned}\right\} \tag{10}$$

Equation (3) reduces to

$$2\frac{\partial F}{\partial \tau}-4\left(\frac{\Omega}{n}\right)^2 F\frac{\partial F}{\partial y}=\frac{\partial P}{\partial y}+\frac{2}{R}\frac{\partial^2 F}{\partial y^2} \tag{11}$$

and serves merely to determine the axial pressure gradient.

Transverse component

On the assumption that the amplitude of the oscillations, i.e. Ω/n, is small, it appears permissible to neglect to first-order the non-linear convection terms in (7), (8) and (11), though retaining the non-linear centrifugal term $(ge^{i\tau})^2$. (Some remarks concerning the validity of this assumption will be made later.) For the transverse flow we then have to solve

$$\frac{d^2 g}{dy^2}-iRg=0$$

with $g(0)=1$ and $g(1)=0$. The solution is

$$g=\frac{\sinh\sqrt{(iR)}\,(1-y)}{\sinh\sqrt{(iR)}}. \tag{12}$$

Equation (12) leads to, in real notation,

$$\frac{v}{r\Omega}=\frac{\begin{aligned}&[\cos\sqrt{(\tfrac{1}{2}R)}\,y\cosh\sqrt{(\tfrac{1}{2}R)}\,(2-y)-\cos\sqrt{(\tfrac{1}{2}R)}\,(2-y)\cosh\sqrt{(\tfrac{1}{2}R)}\,y]\cos nt\\&+[\sin\sqrt{(\tfrac{1}{2}R)}\,y\sinh\sqrt{(\tfrac{1}{2}R)}\,(2-y)-\sin\sqrt{(\tfrac{1}{2}R)}\,(2-y)\sinh\sqrt{(\tfrac{1}{2}R)}\,y]\sin nt\end{aligned}}{\cosh\sqrt{(2R)}-\cos\sqrt{(2R)}}. \tag{13}$$

Expanding this for small values of the Reynolds number, we get

$$\frac{v}{r\Omega}=(1-y)\left\{\left[1-\frac{R^2}{360}y(8+8y-12y^2+3y^3)\right]\cos nt+\frac{R}{6}y\,(2-y)\sin nt\right\}+O(R^3), \tag{14}$$

with amplitude approximately

$$\frac{|v|}{r\Omega}\approx(1-y)\left[1-\frac{R^2}{180}y(2-y)\,(2-2y+y^2)\right] \tag{15}$$

and phase angle

$$\tan^{-1} \tfrac{1}{6} Ry(2-y). \tag{16}$$

For large R, (13) becomes

$$\frac{v}{r\Omega} \sim e^{-\sqrt{(\frac{1}{2}R)}y} \cos\left(nt - \sqrt{(\tfrac{1}{2}R)}\, y\right), \tag{17}$$

the well-known shear-layer solution, whose magnitude is

$$\frac{|v|}{r\Omega} = e^{-\sqrt{(\frac{1}{2}R)}y}. \tag{18}$$

Numerical evaluation of $|v|/r\Omega$ from (13), (15) and (18) for various values of R indicates that the approximation (15) is valid for $R < 10$, and the asymptotic form (18) for $R > 20$. Curves illustrating $|v|/r\Omega$ for $R = 5$, 50 and 200 are given in figure 1, the first derived from (15), the two latter from (18).

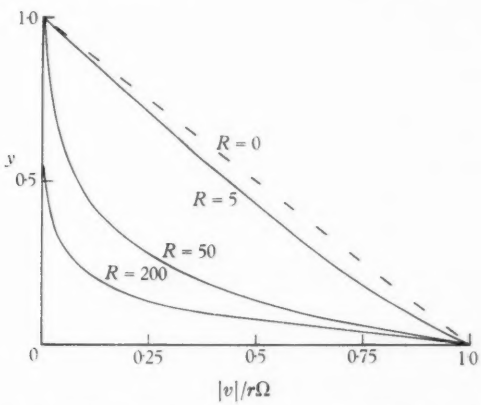

FIGURE 1. One disk oscillating: amplitude of transverse velocity $|v|/r\Omega$ for $R = 5$, 50, 200.

We see that for small Reynolds numbers the fluid has transverse motion for all $0 \leqslant y \leqslant 1$. In the limit $R \to 0$, the velocity profile is linear in y (the broken line in figure 1) with zero-phase angle. For non-zero R, the profile assumes the form of a polynomial in y, and the fluid acquires a phase lag with respect to the oscillations of the plate. The curve $R = 5$ shows that $|v|/r\Omega$ decreases with increasing R; at the same time this decrease is less for small y than for large y. That is, there is already a trend towards concentration of the moving fluid near the oscillating plate.

At about $R = 50$, a boundary layer adjacent to the rotating disk becomes apparent, and its thickness has order of magnitude

$$y \sim \frac{1}{\sqrt{R}} = \frac{1}{d}\sqrt{\frac{\nu}{n}} \quad \text{or} \quad z \sim \frac{d}{\sqrt{R}} = \sqrt{\frac{\nu}{n}}. \tag{19}$$

Thus for large R the presence of the stationary disk has no effect on the transverse motion whose velocity profile is exactly that in the case of a single disk in an otherwise unbounded fluid.

From equation (14), the skin friction for small R on the disk $z = 0$ is

$$\mu\left(\frac{\partial v}{\partial z}\right)_{z=0} \approx -\frac{\mu r\Omega}{d}\left[\left(1+\frac{R^2}{45}\right)\cos nt - \frac{R}{3}\sin nt\right] \tag{20}$$

and on the disk $z = d$ is

$$\mu\left(\frac{\partial v}{\partial z}\right)_{z=d} \approx -\frac{\mu r\Omega}{d}\left[\left(1-\frac{7R^2}{360}\right)\cos nt + \frac{R}{6}\sin nt\right]. \tag{21}$$

When $R \to 0$, the shearing forces are equal on the two disks. As R increases, the shear on the rotating disk increases in magnitude, while that on the stationary disk decreases.

Similarly for large R, from equation (17)

$$\mu\left(\frac{\partial v}{\partial z}\right)_{z=0} \sim -\frac{\mu r\Omega}{d}\sqrt{\frac{R}{2}}\,(\cos nt - \sin nt) \tag{22}$$

and

$$\mu\left(\frac{\partial v}{\partial z}\right)_{z=d} \sim -\frac{\mu r\Omega}{d}\sqrt{(2R)}\,e^{-\sqrt{(\frac{1}{2}R)}} \cong 0. \tag{23}$$

Steady radial-axial component

Reverting to equation (7), we see that the radial-axial flow will be given by

$$\frac{\partial^2 F}{\partial y\,\partial \tau} - (g\,e^{i\tau})^2 = -K(\tau) + \frac{1}{R}\frac{\partial^3 F}{\partial y^3}, \tag{24}$$

provided the non-linear convective terms can again be neglected. From (12) we obtain

$$(g\,e^{i\tau})^2 = \frac{1}{2}\left[\frac{\cosh\lambda y_1 - \cos\lambda y_1}{\cosh\lambda - \cos\lambda}\right] + \frac{1}{2}\left[\frac{\cosh(1+i)\lambda y_1 - 1}{\cosh(1+i)\lambda - 1}\right]e^{2i\tau}, \tag{25}$$

where

$$\lambda \equiv \sqrt{(2R)}, \quad y_1 = 1 - y.$$

This suggests that there are solutions of the form

$$F(y,\tau) = f(y) + h(y)\,e^{2i\tau} \tag{26}$$

and

$$K(\tau) = K_0 + K_1 e^{2i\tau}. \tag{27}$$

Substitution of (25)–(27) into (24) yields

$$\frac{2}{\lambda^2}\frac{d^3 f}{dy^3} = K_0 - \frac{1}{2}\left[\frac{\cosh\lambda y_1 - \cos\lambda y_1}{\cosh\lambda - \cos\lambda}\right] \tag{28}$$

and

$$\frac{2}{\lambda^2}\frac{d^3 h}{dy^3} - 2i\frac{dh}{dy} = K_1 - \frac{1}{2}\left[\frac{\cosh(1+i)\lambda y_1 - 1}{\cosh(1+i)\lambda - 1}\right]. \tag{29}$$

The boundary conditions are

$$\left.\begin{aligned} f = f' = 0 \quad &\text{on} \quad y = 0 \quad \text{and} \quad y = 1, \\ h = h' = 0 \quad &\text{on} \quad y = 0 \quad \text{and} \quad y = 1. \end{aligned}\right\} \tag{30}$$

The above equations indicate that the radial-axial flow has a mean steady component and a fluctuating component of frequency twice that of the oscillating plate. The radial pressure gradient is similarly compounded of two such terms.

The solution of (28) for the mean steady component is found to be

$$f(y) = \frac{1}{(\cosh\lambda - \cos\lambda)}\left[\frac{1}{4\lambda}(\sinh\lambda y_1 + \sin\lambda y_1) - \frac{1}{4\lambda}(\sinh\lambda + \sin\lambda)(1 - 3y^2 + 2y^3)\right.$$
$$\left. + \tfrac{1}{4}(\cosh\lambda + \cos\lambda)\, y(1 - 2y + y^2) - \tfrac{1}{2}y^2(1-y)\right], \quad (31)$$

$$f'(y) = \frac{1}{(\cosh\lambda - \cos\lambda)}\left[-\tfrac{1}{4}(\cosh\lambda y_1 + \cos\lambda y_1) + \frac{3}{2\lambda}(\sinh\lambda + \sin\lambda)\, y(1-y)\right.$$
$$\left. + \tfrac{1}{4}(\cosh\lambda + \cos\lambda)(1 - 4y + 3y^2) - \tfrac{1}{2}y(2-3y)\right] \quad (32)$$

with
$$K_0 = \frac{3}{\lambda^3}\left[\frac{2\lambda + \lambda(\cosh\lambda + \cos\lambda) - 2(\sinh\lambda + \sin\lambda)}{\cosh\lambda - \cos\lambda}\right]. \quad (33)$$

With λ and y_1 replaced by $\sqrt{(2R)}$ and $1-y$, these expressions reduce to, for small Reynolds numbers,

$$f \approx \frac{R}{120}y^2(1-y)^2(3-y) + O(R^3), \quad (34)$$

$$f' \approx \frac{R}{120}y(1-y)(6 - 15y + 5y^2) + O(R^3) \quad (35)$$

and
$$K_0 \approx \tfrac{3}{20} + O(R^2). \quad (36)$$

For large R the corresponding approximations are

$$f \sim \tfrac{1}{4}y(1-y)^2 - \frac{1}{4\sqrt{(2R)}}(1-y)^2(1+2y) + \frac{1}{4\sqrt{(2R)}}\, e^{-\sqrt{(2R)}\,y}, \quad (37)$$

$$f' \sim \tfrac{1}{4}(1-y)(1-3y) + \frac{3}{2\sqrt{(2R)}}\, y(1-y)\,\tfrac{1}{4}\, e^{-\sqrt{(2R)}\,y} \quad (38)$$

and
$$K_0 \sim \frac{3}{R}\left(\frac{1}{2} - \frac{1}{\sqrt{(2R)}}\right). \quad (39)$$

These solutions are illustrated in figures 2 and 3. Figure 2 depicts schematically a typical streamline of the radial-axial steady flow at each of the selected Reynolds numbers $R = 5$, 50, 200; figure 3 shows the dimensionless radial velocity $f' \equiv nu/r\Omega^2$. When $R = 5$, $f' = 0$ at $y = 0{\cdot}47$ and the curves for $y < 0{\cdot}47$ and $y > 0{\cdot}47$ have almost the same shape. As R increases, however, there is a marked departure from this symmetry. When $R = 200$ we see that u is positive for $y < 0{\cdot}38$, where both centrifugal force and pressure gradient are active. In this region the exponential term in (38) is of the same order of magnitude as the first term and the profile is of the boundary-layer type. For $y > 0{\cdot}38$ it is seen from figure 1 that the centrifugal force is vanishingly small, and the flow near the stationary disk behaves essentially like Poiseuille flow with the pressure gradient (39).

It is important to note here that a solution for the steady radial-axial flow has been obtainable in which inertia terms are neglected, and yet all the boundary conditions are satisfied. Such a solution could not be found in the single-disk problem (Rosenblat 1959). An examination of the behaviour at high Reynolds numbers throws light on the contrasting features of the two problems.

In both cases centrifugal force, acting within a boundary layer of thickness $\sqrt{(\nu/n)}$, causes fluid to be thrown radially outwards. As compensation, fluid is drawn inwards along the axis towards the moving disk. In the single-disk case, the quantity of fluid required for this purpose can be obtained in a purely axial motion from, in effect, a source at infinity whose strength is determined by continuity considerations. Hence no radial flow takes place at large z, and there

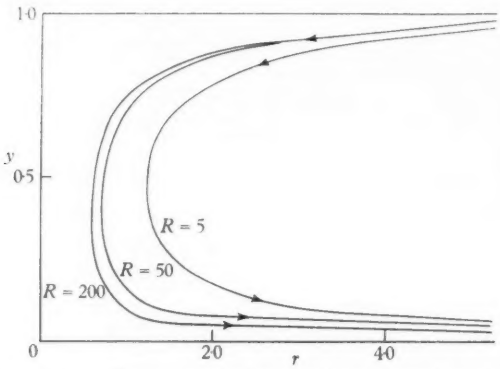

FIGURE 2. One disk oscillating: typical streamlines of steady radial-axial flow for $R = 5, 50, 200$.

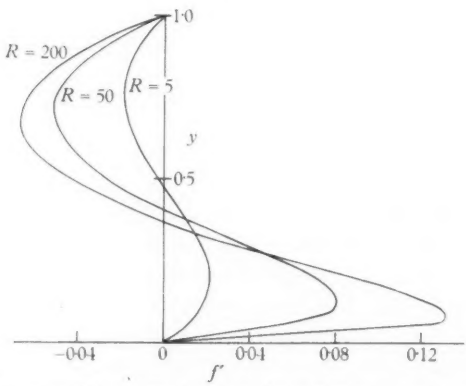

FIGURE 3. One disk oscillating: steady radial velocity $f' = nu_s/r\Omega^2$ for $R = 5, 50, 200$.

is no radial pressure gradient. When a second disk is present, however, the condition $w = 0$ on $z = d$ has to be satisfied. Consequently the fluid thrown radially outwards near the oscillating disk must be balanced by fluid sucked radially inwards. To maintain this inward flow, a radial pressure gradient is induced.

Again in the single-disk problem the centrifugal force is zero outside the boundary layer. The hitherto-neglected inertia terms become comparable in magnitude with the viscous term and hence important. The result is the formation

of a second boundary layer within which the steady radial flow takes place. In the present problem, on the other hand, although outside the boundary layer the non-linear inertia terms are again large compared with the vanishingly small centrifugal force, they are still negligible in relation to the radial pressure gradient which now dominates (in general, see later). Hence the boundary conditions are satisfied and there is no second layer formed.

Fluctuating radial-axial flow

Equation (29) yields the time-dependent component of the radial-axial flow. For low Reynolds numbers the solution is found to be

$$h = \frac{R}{120} y^2(1-y)^2 \left[(3-y) - \frac{iR}{120}(29+167y-150y^2+30y^3)\right] + O(R^3), \tag{40}$$

$$h' = \frac{R}{120} y(1-y) \times \left[(6-15y+5y^2) - \frac{iR}{120}(58+385y-143y^2+1050y^3-210y^4)\right] + O(R^3) \tag{41}$$

and

$$K_1 = \frac{3}{20} - \frac{109iR}{4200} + O(R^2). \tag{42}$$

For high R we obtain

$$8i(2-\sqrt{(2iR)})\,h \sim \frac{(\sqrt{2}-2)(\sqrt{(2iR)}-1)}{\sqrt{(2iR)}} - (\sqrt{2}-2)\,y + \frac{(2-\sqrt{(2iR)})}{\sqrt{(iR)}} e^{-2\sqrt{(iR)}\,y} + \frac{(2\sqrt{(2iR)}-2-\sqrt{2})}{\sqrt{(2iR)}} e^{-\sqrt{(2iR)}\,y} + \frac{(\sqrt{2}-2)}{\sqrt{(2iR)}} e^{-\sqrt{(2iR)}(1-y)}, \tag{43}$$

$$8i(2-\sqrt{(2iR)})\,h' \sim 2-\sqrt{2}-2(2-\sqrt{(2iR)})\,e^{-2\sqrt{(iR)}\,y} - (2\sqrt{(2iR)}-2-\sqrt{2})\,e^{-\sqrt{(2iR)}\,y} + (\sqrt{2}-2)\,e^{-\sqrt{(2iR)}(1-y)} \tag{44}$$

and

$$K_1 \sim \frac{2-\sqrt{2}}{4(\sqrt{(2iR)}-2)}. \tag{45}$$

The principal feature of this component of the flow is that at high Reynolds numbers a boundary layer forms near the stationary disk as well as near the rotating disk—in contrast to the steady component. This arises from the last term in equation (44). When y is nearly 1, (44) reduces to

$$h' \sim \frac{(\sqrt{2}-2)}{8i(\sqrt{(2iR)}-2)}\,[1-e^{-\sqrt{(2iR)}(1-y)}],$$

a typical boundary-layer profile, which is very similar to the solution for flow in a pipe under a periodic pressure gradient (Schlichting 1955, p. 199). In both cases the formation of a boundary layer is due to the fact that the vorticity diffusing away from the wall is constantly changing in sign.

Outside the two layers the velocity—given then by the first term of (44)—is independent of y, since only the constant pressure gradient is there active.

Remarks

Finally, we examine the permissibility of neglecting the inertia terms of equations (7) and (8), with particular reference to flow at high Reynolds numbers. From (38) and (39) it is seen that for large $R, f' = O(1)$ and $K_0 = O(1/R)$. Therefore

the term $(\Omega/n)^2 f'^2$ which occurs in equation (7) would appear to be small compared with the linear terms if

$$(\Omega/n)^2 \ll 1/R.$$

Since $1/\sqrt{R} = (1/d)\sqrt{(\nu/n)}$, and Ω/n is the amplitude of the disk's oscillations, we can say that equation (28) for f and f' is a valid approximation provided that

$$\left.\begin{aligned} \text{amplitude of oscillations} &\ll \frac{\text{boundary-layer thickness}}{\text{distance between disks}}, \\ \frac{\Omega}{n} &\ll \sqrt{\frac{\nu}{n}}\Big/ d. \end{aligned}\right\} \tag{46}$$

An alternative way of expressing this condition is as follows. Since by equation (6) the steady radial component is $u_s = (r\Omega^2/n) f'$, the rate of convection by the radial flow through a typical distance r is Ω^2/n. Also the rate at which vorticity diffuses through a distance d is ν/d^2. Hence (46) is equivalent to

$$\left.\begin{aligned} &\text{rate of convection by } u_s \ll \text{rate of diffusion through distance } d, \\ \text{i.e.} \quad &\Omega^2/n \ll \nu/d^2. \end{aligned}\right\} \tag{47}$$

The right-hand side of (47) represents the influence of the second disk. If this is absent, $d \to \infty$, $\nu/d^2 \to 0$ so that convection is always significant—analogous to the result obtained in the single-disk problem. In the present case inertia need be included only if (46) or (47) is not satisfied. We would then have to solve a complicated non-linear equation very similar to that encountered by Batchelor (1951) and Stewartson (1953) for the steadily rotating disks.

These difficulties arise only for the steady radial-axial component of velocity. For it is quickly seen that linearization of the equations determining the transverse and fluctuating radial components does not require such a stringent condition. In these cases it is in fact only necessary that the amplitude Ω/n be small compared with unity.

3. Both disks oscillating

We now consider the case where the two disks are oscillating with the same frequency and angular speed but 180° out of phase. This is analogous to the problem, studied by Stewartson, of disks rotating steadily with the same speeds in opposite directions. As in that problem we anticipate that the results will be symmetrical (or anti-symmetrical) about the plane $y = \frac{1}{2}$.

The boundary conditions (5) are replaced by

$$\left.\begin{aligned} u = w = 0, \quad v = r\Omega e^{int} \quad &\text{on} \quad z = 0, \\ u = w = 0, \quad v = -r\Omega e^{int} \quad &\text{on} \quad z = d. \end{aligned}\right\} \tag{5a}$$

Equations (1)–(4) may again be transformed using (6) and for the transverse flow lead to

$$\frac{d^2 g}{dy^2} - iRg = 0,$$

as previously, but with $g(0) = 1$ and $g(1) = -1$. The solution now is

$$g = \frac{\sinh\sqrt{(iR)}\,(1-y) - \sinh\sqrt{(iR)}\,y}{\sinh\sqrt{(iR)}}. \tag{12a}$$

For small Reynolds numbers this yields a velocity profile

$$\frac{v}{r\Omega} = (1-2y)\left\{\left[1-\frac{R^2}{360}y(1-y)(1+3y-3y^2)\right]\cos nt + \frac{R}{6}y(1-y)\sin nt\right\} + O(R^3). \tag{14a}$$

Hence the amplitude is given by

$$\frac{|v|}{r\Omega} = (1-2y)\left[1-\frac{R^2}{360}y(1-y)(1-2y+2y^2)\right] \tag{15a}$$

and the phase lag is $\tan^{-1}\frac{1}{6}Ry(1-y)$. (16a)

The skin friction is given by

$$\mu\left(\frac{\partial v}{\partial z}\right)_{z=0} = \mu\left(\frac{\partial v}{\partial z}\right)_{z=d} = -\frac{2\mu r\Omega}{d}\left[\left(1+\frac{R^2}{720}\right)\cos nt - \frac{R}{12}\sin nt\right]. \tag{20, 21a}$$

These approximations are found to be valid for about $R < 40$. The amplitude profile for $R = 20$, illustrated in figure 4, is antisymmetrical about the plane

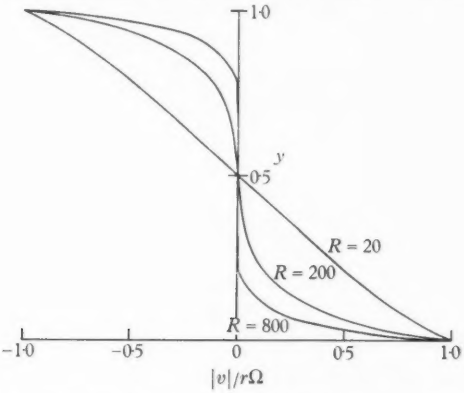

FIGURE 4. Two disks oscillating: amplitude of transverse velocity $|v|/r\Omega$ for $R = 20, 200, 800$.

$y = \frac{1}{2}$ in which there is zero transverse flow. The shearing forces on the two disks are equal in magnitude, though they will be opposite in sign.

The asymptotic solution, useful *for* $R > 80$, is

$$\frac{v}{r\Omega} \sim e^{-\sqrt{(\frac{1}{2}R)}y}\cos\left[nt-\sqrt{(\tfrac{1}{2}R)}\,y\right] - e^{-\sqrt{\frac{1}{2}(R)}(1-y)}\cos\left[nt-\sqrt{(\tfrac{1}{2}R)}\,(1-y)\right], \tag{17a}$$

and this leads to

$$\mu\left(\frac{\partial v}{\partial z}\right)_{z=0} = \mu\left(\frac{\partial v}{\partial z}\right)_{z=d} \sim -\frac{\mu r\Omega}{d}\sqrt{(\tfrac{1}{2}R)}\,(\cos nt - \sin nt). \tag{22, 23a}$$

Figure 4 shows also the velocity amplitude for $R = 200, 800$ derived from (17*a*). It is seen that a boundary layer of thickness $z \sim \sqrt{(\nu/n)}$ forms adjacent to both of the disks. The expression for the skin friction is identical with (22), when one disk is stationary.

For the radial-axial flow equation (24) again holds, with the same boundary conditions. Neglect of the inertia terms is allowable here also provided the

condition (46) is satisfied. The substitutions (26) and (27) yield two equations analogous to (28) and (29), with a difference in the last term in each owing to the changed value of $(g\,e^{i\tau})^2$.

After some tedious algebra we obtain the following results for the mean steady component of the flow. For small R,

$$f = \frac{R}{60} y^2(1-y)^2(1-2y) + O(R^3), \tag{34a}$$

$$f' = \frac{R}{30} y(1-y)(1-5y+5y^2) + O(R^3) \tag{35a}$$

and

$$K_0 = \tfrac{1}{10} + O(R^2). \tag{36a}$$

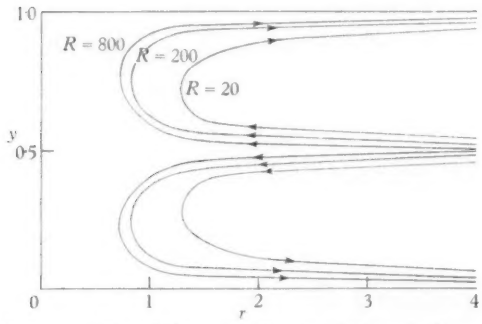

FIGURE 5. Two disks oscillating: typical streamlines of steady radial-axial flow for $R = 20, 200, 800$.

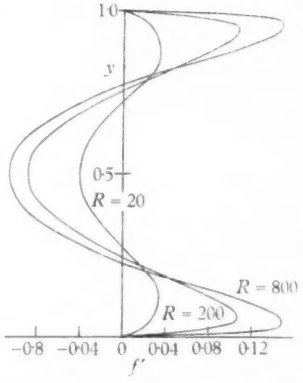

FIGURE 6. Two disks oscillating: steady radial velocity $f' = nu_s/r\Omega^2$ for $R = 20, 200, 800$.

For large Reynolds numbers,

$$f \sim \tfrac{1}{4}y(1-y)(1-2y) - \frac{1}{4\sqrt{(2R)}}(1-2y)(1+2y-2y^2) + \frac{1}{4\sqrt{(2R)}}\left[e^{-\sqrt{(2R)}\,y} - e^{-\sqrt{(2R)}(1-y)}\right], \tag{37a}$$

$$f' \sim \tfrac{1}{4}(1-6y+6y^2) + \frac{3}{\sqrt{(2R)}}y(1-y) - \tfrac{1}{4}\left[e^{-\sqrt{(2R)}\,y} + e^{-\sqrt{(2R)}(1-y)}\right] \tag{38a}$$

and

$$K_0 \sim \frac{3}{R}\left(1 - \frac{2}{\sqrt{(2R)}}\right). \tag{39a}$$

Figure 5 depicts representative streamlines of this flow at $R = 20, 200, 800$. As might be expected there is symmetry about the plane $y = \frac{1}{2}$ and no axial flow across it. In this sense this plane acts as an interface separating the fluid into two self-contained portions, in each of which there is axial flow towards the moving disk. The pressure gradient at high R given by (39a) is twice that of § 2, as it has to counterbalance the flow in two boundary layers. In both cases, however, this pressure gradient is quite small at large Reynolds numbers, which corresponds to a result obtained by Stewartson.

In figure 6 we see the radial velocity component at each of the three values of the Reynolds number. In all cases f' is a minimum (i.e. maximum inflow) when

$y = \frac{1}{2}$. For $R = 20$ it is zero on planes $y = 0{\cdot}27$ and $0{\cdot}73$. Between these and the walls there is radial outflow, due to the predominance of centrifugal action. For $0{\cdot}27 < y < 0{\cdot}73$ there is an inflow as the pressure gradient is then the main factor.

At high Reynolds numbers the profile has the character of a boundary layer near both disks, for about $y < 0{\cdot}2$ and $y > 0{\cdot}8$. In the main body of the fluid its shape is described by a quadratic in y, which is well known as the behaviour of a fluid under constant pressure gradient.

REFERENCES

BATCHELOR, G. K. 1951 *Quart. J. Mech. Appl. Math.* **4**, 29.

ROSENBLAT, S. 1959 *J. Fluid Mech.* **6**, 206.

SCHLICHTING, H. 1955 *Boundary Layer Theory.* London: Pergamon Press.

STEWARTSON, K. 1953 *Proc. Camb. Phil. Soc.* **49**, 333.

An experimental investigation of the effect of ejecting a coolant gas at the nose of a bluff body

By C. H. E. WARREN
Royal Aircraft Establishment, Farnborough, Hants.

(Received 29 December 1959)

An experimental investigation has been made of the effect of ejecting nitrogen and helium coolant gases at the nose of a bluff body at a nominal Mach number of 5·8. The gases were ejected with 'swirl', to encourage them to flow tangentially to the model surface at ejection, and also straight out. Measurements were made of the pressure and temperature on the surface of the model at incidences of 0, 4, 8°, and for a range of coolant gas flows. From these measurements the flow patterns and distributions of heat flux were deduced.

It was found that ejection with swirl did not in fact lead to an easing of the heating problem because the high tangential velocity with which the coolant was injected into the boundary layer increased the wall shear stress, and hence, by the Reynolds analogy, the heat flux, so that it predominated over the reduced driving temperature difference associated with the cooled boundary layer.

With straight-out ejection it was found that the heat alleviation capabilities of the ejected coolant were reduced considerably if the flow rate was sufficiently large that the bow shock wave was bulged out. However, provided that the external flow is not disturbed, straight-out ejection provides an effective way of reducing the heat flux.

1. Introduction

A body travelling at high speeds through the atmosphere experiences aerodynamic heating. Ways of alleviating the problems so incurred are accordingly of interest. One way is to eject a cool gas from the nose of the body. The gas, by flowing back over the body, forms a 'heat buffer' between the hot air stream and the body. This paper described some experiments that were made to investigate some of the fluid dynamic aspects of such a scheme, and, particularly, to determine the effect on the local rates of heat transfer.

In an earlier investigation McMahon (1958) studied the effect of ejecting a cool gas from the nose of a blunt body. He tried various methods of ejecting the gas, and observed the associated flow patterns. In addition, he measured the pressure distributions on the body, and obtained some measurements of the overall rates of heat transfer over fairly large segments of the body. Initially, McMahon ejected a coolant gas straight out at the nose in a direction opposed to the main air stream, but the flow studies and pressure distributions indicate severe disturbances to the flow field. It was thought, somewhat naturally, that ejection in this manner would not be satisfactory as a means of

reducing the rates of heat transfer. Accordingly deflector caps were fitted over the ejection orifice in an attempt to direct the coolant gas tangentially to the body surface. The investigation reported here started from this premise. That is, the aim in ejection should be to make the gas flow tangentially to the body surface, and thereby ensure that the inner part of the boundary layer is composed of cool gas. It was decided, however, that instead of using deflector caps, the ejected coolant would be encouraged to flow tangentially to the body surface by giving it some swirl in the ejection pipe. It was hoped that the centrifugal effect of the swirl would cause the coolant to flow radially outwards at ejection, and that the Coanda effect would subsequently cause it to adhere to the surface. The scheme worked, except at the largest rates of coolant ejection, but it was found that ejection in this manner is not a satisfactory method of easing the heating problem. Although the cool layers of coolant gas reduce the driving temperature difference, the high tangential velocity with which the coolant is injected into the boundary layer increases the wall stress considerably, and hence, by the Reynolds analogy, the heat flux. The results indicate that the effect of the increased shear predominates, at least for the conditions considered here. The matter was not, therefore, pursued further.

In view of these results attention was directed once more to straight-out ejection, for McMahon had subsequently found that this method of ejection actually produced an effective 'blanketing' of the body. Two flow régimes were found. Except at the smaller flow rates the coolant gas emerged as a forward-directed jet, causing the bow shock wave to bulge out in much the same way as with a solid spike (see, for example, Bogdonoff & Vas (1959)). The normal flow pattern is replaced by one in which the main air flow separates ahead of the model, thereby leaving a roughly conical 'dead-air' region in the vicinity of the nose. The flow external to the boundary layer, instead of having a stagnation point at the nose, now has a 'stagnation circle' where the incident flow meets the body. McMahon found that the pressures on the body within the dead-air region are greatly reduced compared with the pressures for no ejection. The results reported here show that, associated with these reduced pressures, there are greatly reduced values of heat flux. However, in the vicinity of the stagnation circle the pressures are somewhat above their values for no ejection. Associated with this there is an increased heat flux in a region around the stagnation circle. The nett result is that, although the region of severest heating is shifted, the overall heating is not greatly reduced, at least not unless large coolant flow rates are employed.

The second flow régime occurs when the coolant flow rate is sufficiently small that the coolant gas does not cause the bow shock wave to bulge out. With the external flow sensibly undisturbed, relatively large reductions in heat flux are obtained. The reductions in total heat transfer over the body are of the order of the 'heat capacity' of the coolant gas, defined for this purpose as the amount of heat that the gas can absorb in having its temperature raised from that just before ejection to the stagnation temperature of the main air stream.

The work reported here is an experimental determination of the local rates of heat transfer over a bluff body for various flow rates of a coolant gas, either

nitrogen or helium, ejected either straight out or with swirl, in the manner already described. The momentum flow rate of the ejected coolant was not varied independently of the mass flow rate. To do so would be one way of extending the present work, for it would be extremely interesting to eject coolant gas at larger rates of mass flow, but with insufficient momentum to cause the bow shock wave to bulge out.

2. Brief description of the experiments

The experiments were made in the 5 in. × 5 in. hypersonic wind tunnel of the Guggenheim Aeronautical Laboratory at the California Institute of Technology. The nominal Mach number was 5·8, and the Reynolds number per inch based on free-stream conditions was about 0·2 million. At this Reynolds number and Mach number it was assured that the boundary layer on the model was laminar.

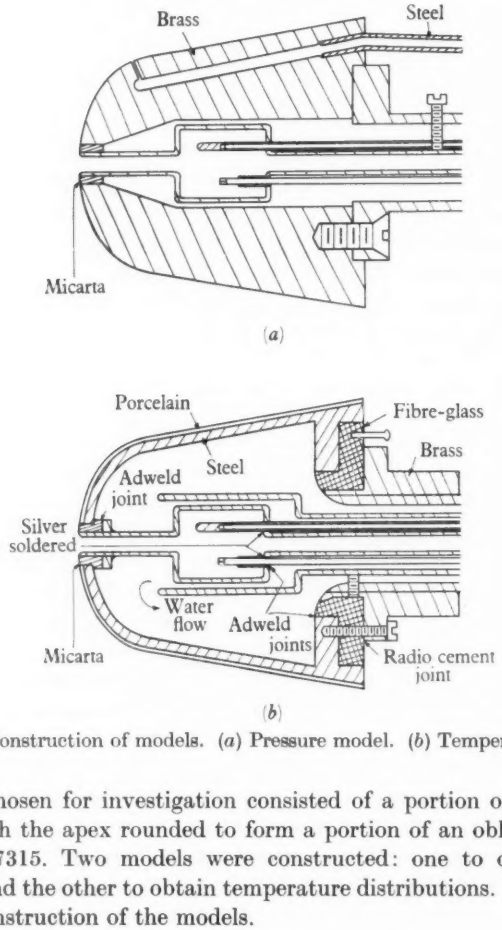

FIGURE 1. Construction of models. (*a*) Pressure model. (*b*) Temperature model.

The shape chosen for investigation consisted of a portion of a cone of 10° semi-angle, with the apex rounded to form a portion of an oblate spheroid of eccentricity 0·7315. Two models were constructed: one to obtain pressure distributions and the other to obtain temperature distributions. Figure 1 shows the internal construction of the models.

The pressure model was constructed of brass with nine conventional static pressure orifices of 0·016 in. diameter. Figure 2 shows the position of the pressure orifices, which were located helically on eight meridians. All pressures have been quoted as pressure coefficients, C_P, defined by

$$C_P = \frac{P - P_\infty}{\frac{1}{2}\rho_\infty V_\infty^2},$$

where P_∞, ρ_∞ and V_∞ are respectively the pressure, density and speed of the freestream. C_P has been normalized by dividing it by the pressure coefficient, C_{P_0}, at the nose for zero incidence and with no coolant ejection; which is, of course, the pressure coefficient behind a normal shock at the tunnel Mach number.

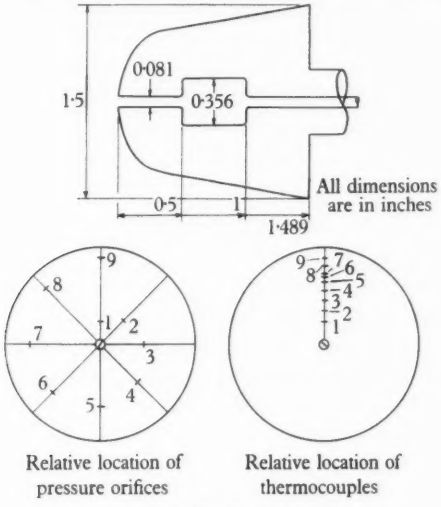

FIGURE 2. Geometry of models.

The temperature model was constructed of a mild steel with a wall thickness of 0·050 in., and coated with a layer of porcelain of thickness 0·020 in. Along one meridian of the temperature model nine thermocouples were formed by cementing a constantan wire of 0·001 in. diameter on the model, and then removing the cement coating at nine precisely located points with a knife blade. It thus became possible to make contact with the wire by means of silver paint at these nine points, thereby forming nine silver-constantan junctions (see figure 2). Painted silver leads connected the thermocouples so formed to turret posts set in fibre-glass on the base of the model. Some heat-meters also were installed on the temperature model with which it was hoped to measure the heat flux directly. However, unsatisfactory results were obtained with them, which will not be reported here.

The temperature model was cooled by water, the inflow being within the return-flow (see figure 1). The flow rate was on the average about 0·17 U.S. gallons per minute, varying at most by a factor of 2. The inflow water temperature whenever measured was always within 1 °F of 76 °F, and the maximum

measured temperature rise overall, that is due to the heat picked up not only in the model but also in the attendant piping, was never greater than 7 °F, and usually less than 3 °F. It can be shown (Warren 1958) that the heat flux, $\dot{q}$, at a particular point across a thin skin of low thermal conductivity is fairly uniform, and is given very closely by

$$\dot{q} = \frac{k}{\delta}(T - T_i),$$

where k is the thermal conductivity of the skin material, δ is the thickness of the skin, T is the temperature of the outer surface at the particular point, and T_i is the corresponding temperature of the inner surface.

Since the thermal conductivity of porcelain is about one-sixtieth of that of steel, it is not unreasonable to assume that most of the temperature drop across the wall of the model occurs in the 0·020 in. layer of porcelain, and that the inner surface of the porcelain is not far removed from the water temperature, which, in the model, was about 80 °F. In view of the failure to obtain satisfactory results with the heat-meters, normalized local rates of heat transfer were obtained from the measurements of surface temperature by assuming that

$$\frac{\dot{q}}{\dot{q}_0} = \frac{T - T_i}{T_0 - T_i},$$

where $\dot{q}_0$ is the heat flux at the nose for zero incidence and with no coolant ejection, T is the measured surface temperature, T_0 is the surface temperature at the nose for zero incidence and with no coolant ejection (measured to be 130 °F), and T_i is the inner surface temperature, assumed to be 80 °F.

The nitrogen and helium gases used in the ejection studies were fed into the model via a pipe within the inflow water pipe. This procedure ensured that the coolant gas reached the model at a fairly constant temperature. Within the model the gas entered a plenum chamber (see figure 1) where a pressure probe and an iron-constantan thermocouple enabled the pressure and temperature of the gas to be determined. From the plenum chamber the gas was conveyed to the nose of the model through an ejection pipe of 0·081 in. inside diameter and 0·5 in. long, the edges of the ejection hole being rounded to a radius of about 0·02 in. The same physical parts for the coolant ejection were used in both the pressure and temperature models. The coolant mass flow rate, $\dot{m}$, has been quoted as a mass flow coefficient, $C_{\dot{m}}$, based on the free-stream mass flow rate through a capture area equivalent to the frontal area of the model, so that

$$C_{\dot{m}} = \frac{\dot{m}}{\rho_\infty V_\infty \pi(\frac{1}{2}D)^2},$$

where D is the model base diameter.

The swirl that was given to the coolant in some of the tests was obtained by inserting in the ejection pipe a twisted strip of brass 0·01 in. thick and 0·5 in. long. The strip was twisted through one complete turn clockwise, so that the helical advance angle at the wall was about 63°. It was appreciated that such a device would not produce initially a rotationally symmetric coolant flow, but it was hoped that, once away from the ejection orifice, the flow would

even out. On the pressure model the setting of the swirler at the ejection orifice made an angle of about 40° with the meridian through pressure orifices 1 and 9, as indicated in figure 2. On the temperature model two positions were tested: one made an angle of about 45° with the meridian through the thermocouples, as indicated in figure 2, and the other made an angle of about 90°.

Further details of the experiments, together with all the results obtained, are given elsewhere (Warren 1958). Only a selection of the results are presented here.

3. Results for no ejection

Distributions of pressure and heat flux in the plane of incidence with no ejection at incidences of 0, 4 and 8° are shown in figures 3 and 4, in terms of the distance, s, from the model nose along a meridian. It was found that there is no noticeable variation of pressure or heat flux with incidence in the meridian plane normal to the plane of incidence, at least up to an incidence of 8°.

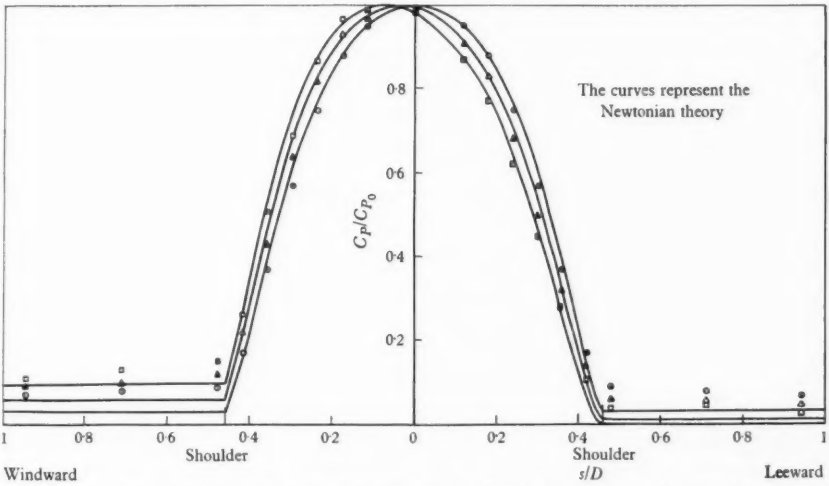

FIGURE 3. Distributions of pressure in the plane of incidence for no ejection ($C_{\dot{m}} = 0$). ⊙, $\alpha = 0°$; △, $\alpha = 4°$; ⊡, $\alpha = 8°$.

The pressure results are in fair agreement with Newtonian theory, which states that the pressure is given by

$$\frac{C_P}{C_{P_0}} = \sin^2 \eta,$$

where η is the angle of the surface to the direction of motion, except on the conical portion, where the Newtonian approach underestimates the pressure. The pressure results are also in good agreement with those of Richards (1957), who earlier tested a model of nominally identical geometry.

The heat flux results at zero incidence are in fair agreement with calculations based on the theory of Lees (1956). In these calculations the measured, as

distinct from the theoretical, pressure distribution was used, and allowance was made for the small effects associated with a pressure gradient. The poor agreement over the conical portion may be associated with the measurements, for the method whereby the heat flux is derived is of least accuracy when the heat flux itself is small. Calculations based on the theory of Cohen & Reshotko (1956), although more difficult to perform, were in substantial agreement with those based on the theory of Lees.

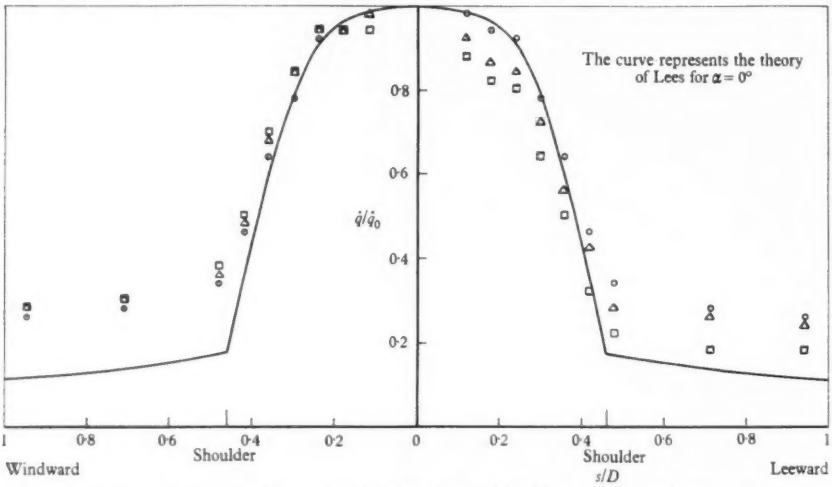

FIGURE 4. Distributions of heat flux in the plane of incidence for no ejection ($C_m = 0$). ⊙, $\alpha = 0°$; △, $\alpha = 4°$; □, $\alpha = 8°$.

4. Variation of ejection conditions with coolant flow rate

On the assumption of one-dimensional flow in the coolant gas pipe, the Mach number in the plenum chamber never exceeds 0·03, based on the measurements of mass flow rate and of pressure and temperature in the plenum chamber. The plenum chamber pressures and temperatures can therefore be treated as representing total conditions. On this assumption, and again that of one-dimensional flow, the Mach number, M_e, at the entry to the final ejection pipe can be calculated. This Mach number is shown in figures 5 and 6. The constancy of Mach number shown in figure 5 for mass flow coefficients above about 0·005 for nitrogen or 0·0015 for helium is evidence that, for ejection with swirl, the flow in the swirl pipe is choked. Figure 6 shows that for straight-out ejection the onset of choking is delayed to a mass flow coefficient about 0·008 for nitrogen and 0·0025 for helium. The Mach numbers themselves should be treated as qualitative only, owing to the assumption of one-dimensional flow made in their derivation, and to the fact that Mach number is extremely sensitive to area ratio near a Mach number of unity.

For straight-out ejection the momentum flow rate of the ejected gas can be calculated, again on a one-dimensional flow assumption, and ignoring any losses in the final ejection pipe, which are estimated to be small. The calculated

momentum flow rates are shown in figure 7 as momentum flow coefficients $C_{\dot{\mu}}$, defined as

$$C_{\dot{\mu}} = \frac{\dot{m}V_{ej}}{\rho_\infty V_\infty^2 \pi(\frac{1}{2}D)^2},$$

where V_{ej} is the velocity of ejection. It will be noted that for small mass flow rates, such that the flow in the ejection pipe is not choked, the momentum flow rate for helium, and hence its speed of ejection, is about seven times that for nitrogen for the same mass flow rate, as would be expected from the relative densities of helium and nitrogen.

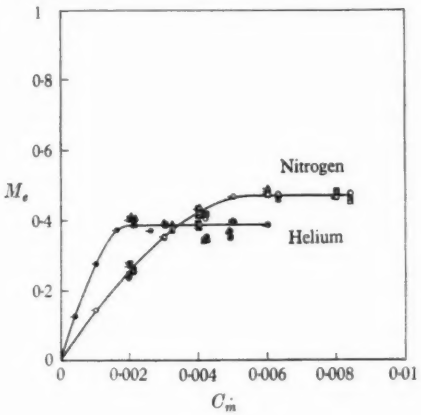

FIGURE 5

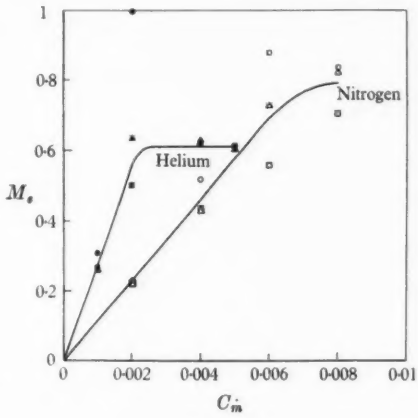

FIGURE 6

FIGURE 5. Mach number of coolant at entry to the final swirl pipe for ejection with swirl. ○ ●, $\alpha = 0°$; △ ▲, $\alpha = 4°$; □ ■, $\alpha = 8°$. The flagged points are for the pressure model, the unflagged points are for the temperature model.

FIGURE 6. Mach number of coolant at entry to the final ejection pipe for straight-out ejection. ○ ●, $\alpha = 0°$; △ ▲, $\alpha = 4°$; □ ■, $\alpha = 8°$.

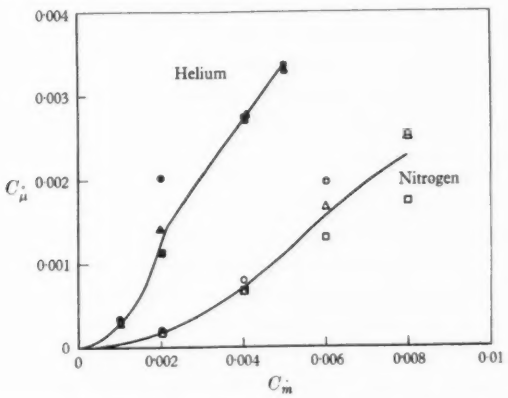

FIGURE 7. Variation of coolant momentum flow with coolant mass flow for straight-out ejection. ○ ●, $\alpha = 0°$; △ ▲, $\alpha = 4°$; □ ■, $\alpha = 8°$.

5. Effects of ejection on the flow pattern

The effects of ejection on the flow pattern can be deduced from an examination of the schlieren photographs and the measured surface pressure distributions.

For straight-out ejection at very small flow rates no noticeable change in the schlieren picture occurs (see figures 8*a*,*b*, plate 1). At a certain critical flow rate, however, the bow shock wave begins to bulge out (see figure 8*c*, plate 1). This critical flow rate appears to increase with increase in incidence (see figures 8*g*,*h*, plate 2). At zero incidence it occurs at a mass flow coefficient of about 0·003 with nitrogen and of about 0·001 with helium. From figure 7 we

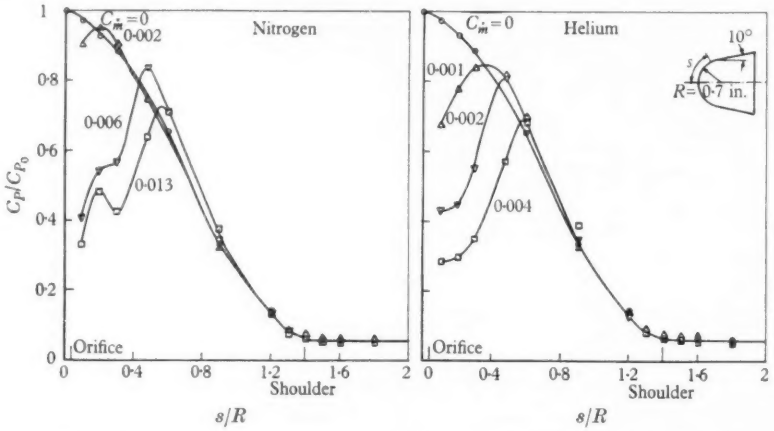

FIGURE 9. Distributions of pressure at zero incidence ($\alpha = 0°$) for straight-out ejection. (McMahon's results for a sphere-cone model.) $C_{\dot{m}} = \dot{m}/\rho_\infty V_\infty \pi R^2$.

see that these mass flow coefficients correspond to a momentum flow coefficient in each case of about 0·00035,* thereby confirming the work of Lam (1959) who suggests that the flow pattern is determined, at small flow rates, by the momentum flow coefficient of the ejected gas. Above the critical flow rate the bow shock wave is bulged out, and from the results of McMahon (1958) there is an associated marked change in the surface pressure distribution. McMahon studied the same problem on a model of about the same size, but having a spherical instead of a spheroidal nose, and an ejection orifice smaller by about 25 %. His tests were made at the same Mach number and about the same Reynolds number. His results are shown in figure 9. It will be noted that the surface-pressure distribution is not markedly changed for a mass flow coefficient of 0·002 with nitrogen, corresponding to an unbulged bow shock wave. For all other mass flow coefficients shown, however, there are marked changes, corresponding to bulged bow shock waves. The pressure distributions are in fact similar to those that occur when a spike protrudes from the nose of a model,

* This momentum flow coefficient based on model base area is equivalent to a momentum flow coefficient of 0·12 based on ejection orifice area.

implying that the ejected gas acts as a 'gas spike'. It will be seen from figure 9 that ejection reduces the pressures in the vicinity of the nose. At the smaller flow rates there is, somewhat surprisingly, an associated reduction in the plenum chamber pressure, P_p (see figure 10). Moreover, the plenum chamber pressure varies appreciably with incidence at the smaller flow rates. This is presumably because the conditions at the ejection orifice vary appreciably with incidence. With helium when the mass flow coefficient is above about 0·003 this dependence on incidence disappears: this is no doubt associated with the fact that above this flow rate the flow in the ejection pipe is choked, as mentioned in §4. With nitrogen the plenum chamber pressure depends on incidence at all flow rates up to that corresponding to a mass flow coefficient of 0·008, the maximum tested: this too is in keeping with the result, obtained in §4, that the flow in the ejection pipe is unchoked for mass flow coefficients less than 0·008.

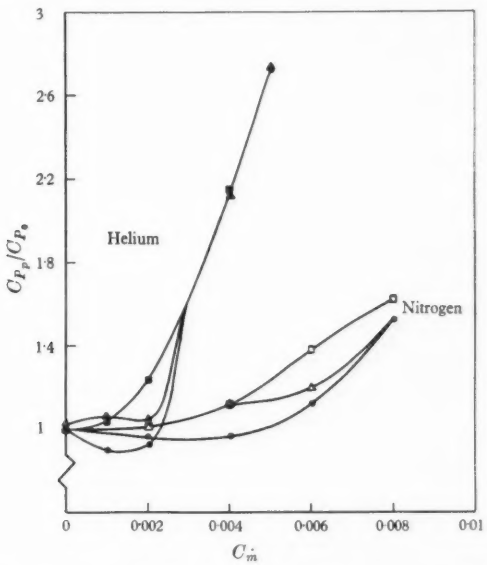

FIGURE 10. Plenum chamber pressure for straight-out ejection.
○ ●, $\alpha = 0°$; △ ▲, $\alpha = 4°$; □ ■, $\alpha = 8°$.

For ejection with swirl the critical flow rate above which the bow shock wave begins to bulge out is greater than for straight-out ejection (see figures 8*c*, *d*, *i* and *j*, plates 1, 2). It would appear, therefore, that the swirler is achieving its desired effect. At zero incidence the critical flow rate occurs at a mass flow coefficient of about 0·008 with nitrogen and of about 0·003 with helium. For ejection with swirl the concept of a momentum flow rate is not so easy to formulate, but it is interesting to note that the ratio of the two critical mass flow rates for ejection with swirl is roughly the same as the corresponding ratio for straight-out ejection, namely about $\sqrt{7}:1$. For ejection with swirl, however, it was found that the critical flow rate decreases with increase in incidence

(see figures 8*d*, *e* and *f*, plate 1). The variations in the surface pressure distribution for ejection with swirl (as measured in the model of the present investigation) are shown in figures 11 and 12. As noted also in the results for straight-out ejection the surface-pressure distributions at zero incidence (figure 11) are not

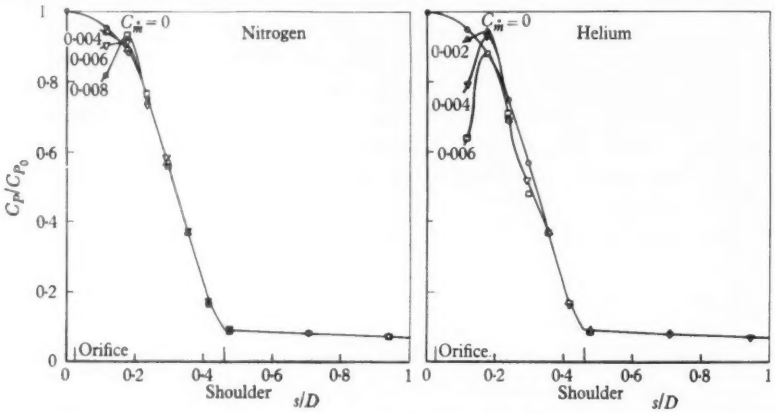

FIGURE 11. Distributions of pressure at zero incidence ($\alpha = 0°$) for ejection with swirl.

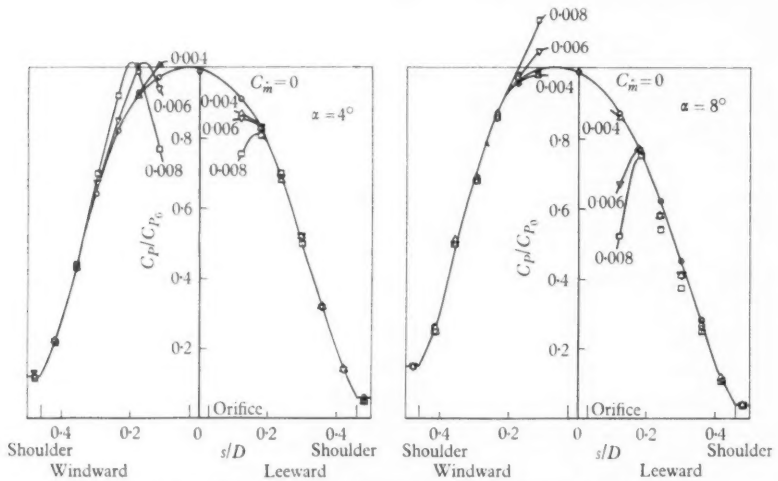

FIGURE 12. Distributions of pressure in the plane of incidence for the ejection with swirl of nitrogen.

markedly changed for mass flow coefficients for which the schlieren pictures indicate an unbulged bow shock wave (mass flow coefficients less than about 0·008 with nitrogen and less than about 0·003 with helium), but there are marked changes corresponding to bulged bow shock waves.

The variations in plenum chamber pressure are shown in figure 13. The plenum chamber pressures do not vary noticeably with incidence: this is no doubt because, with swirl, the flow in the swirl pipe is choked when the mass

flow coefficient is above about 0·005 for nitrogen or 0·0015 for helium (see §4); and up to these flow rates, as we have seen, the bow shock wave is not bulged out, the flow ahead of the body is little affected, and the pressures in the vicinity of the nose do not vary much with either incidence or coolant flow rate.

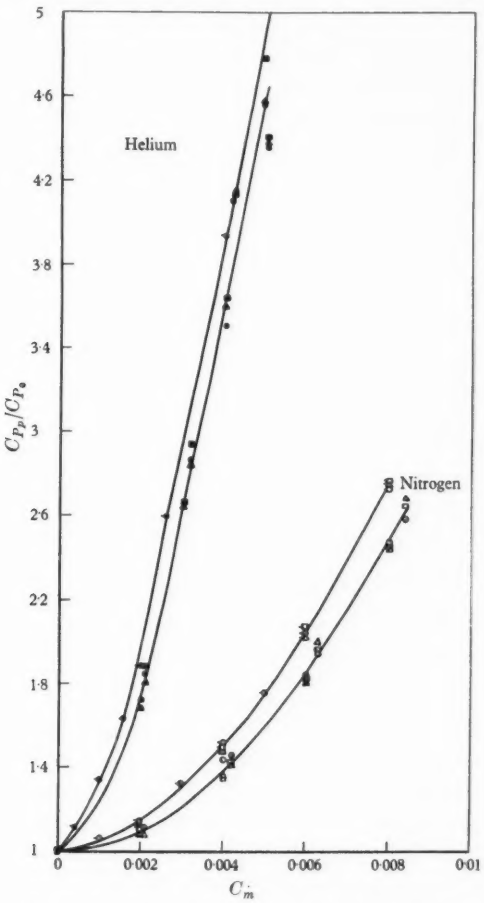

FIGURE 13. Plenum chamber pressure for ejection with swirl. ⊙ ●, $\alpha = 0°$; △ ▲, $\alpha = 4°$; □ ■, $\alpha = 8°$. The flagged points are for the pressure model, which was uncooled; the unflagged points are for the temperature model.

It will be noted, however, by comparing figures 10 and 13 that, for the same mass flow rate, much greater driving pressures are required for ejection with swirl than for straight-out ejection. The slightly greater driving pressures required with the pressure model compared with the temperature model, indicated in figure 13, are because the pressure model was uncooled, and accordingly the temperatures in the plenum chamber were some 100 °F higher than with the temperature model.

6. Effect of ejection on the distribution of heat flux

The distributions of heat flux for ejection with swirl at zero incidence are shown in figure 14. Results are shown for one flow rate with each coolant, the flow rates chosen being ones for which the schlieren and pressure studies considered in §5 indicated that the swirler was working, in the sense that the bow shock wave was not bulged out (see figures 8*d*, *j*, plates 1, 2) and the distributions of pressure were not markedly different from the case of no ejection (see figure 11). The first thing that one notices in figure 14 is that the results depend

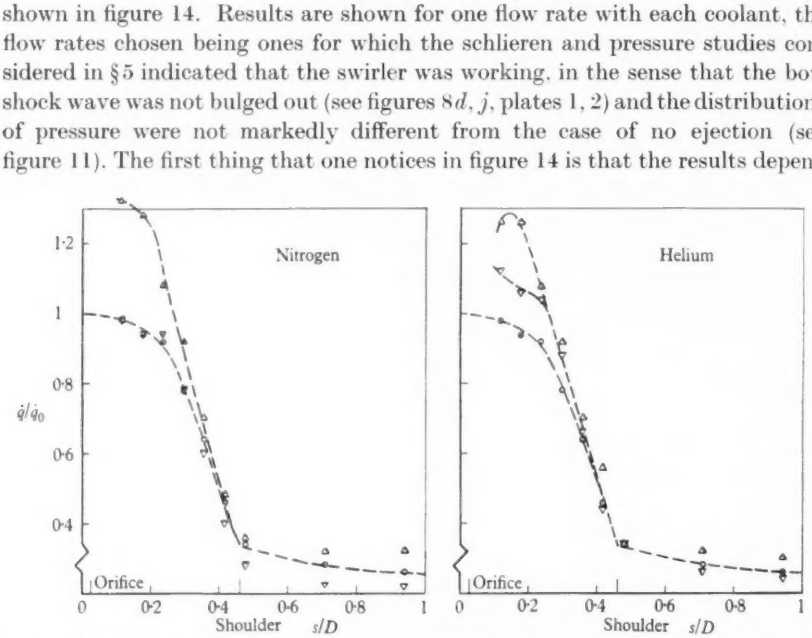

FIGURE 14. Distributions of heat flux at zero incidence ($\alpha = 0°$) for ejection with swirl.
Nitrogen: ⊙, $C_{\dot{m}} = 0$; △, $C_{\dot{m}} = 0{\cdot}006$, swirler at 45°; ▽, $C_{\dot{m}} = 0{\cdot}006$, swirler at 90°.
Helium: ⊙, $C_{\dot{m}} = 0$; △, $C_{\dot{m}} = 0{\cdot}002$, swirler at 45°; ▽, $C_{\dot{m}} = 0{\cdot}002$, swirler at 90°.

critically upon the setting of the swirler, implying that the swirler is not giving a rotationally symmetric distribution of coolant gas over the model. In view of these results an attempt should have been made to obtain a more nearly rotationally symmetric distribution of coolant gas. However, the main observation obtained from figure 14, and from other results not shown here, is that ejection with swirl seems to lead to an increase in heat flux. Accordingly the matter was not pursued, but attention directed instead to straight-out ejection.

An explanation of the increase in heat flux produced by ejection with swirl is provided by the Reynolds analogy, which states that the ratio of the Nusselt number to the product of the surface friction coefficient and the Reynolds number is a constant depending upon the surface temperature and the longitudinal pressure gradient, or

$$\dot{q} \propto \frac{k(T_a - T)}{\mu V_b}\,\tau,$$

where T is the surface temperature, T_a is the adiabatic surface temperature (that is the surface temperature for which the heat flux is zero), V_b is the velocity at the external edge of the boundary layer, τ is the surface shear stress, k is the thermal conductivity, and μ is the dynamic viscosity.

Now the main effect of the introduction of a coolant is to reduce the driving temperature difference $(T_a - T)$, and this is the basis on which it works, but in ejection with swirl the coolant is injected tangentially into the boundary layer at the nose with very high velocity, much greater than the average velocity of the uninjected boundary layer, with the result that the surface shear stress is increased manyfold. The results obtained seem to indicate that the increase in τ outweighs the reduction in $(T_a - T)$ and the changes in the other quantities, particularly k and μ. If tangential injection into a boundary layer is to be instrumental in reducing heat flux it must be done with much less momentum for a given mass flow than was achieved in these experiments.

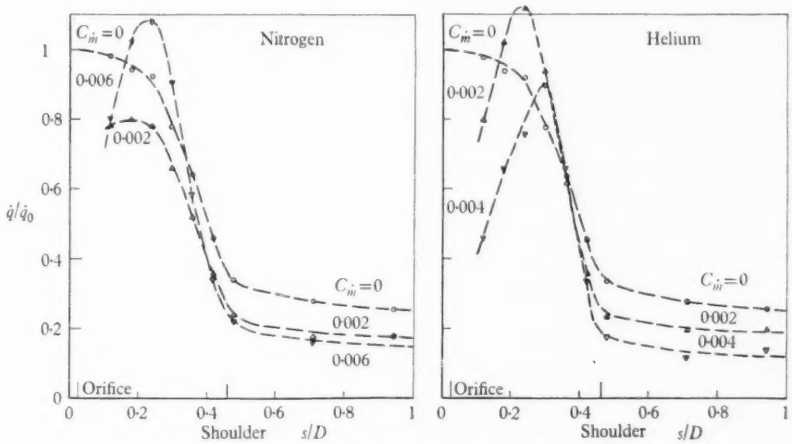

FIGURE 15. Distributions of heat flux at zero incidence ($\alpha = 0°$) for straight-out ejection.

The distribution of heat flux for straight-out ejection at zero incidence are shown in figure 15. The curve for nitrogen at a mass flow coefficient of 0·002 is of a markedly different shape from the curves for the other three cases. Moreover, it corresponds to a reduction in heat flux along the entire body profile. From the schlieren and pressure studies considered in §5 this case is one for which the coolant is introduced with sufficiently little momentum that it does not cause the bow shock wave to bulge out (see figure 8*b*, plate 1), or the pressure distribution to be markedly different from the case of no ejection (see figure 9). The other three cases (nitrogen at a mass flow coefficient of 0·006 and helium at mass flow coefficients of 0·002 and 0·004) all correspond to bulged bow shock waves (see figures 8*c*, *i*, plates 1, 2), and markedly different pressure distributions (see figure 9). In these cases although large reductions in heat flux are obtained in the vicinity of the nose, there is an increase further round the profile, where s/D is about 0·25. These results agree with those of McMahon (1958). He found large reductions in the average heat flux over the nose sector of a sphere of 60° included angle, but considerably smaller reductions over a sector of 120° included angle.

The explanation of these results is provided by considering the associated flow patterns. As shown in §5, in these cases the ejected gas acts as a 'gas spike', causing the main air flow to separate ahead of the model thereby leaving a roughly conical 'dead-air' region in the vicinity of the nose. The flow external to the boundary layer, instead of having a stagnation point at the nose, now has a 'stagnation circle' where the incident flow meets the body, along which the heat flux is increased compared with the heat flux at the same station for no ejection. Inside the dead-air region the pressure is greatly reduced (see figure 9), and this reduction in pressure is largely responsible for the reduced heat flux in the vicinity of the nose.

It is of interest to consider the ratio of the reductions in total heat transfer to the 'heat capacity' of the ejected gas, taken as

$$\dot{m}c_p(T_s - T_p).$$

This expression represents the amount of heat that the gas can absorb when its temperature is raised from that in the plenum chamber, T_p, to the stagnation temperature of the main air flow, T_s; c_p is the specific heat of the gas at constant pressure. For nitrogen ejected straight out at a mass flow coefficient of 0·002, corresponding to an unbulged bow shock wave, the ratio of the reduction in total heat transfer up to the station $s/D = 1$ to the 'heat capacity' of the ejected gas is about 1·1. That this is greater than unity implies that the nitrogen is acting more than as a blanket; that is, a greater reduction in heat transfer is being achieved than would correspond to the absorption by the nitrogen of the heat that would otherwise have been transferred to the model. The ratio of the reduction in total heat transfer up to the shoulder ($s/D = 0{\cdot}459$) to the 'heat capacity' of the ejected gas is about 0·4, which is still remarkably high. These figures should be compared with those for helium for the same mass flow rate, remembering that in this case the shock wave is now bulged out (see figure 8*i*, plate 2). The ratio of the reduction in total heat transfer up to the station $s/D = 1$ to the 'heat capacity' of the ejected gas is about 0·1, which is less than one-tenth of the value with nitrogen: the ratio based on the total heat transfer up to the shoulder is roughly zero.

The implication of these results seems to be that if the gas can be ejected without causing the bow shock wave to bulge out, as is the case with nitrogen ejected at a mass flow coefficient of 0·002, then a steady reduction in heat flux with increase in flow rate should be achieved. This state of affairs can be achieved by arranging that the mass flow rate be increased without increasing the momentum flow rate, so that on impingement with the air the coolant is directed around the body without too much mixing and consequent reduction of its heat alleviation properties. The importance of this observation is brought out by the results for nitrogen and helium ejected at a mass flow coefficient of 0·002 already referred to. Although it has five times the heat capacity and is one-seventh of the density, implying a thicker layer for the same mass flow rate and velocity, helium is not as effective as nitrogen in reducing the heat flux at this flow rate simply because its heat alleviation properties are enormously reduced by mixing. It would obviously be extremely

interesting to extend these experiments by varying the ejection pipe in such a way that the mass flow rate with a given gas could be varied independently of the momentum flow rate. In this way it should be possible to delay bulging the bow shock wave to higher mass flow rates, and substantial reductions in heat flux for quite small mass flow rates should thereby be achieved.

The effect of incidence on the distribution of heat flux for straight-out ejection is shown in figure 16 for nitrogen. Qualitatively the results are similar to those at zero incidence. At a mass flow coefficient of 0·002, corresponding to an unbulged bow shock wave, the heat flux is reduced less on the windward meridian than on the leeward meridian; and at an incidence of 8° ejection is having very little effect on the windward meridian. At a mass flow coefficient of 0·006, corresponding to a bulged bow shock wave, the heat flux is greater, over most of the model, than the heat flux at the lower flow rate, and on the windward meridian it is greater than with no ejection.

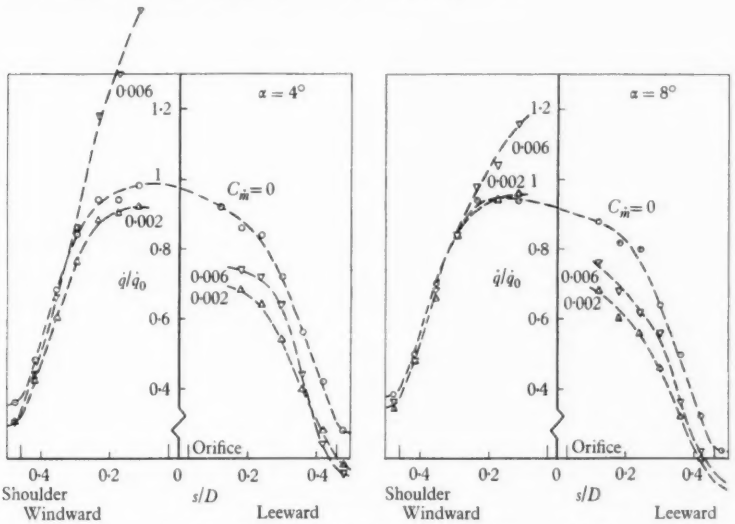

FIGURE 16. Distributions of heat flux in the plane of incidence for the straight-out ejection of nitrogen.

7. Conclusions

In the course of the investigation three ways of ejecting a coolant gas from the nose of a bluff body have become apparent, and something has been learned about the heat transfer rates associated with them.

The method that was tried initially was to encourage the coolant gas to flow tangentially to the model surface at ejection by giving it some swirl in the ejection pipe. The method was successful in the sense that, at the smaller flow rates, the coolant gas was ejected with very little disturbance to the flow external to the boundary layer, as witnessed by the pressure distributions and schlieren studies. However, this method of ejection is not satisfactory as a means of easing the heating problem. Although the cool layers of coolant gas

reduce the driving temperature difference the high tangential velocity with which the coolant is injected into the boundary layer increases the surface shear considerably, and hence, by the Reynolds analogy, the heat flux. The results indicate that the effect of the increased shear predominates, at least for the conditions considered here. This method of ejection was therefore abandoned.

Attention was then centred on straight-out ejection, but here two flow régimes were found. Except at the smaller flow rates the coolant gas acts as a 'gas spike', causing the bow shock wave to bulge out and the main air flow to separate ahead of the model, thereby leaving a roughly conical 'dead-air' region in the vicinity of the nose. The flow external to the boundary layer, instead of having a stagnation point at the nose, now has a 'stagnation circle'. Inside the dead-air region the pressure is greatly reduced compared with the case of no ejection, and, associated with this reduced pressure, there is a greatly reduced heat flux. However, in the vicinity of the stagnation circle the pressure is somewhat above its value for the case of no ejection, and associated with this there is an increased heat flux. The nett result is that, although the region of severest heating is shifted, the overall heat transfer rate is not greatly reduced, at least not unless large flow rates are employed.

At the smaller flow rates the momentum of the ejected gas is not sufficient to disturb the external flow appreciably. The critical flow rate corresponds to a momentum flow coefficient of about 0·00035. With nitrogen this corresponds to a mass flow coefficient of 0·003, and with helium to a mass flow coefficient of 0·001. This method of ejection was investigated with nitrogen at a mass flow coefficient of 0·002, and under these conditions relatively large reductions in heat flux were obtained all over the model. The reductions in total heat transfer were of the order of the 'heat capacity' of the coolant nitrogen, where the 'heat capacity' is defined for this purpose as the amount of heat that the gas can absorb in having its temperature raised from that just before ejection (i.e. in the plenum chamber) to the stagnation temperature of the main air stream. In comparison, for the straight-out ejection of helium at the same mass flow coefficient of 0·002, but a case in which the bow shock wave is now bulged out, the reduction in total heat transfer over the model was no more than one-tenth of the 'heat capacity' of the coolant helium.

Clearly the method of ejecting straight out, but without sufficient momentum to cause the blow shock wave to bulge out, seems extremely promising as a means of alleviating the heating problem. It would form an obvious and interesting extension of the present experiments to be able to vary the momentum flow rates and mass flow rates of an ejected coolant independently. This could be done by varying the size of the ejection pipe.

This investigation was made under Army Ordnance Contract No. DA-04-495-Ord-19 whilst the author was at the Guggenheim Aeronautical Laboratory, California Institute of Technology, on a Harkness Fellowship of the Commonwealth Fund of New York.

(*a*) (*b*) (*c*) (*d*) (*e*) (*f*)

FIGURE 8 (plate 1). Schlieren photographs. (*a*) No ejection, $C_{\dot{m}} = 0$; $\alpha = 0°$. (*b*) Nitrogen ejected straight out, $C_{\dot{m}} = 0{\cdot}002$; $\alpha = 0°$. (*c*) Nitrogen ejected straight out, $C_{\dot{m}} = 0{\cdot}004$; $\alpha = 0°$. (*d*) Nitrogen ejected with swirl, $C_{\dot{m}} = 0{\cdot}006$; $\alpha = 0°$. (*e*) Nitrogen ejected with swirl, $C_{\dot{m}} = 0{\cdot}006$; $\alpha = 4°$. (*f*) Nitrogen ejected with swirl, $C_{\dot{m}} = 0{\cdot}006$; $\alpha = 8°$.

(*Facing p.* 416)

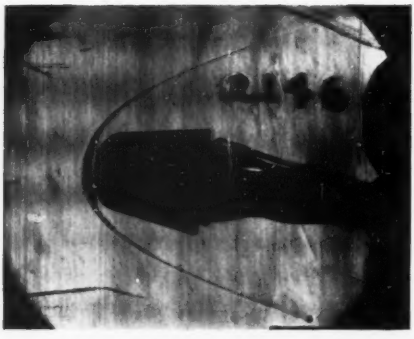

(*g*)

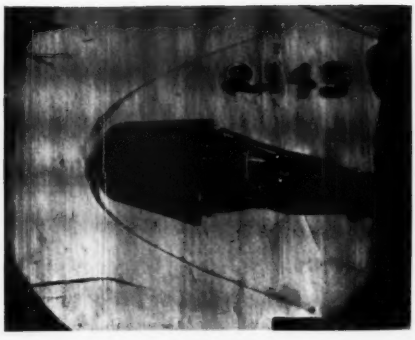

(*h*)

(*i*)

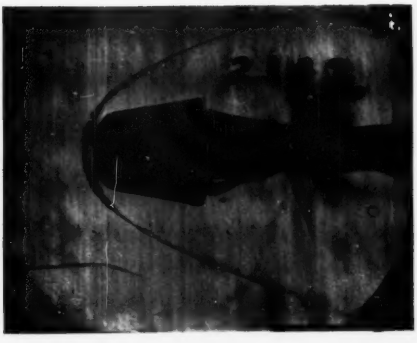

(*j*)

FIGURE 8 (plate 2). Schlieren photographs. (*g*) Nitrogen ejected straight out, $C_m = 0{\cdot}004$; $\alpha = 8^\circ$. (*h*) Nitrogen ejected straight out, $C_m = 0{\cdot}006$, $\alpha = 8^\circ$. (*i*) Helium ejected straight out, $C_m = 0{\cdot}002$, $\alpha = 0^\circ$. (*j*) Helium ejected with swirl, $C_m = 0{\cdot}002$; $\alpha = 0^\circ$.

Bo

Co

La

Le

Mc

Ri

W

REFERENCES

BOGDONOFF, S. M. & VAS, I. E. 1959 Preliminary investigations of spiked bodies at hypersonic speeds. *J. Aero/Space Sci.* **26**, 65–74.

COHEN, C. B. & RESHOTKO, E. 1956 The compressible laminar boundary layer with heat transfer and arbitrary pressure gradient. *N.A.C.A. Report* 1294.

LAM, S. H. 1959 Interaction of a two-dimensional inviscid incompressible jet facing a hypersonic stream. *AFOSR TN* 59-274, *Report*, no. 447.

LEES, L. 1956 Laminar heat transfer over blunt-nosed bodies at hypersonic flight speeds. *Jet Propulsion*, **26**, 259–69.

MCMAHON, H. M. 1958 An experimental study of the effect of mass injection at the stagnation point of a blunt body. California Institute of Technology Guggenheim Aeronautial Laboratory Hypersonic Research Project Memorandum, no. 42.

RICHARDS, H. K. 1957 An experimental investigation of heat transfer rates on a blunt body in hypersonic flow. California Institute of Technology Guggenheim Aeronautical Laboratory Ae E Thesis.

WARREN, C. H. E. 1958 An experimental investigation of the effect of ejecting a coolant gas at the nose of a blunt body. California Institute of Technology Guggenheim Aeronautical Laboratory Hypersonic Research Project Memorandum, no. 47.

On Kelvin's ship-wave pattern

By F. URSELL

Department of Applied Mathematics and Theoretical Physics, University of Cambridge

(Received 25 October 1959)

When a concentrated pressure travels with constant velocity over the free surface of water, it carries with it a familiar pattern of ship waves. Let viscosity and surface tension be neglected, let the free-surface condition be linearized, let the depth of water be assumed infinite, and let initial transient effects be ignored. Then, as is well known, the wave motion everywhere can be found by standard methods in the form of a double integral. The wave pattern at a great distance behind the disturbance can be found by an application of the ordinary method of stationary phase, which shows that the wave amplitude is considerable inside an angle bounded by the two horizontal rays $\theta = \pm\theta_c$ from the disturbance, where $\theta_c = \sin^{-1}\frac{1}{3} \doteqdot 19\frac{1}{2}°$. But the method fails in two regions, near the track $\theta = 0$ of the pressure point, and near the critical lines $\theta = \pm\theta_c$.

These two regions are treated in the present paper. It is shown that near $\theta = 0$ the linearized surface elevation oscillates with indefinitely increasing amplitude and indefinitely decreasing wavelength. (This result holds only when the pressure is concentrated at a point and applied at the free surface.) Near the critical lines the surface elevation at a greater distance behind the pressure point can be expressed in terms of Airy functions, and this expression goes over into the known wave pattern inside the critical angle. It is shown that near the critical lines the crest length increases as the cube root of the distance, and that the separation between crests remains constant. Contour maps of the wave surface are given for three distances behind the moving pressure point.

1. Introduction

When a disturbance (e.g. a ship) travels on a water surface, it carries with it a familiar pattern of bow and stern waves which was first explained mathematically by Lord Kelvin (Sir W. Thomson 1891). Instead of ship waves he considered the waves generated by a prescribed pressure distribution moving with a constant velocity U and acting on the water surface. The magnitude of the pressure and the resulting wave slope were assumed to be so small that the equations of motion could be linearized; viscosity and surface tension were neglected. Under these assumptions it is sufficient (in principle) to calculate the waves due to a moving concentrated pressure point; the effect of a distribution of surface pressure can thence be found by integration. Kelvin showed, apparently by using his principle of stationary phase, that the characteristic wave pattern of a pressure point is the superposition of two sets of waves effectively confined between the two vertical planes $\theta = \pm\theta_c \doteqdot \pm 19\frac{1}{2}$, where the co-ordinates are taken as in § 2 below;

for a figure see Lamb (1932, §256). A simple argument using such ideas was given by Havelock (1908, p. 417), and by Lamb (1932, §256). All these results are valid at a distance of many wavelengths behind the pressure point; near the pressure point the principle of stationary phase is not applicable. It was found that near the critical lines $\theta = \pm\theta_c$ the amplitude is much larger than elsewhere at the same distance from the pressure point, and the simplest form of the principle of the stationary phase could not be used there. (Kelvin predicted infinite amplitudes on $\theta = \theta_c$; the amplitude variation on $\theta = \theta_c$ was first given correctly by Havelock (1908, see equation (4.1) below).) The study of the wave pattern near, but not actually on, a critical line is more difficult and was undertaken by Hogner (1923) who was able to write the surface elevation as the sum of a double and of a single integral, and to show that only the latter is significant at a large distance behind the pressure point. This is convenient because the application of the methods of steepest descents and of stationary phase to single integrals is simple. There are, however, some difficulties in his work. First, the single integral has one finite limit of integration, and this leads to complications (see p. 19 of his paper). Secondly, near the lines $\theta = \pm\theta_c$, where a single asymptotic expression in terms of Airy functions would be expected (cf. equation (4.12) below), Hogner's expression changes its form as θ passes through θ_c (Hogner, 1923, equations (82), (83)).

A new treatment of the problem has been given by Peters (1949). The surface elevation was obtained by him in a form similar to Hogner's, as the sum of a double and a single integral where again only the latter contributes significantly to the waves far behind the pressure point; but Peters's integral, unlike Hogner's, has both limits of integration at infinity. By an immediate application of the method of steepest descents he found expressions which are valid when θ is not near θ_c. An expression was also given for θ on and near $\theta = \theta_c$; but this is valid only when $N^{\frac{2}{3}}|\theta - \theta_c|$ is small, see §4 below.

While the work of Peters has thus reduced the problem of finding the waves far behind the pressure point to the asymptotic evaluation of a single integral containing a large parameter, there are two regions which have not yet received adequate treatment, and these will be considered in the present paper. One is the vicinity of the track of the pressure point where θ and z are small. The limits are non-uniform: we shall see by applying the method of steepest descents that the amplitude tends to ∞ as θ tends to 0 on $z = 0$ (but on $\theta = 0$ it is finite as z tends to 0). The other region is the neighbourhood of $\theta = \theta_c$, where an expression in terms of Airy functions will be given; here the method of Chester, Friedman & Ursell (1957) is applicable, and the expression is valid in some finite angle including the line $\theta = \theta_c$.

2. The elevation due to a travelling pressure point

Peters has calculated the velocity potential and the surface elevation $\zeta(x, y; U, g)$ above the mean water level. In this calculation the exact free-surface condition has been replaced by its linearized approximation. Take the origin of co-ordinates travelling with the surface pressure point, the x-axis horizontal along the track of the disturbance, and the y-axis horizontal at

right angles to the x-axis. Write $K = g/U^2$ and define N and θ by the equations

$$Kx = N\cos\theta, \quad Ky = N\sin\theta. \tag{2.1}$$

The critical angle θ_c is defined by

$$\theta_c = \sin^{-1}\tfrac{1}{3} = \tan^{-1}\frac{1}{2\sqrt{2}} \doteqdot 19\tfrac{1}{2}^\circ;$$

and the total force acting on the fluid is denoted by P_0.

Then Peters's expressions for $\zeta(x, y)$ are:

for $x > 0$

$$\zeta(x, y) = \zeta_1(x, y) + \zeta_2(x, y),$$

where

$$\frac{\pi^2\rho U^2}{P_0}\zeta_1(x, y) = \int_0^\infty dk\, k^2 e^{-kx}\int_0^{\frac{1}{2}\pi} d\gamma \frac{\sin^2\gamma\cos(ky\cos\gamma)}{K^2 + k^2\sin^2\gamma},$$

and

$$\begin{aligned} -\frac{\pi\rho g}{P_0 K^2}\zeta_2(x, y) &= 2\lim_{z\to 0}\int_0^\infty (1+u^2)\cos\{Kyu\sqrt{(1+u^2)}\}\sin\{Kx\sqrt{(1+u^2)}\}\exp\{-Kz(1+u^2)\}\,du \\ &= \operatorname{im}\lim_{z\to 0}\int_{-\infty}^\infty (1+u^2)\exp[iN\{(\cos\theta - u\sin\theta)\sqrt{(1+u^2)}\}]\exp\{-Kz(1+u^2)\}\,du; \end{aligned} \tag{2.2}$$

while for $x < 0$, $\zeta(x, y) = \zeta_1(-x, y)$. At the pressure point $x = 0$, $y = 0$ the integrals diverge.

It appears impossible to express ζ_1 and ζ_2 in terms of known functions, but asymptotic expansions for the amplitude at a large distance ($N \gg 1$) behind the pressure point can be found, and these show that the contribution of ζ_1 is negligible inside the critical angle $|\theta| \leqslant \theta_c$. For according to P, p. 142,*

$$\frac{\pi^2\rho K^2 U^2}{P_0}\zeta_1(x, y) = \frac{\pi}{(x^2+y^2)^{\frac{1}{2}}} - \frac{3\pi y^2}{2(x^2+y^2)^{\frac{5}{2}}} - \int_0^\infty dk\, k^4 e^{-kx}\int_0^{\frac{1}{2}\pi} d\gamma \frac{\cos(ky\cos\gamma)}{k^2 + K^2\sin^2\gamma}; \tag{2.3}$$

and when the substitution $k = Ku\sin\gamma$ is made in the double integral, this becomes

$$\begin{aligned} &\int_0^\infty du\int_0^{\frac{1}{2}\pi} d\gamma \frac{(K\sin\gamma)^3 u^4}{1+u^2}\exp(-Kxu\sin\gamma)\cos(Kyu\sin\gamma\cos\gamma) \\ &\quad = \frac{1}{2}\int_0^\pi d\gamma (K\sin\gamma)^3\int_0^\infty du\frac{u^4}{1+u^2}\exp(-Kxu\sin\gamma - iKyu\sin\gamma\cos\gamma) \\ &\quad = \frac{1}{2}\int_0^\pi d\gamma (K\sin\gamma)^3 F_0(Kx\sin\gamma + iKy\sin\gamma\cos\gamma), \end{aligned} \tag{2.4}$$

where by definition

$$F_0(Z) \equiv \int_0^\infty \frac{u^4 e^{-uZ}}{1+u^2}\,du = \frac{2}{Z^3} - \frac{1}{Z} + \int_0^\infty \frac{e^{-uZ}}{1+u^2}\,du.$$

* References preceded by the letters H or P are to Hogner (1923) or Peters (1949), respectively.

The last integral is related to the exponential integral (Jeffreys & Jeffreys 1946, p. 443), and it can be shown that for re $Z > 0$ and $|Z| \leqslant 1$ we have

$$|F_0(Z)| < A|Z|^{-3};$$

while for re $Z > 0$ and $|Z| > 1$ we have $|F_0(Z)| < A|Z|^{-5}$, by the method of steepest descents. To find a bound for (2.4), write it as

$$\frac{1}{2}\int_0^{\frac{1}{6}\pi} + \frac{1}{2}\int_{\frac{1}{6}\pi}^{\frac{5}{6}\pi} + \frac{1}{2}\int_{\frac{5}{6}\pi}^{\pi} = I_1 + I_2 + I_3, \text{ say.}$$

In I_1 introduce the new variable $\beta = Kx\sin\gamma + iKy\sin\gamma\cos\gamma$; then

$$\left|\frac{d\beta}{d\gamma}\right| = |Kx\cos\gamma + iKy\cos 2\gamma| \geqslant \tfrac{1}{2}|Kx + iKy| = \tfrac{1}{2}N,$$

and

$$|K\sin\gamma| = |\beta(x+iy\cos\gamma)^{-1}| < 2\beta|x+iy|^{-1} = 2\beta KN^{-1}.$$

Thus,

$$|I_1| \leqslant \frac{1}{2}\int_0^{\infty} |2\beta|^3 K^3 N^{-3} |F_0(\beta)| 2N^{-1}|d\beta| < AK^3N^{-4}. \tag{2.5}$$

Similarly,

$$|I_3| < AK^3N^{-4}.$$

To find a bound for I_2, deform the path of integration in the γ-plane to pass below $\gamma = \frac{1}{2}\pi$; on the new path, the real part of $Kx\sin\gamma + iKy\sin\gamma\cos\gamma$ is positive, and

$$|Kx\sin\gamma + iKy\sin\gamma\cos\gamma| > A|Kx + iKy|$$

which is uniformly large when N is large. Thus

$$|I_2| \leqslant A\int_{\frac{1}{6}\pi}^{\frac{5}{6}\pi} K^3N^{-5}|d\gamma| < AK^3N^{-5}, \tag{2.6}$$

and equations (2.5) and (2.6) show that the double integral in (2.3) is $O(K^3N^{-4})$. Thus ζ_1 is of order N^{-3} everywhere, while ζ_2 is of order $N^{-\frac{1}{2}}$ inside the critical angle, and exponentially small outside the critical angle, see P, equations (5.2), (5.4). Thus, ζ_2 is dominant inside the critical angle, ζ_1 outside. We are considering the asymptotic form of $\zeta(x, y)$ for large $N = K|x+iy|$; the expressions (2.3) and P (5.2), (5.4) are adequate except near $\theta = 0$ and $\theta = \pm\theta_c$. (They will not be quoted here; see, however, § 4 below.) We shall now obtain new expansions valid near $\theta = 0$ and $\theta = \theta_c$.

3. The track of the pressure point

We shall have to evaluate (2.2) for small θ, where, by reason of the symmetry of the pattern, we shall take $\theta \geqslant 0$. If we attempt to find the limit in (2.2) by putting $z = 0$ in (2.2) we see that the resulting integral does not converge. This difficulty is avoided if the path of integration is deformed before z is placed equal to 0. The new path is chosen so that

$$\exp[iN\{(\cos\theta - u\sin\theta)\sqrt{(1+u^2)}\}] \tag{3.1}$$

tends to zero rapidly as $|u| \to \infty$ along the new path, and there are two cases, $\theta = 0$ and $\theta > 0$, which must be considered separately.

(i) If $\theta = 0$, take a path of integration along the straight line from $u = -\infty\exp(\frac{1}{8}\pi i)$ through $u = 0$ to $\infty\exp(\frac{1}{8}\pi i)$, say. Along this path

$\exp\{iN\sqrt{(1+u^2)}\} \to 0$ as $|u| \to \infty$, and $\exp\{-Kz(1+u^2)\}$ is uniformly bounded for all u on the path and all $z \geqslant 0$. Thus, this integral is uniformly convergent as $z \to 0$, and

$$-\frac{\pi\rho g}{P_0K^2}\zeta_2(x,0) = \operatorname{im}\int_{-\infty\exp(\frac{1}{8}\pi i)}^{\infty\exp(\frac{1}{8}\pi i)} (1+u^2)\exp\{iN\sqrt{(1+u^2)}\}\,du. \tag{3.2}$$

(Clearly a good deal of latitude is allowed in the choice of the path.) This may be written in terms of Bessel functions, (P, p. 140, cf. Hogner 1924, p. 7):

$$\zeta_2(x,0) = \frac{P_0K^2}{4\rho g}\{3Y_1(Kx) - Y_3(Kx)\} \sim -\frac{P_0K^2}{\rho g}\left(\frac{2}{\pi Kx}\right)^{\frac{1}{2}}\cos(Kx - \tfrac{1}{4}\pi), \tag{3.3}$$

and so ζ_2 is finite when Kx is positive.

(ii) If $\theta > 0$, take a path of integration along the straight line from $u = -\infty\exp(\frac{1}{8}\pi i)$ to $u = 0$, and thence along the straight line to $u = \infty\exp(-\frac{1}{8}\pi i)$ Along this path the expression (3.1) tends to 0 as $|u| \to \infty$, and $\exp\{-Kz(1+u^2)\}$ is uniformly bounded. Thus, as in (i), the integral is uniformly convergent as $z \to 0$ for fixed θ, and

$$-\frac{\pi\rho g}{P_0K^2}\zeta_2(x,y) = \operatorname{im}\int_{-\infty\exp(\frac{1}{8}\pi i)}^{\infty\exp(-\frac{1}{8}\pi i)} (1+u^2)\exp[iN\{(\cos\theta - u\sin\theta)\sqrt{(1+u^2)}\}]\,du. \tag{3.4}$$

We note that the limits of integration in (3.2) and (3.4) are different, and we are led to suspect singular behaviour near $\theta = 0$. This is confirmed by the following calculation. First, deform the path of (3.4) into two paths of steepest descent through the two saddle points. These points are the roots of

$$(d/du)\{(\cos\theta - u\sin\theta)\sqrt{(1+u^2)}\} = 0,$$

i.e. the roots of $\quad u\cos\theta - (1+2u^2)\sin\theta = 0,$

i.e. the points

$$u_+(\theta) = \tfrac{1}{4}\{\cot\theta + \sqrt{(\cot^2\theta - 8)}\} \quad \text{and} \quad u_-(\theta) = \tfrac{1}{4}\{\cot\theta - \sqrt{(\cot^2\theta - 8)}\}, \tag{3.5}$$

which are real if $\theta < \theta_c$ as we may suppose in this section. The paths of steepest descent are sketched in P, fig. 5, in the plane of a convenient variable $\tau = \sinh^{-1}u$ in terms of which the function

$$F(u) \equiv (\cos\theta - u\sin\theta)\sqrt{(1+u^2)} \tag{3.6}$$

is single-valued. The paths of steepest descent $C_-(\theta), C_+(\theta)$ in the cut u-plane are their conformal images and are shown schematically in figure 1.

The path of (3.4) can be deformed into $C_- + C_+$. Consider the behaviour of the integral as $\theta \to 0$. It is easy to see that the integrand tends to zero uniformly as $|u| \to \infty$ along $C_-(\theta)$, and so, as $\theta \to 0$,

$$\begin{aligned}\int_{C_-} &\to \int_{-\infty\exp(\frac{3}{4}\pi i)}^{\infty\exp(\frac{1}{4}\pi i)} (1+u^2)\exp\{iN\sqrt{(1+u^2)}\}\,du \\ &= \int_{-\infty\exp(\frac{1}{4}\pi i)}^{\infty\exp(\frac{1}{4}\pi i)} (1+u^2)\exp\{iN\sqrt{(1+u^2)}\}\,du,\end{aligned}$$

whence $\qquad \operatorname{im}\int_{C_-} \to -\tfrac{1}{4}\{3Y_1(Kx) - Y_3(Kx)\},$

see equation (3.3)).

As for the integral along $C_+(\theta)$, we note that $u_+(\theta) \sim \frac{1}{2}\cot\theta \to \infty$; thus $C_+(\theta)$ moves off to infinity as $\theta \to 0$. Introduce a new variable $v = u\tan\theta$, in terms of which

$$\int_{C_+} = \cot^3\theta \int_{\infty \exp(\frac{1}{3}\pi i)}^{\infty \exp(-\frac{1}{3}\pi i)} (v^2 + \tan^2\theta) \exp\left[\frac{iN\cos^2\theta}{\sin\theta}\{(1-v)\sqrt{(v^2+\tan^2\theta)}\}\right] dv. \tag{3.7}$$

The expression $\{\}$ has a saddle point at $v_+(\theta) = u_+(\theta)\tan\theta = \frac{1}{4}(1+\sqrt{(1-8\tan^2\theta)})$, which remains finite as $\theta \to 0$; and the expression $(N\cos^2\theta/\sin\theta) = M$ is a large

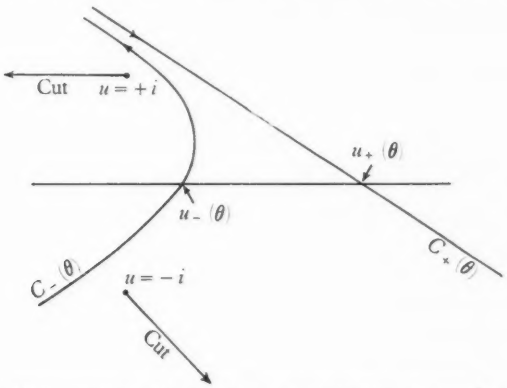

FIGURE 1. Deformation of the contour of integration for small values of θ.

parameter tending to ∞ as $\theta \to 0$ (whether N is large or not). If we apply the ordinary method of steepest descents (see, for example, Jeffreys & Jeffreys 1946, §17.04) to (3.7), we find (the details are omitted) that

$$\int_{C_+} \sim \frac{\cot^3\theta}{4M^{\frac{1}{2}}} \pi^{\frac{1}{2}} \exp\{iMf(\theta) - \tfrac{1}{4}\pi i\}, \quad \text{whence near } \theta = 0$$

$$-\frac{\pi\rho g}{P_0 K^2}\zeta_2(x,y) = \mathrm{im}\int_{C_+}$$

$$= \tfrac{1}{4}\pi^{\frac{1}{2}} N^{-\frac{1}{2}} (\sin\theta)^{-\frac{5}{2}} \sin\left(\frac{N\cos^2\theta}{\sin\theta} f(\theta) - \tfrac{1}{4}\pi\right) + o(N^{-\frac{1}{2}}(\sin\theta)^{-\frac{5}{2}}), \tag{3.8}$$

where by definition

$$f(\theta) \equiv \frac{3^{\frac{3}{2}}}{16}(1 - \tfrac{1}{3}\sqrt{(1-8\tan^2\theta)})^{\frac{3}{2}}(1+\sqrt{(1-8\tan^2\theta)})^{\frac{1}{2}},$$

$$\to \tfrac{1}{4} \quad \text{as} \quad \theta \to 0.$$

The equation (3.8) shows that the free surface oscillates with infinitely increasing amplitude and infinitely decreasing wavelength as $\theta \to 0$. This behaviour may be compared with the behaviour of waves due to a concentrated initial pressure (Lamb 1932, §239), and is responsible for the infinite wave resistance of the surface pressure point. (For a submerged pressure point or distributed pressure the amplitude on $\theta = 0$ and wave resistance are finite.) We note again that to obtain (3.8) it was not necessary to assume that N is large.

4. The neighbourhood of the critical lines

We have noted in § 1 that existing expansions are inadequate in various ways near $\theta = \pm\theta_c$. On the line $\theta = \theta_c$ itself, the function $F(u)$ of (3.6) has a double zero, and the saddle points $u_+(\theta), u_-(\theta)$ coalesce into a saddle point of higher order at $u = 1/\sqrt{2}$ which is easily treated by the method of steepest descents. Peters (equations (5.3), (5.5) with an error in sign in (5.3)) has shown that

$$-\frac{\pi\rho g}{P_0 K^2}\zeta_2(x, x\tan\theta_c)$$

$$\sim \frac{3^{\frac{1}{6}}}{2^{\frac{2}{3}}}\frac{\Gamma(\frac{1}{3})}{N^{\frac{1}{3}}}\sin\left(\frac{3^{\frac{1}{2}}}{2}N\right) - \frac{3^{\frac{7}{6}}}{2^{\frac{5}{3}}}\frac{\Gamma(\frac{2}{3})}{N^{\frac{2}{3}}}\cos\left(\frac{3^{\frac{1}{2}}}{2}N\right), \tag{4.1}$$

where $$N = Kx\sec\theta_c.$$

Thus, on (and presumably near) $\theta = \theta_c$, the amplitude decreases as $N^{-\frac{1}{3}}$, while elsewhere it decreases as $N^{-\frac{1}{2}}$ (see P (5.2), (5.4)), and so the waves are prominent near $\theta = \theta_c$ when N is large. We shall now obtain an asymptotic expression which is valid in a finite angle inciuding the line $\theta = \theta_c$. This is to be compared with Hogner's equations (H (82), (83)) which change in form as the line $\theta = \theta_c$ is crossed; it is believed that these hold when $N^{\frac{2}{3}}|\theta - \theta_c|$ is large and $N^{\frac{1}{3}}|\theta - \theta_c|$ is small, but their precise region of validity has not been investigated. Our asymptotic formula will be derived by the method of Chester *et al.* (1957) and will involve the Airy function (see Jeffreys & Jeffreys 1946, § 17.07)

$$\mathrm{Ai}(Z) = \frac{1}{2\pi i}\int_{\infty\exp(-\frac{1}{3}\pi i)}^{\infty\exp(\frac{1}{3}\pi i)} \exp(\tfrac{1}{3}t^3 - Zt)\,dt, \tag{4.2}$$

$$= \frac{1}{\pi}\int_0^\infty \cos(\tfrac{1}{3}t^3 + Zt)\,dt$$

when Z is real. Since in (4.2) the argument of the exponential is a cubic polynomial, comparison with (3.4) suggests the introduction of a new complex variable v by the implicit relation

$$F(u,\theta) \equiv (\cos\theta - u\sin\theta)\sqrt{(1+u^2)} = -\tfrac{1}{3}v^3 + \mu(\theta)\,v - \nu(\theta), \tag{4.3}$$

where $\mu(\theta)$ and $\nu(\theta)$ are to be chosen so as to make the transformation regular in a uniform neighbourhood of $u = 1/\sqrt{2}$ for all θ sufficiently close to θ_c. The segments of the path of integration of (3.4) lying outside this neighbourhood are deformed into segments of paths of steepest descent from the saddle points, and the contribution from these is negligible, as in the ordinary method of steepest descents. The only significant contribution thus comes from the neighbourhood of the (nearly coincident) saddle points where the transformation (4.3) is applicable.

On differentiating (4.3), keeping θ fixed, we get

$$\frac{\partial F(u,\theta)}{\partial u}\frac{du}{dv} = -v^2 + \mu(\theta). \tag{4.4}$$

The left-hand side vanishes when $u = u_{\pm}(\theta)$, the right-hand side when $v = \pm\mu^{\frac{1}{2}}(\theta)$. If the (u, v)-transformation is to be regular, these points must correspond, and so, from (4.3),

$$\left.\begin{aligned} F(u_+, \theta) &\equiv (\cos\theta - u_+ \sin\theta)\sqrt{(1+u_+^2)} = \tfrac{2}{3}\mu^{\frac{3}{2}}(\theta) - \nu(\theta), \\ F(u_-, \theta) &\equiv (\cos\theta - u_- \sin\theta)\sqrt{(1+u_-^2)} = -\tfrac{2}{3}\mu^{\frac{3}{2}}(\theta) - \nu(\theta), \end{aligned}\right\} \tag{4.5}$$

where $u_+(\theta)$ and $u_-(\theta)$ are known functions of θ, see equation (3·5). These equations are readily solved for $\mu(\theta)$ and $\nu(\theta)$

$$\mu^{\frac{3}{2}}(\theta) = \frac{3^{\frac{5}{2}}}{64}\frac{\cos^2\theta}{\sin\theta}\{(1+Q)^{\frac{1}{2}}(1-\tfrac{1}{3}Q)^{\frac{3}{2}} - (1-Q)^{\frac{1}{2}}(1+\tfrac{1}{3}Q)^{\frac{3}{2}}\}, \tag{4.6}$$

$$\nu(\theta) = -\frac{3^{\frac{3}{2}}}{32}\frac{\cos^2\theta}{\sin\theta}\{(1+Q)^{\frac{1}{2}}(1-\tfrac{1}{3}Q)^{\frac{3}{2}} + (1-Q)^{\frac{1}{2}}(1+\tfrac{1}{3}Q)^{\frac{3}{2}}\}, \tag{4.7}$$

where $Q \equiv \sqrt{(1-8\tan^2\theta)}$. By expanding these expressions it can be shown that $\mu(\theta)$ and $\nu(\theta)$ involve only even powers of Q and are therefore regular functions of θ.

This also follows from the general theory (Chester *et al.* 1957), which shows further that with these values of $\mu(\theta)$ and $\nu(\theta)$ the transformation (4.3) is indeed uniformly regular, and that the points $u = u_{\pm}(\theta), v = \pm\mu^{\frac{1}{2}}(\theta)$ correspond. Following the procedure explained by Chester *et al.* (1957) we change the variable of integration in (3.4) to v, and expand $(1+u^2)\,du/dv$ in the form

$$(1+u^2)\frac{du}{dv} = \sum_0^\infty p_m(\theta)\,(v^2-\mu(\theta))^m + v\sum_0^\infty q_m(\theta)\,(v^2-\mu(\theta))^m,$$

which holds uniformly when v and $\theta - \theta_c$ are sufficiently small. The theory shows that the asymptotic expansion of (3.4) is

$$\Sigma p_m(\theta)\int (v^2-\mu(\theta))^m \exp[iN(-\tfrac{1}{3}v^3+\mu v-\nu)]\,dv + \Sigma q_m(\theta)\int v(v^2-\mu(\theta))^m \exp[iN(-\tfrac{1}{3}v^3+\mu v-\nu)]\,dv,$$

where the integration can be extended with a negligible error from $-\infty\exp(\frac{1}{6}\pi i)$ to $\infty\exp(-\frac{1}{6}\pi i)$, cf. P, fig. 6. To obtain the dominant terms it is sufficient to calculate the leading coefficients $p_0(\theta)$ and $q_0(\theta)$. On putting $u = u_{\pm}(\theta), v = \pm\mu^{\frac{1}{2}}(\theta)$, we find that

$$(1+u_{\pm}^2)\left(\frac{du}{dv}\right)_{\pm} = p_0(\theta) \pm \mu^{\frac{1}{2}}(\theta)\,q_0(\theta),$$

and the left-hand side is known when du/dv is known at $v = \pm\mu^{\frac{1}{2}}(\theta)$.

But, from (4.4),

$$\frac{\partial^2 F}{\partial u^2}\left(\frac{du}{dv}\right)^2 + \frac{\partial F}{\partial u}\frac{d^2u}{dv^2} = -2v,$$

whence

$$\left(\frac{\partial^2 F}{\partial u^2}\right)_{\pm}\left(\frac{du}{\partial v}\right)_{\pm}^2 = \mp 2\mu^{\frac{1}{2}}, \tag{4.8}$$

where

$$\left(\frac{\partial^2 F}{\partial u^2}\right)_{\pm} = \mp\frac{4}{3^{\frac{1}{2}}}\sin\theta\,Q(1\pm Q)^{-\frac{1}{2}}(1\mp\tfrac{1}{3}Q)^{-\frac{1}{2}}, \tag{4.9}$$

as is easily shown. The sign of $(du/dv)_\pm$ is positive for small $\theta-\theta_c$, since $u=u_\pm$, $v=\pm\mu^{\frac{1}{2}}$ correspond. Thus, from (4.8) and (4.9),

$$(1+u_\pm^2)\left(\frac{du}{dv}\right)_\pm = \frac{3^{\frac{3}{4}}}{2^{\frac{3}{2}}}\frac{\cos^2\theta}{\sin^{\frac{5}{2}}\theta}\left(\frac{\mu(\theta)}{1-8\tan^2\theta}\right)^{\frac{1}{4}}(1\pm Q)^{\frac{3}{4}}(1\mp\tfrac{1}{3}Q)^{\frac{3}{4}},$$

whence

$$p_0(\theta)=\frac{3^{\frac{3}{4}}}{2^{\frac{11}{2}}}\frac{\cos^2\theta}{\sin^{\frac{5}{2}}\theta}\left(\frac{\mu(\theta)}{1-8\tan^2\theta}\right)^{\frac{1}{4}}\{(1+Q)^{\frac{3}{4}}(1-\tfrac{1}{3}Q)^{\frac{3}{4}}+(1-Q)^{\frac{3}{4}}(1+\tfrac{1}{3}Q)^{\frac{3}{4}}\} \tag{4.10}$$

and

$$q_0(\theta)=\frac{3^{\frac{3}{4}}}{2^{\frac{11}{2}}}\frac{\cos^2\theta}{\sin^{\frac{5}{2}}\theta}\left(\frac{\mu(\theta)}{1-8\tan^2\theta}\right)^{-\frac{1}{4}}Q^{-1}\{(1+Q)^{\frac{3}{4}}(1-\tfrac{1}{3}Q)^{\frac{3}{4}}-(1-Q)^{\frac{3}{4}}(1+\tfrac{1}{3}Q)^{\frac{3}{4}}\}, \tag{4.11}$$

where $Q=N(1-8\tan^2\theta)$; the functions $p_0(\theta)$ and $q_0(\theta)$ are regular near $\theta=\theta_c$. We thus see that the integral (3.4) is asymptotically

$$p_0(\theta)\int\exp[iN(-\tfrac{1}{3}v^3+\mu v-\nu)]\,dv+q_0(\theta)\int v\exp[iN(-\tfrac{1}{3}v^3+\mu v-\nu)]\,dv$$

$$=-ip_0(\theta)\int\exp[N(\tfrac{1}{3}w^3+\mu w-i\nu)]\,dw-q_0(\theta)\int w\exp[N(\tfrac{1}{3}w^3+\mu w-i\nu)]\,dw,$$

where $w=iv$ and the integration is from $w=\infty\exp(-\frac{1}{3}\pi i)$ to $w=\infty\exp(\frac{1}{3}\pi i)$. But these integrals are multiples of the Airy function (4.2) and of its derivative. Thus the integral in (3.4) is asymptotically

$$2\pi i\exp(-iN\nu(\theta))\{-iN^{-\frac{1}{3}}p_0(\theta)\,\mathrm{Ai}(-N^{\frac{2}{3}}\mu(\theta))+N^{-\frac{2}{3}}q_0(\theta)\,\mathrm{Ai}'(-N^{\frac{2}{3}}\mu(\theta))\}.$$

Higher terms in the expression are of order $N^{-\frac{4}{3}}\,\mathrm{Ai}$, $N^{-\frac{5}{3}}\,\mathrm{Ai}'$ at most. The amplitude $\zeta_2(x,y)$ is obtained from the imaginary part, cf. equation (3.4)

$$\frac{\rho g}{2P_0K^2}\zeta_2(x,y)\sim\frac{p_0(\theta)}{N^{\frac{1}{3}}}\,\mathrm{Ai}(-N^{\frac{2}{3}}\mu(\theta))\sin(N\nu(\theta))$$

$$-\frac{q_0(\theta)}{N^{\frac{2}{3}}}\,\mathrm{Ai}'(-N^{\frac{2}{3}}\mu(\theta))\cos(N\nu(\theta)), \tag{4.12}$$

where $\mu(\theta)$, $\nu(\theta)$, $p_0(\theta)$, $q_0(\theta)$ are defined by equations (4.6), (4.7), (4.10), (4.11), respectively, and are regular near $\theta=\theta_c$. It can be shown that near $\theta=\theta_c$.

$$\left.\begin{aligned}\mu(\theta)&=-\frac{3}{2^{\frac{2}{3}}}(\theta-\theta_c)+O((\theta-\theta_c)^2),\\ \nu(\theta)&=-\frac{3^{\frac{1}{2}}}{2}+\frac{3^{\frac{1}{2}}}{2^{\frac{1}{3}}}(\theta-\theta_c)+O((\theta-\theta_c)^2),\end{aligned}\right\} \tag{4.13}$$

and that

$$p_0(\theta_c)=\frac{3^{\frac{3}{4}}}{2^{\frac{3}{2}}},\quad q_0(\theta_c)=\frac{15}{2^{\frac{5}{2}}}.$$

Values of the functions $\mu(\theta)$, $\nu(\theta)$, $p_0(\theta)$, $q_0(\theta)$ are shown in Table 1. The functions Ai and Ai′ are tabulated by Miller (1946).

Equation (4.12) gives the wave pattern far behind the travelling pressure point; from the general theory (Chester *et al.* 1957) it follows that it is valid in

θ (degrees)	$\mu(\theta)$	$\nu(\theta)$	$p_0(\theta)$	$q_0(\theta)$
10·00	0·532	−1·227	9·484	11·131
10·25	0·510	−1·210	8·890	10·545
10·50	0·488	−1·193	8·348	10·002
10·75	0·468	−1·177	7·852	9·500
11·00	0·448	−1·162	7·397	9·035
11·25	0·429	−1·147	6·979	8·603
11·50	0·410	−1·133	6·594	8·201
11·75	0·392	−1·120	6·239	7·826
12·00	0·374	−1·107	5·911	7·476
12·25	0·357	−1·095	5·670	7·148
12·50	0·340	−1·083	5·326	6·842
12·75	0·324	−1·071	5·065	6·555
13·00	0·308	−1·060	4·822	6·285
13·25	0·293	−1·050	4·596	6·032
13·50	0·278	−1·039	4·385	5·793
13·75	0·263	−1·030	4·189	5·569
14·00	0·249	−1·020	4·005	5·357
14·25	0·235	−1·011	3·833	5·157
14·50	0·221	−1·002	3·672	4·967
14·75	0·208	−0·993	3·521	4·788
15·00	0·195	−0·984	3·379	4·619
15·25	0·182	−0·976	3·246	4·458
15·50	0·169	−0·968	3·120	4·306
15·75	0·157	−0·961	3·002	4·161
16·00	0·145	−0·953	2·891	4·023
16·25	0·133	−0·946	2·786	3·892
16·50	0·122	−0·939	2·686	3·768
16·75	0·111	−0·932	2·593	3·649
17·00	0·100	−0·925	2·504	3·536
17·25	0·089	−0·918	2·420	3·428
17·50	0·078	−0·912	2·340	3·324
17·75	0·067	−0·906	2·265	3·226
18·00	0·057	−0·899	2·193	3·131
18·25	0·047	−0·894	2·125	3·041
18·50	0·037	−0·888	2·060	2·955
18·75	0·027	−0·882	1·999	2·872
19·00	0·018	−0·876	1·940	2·793
19·25	0·008	−0·871	1·884	2·716
19·50	−0·001	−0·865	1·831	2·643
19·75	−0·010	−0·860	1·780	2·573
20·00	−0·019	−0·855	1·732	2·506

TABLE 1. The coefficient functions $\mu(\theta)$, $\nu(\theta)$, $p_0(\theta)$, $q_0(\theta)$ occurring in equation (4.12) for the elevation

some finite angle including $\theta = \theta_c$ and it reduces to the equations of Peters (P (5.2), (5.4)) when $|N^{\frac{2}{3}}\mu(\theta)|$ is large, as can be shown by using the asymptotic expressions

$$\left.\begin{aligned} \mathrm{Ai}(X) &\sim \tfrac{1}{2}\pi^{-\frac{1}{2}}X^{-\frac{1}{4}}\exp(-\tfrac{2}{3}X^{\frac{3}{2}}), \quad \mathrm{Ai}'(X) \sim -\tfrac{1}{2}\pi^{-\frac{1}{2}}X^{\frac{1}{4}}\exp(-\tfrac{2}{3}X^{\frac{3}{2}}),\\ \mathrm{Ai}(-X) &\sim \pi^{-\frac{1}{2}}X^{-\frac{1}{4}}\cos(\tfrac{2}{3}X^{\frac{3}{2}}-\tfrac{1}{4}\pi), \quad \mathrm{Ai}'(-X) \sim \pi^{-\frac{1}{2}}X^{\frac{1}{4}}\cos(\tfrac{2}{3}X^{\frac{3}{2}}-\tfrac{3}{4}\pi), \end{aligned}\right\} \tag{4.14}$$

valid when X is large and positive. The equation (P (5.5)) is obtained by supposing that $N^{\frac{2}{3}}\mu(\theta)$ is small, expanding the Airy function in powers of $\theta - \theta_c$ and retaining only the first two terms.

5. Description of the wave pattern

Let us consider first the well-known pattern some distance inside the critical lines where the Airy functions may be replaced by their asymptotic expansions in terms of circular functions. When N is large, the surface elevation in this region is of the form (see P (5.2))

$$\frac{A_1(\theta)}{N^{\frac{1}{2}}}\cos\{Nf_1(\theta)+\epsilon_1\}+\frac{A_2(\theta)}{N^{\frac{1}{2}}}\cos\{Nf_2(\theta)+\epsilon_2\}. \tag{5.1}$$

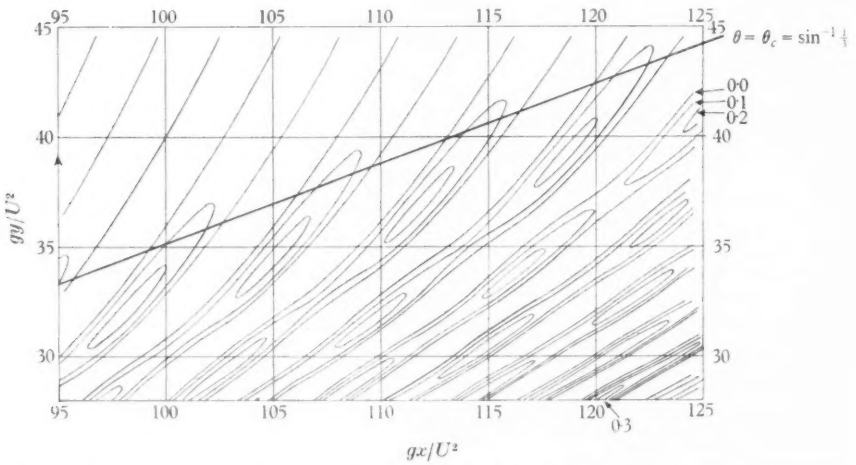

FIGURE 2. Contours of equal magnitude of the dimensionless surface elevation $\rho U^4\zeta_2(x, y)/2gP_0$ due to a concentrated force P_0 moving with velocity U, for $gr/U^2 = 2\pi r/\lambda$ near 100. (Here r denotes the distance from the disturbance, λ the wavelength of waves moving with phase velocity U.) For the sake of clarity only positive values of the elevation are shown. Note that the largest elevation in the figure occurs near the point (120·2, 28), not near $\theta = \theta_c$.

The curves of constant phase corresponding to each term are of the form

$$rf(\theta) = \text{const.};$$

that is, they are geometrically similar with respect to the origin (see also, Lamb 1932, §256). The amplitude of each term falls off like $r^{-\frac{1}{2}}$. The total surface elevation, being the sum of two terms, does not exhibit exact similarity with respect to the origin, but the amplitude is almost periodic along radii from the origin.

Next let us consider the surface elevation (4.12) near the critical line $\theta = \theta_c$ when N is large. For very large N and bounded values of $N^{\frac{2}{3}}|\theta-\theta_c|$ the first term in (4.12) is dominant. Thus, the nodal lines (contours of zero surface elevation) lie near those curves where the first term vanishes, that is, near those curves where either $\sin(N\nu(\theta))$ or $\mathrm{Ai}(-N^{\frac{2}{3}}\mu(\theta))$ vanishes, that is,

$$\text{near } N\nu(\theta) = m\pi, \quad \text{where } m \text{ is any large integer,} \tag{5.2}$$

and

$$\text{near } N^{\frac{2}{3}}\mu(\theta) = |a_1|, |a_2|, \ldots, |a_s|, \ldots, \tag{5.3}$$

where $a_s < 0$ is the sth zero of Ai (z). It follows from (4.13) that the curves (5.2) are ultimately equidistant straight lines crossing $\theta = \theta_c$ at an angle $\tan^{-1} 1/\sqrt{2}$ that is, inclined at an angle $\tan^{-1}\sqrt{2} = \frac{1}{4}\pi + \frac{1}{2}\theta_c \doteqdot 54\frac{3}{4}°$, to the track of the disturbance, as was stated by Kelvin (W. Thomson 1891, p. 485). As for the curves (5.3), it follows from (4.13) that they are approximately of the form

$$Kp \doteqdot \frac{2^{\frac{1}{2}}}{3}(Kr)^{\frac{1}{3}}|a_s|,$$

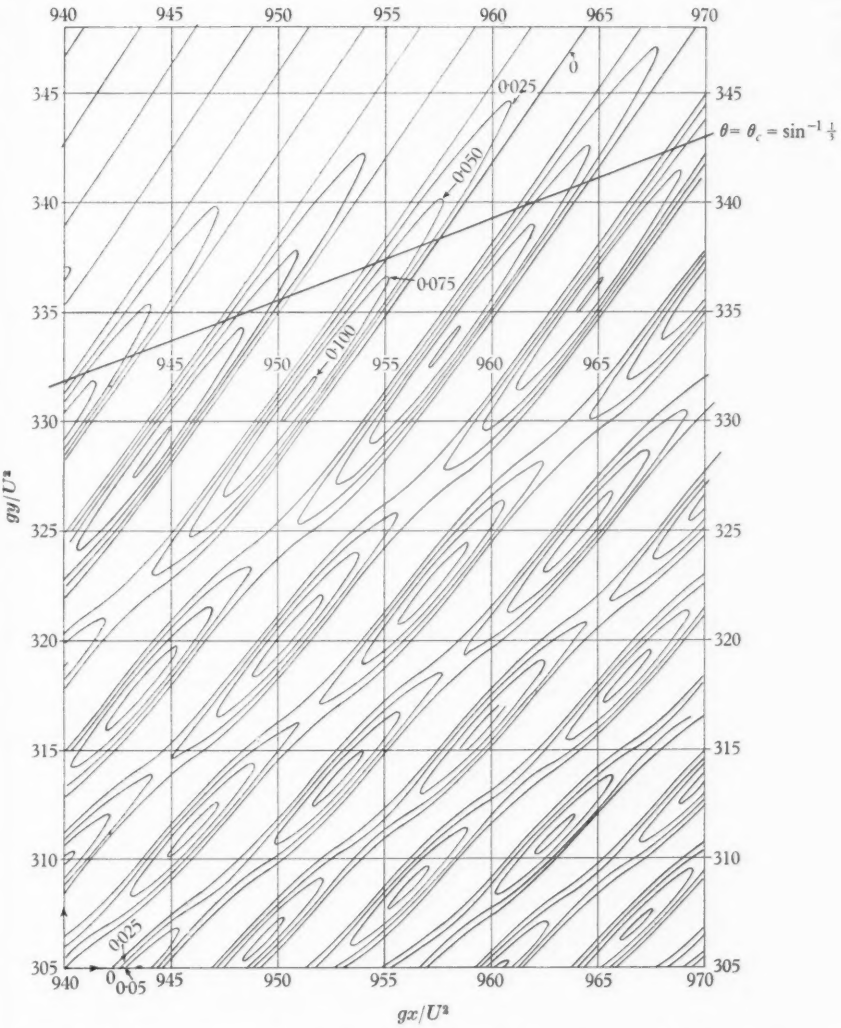

FIGURE 3. Contours of equal magnitude of the dimensionless surface elevation $\rho U^4 \zeta_2(x, y)/2gP_0$, for gr/U^2 near 1000. For the sake of clarity only positive values of the elevation are shown. The elevation again exceeds 0·08 near the point (963, 285).

where p is the perpendicular distance from $\theta = \theta_c$ and r is the distance from the origin. These curves lie inside the critical lines, and it is seen that p increases only slowly with distance from the origin. Thus, the curves (5.2) and (5.3) combine to form a net of (approximate) parallelograms: the sides parallel to $\theta = \theta_c$ are of nearly constant length, while the length of the sides parallel to $\theta = \frac{1}{4}\pi + \frac{1}{2}\theta_c$ increases as the cube root of the distance. The amplitude due to the first term in (4.12) varies with distance as $N^{-\frac{1}{3}}$ and this is ultimately much larger (by a factor

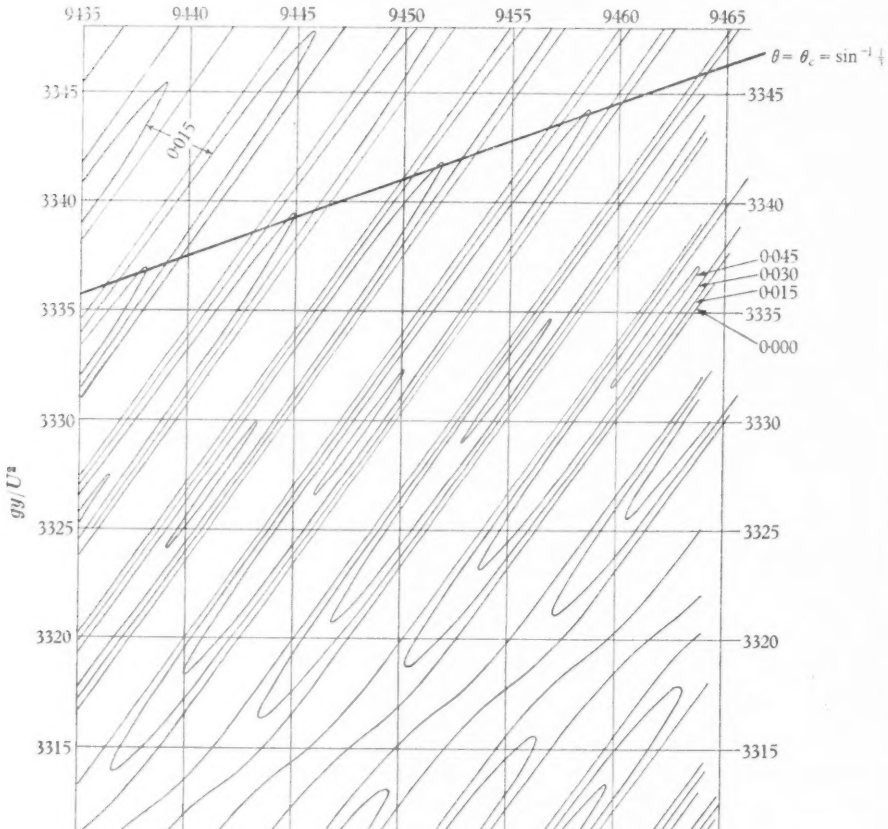

FIGURE 4. Contours of equal magnitude of the dimensionless surface elevation $\rho U^4 \zeta_2(x, y)/2gP_0$, for gr/U^2 near 10,000. For the sake of clarity only positive values of the elevation are shown. Note the progressive lengthening of the crests with distance from the disturbance, as shown by figures 2 to 4.

$N^{\frac{1}{6}}$) than the term $N^{-\frac{1}{2}}$ describing the variation with distance well inside the critical angle. Thus, ultimately the largest waves are near the critical lines $\theta = \pm\theta_c$ and near $\theta = 0$ where the linearized theory predicts infinite amplitude and infinitesimal wave length.

Figures 2, 3 and 4 show contours of equal surface elevation computed from (4.12) for three distances, near $N = 100$, 1000 and 10,000, respectively, where $N = gr/U^2 = 2\pi r/\lambda$, and λ is the wavelength of a regular wave-train travelling with phase velocity U. In each case the nodal lines lie near the boundaries of the parallelograms mentioned above. There are striking phase changes near the zeros of Ai $(-N^{\frac{2}{3}}\mu(\theta))$; these arise from the presence of the second term in (4.12). The lengthening of the crests with increasing N is clearly shown. Figure 3 ($N \doteqdot 1000$) resembles closely the contour map computed by Hogner (1923).

In figure 2 ($N \doteqdot 100$) the largest amplitudes occur near the point (120·2, 28) which is not near $\theta = \theta_c$ where they would be expected. The reason is that the quotient $N^{-\frac{1}{6}}$ obtained in the last paragraph but one is about 0·46 and differs little from unity. The reduction in wave height by this factor is more than compensated by the fairly rapid increase in $p_0(\theta)$ and $q_0(\theta)$ as θ decreases from θ_c; see Table 1 above. Even when N is near 10,000, the quotient $N^{-\frac{1}{6}}$ is still about 0·22. Thus the concentration of amplitude near the critical lines is not very striking (much less so than is suggested by Havelock's comparison (1908, Table 2) of the amplitude on the critical lines with the amplitude of transverse waves on $\theta = 0$).

In the computations it is assumed that the pressure is concentrated at a point on the free surface. If the pressure is distributed over an area, the resulting amplitude is obtained by an integration over the area, and in regions where the wavelength is short (compared to the dimensions of the pressure area) the amplitude will be reduced by destructive interference. In particular the infinite amplitude predicted near the track of the disturbance will not be observed. Similar remarks apply when the waves are due to a submerged instead of a surface source.

Mr H. P. F. Swinnerton-Dyer computed for me the co-ordinates of points on the contours of equal elevation which are shown in figures 2, 3 and 4. His help and advice is most gratefully acknowledged.

REFERENCES

Chester, C., Friedman, N. & Ursell, F. 1957 *Proc. Camb. Phil. Soc.* **53**, 399–511.

Havelock, T. H. 1908 *Proc. Roy. Soc.* A, **81**, 398–430.

Hogner, E. 1923 *Ark. Mat. Astr. Fys.* **17**, no. 12, 1–50.

Hogner, E. 1924 *Ark. Mat. Astr. Fys.* **18**, no. 10, 1–9.

Jeffreys, H. & Jeffreys, B. S. 1946 *Mathematical Physics.* Cambridge University Press.

Lamb, H. 1932 *Hydrodynamics*, 6th ed. Cambridge University Press.

Miller, J. C. P. 1946 *The Airy Integral.* Brit. Assn. Math. Tables, Part-vol. B, Cambridge University Press.

Peters, A. S. 1949 *Commun. Pure Appl. Math.* **2**, 123–48.

Thomson, W. (Lord Kelvin). 1891 *Popular Lectures and Addresses*, Vol. 3, 481–8. London: Macmillan.

Magnetohydrodynamic flow of a viscous fluid past a sphere

By RICHARD VAN BLERKOM
International Business Machines Corporation

(Received 15 December 1959)

The flow of a viscous incompressible electrically conducting fluid past a sphere is studied; the uniform ambient flow field is colinear with the ambient uniform magnetic field. The force exerted on the sphere is computed for various conductivities and Reynolds numbers; of particular interest is the distinction in behaviour between the flow with ambient particle speed greater than ambient Alfvén speed and that with particle speed less than Alfvén speed.

1. Introduction

The flow of a viscous incompressible fluid past an obstacle at low Reynolds number has been the subject of many investigations. The rigorous analysis of this problem requires the solution of the non-linear Navier–Stokes differential equations. Stokes (1945), Oseen (1910), and Lewis & Carrier (1949) have formulated linear problems whose relevant solutions are good approximations to the observed physical facts. The linearized problems have been solved for flow past a sphere by Lamb (1945) and by Goldstein (1929) and the drag on the sphere has also been found. We shall use the same methods of linearization to study the flow of a viscous, incompressible, and electrically conducting fluid past an obstacle when the magnetic field and velocity are constant and parallel far from the obstacle. A detailed solution will be obtained for a sphere and a method of solution for other geometries will be indicated. The modification introduced in a uniform flow by an externally applied point force will be described.

2. The flow past a sphere

The magnetohydrodynamic flow of an incompressible viscous electrically conducting fluid of constant properties is governed by Maxwell's equations and the laws of conservation of mass and momentum. In m.k.s. units these equations take the form

$$\rho\left\{\frac{\partial \mathbf{V}'}{\partial t}+[\mathbf{V}'.\nabla')\,\mathbf{V}'\right\}=-\nabla' p'+\rho\nu\nabla'^2\mathbf{V}'+\mu\mathbf{j}\times\mathbf{H}', \tag{2.1}$$

$$\operatorname{div}\mathbf{V}'=0, \tag{2.2}$$

$$\operatorname{curl}\mathbf{H}'=\mathbf{j}, \quad \operatorname{div}\mathbf{H}'=0, \tag{2.3}$$

$$\operatorname{curl}\mathbf{E}=0. \tag{2.4}$$

These are supplemented by the constitutive relation

$$\mathbf{j}=\sigma[\mathbf{E}+\mu\mathbf{V}'\times\mathbf{H}']. \tag{2.5}$$

Here, $\mathbf{V}'$ is the fluid velocity, $\mathbf{H}'$ is the magnetic field, $\mathbf{E}$ is the electric field, σ is the electrical conductivity, ρ is the mass density, μ is the magnetic permeability, and ν is the kinematic viscosity. The differentiations are taken with respect to the physical variables x', y', z'.

The differential equations can be put in a dimensionless form by introducing the following substitutions:

$$\mathbf{V} = \frac{\mathbf{V}'}{U}, \quad p = \frac{a}{\rho\nu U}p', \quad x = \frac{x'}{a}, \quad y = \frac{y'}{a}, \quad z = \frac{z'}{a} \quad \text{and} \quad \mathbf{H} = \frac{\mathbf{H}'}{H_0}.$$

Here, U is a characteristic velocity of the problem, H_0 is a characteristic magnetic field, a is a characteristic length and the differentiations are with respect to x, y and z. In the problems we are considering U is the undisturbed velocity and H_0 is the magnetic field far from the obstacle. For steady-state problems, $\partial\mathbf{V}/\partial t = 0$ and (2.1) to (2.5) take the form

$$R(\mathbf{V}.\nabla)\mathbf{V} = -\nabla p + \nabla^2\mathbf{V} + \frac{\mu H_0 a^2}{\rho\nu U}\mathbf{j}\times\mathbf{H}, \tag{2.6}$$

$$\operatorname{div}\mathbf{V} = 0, \tag{2.7}$$

$$\operatorname{curl}\mathbf{H} = \frac{a}{H_0}\mathbf{j}, \quad \operatorname{div}\mathbf{H} = 0, \tag{2.8}$$

$$\operatorname{curl}\mathbf{E} = 0, \tag{2.9}$$

$$\mathbf{j} = \sigma\{\mathbf{E} + \mu U H_0 \mathbf{V}\times\mathbf{H}\}. \tag{2.10}$$

If we substitute (2.8) into (2.6) and use the vector identity

$$(\operatorname{curl}\mathbf{H})\times\mathbf{H} = (\mathbf{H}.\nabla)\mathbf{H} - \tfrac{1}{2}\nabla(\mathbf{H}.\mathbf{H}),$$

we obtain

$$R(\mathbf{V}.\nabla)\mathbf{V} = -\nabla p_0 + \nabla^2\mathbf{V} + \frac{M^2}{R_m}(\mathbf{H}.\nabla)\mathbf{H}, \tag{2.11}$$

where

$$p_0 = p + \frac{M^2}{2R_m}\mathbf{H}.\mathbf{H}. \tag{2.12}$$

Here, R_m is the magnetic Reynolds number given by $R_m = Ua\mu\sigma$ and M is the Hartmann number given by $M = \mu H_0 a(\sigma/\rho\nu)^{\frac{1}{2}}$. The ratio R_m/R is a measure of the relative importance of magnetic and viscous effects.

If we take the curl of (2.10) and make use of (2.7) and (2.9) and the vector identities

$$\operatorname{curl}(\operatorname{curl}\mathbf{H}) = \nabla(\operatorname{div}\mathbf{H}) - \nabla^2\mathbf{H} = -\nabla^2\mathbf{H} \tag{2.13a}$$

and

$$\operatorname{curl}(\mathbf{V}\times\mathbf{H}) = (\mathbf{H}.\nabla)\mathbf{V} - (\mathbf{V}.\nabla)\mathbf{H} + \mathbf{V}(\nabla.\mathbf{H}) - \mathbf{H}(\nabla.\mathbf{V}), \tag{2.13b}$$

we obtain

$$\nabla^2\mathbf{H} = -R_m\{(\mathbf{H}.\nabla)\mathbf{V} - (\mathbf{V}.\nabla)\mathbf{H}\}. \tag{2.14}$$

We shall confine our attention to problems in which the fluid flows past an axially symmetric obstacle in an otherwise unbounded domain with an ambient velocity $\mathbf{i}V_0$ and magnetic field $\mathbf{i}H_0$ which are uniform and directed along the symmetry axis of the object. Chester (1957) has treated this problem following a Stokes-like analysis; he computed the drag on a sphere to be

$$D = D_s\{1 + \tfrac{3}{8}M + \tfrac{7}{960}M^2 - \tfrac{43}{7680}M^3 + O(M^4)\}, \tag{2.15}$$

where

$$D_s = 6\pi\rho\nu a U. \tag{2.16}$$

We shall invoke an analysis similar to that of Oseen, although the motivation stems from the Carrier–Lewis approximation technique as used by Greenspan & Carrier (1959). In this technique one anticipates that the mathematical model retains significance when each of the undifferentiated quantities in the convective terms of equations (2.11) and (2.14) is replaced by an appropriate average which is taken to be some fraction of the free-stream values. In this paper, we shall take these functions to be unity, so that we shall treat a mathematical problem which is identical with that which would arise if the Oseen philosophy were followed. It should be noted, however, that the equations which would be obtained with a more appropriate choice of these averages would have solutions which are related to those obtained here by the formulas

$$\mathbf{V}_1(\mathbf{r}, C_1, C_2, C_3, R, R_m, \beta) = \mathbf{V}\left(\mathbf{r}, 1, 1, 1, \frac{R}{C_1}, \frac{R_m}{C_3}, \frac{C_1\beta}{C_2}\right), \tag{2.17a}$$

$$\mathbf{H}_1(\mathbf{r}, C_1, C_2, C_3, R, R_m, \beta) = \mathbf{H}\left(\mathbf{r}, 1, 1, 1, \frac{R}{C_1}, \frac{R_m}{C_3}, \frac{C_1\beta}{C_2}\right), \tag{2.17b}$$

where $C_1\mathbf{i}, C_2\mathbf{i}, C_3\mathbf{i}, C_4\mathbf{i}$ are the quantities which replace $\mathbf{V}, \mathbf{H}, \mathbf{H}, \mathbf{V}$, respectively, as they appear in (2.11) and (2.14).

With the foregoing, (2.11) and (2.14) become

$$R\frac{\partial \mathbf{V}}{\partial x} = -\nabla p_0 + \nabla^2\mathbf{V} + \frac{M^2}{R_m}\frac{\partial \mathbf{H}}{\partial x}, \tag{2.18}$$

$$\frac{1}{R_m}\nabla^2\mathbf{H} = \frac{\partial}{\partial x}(\mathbf{H} - \mathbf{V}). \tag{2.19}$$

Since the problem has been linearized superposition may be used; we write $\mathbf{V} = \mathbf{i} + \mathbf{v}$ and $\mathbf{H} = \mathbf{i} + \mathbf{h}$. The boundary conditions require that $\mathbf{v}$ and $\mathbf{h}$ tend to zero as the distance from the obstacle goes to infinity, that $\mathbf{v} = -\mathbf{i}$ at the obstacle surface, and that h_t and μh_n be continuous at the obstacle surface. Here, h_n and h_t are, respectively, the component of magnetic field that is normal to the obstacle and the component that is tangent to the obstacle.

Equations (2.18) and (2.19) can be simplified in the following way. We define

$$\mathbf{v}_1 = \mathbf{v} - \frac{\alpha_1}{R_m}\mathbf{h}, \tag{2.20}$$

$$\mathbf{v}_2 = \mathbf{v} - \frac{\alpha_2}{R_m}\mathbf{h}, \tag{2.21}$$

where the α_j are the roots of

$$\alpha^2 + (R - R_m)\alpha - M^2 = 0. \tag{2.22}$$

We then obtain

$$R_1\frac{\partial \mathbf{v}_1}{\partial x} = -\nabla p_0 + \nabla^2\mathbf{v}_1, \tag{2.23}$$

$$R_2\frac{\partial \mathbf{v}_2}{\partial x} = -\nabla p_0 + \nabla^2\mathbf{v}_2, \tag{2.24}$$

where $R_j = R + \alpha_j$. Each of these equations is identical with that encountered in the classical Oseen treatment of viscous fluid problems and our investigation will parallel closely that of Oseen.

It is easily seen that

$$\mathbf{v} = \frac{1}{R_2 - R_1}\left[(R_2 - R)\,\mathbf{v}_1 - (R_1 - R)\,\mathbf{v}_2\right], \tag{2.25}$$

$$\mathbf{h} = \frac{R_m}{R_2 - R_1}\left[\mathbf{v}_1 - \mathbf{v}_2\right], \tag{2.26}$$

$$\operatorname{div}\mathbf{v}_1 = \operatorname{div}\mathbf{v}_2 = 0, \tag{2.27}$$

and that the 'modified' Reynolds numbers R_i are the roots of

$$R_i^2 - (R + R_m)\,R_i + (RR_m - M^2) = 0, \tag{2.28}$$

and are always real.

We define

$$\beta = \frac{\mu H_0^2}{\rho U^2} = \frac{M^2}{RR_m} \tag{2.29}$$

and note that, for $\beta < 1$, each of the 'modified' Reynolds numbers is positive, but for $\beta > 1$ there is a positive and a negative 'modified' Reynolds number. These two cases will be considered separately. When $\beta = 1$ the 'modified' Reynolds numbers are $R + R_m$ and zero.

It is convenient to follow Lamb (1945) and introduce the potential $\overline{\chi}_j$ such that

$$V_j = -\overline{\chi}_j\,\mathbf{i} + R_j^{-1}\operatorname{grad}\overline{\chi}_j + \operatorname{grad}\sum_{n=0}^{\infty} A_{nj}\frac{\partial^n(r^{-1})}{\partial x^n}. \tag{2.30}$$

In order that (2.23) and (2.24) be satisfied it is necessary that

$$\left[\nabla^2 - R_j\frac{\partial}{\partial x}\right]\overline{\chi}_j = 0. \tag{2.31}$$

Furthermore,

$$p_0 = -\sum_{n=0}^{\infty} A_{nj} R_j^{-1}\frac{\partial^{n+1}(r^{-1})}{\partial x^{n+1}}. \tag{2.32}$$

The axially symmetric solution to (2.31) that vanishes at infinity is

$$\overline{\chi}_j = \mathrm{e}^{\frac{1}{2}(R_j)x}\sum_{n=0}^{\infty} B_{jn}\,\chi_n(|R_1|\,r)\,P_n(\cos\theta), \tag{2.33}$$

where θ is the polar angle measured in spherical co-ordinates (r, θ, ω) and

$$\chi_n(x) = (2n+1)\left(\frac{\pi}{x}\right)^{\frac{1}{2}} K_{n+\frac{1}{2}}\left(\frac{x}{2}\right). \tag{2.34}$$

Here, K_n is the modified Bessel function of the second kind.

It follows from (2.8), (2.26), (2.30) and (2.31) that the current paths are circles which have their centres on the x-axis. From the axial symmetry of the problem, equation (2.10), and Kirchhoff's law, we deduce that $\mathbf{E} = 0$ everywhere in the fluid. Inside the spherical obstacle the electric and magnetic fields are governed by Maxwell's equations and the charge conservation equations which, in m.k.s. units, are given by

$$\left.\begin{aligned} \operatorname{curl}\mathbf{h}_i = \frac{a}{H_0}\mathbf{j}_i, \quad \operatorname{div}\mathbf{h}_i = 0, \quad \mathbf{j}_i = \sigma_i\mathbf{E}_i, \\ \operatorname{curl}\mathbf{E}_i = 0, \quad \operatorname{div}\sigma_i\mathbf{E}_i = 0. \end{aligned}\right\} \tag{2.35}$$

Since the electric field vanishes in the fluid and on the boundary of the sphere, it follows that $\mathbf{E}_i = 0$ and that

$$\mathbf{h}_i = -\operatorname{grad} \sum_{n=0}^{\infty} D_n r^n P_n(\cos\theta). \tag{2.36}$$

We now follow the method of Goldstein (1929) and write the boundary conditions at the surface of the sphere ($r = 1$) in the form

$$\frac{(n+1)(-1)^n}{n!}\frac{R_m}{R}A_n - \frac{1}{2(R_2-R_1)}\sum_{m=0}^{\infty}\sum_{j=1}^{2}(-1)^j(R_m-R_j)B_{jm}\sigma_{n,m}(R_j) = \begin{cases}0 & (n=0,2,3,\ldots),\\ 1 & (n=1),\end{cases} \tag{2.37}$$

$$\frac{(-1)^n}{n!}\frac{R_m}{R}A_n + \frac{1}{2(R_2-R_1)}\sum_{m=0}^{\infty}\sum_{j=1}^{2}(-1)^j(R_m-R_j)B_{jm}\tau_{n,m}(R_j) = \begin{cases}0 & (n=2,3,\ldots),\\ 1 & (n=1),\end{cases} \tag{2.38}$$

$$\frac{(-1)^n(n+1)}{n!}\frac{R_m}{R}A_n - \frac{R_m}{2(R_2-R_1)}\sum_{m=0}^{\infty}\sum_{j=1}^{2}(-1)^j B_{jm}\sigma_{n,m}(R_j) = -\frac{\mu_s}{\mu}nD_n - \delta_{1n} \quad (n=0,1,2,\ldots), \tag{2.39}$$

$$\frac{(-1)^n}{n!}\frac{R_m}{R}A_n + \frac{R_m}{2(R_2-R_1)}\sum_{m=0}^{\infty}(-1)^j B_{jn}\tau_{n,m}(R_j) = D_n + \delta_{1n} \quad (n=1,2,\ldots), \tag{2.40}$$

where

$$\sigma_{n,m}(R_1 r) = 2\{\chi_n'(|R_1|r)\psi_{n,m}(|R_1|r) - \chi_m(|R_1|r)\psi_{n,m}'(|R_1|r)\}\left(\frac{|R_1|}{R_1}\right)^n \tag{2.41}$$

and

$$\tau_{n,m}(R_1 r) = \frac{2\chi_m(|R_1|r)}{R_1}\{2X_{n,m}(|R_1|r) - \Psi_{n,m}(|R_1|r)\}\left(\frac{|R_1|}{R_1}\right)^n. \tag{2.42}$$

The functions $X_{n,m}$ and $\Psi_{n,m}$ are given by

$$\begin{aligned}X_{n,m} = {} & \frac{m(2n+1)}{n+1}\frac{(2m)!\,(2n)!}{(2n+2m)!}\left(\frac{(n+m)!}{(n)!\,(m)!}\right)^2 \\ & \times\left\{\frac{\psi_{n+m-1}}{\xi} + \frac{3(n-1)}{(2n-1)}\frac{m-1}{2m-1}\frac{2n+2m-1}{n+m}\frac{\psi_{n+m-3}}{\xi} + \frac{1.3.5}{2!}\frac{(n-1)(n-2)}{(2n-1)(2n-3)}\right. \\ & \times\frac{(m-1)(m-2)}{(2m-1)(2m-3)}\frac{(2n+2m-1)(2n+2m-3)}{(n+m)(n+m-1)}\frac{\psi_{n+m-5}}{\xi} \\ & + \ldots + \frac{1.3\ldots(2r+1)}{r!}\frac{(n-1)\ldots(n-r)}{(2n-1)\ldots(2n-2r+1)}\frac{(m-1)\ldots(m-r)}{(2m-1)\ldots(2m-2r+1)} \\ & \times\frac{(2n+2m-1)\ldots(2n+2m+2n+1)}{(n+m)\ldots(n+m-r+1)}\frac{\psi_{n+m-2r-1}}{\xi} \\ & \left. + \ldots + \frac{(n-1)\ldots(n-m+1)}{(2n-1)\ldots(2n-2m+3)}\frac{(2n+2m-1)\ldots(2n+3)}{(n+m)\ldots(n+2)}\frac{\psi_{n-m+1}}{\xi}\right\}\end{aligned} \tag{2.43}$$

and

$$\Psi_{n,m} = \frac{(2m)!\,(2n+1)!}{(2n+2m+1)!}\left(\frac{(n+m)!}{(n)!\,(m)!}\right)^2\left\{\psi_{n+m} + \frac{n}{2n-1}\frac{m}{2m-1}\frac{2n+2m+1}{n+m}\psi_{n+m-2}\right.$$

$$+\frac{1.3}{2!}\frac{n(n-1)}{(2n-1)(2n-3)}\frac{m(m-1)}{(2m-1)(2m-3)}\frac{(2n+2m+1)(2n+2m-1)}{(n+m)(n+m-1)}\psi_{n+m-4}$$

$$+\ldots+\frac{1.3.5\ldots(2r-1)}{r!}\frac{n(n-1)\ldots(n-r+1)}{(2n-1)(2n-3)\ldots(2n-2r+1)}$$

$$\times\frac{m(m-1)\ldots(m-r+1)}{(2m-1)(2m-3)\ldots(2m-2r+1)}$$

$$\times\frac{(2n+2m+1)(2n+2m-1)\ldots(2n+2m-2r+3)}{(n+m)(n+m-1)\ldots(n+m-r+1)}\psi_{n+m-2r}$$

$$+\ldots+\frac{n(n-1)\ldots(n-m+1)}{(2n-1)(2n-3)\ldots(2n-2m+1)}$$

$$\left.\times\frac{(2n+2m+1)(2n+2m-1)\ldots(2n+3)}{(n+m)(n+m-1)\ldots n+1}\psi_{n-m}\right\}, \tag{2.44}$$

where

$$\psi_n(x) = (2n+1)\left(\frac{\pi}{x}\right)^{\frac{1}{2}} I_{n+\frac{1}{2}}\left(\frac{x}{2}\right). \tag{2.45}$$

Equation (2.37) is the condition $v_r = -\cos\theta$, equation (2.38) is the condition $v_\theta = \sin\theta$, equation (2.39) expresses the continuity of μh_r and equation (2.40) represents the continuity of h_θ. The infinite system of equations is approximated to order q by considering (2.37) for $n = 0, 1, \ldots, q$; (2.38) for $n = 1, \ldots, q$; (2.39) for $n = 0, 1, \ldots, q-1$; and (2.40) for $n = 1, 2, \ldots, q$. This yields $4q+1$ equations for the $4q+1$ unknowns $A_0, A_1, \ldots, A_q$; $B_{10}, B_{11}, \ldots, B_{1q-1}$; $B_{20}, B_{21}, \ldots, B_{2q-1}$; $D_1, D_2, \ldots, D_q$ with the rest of the A_n, B_{jn-1}, D_n taken as zero. Numerical results for the constants were obtained using a second-order approximation and several values of the 'modified' Reynolds number. For small 'modified' Reynolds numbers it was found that A_0, A_1, B_{10}, B_{20} and D_1 are all much greater than A_2, B_{11}, B_{21} and D_2.

The drag D on a solid obstacle is obtained by applying Newton's second law of motion to the fluid surrounding the obstacle and bounded by a surface S which is everywhere far from the obstacle. The total force exerted on the fluid within S is the sum of the viscous force exerted by the obstacle $(-D)$, the force exerted by the fluid outside S, plus the ponderomotive force.

We are able to show by direct calculation from the results of § 2 that for small 'modified' Reynolds numbers the ponderomotive force $\{\beta R(\operatorname{curl}\mathbf{H})\times\mathbf{H}\}$ is small compared with the viscous forces $\nu\nabla^2\mathbf{V}$ in all parts of the fluid provided that $\mu = \mu_s$. This restriction on the permeabilities is necessary so that near the sphere $\mathbf{H} \approx \mathbf{i}$. Hence in computing the drag we neglect the body force. This calculation can be carried out by an extension of the process used by Lamb in showing for small Reynolds number that $(\operatorname{curl}\mathbf{V})\times\mathbf{V}$ may be neglected compared with viscous forces in a non-conducting fluid.

We continue in a manner similar to that used by Goldstein (1929) and obtain

$$C_D = \frac{D}{\rho U^2 a^2} = -\frac{R_m}{R}(1-\beta)\int \frac{\partial \phi}{\partial n} dS. \tag{2.46}$$

For flow past a spherical object we obtain

$$C_D = \frac{4\pi R_m}{R}(1-\beta)A_0 \quad (\mu = \mu_s). \tag{2.47}$$

The first-order solution for small 'modified' Reynolds numbers yields

$$C_D \approx \frac{6\pi}{R}(1+\tfrac{3}{8}R+O(R_i^2)) \quad (\beta \leqslant 1), \tag{2.48a}$$

$$C_D \approx \frac{6\pi}{R}\left[1-\frac{3R}{8}\left(\frac{R_m-2R_m\beta-R}{|R_2-R_1|}\right)\right] \quad (\beta \geqslant 1), \tag{2.48b}$$

when $\mu = \mu_s$.

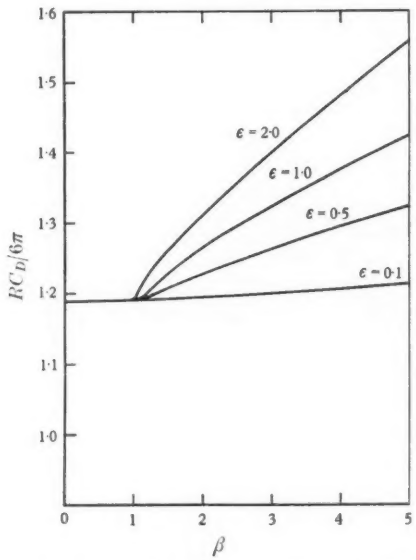

FIGURE 1. Drag coefficient *versus* β. $\epsilon = R_m/R$, $R = 0{\cdot}5$.

Numerical values were obtained for C_D at $R = \frac{1}{2}$ for several values of R_m and β, where all terms up to those of order R_i^2 were retained and it was found that (2.48*a*) and (2.48*b*) were changed by about 1 %. These results are plotted in figure 1. This does not mean that the error in these formulas for C_D is as small as 1 %, since this error is dependent on the accuracy of the linearization.

In order to obtain additional insight, the results of § 2 were used to obtain numerical values for the x-components of particle velocity and magnetic field along the lines $(0, 0, z)$, $(5, 0, z)$ and, for the subsonic case, $(-5, 0, z)$, with $R = R_m = 0{\cdot}25$ and $\mu = \mu_s$. The results are shown in figure 2. It was found that both the particle velocity and magnetic field are independent of β for $0 \leqslant \beta \leqslant 1$.

In fact, in both the supersonic and the subsonic case ($\beta = 2$), the magnetic field was found to be small (less than 0·1) and hence was not plotted. If the sphere has a permeability different from that of the fluid, the magnetic field is distorted near the sphere but the effects are unimportant elsewhere.

As was mentioned previously, Chester (1957) extended the Stokes-type approximation for the flow past a sphere. This is equivalent to the linearization we have used, if the special case R and $R_m \to 0$, β large and $\mu = \mu_s$ is considered. This yields 'modified' Reynolds numbers of $\pm M$ and a drag, particle velocity and magnetic field which are all in agreement with Chester's results.

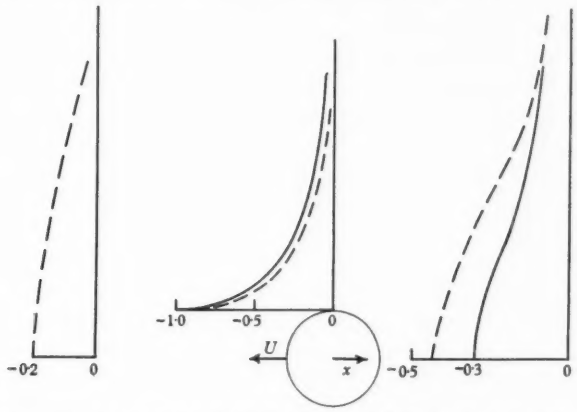

FIGURE 2. x-component of particle velocity *versus* position; $R = R_m = 0{\cdot}25$. The positions of the origins of the three graphs indicate the values of x at which $u(x, y)$ is plotted as a function of y. —, $\beta \leqslant 1$; – – –, $\beta = 2$.

3. The point-force problem

We shall discuss here the flow field and magnetic field which arise when an externally applied point force acts on a fluid which otherwise would have uniform velocity and magnetic field. Such a description is of interest because it will be a major contribution to the description of the flow past objects such as that considered in § 2, and because it can be displayed in closed form with easy interpretation.

The governing equations are (2.14) and (2.11) modified only by the inclusion of the point-force contribution. That is,

$$R(\mathbf{V}.\nabla)\,\mathbf{V} + \nabla p_0 - \nabla^2\mathbf{V} + \frac{M^2}{R_m}(\mathbf{H}.\nabla)\,\mathbf{H} = -F\delta(r)\,\mathbf{i}, \tag{3.1}$$

with

$$\delta(r) = \delta(x-0, y-0, z-0),$$

where $\delta(r)$ is the Dirac delta function and $-F\delta(r)\,\mathbf{i}$ is the force per unit volume applied at the origin. The equations of motion are put into dimensionless form and linearized, and linear combinations are taken in the same manner as in § 2. In this problem we define the characteristic length by

$$a = \sqrt{\frac{(6\pi\rho\nu U)}{F}}. \tag{3.2}$$

The exact solution to the linear problem is found to be

$$\mathbf{v}_j = -\frac{3}{2}\frac{\exp\left[-\frac{1}{2}|R_j|r+\frac{1}{2}(R_j)x\right]}{r}\mathbf{i}+\frac{3}{2R_j}\nabla\left(\frac{\exp\left[-\frac{1}{2}|R_j|r+\frac{1}{2}(R_j)x\right]}{r}\right)-\frac{3}{2R_j}\nabla\left(\frac{1}{r}\right), \tag{3.3}$$

and

$$p_0 = +\frac{3}{2}\frac{\partial}{\partial x}\left(\frac{1}{r}\right). \tag{3.4}$$

Expressions for $\mathbf{v}$ and $\mathbf{h}$ are obtained from (2.25) and (2.26). We note that at the origin the velocity becomes infinite as r^{-1} and is directed along the positive x-axis, while $\mathbf{h} = 0$.

At this point it is appropriate to compare our results for $\beta < 1$ with those for $\beta > 1$. The wake for the magnetohydrodynamic flow is the region in which $\exp\left[-\frac{1}{2}|R_j|r+\frac{1}{2}(R_j)x\right]$ is not small. In the wake the particle velocity and magnetic field vary as r^{-1} far from the origin, while in the region outside the wake they vary as r^{-2}. For $0 \leqslant \beta \leqslant 1$, the wake appears near the positive x-axis. However, for $\beta > 1$ the wake appears not only near the positive x-axis, but also near the negative x-axis.

We now find it convenient to turn our attention to the co-ordinate system in which the fluid is at rest at infinity. From (2.25), (2.26) and (3.3), it follows that far from the origin at points outside the wake for $\beta < 1$ the velocity and magnetic field are as if due to a source located at the origin and of strength $6\pi R_m/R_1R_2$. There is an equal inward flux along the wake near the x-axis. If $\beta > 1$, the magnetic field outside the wake is the same as that due to a sink at the origin, which is offset by concentrated outward flows near both the positive and the negative x-axes; the velocity is that which would be due to a sink equivalent to the magnetic field sink and, in addition, there is an inward flux near the positive x-axis, both of which are balanced by an outward flux along the negative x-axis. The results for $\beta = 1$ are obtained by considering what happens in the limit as $\beta \to 1-$ or $1+$. These limits yield the same conclusions. There is a net influx of particles near the positive x-axis which is balanced by a source at the origin. The essentially different behaviour for $\beta < 1$ and $\beta > 1$ may be explained by noting that, if $\beta = 1$,

$$U = \sqrt{\left(\frac{\mu}{\rho}\right)}H_0, \tag{3.5}$$

which is equal to the Alfvén wave speed. Hence, for $\beta < 1$ the free-stream velocity is greater than the Alfvén velocity and for $\beta > 1$ the free-stream velocity is less than the Alfvén speed.

4. The infinite conductivity case

We shall now discuss the flow past an obstacle of a fluid which has infinite conductivity. For $\sigma \to \infty$ ($R_m \to \infty$) a possible solution to (2.7), (2.11) and (2.14) is $\mathbf{h} = \mathbf{v}$, which reduces the problem to the form

$$\left[\nabla^2 - R(1-\beta)\frac{\partial}{\partial x}\right]\mathbf{v} = \operatorname{grad} p_0, \tag{4.1}$$

$$\nabla . \mathbf{v} = 0. \tag{4.2}$$

These equations are identical with the equations of motion for a non-conducting fluid flow with Reynolds number $R(1-\beta)$ and pressure p_0. For $\beta > 1$, we deduce that the disturbance velocity is equivalent to the disturbance velocity due to the flow of a non-conducting fluid which, far from the obstacle, is in the direction of the negative x-axis and which has a Reynolds number $R(\beta-1)$. Hence, if we can satisfy the boundary conditions on the velocity in the problem in which there is no magnetic field, then we can satisfy the boundary conditions on velocity in the magnetohydrodynamical problem. The magnetic field satisfies the same boundary conditions at the obstacle ($\mathbf{H} = 0$) as the velocity as long as the obstacle has the same permeability as the fluid. The magnetic field inside the sphere is zero and the electric field is everywhere equal to zero by the same argument as in the previous section. For $\beta = 1$, (4.9) reduces to the equation obtained by Stokes for a non-conducting fluid. Naturally the suitability of this model can only be determined by the degree of agreement with experimental results.

The work reported in this paper is an extract from a thesis submitted in April 1959 in partial fulfilment of the requirements for the degree of Ph.D. in applied mathematics at Harvard University.

REFERENCES

CHESTER, W. 1957 The effect of a magnetic field on Stokes flow in a conducting fluid. *J. Fluid Mech.* **3**, 304.

GOLDSTEIN, S. 1929 The forces on a solid body moving through viscous fluid and the steady flow of viscous fluid past a fixed spherical obstacle at small Reynolds numbers. *Proc. Roy. Soc.* A, **123**, 216.

GREENSPAN, H. P. & CARRIER, G. F. 1959 The magnetohydrodynamic flow past a flat plate. *J. Fluid Mech.* **6**, 77.

LAMB, H. 1945 *Hydrodynamics.* New York: Dover.

LEWIS, J. A. & CARRIER, G. F. 1949 Some remarks on the flat plate boundary layer. *Quart. Appl. Math.* **7**, 228.

OSEEN, C. W. 1910 Ueber die Stokes' sche formel, und uber eine verwandte aufgabe in der hydrodynamik. *Arkiv. f. math.* 29.

STOKES, G. G. 1945 On the theory of the internal friction in fluids in motion. *Trans. Camb. Phil. Soc.* **8**, 287.

Standing surface waves of finite amplitude

By IRADJ TADJBAKHSH AND JOSEPH B. KELLER
Institute of Mathematical Sciences, New York University

(Received 21 December 1959)

Gravity waves on the surface of an inviscid incompressible fluid of finite depth are considered. The waves are assumed to be periodic in time and in the horizontal direction. The surface profile, potential function, pressure and frequency of the motion are determined (to third order) as series in powers of the amplitude divided by the wavelength. It is found that the frequency increases with amplitude for depths less than a certain multiple of the wavelength and decreases with increasing amplitude for greater depths. Graphs of the surface profile and of the pressure as a function of depth are included.

1. Introduction

Gravity waves on the surface of a liquid are governed by non-linear equations. In the classical theory of such waves, the equations are linearized. Thus, the results of that theory yield the linear terms in the expansion of the wave motion in powers of the amplitude. We shall determine two additional terms in this expansion for standing waves in a liquid of uniform finite depth. Our results will then exhibit various deviations from those of the linear theory. For example, the period will depend upon the amplitude, the motion will not be sinusoidal in time nor in space, and the maximum elevation will not equal the minimum depression. These effects become more pronounced the larger the amplitude. They are described and depicted graphically in § 4.

Similar results have been obtained for liquid of infinite depth by Penney & Price (1952). Our results for the wave profile and the period coincide with theirs when we permit the depth to become infinite. However, our analysis indicates that in the expression for the fluid pressure there are additional terms, independent of the vertical distance, which they have not taken into account. Airy, Stokes, Rayleigh and others have obtained analogous results for progressing waves.

We formulate the problem in the next section and solve it by a perturbation method in § 3. Then we discuss the results in § 4 where some graphs are also given. In the Appendix we show how the method of Penney & Price can be modified to yield the same results, although it requires more labour than our method.

2. Formulation

Let us consider the time-periodic irrotational two-dimensional motion of an inviscid incompressible fluid bounded below by a rigid horizontal bottom and above by a free surface. We suppose the motion to be periodic in the horizontal

direction and symmetric about the vertical plane $x = 0$. Then we may confine our attention to the fluid between that plane and a parallel plane one half wavelength from it. Let λ denote the wavelength, $k = 2\pi/\lambda$ the propagation constant, $k^{-1}h$ the mean depth of the liquid, $k^{-1}x$ and $k^{-1}y$ the distances along the horizontal and vertical axes, respectively, g the acceleration of gravity, $(kg)^{\frac{1}{2}}\omega$ the angular frequency and $(kg)^{-\frac{1}{2}}\omega^{-1}t$ the time. In addition let a be a measure of the wave amplitude, the precise meaning of which will become clear later. Then we define $\epsilon = ka$ and let $\epsilon k^{-1}\eta(x,t)$ denote the elevation of the surface above the mean level given by the plane $y = 0$. Finally, we introduce the potential function $\epsilon g^{\frac{1}{2}}k^{-\frac{3}{2}}\phi(x,y,t)$.

In terms of the dimensionless quantities which we have just introduced, the equations which govern the motion are

$$\Delta\phi = 0 \quad \text{in} \quad 0 \leqslant x \leqslant \pi, \ -h \leqslant y \leqslant \epsilon\eta(x,t), \tag{1}$$

$$\eta + \omega\phi_t + \tfrac{1}{2}\epsilon(\phi_x^2 + \phi_y^2) = 0 \quad \text{on} \quad y = \epsilon\eta(x,t), \tag{2}$$

$$\phi_y = \omega\eta_t + \epsilon\phi_x\eta_x \quad \text{on} \quad y = \epsilon\eta(x,t), \tag{3}$$

$$\frac{\partial\phi}{\partial n} = 0 \quad \text{on} \quad x = 0, \ x = \pi, \ y = -h, \tag{4}$$

$$\int_0^\pi \eta(x,t)\,dx = 0, \tag{5}$$

$$\nabla\phi(x,y,t+2\pi) = \nabla\phi(x,y,t), \tag{6}$$

$$\int_0^\pi\int_0^{2\pi} \eta(x,t)\cos t\,\cos x\,dt\,dx = 0, \tag{7}$$

$$\int_{-h}^0\int_0^\pi\int_0^{2\pi} \phi(x,y,t)\,\cos t\,\cos x\,dt\,dx\,dy = \tfrac{1}{2}\pi^2(\tanh h)^{\frac{1}{2}}. \tag{8}$$

Equation (1) expresses the incompressibility of the fluid; (2) is the condition that the pressure at the surface, as obtained from Bernoulli's equation, be constant; (3) is the condition that a particle on the surface remain on the surface; (4) asserts that the bottom $y = -h$ is rigid and that $x = 0$ and $x = \pi$ are planes of symmetry of the motion; (5) is the condition that the mean surface is $y = 0$; (6) asserts the periodicity of the velocity components; (7) and (8) fix the phase and amplitude of the motion. Equation (8) shows that in the dimensional units, a is proportional to the Fourier coefficient of $\eta(x,t)$ with respect to the linearized surface profile $\sin t\,\cos x$. In fact a is just the amplitude of the linearized surface wave motion.

The pressure $p(x,y,t)$ is given by Bernoulli's equation

$$\frac{k}{\rho g}(p - p_0) = -y - \epsilon\omega\phi_t - \tfrac{1}{2}\epsilon^2(\phi_x^2 + \phi_y^2). \tag{9}$$

Here p_0 denotes the pressure of the atmosphere above the fluid and ρ denotes the constant density of the fluid.

The problem we consider is that of determining the dimensionless surface profile $\eta(x,t)$, the dimensionless potential function $\phi(x,y,t)$ and the dimensionless angular frequency ω satisfying equations (1) to (8). We note that the solution

also depends upon the dimensionless depth h, which is proportional to the actual depth divided by the wavelength, and the dimensionless constant $\epsilon = ka$, which is proportional to the linearized amplitude divided by the wavelength. We shall solve the problem by determining the first three terms in the expansion of the solution in powers of ϵ. Additional terms can be found by continuing our procedure.

We shall find that, for certain values of h, the problem we have formulated does not have a unique solution. This lack of uniqueness does not refer to the arbitrary constant which may be added to ϕ. These values of h are those for which the linear theory yields, for some harmonic (in space), a frequency (in time) which is an integral multiple of the fundamental frequency. According to the linear theory the frequency of the nth spatial harmonic is $(n \tanh nh)^{\frac{1}{2}}$. Thus we can make the problem have a unique solution by imposing the condition

$$\frac{n \tanh nh}{\tanh h} \neq (\text{integer})^2 \quad (n = 2, 3, \ldots). \tag{10}$$

Of course the solution we shall obtain will be a solution for any value of h, but it will not be the only solution satisfying (1) to (8) unless h satisfies (10).

3. Perturbation solution

We assume that η, ϕ and ω have limits η^0, ϕ^0 and ω_0 as ϵ tends to zero. If we set $\epsilon = 0$ in equations (1) to (8), we find that all but (2) and (3) are unchanged in form while these two become

$$\eta^0 + \omega_0 \phi^0_t = 0 \quad \text{on} \quad y = 0, \tag{2^0}$$

$$\phi^0_y - \omega_0 \eta^0_t = 0 \quad \text{on} \quad y = 0. \tag{3^0}$$

The zero-order problem, with (2^0) and (3^0) instead of (2) and (3), is just the classical linear problem. It has the unique solution

$$\eta^0 = \sin t \cos x, \tag{11}$$

$$\phi^0 = \frac{\omega_0}{\sinh h} \cos t \cos x \cosh (y + h), \tag{12}$$

$$\omega_0^2 = \tanh h. \tag{13}$$

We now assume that η, ϕ and ω have derivatives with respect to ϵ at $\epsilon = 0$ and we denote them by η^1, ϕ^1 and ω_1. Then we differentiate equations (1) to (8) with respect to ϵ and let ϵ tend to zero. In differentiating (2) and (3) we utilize the relation

$$\frac{d}{d\epsilon} \phi(x, \epsilon\eta, t, \epsilon) = \left[\frac{\partial}{\partial \epsilon} + (\eta + \epsilon\eta_\epsilon) \frac{\partial}{\partial y}\right] \phi. \tag{14}$$

Upon differentiating (2) and (3), but before setting $\epsilon = 0$, we obtain

$$\begin{aligned} \eta_\epsilon + \omega_\epsilon \phi_t + \omega[\phi_{t\epsilon} + (\eta + \epsilon\eta_\epsilon)\phi_{ty}] = &-\tfrac{1}{2}(\phi_x^2 + \phi_y^2) - \epsilon\phi_x[\phi_{x\epsilon} + (\eta + \epsilon\eta_\epsilon)\phi_{xy}] \\ &- \epsilon\phi_y[\phi_{y\epsilon} + (\eta + \epsilon\eta_\epsilon)\phi_{yy}] \quad \text{on} \quad y = \epsilon\eta(x, t), \end{aligned} \tag{15}$$

$$\begin{aligned} \phi_{y\epsilon} + (\eta + \epsilon\eta_\epsilon)\phi_{yy} - \omega_\epsilon \eta_t - \omega\eta_{t\epsilon} = &\eta_x \phi_x + \epsilon\eta_{x\epsilon}\phi_x + \epsilon\eta_x[\phi_{x\epsilon} + (\eta + \epsilon\eta_\epsilon)\phi_{xy}] \\ &\text{on} \quad y = \epsilon\eta(x, t). \end{aligned} \tag{16}$$

When we set $\epsilon = 0$ in the differentiated form of (1) and (4) to (7), these equations retain their form with the superscript 'one' affixed to η and ϕ. From (15), (16) and (8), we obtain

$$\eta^1 + \omega_0 \phi_t^1 = -\tfrac{1}{2}[(\phi_x^0)^2 + (\phi_y^0)^2] - \omega_0 \eta^0 \phi_{ty}^0 - \omega_1 \phi_t^0 \quad \text{on} \quad y = 0, \tag{2^1}$$

$$\phi_y^1 - \omega_0 \eta_t^1 = \eta_x^0 \phi_x^0 - \eta^0 \phi_{yy}^0 + \omega_1 \eta_t^0 \quad \text{on} \quad y = 0, \tag{3^1}$$

$$\int_0^{\pi} \int_0^{2\pi} \eta^1(x,t) \sin t \cos x \, dt \, dx = 0. \tag{8^1}$$

To solve the differentiated equations for η^1, ϕ^1 and ω_1, we first insert into (2^1) and (3^1) the zero-order quantities given by (11) to (13). Upon doing this and simplifying the results, we obtain

$$\eta^1 + \omega_0 \phi_t^1 = \tfrac{1}{8}[(\omega_0^2 - \omega_0^{-2}) + (\omega_0^2 + \omega_0^{-2}) \cos 2x - (3\omega_0^2 + \omega_0^{-2}) \cos 2t$$

$$- (3\omega_0^2 - \omega_0^{-2}) \cos 2t \cos 2x] + \frac{\omega_1}{\omega_0} \sin t \cos x \quad \text{on} \quad y = 0, \tag{17}$$

$$\phi_y^1 - \omega_0 \eta_t^1 = -\frac{1}{2\omega_0} \sin 2t \cos 2x + \omega_1 \cos t \cos x \quad \text{on} \quad y = 0. \tag{18}$$

Next we differentiate (17) with respect to t and eliminate η_t^1 from (17) and (18). This elimination yields

$$\phi_y^1 + \omega_0^2 \phi_{tt}^1 = \tfrac{1}{4}(3\omega_0^3 + \omega_0^{-1}) \sin 2t + \tfrac{3}{4}(\omega_0^3 - \omega_0^{-1}) \sin 2t \cos 2x$$

$$+ 2\omega_1 \cos t \cos x \quad \text{on} \quad y = 0. \tag{19}$$

To determine ϕ^1 we expand it in a Fourier cosine series since by (4), $\phi_x^1 = 0$ at $x = 0$ and $x = \pi$. In order that ϕ^1 satisfy (1) and (4), we find that it must be of the form

$$\phi^1(x,y,t) = \sum_{n=0}^{\infty} A_n(t) \cos nx \cosh n(y+h). \tag{20}$$

Insertion of (20) into (19) yields

$$\omega_0^2 A_{0tt} = \tfrac{1}{4}(3\omega_0^3 + \omega_0^{-1}) \sin 2t, \tag{21}$$

$$\omega_0^2 \cosh h \, . \, A_{1tt} + \sinh h \, . \, A_1 = 2\omega_1 \cos t, \tag{22}$$

$$\omega_0^2 \cosh 2h \, . \, A_{2tt} + 2 \sinh 2h \, . \, A_2 = \tfrac{3}{4}(\omega_0^3 - \omega_0^{-1}) \sin 2t, \tag{23}$$

$$\omega_0^2 \cosh nh \, . \, A_{ntt} + n \sinh nh \, . \, A_n = 0 \quad (n = 3, 4, \ldots). \tag{24}$$

From (6) and (20) we see that all A_n with $n \geqslant 1$ must be periodic in t with period 2π. Then from (10) and (24) it follows that $A_n = 0$ for $n \geqslant 3$. From (10) and (23), we have

$$A_2 = -\frac{3}{16 \cosh 2h} (\omega_0 - \omega_0^{-7}) \sin 2t. \tag{25}$$

The periodicity of A_1 requires $\omega_1 = 0$, and (22) yields

$$A_1 = \alpha_1 \sin t + \beta_1 \cos t. \tag{26}$$

Here α_1 and β_1 are constants so far undetermined. Finally (21) yields

$$A_0 = -\tfrac{1}{16}(3\omega_0 + \omega_0^{-3}) \sin 2t + \alpha_0 t + \beta_0. \tag{27}$$

Here α_0 and β_0 are also undetermined constants.

We now insert the above results into (20), use the resulting expression for ϕ^1 in (17), and solve (17) for η^1. This yields

$$\eta^1 = \tfrac{1}{8}(\omega_0^2 - \omega_0^{-2}) - \omega_0\alpha_0 - \omega_0(\alpha_1 \cos t - \beta_1 \sin t)\cos x \cosh h + \tfrac{1}{8}(\omega_0^2 + \omega_0^{-2})\cos 2x + \tfrac{1}{8}(\omega_0^{-2} - 3\omega_0^{-6})\cos 2t \cos 2x. \quad (28)$$

By applying (7) to η^1 we find $\alpha_1 = 0$. Application of (8^1) to η^1 yields $\beta_1 = 0$. Utilization of (5) leads to

$$\alpha_0 = \tfrac{1}{8}(\omega_0 - \omega_0^{-3}). \quad (29)$$

Now that all constants except the inconsequential β_0 have been determined, the solution η^1, ϕ^1 and ω_1 is completely determined. It is given by

$$\eta^1 = \tfrac{1}{8}[(\omega_0^2 - \omega_0^{-2}) + (\omega_0^{-2} - 3\omega_0^{-6})\cos 2t]\cos 2x, \quad (30)$$

$$\phi^1 = \beta_0 + \tfrac{1}{8}(\omega_0 - \omega_0^{-3})t - \tfrac{1}{16}(3\omega_0 + \omega_0^{-3})\sin 2t - \frac{3}{16\cosh 2h}(\omega_0 - \omega_0^{-7}) \times \sin 2t \cos 2x \cosh 2(y+h), \quad (31)$$

$$\omega_1 = 0. \quad (32)$$

It is interesting to observe that η^1 contains a non-constant term which is independent of t and that ϕ^1 contains t-dependent terms independent of x and y, one of which is not periodic in t.

Let us now assume that η, ϕ and ω have second derivatives with respect to ϵ at $\epsilon = 0$, and let us denote them by η^2, ϕ^2 and ω_2. To determine them we differentiate equations (1) to (8) twice with respect to ϵ and set $\epsilon = 0$. Equations (1) and (4) to (7) remain unchanged in form while (8) takes the form of (8^1), with the superscript 'two' affixed to η and ϕ. The twice differentiated form of (2) and (3) is most easily found by differentiating (15) and (16). To solve the resulting equations we proceed exactly as before. Upon eliminating η^2 from (2^2) and (3^2), we obtain

$$\phi_y^2 + \omega_0^2\phi_{tt}^2 = \alpha_{11}\cos t \cos x + \alpha_{13}\cos t \cos 3x + \alpha_{31}\cos 3t \cos x + \alpha_{33}\cos 3t \cos 3x. \quad (33)$$

Here the constants α_{ij} are given by

$$\left.\begin{aligned} \alpha_{11} &= 2\omega_2 + \tfrac{1}{16}(-9\omega_0^{-7} + 12\omega_0^{-3} + 3\omega_0 + 2\omega_0^5), \\ \alpha_{13} &= \tfrac{1}{16}(\omega_0^{-7} - 5\omega_0 + 2\omega_0^5), \\ \alpha_{31} &= \tfrac{1}{16}(-9\omega_0^{-7} - 62\omega_0^{-3} + 31\omega_0), \\ \alpha_{33} &= \tfrac{3}{16}(9\omega_0^{-7} - 22\omega_0^{-3} + 13\omega_0). \end{aligned}\right\} \quad (34)$$

In solving for ϕ^2 as before we find that α_{11}, the coefficient of $\cos t \cos x$, must vanish. This yields for ω_2 the result

$$\omega_2 = \tfrac{1}{32}(9\omega_0^{-7} - 12\omega_0^{-3} - 3\omega_0 - 2\omega_0^5). \quad (35)$$

Then calculations like those previously given lead to the following solutions for η^2 and ϕ^2

$$\eta^2 = b_{11}\sin t \cos x + b_{13}\sin t \cos 3x + b_{31}\sin 3t \cos x + b_{33}\sin 3t \cos 3x, \quad (36)$$

$$\phi^2 = \beta_2 + \beta_{13}\cos t \cos 3x \cosh 3(y+h) + \beta_{31}\cos 3t \cos x \cosh(y+h) + \beta_{33}\cos 3t \cos 3x \cosh 3(y+h). \quad (37)$$

Here β_2 is arbitrary and the other constants are given by

$$\left.\begin{aligned} b_{11} &= \tfrac{1}{32}(3\omega_0^{-8}+6\omega_0^{-4}-5+2\omega_0^4),\\ b_{13} &= \tfrac{3}{128}(9\omega_0^{-8}+27\omega_0^{-4}-15+\omega_0^4+2\omega_0^8),\\ b_{31} &= \tfrac{1}{128}(3\omega_0^{-8}+18\omega_0^{-4}-5),\\ b_{33} &= \tfrac{3}{128}(-9\omega_0^{-12}+3\omega_0^{-8}-3\omega_0^{-4}+1), \end{aligned}\right\} \tag{38}$$

and

$$\left.\begin{aligned} \beta_{13} &= \frac{1}{128\cosh 3h}(1+3\omega_0^4)(3\omega_0^{-9}-5\omega_0^{-1}+2\omega_0^3),\\ \beta_{31} &= \frac{1}{128\cosh h}(9\omega_0^{-9}+62\omega_0^{-5}-31\omega_0^{-1}),\\ \beta_{33} &= \frac{1}{128\cosh 3h}(1+3\omega_0^4)(-9\omega_0^{-13}+22\omega_0^{-9}-13\omega_0^{-5}). \end{aligned}\right\} \tag{39}$$

4. Discussion

The finite Taylor expansions of $\epsilon\eta$, $\epsilon\phi$ and ω are

$$\epsilon\eta = \epsilon\eta^0(x,t)+\epsilon^2\eta^1(x,t)+\tfrac{1}{2}\epsilon^3\eta^2(x,t)+O(\epsilon^4), \tag{40}$$

$$\epsilon\phi = \epsilon\phi^0(x,y,t)+\epsilon^2\phi^1(x,y,t)+\tfrac{1}{2}\epsilon^3\phi^2(x,y,t)+O(\epsilon^4), \tag{41}$$

$$\omega = \omega_0+\tfrac{1}{2}\epsilon^2\omega_2+O(\epsilon^3). \tag{42}$$

The zero-order solution is given by equations (11) to (13), the first-order solution by (30) to (32) and the second-order solution by (35) to (37).

On the basis of (42) we see that the frequency ω depends upon the 'amplitude' ϵ of the wave motion, as is usually the case for non-linear systems. By examining (35) we find that $\omega_2 = 0$ at $\omega_0 \doteqdot 0{\cdot}89$ which corresponds to $h = h^* \doteqdot 1{\cdot}07$. For $h > h^*$, $\omega_2 < 0$ while for $h < h^*$, $\omega_2 > 0$. Thus, for depths greater than h^*, the fluid behaves like a soft spring, its free vibration frequency decreasing with increasing amplitude. For depths shallower than h^*, the fluid behaves like a hard spring, its free vibration frequency increasing with increasing amplitude.

From (40) and the expressions for η^0, η^1 and η^2, we see that the surface is never flat. It is most nearly so when $t = n\pi$ where n is any integer. Then

$$\epsilon\eta(x,n\pi) = \tfrac{1}{8}\epsilon^2(\omega_0^2+2\omega_0^{-2}-3\omega_0^{-6})\cos 2x. \tag{43}$$

The velocity vanishes throughout the fluid at $t = (n+\frac{1}{2})\pi$. At these times each part of the surface is either at its highest or lowest position. In particular, when n is an even integer, the crest is at $x = 0$ and the profile is given by

$$\epsilon\eta = \left[\epsilon+\frac{\epsilon^3}{256}(9\omega_0^{-8}+6\omega_0^{-4}-15+8\omega_0^4)\right]\cos x+\tfrac{1}{8}\epsilon^2(\omega_0^{-2}+3\omega_0^{-6})\cos 2x$$
$$+\tfrac{3}{256}\epsilon^3(9\omega_0^{-12}+6\omega_0^{-8}+30\omega_0^{-4}-16+\omega_0^4+2\omega_0^8)\cos 3x. \tag{44}$$

The greatest rise occurs at $x = 0$, and it is equal to

$$\epsilon\eta_{\max} = \epsilon+\tfrac{1}{8}\epsilon^2(\omega_0^{-2}+3\omega_0^{-6})+\frac{\epsilon^3}{256}(27\omega_0^{-12}+27\omega_0^{-8}+96\omega_0^{-6}-63+11\omega_0^4+6\omega_0^8). \tag{45}$$

When $t = (n+\frac{1}{2})\pi$, with n an odd integer, the crest is at $x = \pi$. The wave profile at this time may be obtained either by reflecting that given by (44) about $x = \frac{1}{2}\pi$, or replacing ϵ by $-\epsilon$ in (44). A graph of the surface profile for $\epsilon = 0{\cdot}05$ and $h = 0{\cdot}25$ is shown in figure 1.

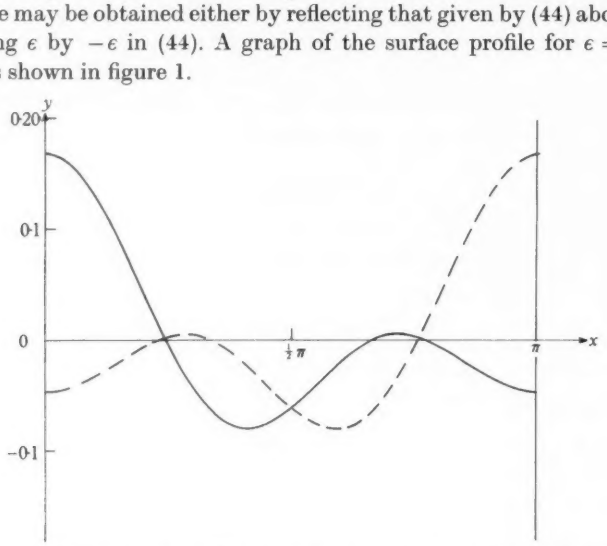

FIGURE 1. Profile of the surface of the standing wave at $t = (n+\frac{1}{2})\pi$, for n even (solid curve) and n odd (broken curve). These curves are based on equation (44) with $\epsilon = 0{\cdot}05$ and $h = 0{\cdot}25$.

When the depth h becomes infinite, our results (40) and (42) become

$$\epsilon\eta = (\epsilon + \tfrac{1}{32}\epsilon^3)\cos x + \tfrac{1}{2}\epsilon^2 \cos 2x + \tfrac{3}{8}\epsilon^3 \cos 3x, \tag{46}$$

$$\omega = 1 - \tfrac{1}{8}\epsilon^2. \tag{47}$$

These results agree with those of Penney & Price who obtained additional terms in this case.

In calculating the pressure from (9) it is convenient to consider those instants when the fluid is at rest. Then in the vertical plane $x = 0$ and at the time of a crest, (9) becomes

$$\begin{aligned}\frac{k}{\rho g}(p - p_0) = -y + \left[\epsilon + \frac{\epsilon^3}{256}(9\omega_0^{-8} - 234\omega_0^{-4} + 81 - 8\omega_0^4)\right]\frac{\cosh(y+h)}{\cosh h} \\ - \epsilon^2\left[\tfrac{1}{2}\omega_0^2 + \tfrac{3}{8}(\omega_0^2 - \omega_0^{-6})\frac{\cosh 2(y+h)}{\cosh 2h}\right] + \frac{\epsilon^3}{256}(1 + 3\omega_0^4)(27\omega_0^{-12} \\ - 63\omega_0^{-8} + 39\omega_0^{-4} - 5 + 2\omega_0^4)\frac{\cosh 3(y+h)}{\cosh 3h} \quad \text{for} \quad -h \leqslant y \leqslant \eta_{\max}.\end{aligned} \tag{48}$$

Upon replacing ϵ by $-\epsilon$ in (48), we obtain the pressure in the vertical plane $x = 0$ at the time of a trough. Graphs of these pressures are shown in figure 2 for $\epsilon = 0{\cdot}05$ and $h = 0{\cdot}25$.

When the depth h becomes infinite, our result (48) becomes

$$\frac{k}{\rho g}(p - p_0) = -y + (\epsilon - \tfrac{19}{32}\epsilon^3)e^y - \tfrac{1}{2}\epsilon^2. \tag{49}$$

This result agrees to the third order with the equation (135) of Penney & Price with the exception of the term independent of y. The difference arises from the fact that Penney & Price did not take into account the contribution of the zero order term in their potential function Φ. Had they done this by utilizing their equation (47), the correct form of their equation (135) to the fifth order would have been

$$p = \frac{\lambda\rho g}{2\pi}\left[-y-\tfrac{1}{2}A^2+\tfrac{3}{32}A^4+(A-\tfrac{19}{32}A^3+\tfrac{755}{1792}A^5)e^y \right.$$
$$\left. -\tfrac{5}{14}A^4e^{2y}-(\tfrac{7}{132}A^5)e^{3y}+(\tfrac{15}{256}A^5)e^{5y}\right].$$

Our solution describes the standing wave which results from the reflexion of a normally incident progressing wave from a wall or breakwater at $x = 0$. It also describes the free vibrations of the liquid contained between two vertical walls one-half wavelength apart. In either of these cases the pressure given by (48) and shown in figure 2 is the pressure on the wall.

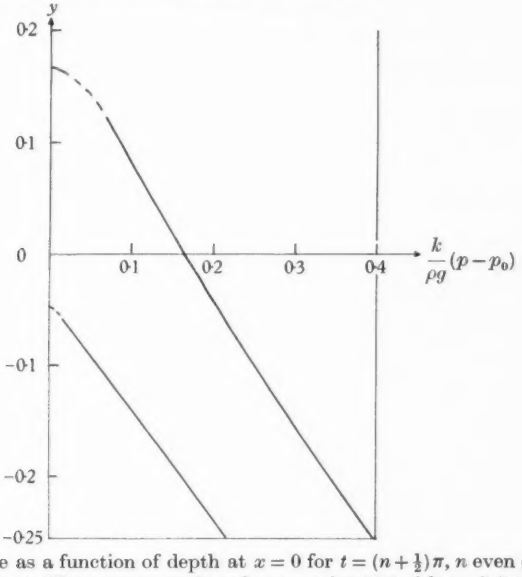

FIGURE 2. Pressure as a function of depth at $x = 0$ for $t = (n+\frac{1}{2})\pi$, n even (upper curve) and n odd (lower curve). These curves are based on equation (48) with $\epsilon = 0{\cdot}05$ and $k = 0{\cdot}255$. The horizontal scale is $k(p-p_0)/\rho g$ and the vertical scale is y. The dashed parts are sketched in to make $p-p_0$ have the value zero at the surface $y = \epsilon\eta_{\max}$ and $y = \epsilon\eta_{\min}$. Equation (48) does not yield $p-p_0 = 0$ at these points since it is correct only through ϵ^3.

Appendix

Following Penney & Price (1952), we write η and ϕ in a form which obviously satisfies (1), (4) and (5). It is

$$\epsilon\eta = \sum_{n=1}^{\infty} \alpha_n(t)\cos nx, \tag{1}$$

$$\epsilon\phi = \sum_{n=-\infty}^{\infty} \beta_n(t)\, e^{ny}\cos nx. \tag{2}$$

To satisfy (4) the coefficients $\beta_n(t)$ and $\beta_{-n}(t)$ must obey the relation

$$e^{inh}\beta_{-n}(t) = e^{-inh}\beta_n(t). \tag{3}$$

Upon inserting (1) and (2) into (2) and (3) of § 2, we obtain the following equations for the determination of α_n, β_n and ω:

$$\alpha_s = -\sum_{n=-\infty}^{\infty} \omega\beta_n'[E(n,s-n)+E(n,s+n)] - \frac{1}{2}\sum_{n=-\infty}^{\infty}\sum_{m=-\infty}^{\infty} mn \times \beta_n\beta_m[E(m+n,s-m+n)+E(m+n,s+m-n)] \quad \text{for} \quad s = 0,1,2,\ldots, \tag{4}$$

$$\omega\alpha_s' = \sum_{n=-\infty}^{\infty} n\beta_n[E(n,s-n)+E(n,s+n)] - \frac{1}{2}\sum_{n=-\infty}^{\infty}\sum_{m=1}^{\infty} mn\,\alpha_m\beta_n \times [E(n,s-m+n)+E(n,s+m-n)-E(n,s-m-n)-E(n,s+m+n)] \quad \text{for} \quad s = 0,1,2,\ldots. \tag{5}$$

Here a prime denotes differentiation with respect to t and the quantity $E(\lambda, s)$ is defined by the equations

$$E(\lambda, \pm s) = \sum_{N=0}^{\infty} \frac{\lambda^N}{2^N N!} S_N(s), \tag{6}$$

$$S_N(\pm s) = \sum_{m=-\infty}^{\infty}\sum_{n=-\infty}^{\infty}\sum_{p=-\infty}^{\infty} \ldots \alpha_m\alpha_n\alpha_p \ldots \alpha_{s-m-n-p}, \ldots, \tag{7}$$

$$\alpha_{-k} = \alpha_k \quad (k = 1,2,3,\ldots). \tag{8}$$

Instead of using the iteration method of Penney & Price, we solve (4) and (5) by assuming that α_n, β_n and ω can be expressed as

$$\epsilon\alpha_s = \sum_{j=s}^{\infty} \alpha_{sj}\epsilon^j, \tag{9}$$

$$\epsilon\beta_s = \sum_{j=|s|}^{\infty} \beta_{sj}\epsilon^j, \tag{10}$$

$$\omega = \sum_{j=0}^{\infty} \omega_j\epsilon^j. \tag{11}$$

Then $E(\lambda, s)$ can be written as

$$E(\lambda, s) = \sum_{j=|s|}^{\infty} E_j(\lambda, s)\epsilon^j. \tag{12}$$

We now insert equations (9) to (12) into (4) and (5) and equate the coefficients of the powers of ϵ. In this way we obtain, for each pair of integers $v \geqslant s \geqslant 0$, the equations

$$\alpha_{sv} = -\sum_{n=-v}^{v}\sum_{j=|n|}^{v}\sum_{k=0}^{j} \omega_k\beta_{n(j-k)}'[E_{v-j}(n,s-n)+E_{v-j}(n,s+n)] - \frac{1}{2}\sum_{n=-v}^{v}\sum_{m=0}^{v}\sum_{j=m}^{v}\sum_{i=|n|}^{v} mn\,\alpha_{mj}\beta_{ni}[E_{v-i-j}(m+n,s-m+n) + E_{v-i-j}(m+n,s+m-n)], \tag{13}$$

$$\sum_{k=0}^{v-s} \omega_k \alpha'_{s(v-k)} = \sum_{n=-v}^{v} \sum_{j=|n|}^{v} n\beta_{nj}[E_{v-j}(n, s-n) + E_{v-j}(n, s+n)]$$

$$-\frac{1}{2} \sum_{n=-v}^{v} \sum_{m=0}^{v} \sum_{j=m}^{v} \sum_{i=|n|}^{v} mn\,\alpha_{mj}\beta_{ni}[E_{v-i-j}(n, s-m+n) + E_{v-i-j}(n, s+m-n)$$

$$- E_{v-i-j}(n, s-m-n) - E_{v-i-j}(n, s+m+n)]. \quad (14)$$

These equations can be solved successively, starting with $s = v = 0$. We have solved them for all s and v satisfying $3 \geqslant v \geqslant s \geqslant 0$. The results are the same as those of § 3, but the labour is greater.

The research reported in this paper has been sponsored by the Office of Naval Research under Contract No. (285) 45.

REFERENCE

PENNEY, W. G. & PRICE, A. T. 1952 *Phil. Trans.* A, **244**, 254.

Exact solutions of the magnetohydrodynamic equations

By W. E. WILLIAMS
Department of Applied Mathematics, Liverpool University

(Received 2 November 1959)

Exact one-dimensional solutions of the magnetohydrodynamic equations of an incompressible fluid are considered. It is shown that one class of plane wave solutions of the linearized equations is also a possible class of solutions of the general equations including the effect of displacement current. A similar result is also established for the solutions for a horizontally stratified fluid. For the particular case when the viscosity is equal to the magnetic diffusivity an exact solution is obtained for the magnetohydrodynamic Rayleigh problem for a semi-infinite plate. It is shown that this solution may be employed directly to give the solution for liquids of small, but not necessarily equal, viscosity and magnetic diffusivity.

1. Introduction

The solution of the linearized equations of magnetohydrodynamics is a topic which has received a considerable amount of attention in recent years. The most comprehensive and systematic work on this subject is that of Baños (1955*a*, *b*), who has considered the detailed form of plane wave solutions of the linearized equations. It has also been observed by certain authors (e.g. Lundquist 1952) that, for an incompressible fluid, the general non-linear equations also possess plane wave solutions similar to those of the linearized equations. It thus seems of interest to consider other conditions under which the general and linear equations of an incompressible fluid possess similar exact solutions.

In the present paper we examine whether there exist similar solutions of the linear and exact equations of motion of an incompressible fluid which are functions of one Cartesian variable z and time.

In §2 we consider the particular class of solutions with no velocity component in the z-direction. If the displacement current is neglected the exact equations are identical with the linearized ones and thus exact solutions of the linear equations are also solutions of the complete equations. In particular the forms of the plane wave solutions of the linear and exact equations are identical. This fact has been observed by Lundquist and others. It is also shown that, without neglecting the displacement current, there exist solutions of the linear equations which are also solutions of the exact equations. For plane waves these are the pressure modes defined by Baños (1955*b*) and are characterized by the fact that the associated Poynting vector is in the direction of propagation.

In §3 the particular case when the external magnetic field is in the z direction is considered. It is shown that, for a horizontally stratified incompressible fluid,

the small amplitude Alfvén wave type solutions obtained by Ferraro (1954) represent possible exact solutions of the equations of motion with the effect of displacement current included. It is also shown that the equations of motion for one-dimensional disturbances in an unbounded fluid are essentially linear and capable of exact solution.

The type of solutions considered in §2 occur in some initial value problems in magnetohydrodynamics; one such problem is the Rayleigh problem for an infinite plate when there is a transverse field present perpendicular to the plate. The solution of this problem has been considered in detail by Ludford (1959) and Chang & Yen (1959). Another class of boundary-value problem satisfying our conditions is the problem of the motion of a viscous fluid bounded by an infinite oscillating plane, and the solution for an insulating plane has been given by Kakutani (1959). The magnetohydrodynamic Rayleigh problem for a half-plane is another case when the general equations are exactly reducible to a linear form. This problem is considered in §4 where it is shown that, when the viscosity is equal to the magnetic diffusivity (conductivity $\times$ permeability)$^{-1}$, the boundary-value problem reduces to a classical one. It is also shown that the first-order solution for small viscosity and diffusivity may be deduced immediately from this special case.

2. General equations

The motion of an incompressible conducting fluid under the action of a constant external magnetic field $\mathbf{H}_0$ is governed by the equations

$$\mu\frac{\partial \mathbf{H}}{\partial t} = -\operatorname{curl}\mathbf{E}, \tag{1}$$

$$\frac{1}{\sigma}(\mathbf{J}-\rho_e\mathbf{v}) = \mathbf{E}+\mu\mathbf{v}(\mathbf{H}_0+\mathbf{H}), \tag{2}$$

$$\rho\frac{d\mathbf{v}}{dt} = -\operatorname{grad}p+\rho_e\mathbf{E}+\mu\mathbf{J}\times(\mathbf{H}_0+\mathbf{H})+\lambda\nabla^2\mathbf{v}, \tag{3}$$

$$\mathbf{J} = \operatorname{curl}\mathbf{H}-\epsilon\frac{\partial \mathbf{E}}{\partial t}, \tag{4}$$

$$\rho_e = \epsilon\operatorname{div}\mathbf{E}, \tag{5}$$

$$\operatorname{div}\mathbf{v} = 0, \tag{6}$$

$$\frac{\partial\rho}{\partial t}+\mathbf{v}.\operatorname{grad}\rho = 0. \tag{7}$$

In the above equations $\mathbf{E}$ and $\mathbf{H}$ denote the induced electric and magnetic fields, $\mathbf{J}$ denotes the current density, $\mathbf{v}$ the fluid velocity and p, ρ and ρ_e the pressure, fluid density and charge density, respectively. It will also be assumed that μ (permeability), ϵ (dielectric constant), σ (conductivity) and λ (coefficient of viscosity) are constant. We also have from Maxwell's equation that

$$\operatorname{div}\mathbf{H} = 0. \tag{8}$$

We now investigate the possibility of obtaining exact solutions of the above equations in which the field components are functions of one Cartesian variable z and of time. Equations (1) and (8) then show that H_z is constant; it may thus be

absorbed into the z-component of $\mathbf{H}_0$ and hence there will be no loss of generality in taking $H_z = 0$. Equations (6) and (7) have, as one solution,

$$v_z = \partial\rho/\partial t = \partial\rho/\partial z = 0$$

and we consider solutions of equations (1)–(5) satisfying these conditions. Equation (7) shows that ρ will be constant if constant at any particular instant.

For the first part of the investigation, it will be assumed that the displacement current may be neglected (i.e. $\rho_e = 0$).

The above assumptions enable (3) to be rewritten

$$\rho\frac{\partial \mathbf{v}}{\partial t} = -\mathbf{k}\frac{\partial}{\partial z}[p + \tfrac{1}{2}\mu(\mathbf{H}_0 + \mathbf{H})^2] + \lambda\frac{\partial^2 \mathbf{v}}{\partial z^2} + \mu H_{0z}\frac{\partial \mathbf{H}}{\partial z}, \tag{9}$$

where $\mathbf{k}$ is the unit vector in the z-direction. Equations (1), (2), (4) and (8) now give

$$\frac{1}{\sigma}\operatorname{curl}\mathbf{J} = -\frac{1}{\sigma}\frac{\partial^2 \mathbf{H}}{\partial z^2} = -\mu\frac{\partial \mathbf{H}}{\partial t} + \mu H_{0z}\frac{\partial \mathbf{v}}{\partial z}. \tag{10}$$

Since $v_z = H_z = 0$ we have, from (9), that

$$\frac{\partial}{\partial z}\{p + \tfrac{1}{2}\mu(\mathbf{H}_0 + \mathbf{H})^2\} = 0. \tag{11}$$

$\mathbf{H}$ may now be eliminated from (9) and (10) to give

$$\left(\rho\frac{\partial}{\partial t} - \lambda\frac{\partial^2}{\partial z^2}\right)\left(\mu\frac{\partial}{\partial t} - \frac{1}{\sigma}\frac{\partial^2}{\partial z^2}\right)\mathbf{v} = \mu^2 H_{0z}^2\frac{\partial^2 \mathbf{v}}{\partial z^2}. \tag{12}$$

Equation (12) has been obtained by Ludford (1959) for the particular case when $\mathbf{v}$ and $\mathbf{H}_0$ are perpendicular, it has also been derived by Dungey (1958) by linearizing the equations of motion.

In view of the fact that our assumptions concerning the form of the solutions have reduced the equations to a linear form it seems of interest to examine whether there exist solutions of the linearized equations which satisfy our assumptions and which may therefore represent solutions of the general equations. Since z is arbitrary it is seen that plane waves satisfy our assumptions, and the propagation of small amplitude plane waves has been considered in detail by Baños (1955*a*, *b*). Baños's work on magnetohydrodynamic waves is confined to the case of an inviscid fluid; in a later investigation (Baños 1956) he has considered the propagation of magneto-elastic waves. With suitable changes of notation the latter work may be used to obtain the results for the propagation of small amplitude plane waves in a viscous fluid.

Baños has shown that the solution of the linearized equations can be split up into two independent classes of solutions which he calls v- and p-modes. The v-modes are solutions which are obtained by requiring that the velocity be perpendicular to both $\mathbf{k}$ and $\mathbf{H}_0$; the pressure associated with such modes is then shown to be zero. The p-mode solutions arise when the fluid velocity is in the plane of $\mathbf{k}$ and $\mathbf{H}_0$ and perpendicular to $\mathbf{k}$; in general the pressure associated with this mode is non-zero. Another difference between the v- and p-modes is that the Poynting vector for the v-modes is in the direction of $\mathbf{H}_0$ whilst that for the

p-modes is parallel to **k**. If the displacement current is neglected the wave-numbers of the v- and p-modes are equal.

We now examine the extent to which Baños's results are applicable to plane wave solutions of the general equations. If it is assumed that **v** and **H** are both proportional to $\exp i(\omega t + kz)$, then equation (12) gives

$$(i\omega\rho + \lambda k^2)(i\omega\mu + k^2\sigma^{-1}) = -\mu^2 H_{0z}^2 k^2. \tag{13}$$

For $\lambda = 0$ equation (13) reduces to one obtained by Baños (1955*b*) and for non-zero λ may be identified with a similar equation derived by Baños (1956) for magneto-elastic waves. Thus, if the displacement current is neglected, the wave-numbers of the plane wave solutions of the exact and linearized equations are equal.

The existence of v- and p-mode types of solution of the general equations will now be considered. It is easily seen that equation (9) may be re-written

$$\rho\frac{\partial \mathbf{v}}{\partial t} = -\mathbf{k}\frac{\partial}{\partial z}(p + \tfrac{1}{2}\mu H^2) + \lambda\frac{\partial^2 \mathbf{v}}{\partial z^2} + \mu\mathbf{J}\times\mathbf{H}_0. \tag{14}$$

Clearly a possible class of solutions of (14) is obtained by setting $p = -\frac{1}{2}\mu H^2$; **v** will then be perpendicular to $\mathbf{H}_0$. Hence, since $v_z = 0$, the velocity is perpendicular to both **k** and $\mathbf{H}_0$. This is precisely the linear **v**-mode and hence we conclude that the exact equations, neglecting displacement currents, possess plane wave solutions of the v-mode type. In the exact solution, however, the pressure associated with this mode is $-\frac{1}{2}\mu H^2$ and not zero; in the linear theory terms of order H^2 are neglected and this would give $p = 0$. Equation (13) shows that there will be two possible v-mode solutions, one of which is essentially a damped Alfvén wave and the other a highly attenuated one which vanishes for zero viscosity or infinite conductivity. **v** will be of the form $A\mathbf{k}\times\mathbf{H}_0\exp i(\omega t + kz)$ and **H** and **E** may be obtained from equations (1) and (10).

It would be logical at this point to consider the existence of p-mode type solutions. It will, however, be shown that in this case it is not necessary to neglect the displacement current and we therefore consider conditions under which the effect of the displacement current may be treated simply. The non-linear effect of the displacement current is due to the charge density term and thus, in order to seek simple solutions, we shall consider only those with $\operatorname{div}\mathbf{E} = 0$. Since our main interest lies in solutions of the plane wave type it may be assumed that $E_z = 0$. If the displacement current is included then (10) becomes

$$-\frac{1}{\sigma}\frac{\partial^2 \mathbf{H}}{\partial z^2} + \epsilon\mu\frac{\partial^2 \mathbf{H}}{\partial t^2} = \mu\frac{\partial \mathbf{H}}{\partial t} + \mu H_{0z}\frac{\partial \mathbf{v}}{\partial z}. \tag{15}$$

Equation (15) shows that **v** and **H** are parallel for plane waves, and equations (2) and (3) thus become

$$\frac{1}{\sigma}\mathbf{J} = \mathbf{E} + \mu\mathbf{v}\times\mathbf{H}_0 \tag{16}$$

$$\rho\frac{\partial \mathbf{v}}{\partial t} = -\operatorname{grad}(p + \tfrac{1}{2}\mu H^2) + \mu\mathbf{J}\times\mathbf{H}_0 + \lambda\frac{\partial^2 \mathbf{v}}{\partial z^2} - \mu\epsilon\frac{\partial \mathbf{E}}{\partial t}\times\mathbf{H}. \tag{17}$$

The only non-vanishing component of the last term on the right-hand side of (17) is that in the z-direction and hence this term may be written as $-\epsilon \operatorname{grad} \psi$, where ψ is a scalar depending on z and t, and hence

$$\rho \frac{\partial \mathbf{v}}{\partial t} = -\operatorname{grad}(p + \tfrac{1}{2}\mu H^2 + \epsilon\psi) + \lambda \frac{\partial^2 \mathbf{v}}{\partial z^2} + \mu \mathbf{J} \times \mathbf{H}_0. \tag{18}$$

Equations (2) and (4) give

$$\frac{1}{\sigma} \mathbf{J} . \mathbf{H}_0 = \mathbf{E} . \mathbf{H}_0, \tag{19}$$

$$\left(1 + \frac{\epsilon}{\sigma} \frac{\partial}{\partial t}\right) \mathbf{J} . \mathbf{H}_0 = \mathbf{H}_0 . \operatorname{curl} \mathbf{H}. \tag{20}$$

From (1) and (19)

$$\left\{\frac{\partial}{\partial t}\left(1 + \frac{\epsilon}{\sigma} \frac{\partial}{\partial t}\right) - \frac{1}{\sigma\mu} \frac{\partial^2}{\partial z^2}\right\} \mathbf{J} . \mathbf{H}_0 = -\frac{H_{0z}}{\mu} \frac{\partial}{\partial z} (\operatorname{div} \mathbf{E}). \tag{21}$$

Thus, since $\operatorname{div} \mathbf{E} = 0$, $\mathbf{J} . \mathbf{H}_0 = \mathbf{E} . \mathbf{H}_0 = 0$ is a possible solution and $\mathbf{E}$ will have the form $\phi \mathbf{k} \times \mathbf{H}_0$ where ϕ is a scalar. From (16)

$$\left(\rho \frac{\partial}{\partial t} - \lambda \frac{\partial^2}{\partial z^2}\right) \operatorname{curl} \mathbf{v} = \mu \operatorname{curl} (\mathbf{J} \times \mathbf{H}_0), \tag{22}$$

and eliminating $\mathbf{v}$ between (15) and (21) gives

$$\left(\frac{\partial}{\partial t} - \nu \frac{\partial^2}{\partial z^2}\right) \operatorname{curl} \left[\operatorname{curl} \left\{\frac{1}{\sigma} \frac{\partial \mathbf{J}}{\partial t} - \frac{\partial \mathbf{E}}{\partial t}\right\}\right] = \frac{\mu^2}{\rho} H_{0z} \frac{\partial^2}{\partial t \, \partial z} \operatorname{curl} (\mathbf{J} \times \mathbf{H}_0), \tag{23}$$

where ν is the kinematic viscosity.

Finally, from (1), (4) and (22),

$$\left(\frac{\partial}{\partial t} - \nu \frac{\partial^2}{\partial z^2}\right) \left\{-\frac{1}{\sigma\mu} \left(\frac{\partial^2}{\partial z^2} - \epsilon\mu \frac{\partial^2}{\partial t^2}\right) + \frac{\partial}{\partial t}\right\} \frac{\partial^2 \phi}{\partial z^2} = \frac{\mu H_{0z}^2}{\rho} \frac{\partial^2}{\partial z^2} \left(\frac{\partial^2}{\partial z^2} - \epsilon\mu \frac{\partial^2}{\partial t^2}\right) \phi. \tag{24}$$

If the displacement current is not neglected then (9) has the form

$$\begin{aligned} \rho \frac{\partial \mathbf{v}}{\partial t} = &-\mathbf{k} \frac{\partial}{\partial z} [p + \tfrac{1}{2}\mu(\mathbf{H}_0 + \mathbf{H})^2 + \epsilon\psi] + \epsilon\mu \mathbf{k} [H_0^2 - H_{0z}^2] \frac{\partial \phi}{\partial t} \\ &+ \epsilon\mu H_{0z} [\mathbf{k} \times (\mathbf{k} \times \mathbf{H}_0)] \frac{\partial \phi}{\partial t} + \mu H_{0z} \frac{\partial \mathbf{H}}{\partial z} + \lambda \frac{\partial^2 \mathbf{v}}{\partial z^2}. \end{aligned} \tag{25}$$

$\mathbf{v}$ is perpendicular to $\mathbf{k}$ and thus from (24)

$$\rho \frac{\partial \mathbf{v}}{\partial t} = \lambda \frac{\partial^2 \mathbf{v}}{\partial z^2} + \epsilon\mu H_{0z} [\mathbf{k} \times (\mathbf{k} \times \mathbf{H}_0)] \frac{\partial \phi}{\partial t} + \mu H_{0z} \frac{\partial \mathbf{H}}{\partial z}, \tag{26}$$

$$\frac{\partial}{\partial z} [p + \tfrac{1}{2}\mu(\mathbf{H}_0 + \mathbf{H})^2 + \epsilon\psi] = \epsilon\mu [H_0^2 - H_{0z}^2] \frac{\partial \phi}{\partial t}. \tag{27}$$

The velocity and magnetic field components are now determined in terms of ϕ from (25) and (26) and the pressure is then given by (27).

If it is assumed that ϕ is proportional to $\exp i(\omega t + kz)$ then (24) becomes

$$(i\omega + \nu k^2) \left\{\frac{1}{\sigma\mu} (k^2 - \epsilon\mu\omega^2) + i\omega\right\} = \frac{\mu H_{0z}^2}{\rho} (\epsilon\mu\omega^2 - k^2). \tag{28}$$

For $\nu = 0$, (28) reduces to the dispersion equation obtained by Baños for the p-modes of an inviscid fluid and with suitable changes of notation is identical with the corresponding equation obtained for magneto-elastic waves. For plane waves $\mathbf{v}$ and $\mathbf{H}$ are parallel and thus equation (26) shows that $\mathbf{v}$ is parallel to $\mathbf{k} \times (\mathbf{k} \times \mathbf{H}_0)$; this is precisely Baños's definition of the p-mode solution and the other field components are identical with the ones obtained by Baños for the linearized equations. Thus the p-mode solutions of the linearized equations are possible solutions of the general magnetohydrodynamic equations. If $\mathbf{H}_0$ and $\mathbf{k}$ are parallel, the appropriate form for $\mathbf{E}$ is then $\phi \mathbf{a} \times \mathbf{H}_0$ and it may then be verified that in this case the p- and v-modes are indistinguishable. For $\mathbf{H}_0$ and $\mathbf{k}$ parallel it is possible to obtain some additional exact solutions of the equations and this point will be considered in more detail in the following section.

The fact that the present method of generating p-mode solutions for plane waves is identical with Baños's is a particular example of a general result (Williams 1960) that the general solution of the linearized equations can be expressed in terms of two independent classes of solutions. One class is generated by a stream function and the other by a one component electric vector potential. For plane waves the first class becomes the v-mode solution and the other the p-mode solution.

3. Wave fronts perpendicular to external fields

The problem considered in the first part of the present section is of a more general nature than that of the previous sections in that we investigate the deviations from the uniform state $\mathbf{E} = \mathbf{H} = 0$ of a horizontally stratified liquid. It is also assumed that the permanent magnetic field is vertical. The propagation of small amplitude disturbances in an incompressible fluid of this type has been examined by Ferraro (1954); the corresponding problem for a compressible fluid has been solved by Ferraro & Plumpton (1958). Ferraro has shown that for an incompressible fluid there will be propagated small amplitude disturbances which are essentially Alfvén waves with a variable velocity. It will now be shown that the exact equations also possess solutions of this type.

The undisturbed pressure and density will be denoted by p_0 and ρ_0, respectively, and the deviations from these quantities by p_1 and ρ_1. Equation (3) now becomes

$$(\rho_0+\rho_1)\frac{d\mathbf{v}}{dt} = -\operatorname{grad}(p_0+p_1)+\rho_e \operatorname{div}\mathbf{E}+\mu\mathbf{J}\times(\mathbf{H}_0+\mathbf{H})-(\rho_0+\rho_1)g\mathbf{k}, \tag{29}$$

where g is the acceleration due to gravity. The static equilibrium condition is

$$\frac{dp_0}{dz} = -\rho_0 g, \tag{30}$$

In order to simplify the analysis it has been assumed that the fluid is inviscid; this assumption is not actually essential and the analysis can in fact be carried out for a varying coefficient of viscosity. One solution of equations (6)–(8) is $v_z = H_z = \rho_1 = 0$, and we consider solutions of the equations which satisfy this condition.

We now attempt to obtain a particular solution of the equations with **v** and **H** parallel; this assumption is made because the solution obtained by Ferraro satisfies it and also it enables the effect of displacement currents to be included. Equations (2) and (4) now show that

$$\left(1+\frac{\epsilon}{\sigma}\frac{\partial}{\partial t}\right)\operatorname{div}\mathbf{E}=0, \tag{31}$$

and a possible class of solutions of (31) will be $\operatorname{div}\mathbf{E}=0=E_z$. From (1), (2) and (4) it may be shown that

$$\left[\mu\frac{\partial}{\partial t}-\frac{1}{\sigma}\left(\frac{\partial^2}{\partial z^2}-\epsilon\mu\frac{\partial^2}{\partial t^2}\right)\right]\mathbf{J}=-\mu\left[\frac{\partial^2}{\partial z^2}-\epsilon\mu\frac{\partial^2}{\partial t^2}\right]\mathbf{v}\times\mathbf{H}_0, \tag{32}$$

and (29) and (32) then give

$$\begin{aligned}\left[\mu\frac{\partial}{\partial t}-\frac{1}{\sigma}\left(\frac{\partial^2}{\partial z^2}-\epsilon\mu\frac{\partial^2}{\partial t^2}\right)\right]\rho_0\frac{\partial\mathbf{v}}{\partial t}-\mu^2H_0^2\left(\frac{\partial^2}{\partial z^2}-\epsilon\mu\frac{\partial^2}{\partial t^2}\right)\mathbf{v}\\ =-\left[\mu\frac{\partial}{\partial t}-\frac{1}{\sigma}\left(\frac{\partial^2}{\partial z^2}-\epsilon\mu\frac{\partial^2}{\partial t^2}\right)\right]\operatorname{grad}P,\end{aligned} \tag{33}$$

where $P=p+\frac{1}{2}\mu H^2+\epsilon\psi$ and ψ is defined as in (18). Since $v_z=0$ and p is a function of z and t only we have that the right-hand side of (33) vanishes and hence

$$\left\{\mu\rho_0\frac{\partial^2}{\partial t^2}-\left(\frac{\partial^2}{\partial z^2}-\epsilon\mu\frac{\partial^2}{\partial t^2}\right)\left(\frac{\rho_0}{\sigma}\frac{\partial}{\partial t}+\mu^2H_0^2\right)\right\}\mathbf{v}=0. \tag{34}$$

v will have the form $\phi\mathbf{a}\times\mathbf{k}$, where ϕ is a scalar solution of (34) and **a** an arbitrary constant vector; the other components may then be expressed in terms of ϕ.

For $\epsilon=\sigma^{-1}=0$ equation (34) reduces to the Alfvén wave equation with a variable velocity $(\mu H_0^2/\rho_0)^{\frac{1}{2}}$ and is the equation obtained by Ferraro by linearizing the equations. Thus we see that for this class of problem, also, there exist solutions of the linearized equations which also represent possible solutions of the general equations.

The above analysis has been concerned more with particular forced solutions of the general equations than with the solution of particular boundary-value problems. It is also of interest, however, to examine the possibility of obtaining exact solutions for initial value problems where the wave fronts are perpendicular to the external magnetic field. The fluid is assumed to occupy an unbounded region of space and the initial density is assumed to be uniform; equation (7) then shows that the density will always be uniform. Equation (3) becomes

$$\rho\left\{\frac{\partial}{\partial t}+v_z(t)\frac{\partial}{\partial z}\right\}\mathbf{v}=-\operatorname{grad}\left[p+\tfrac{1}{2}\mu(\mathbf{H}_0+\mathbf{H})^2\right]+\mu H_{0z}\frac{\partial\mathbf{H}}{\partial z}+\lambda\frac{\partial^2\mathbf{v}}{\partial z^2}. \tag{35}$$

From equations (6) and (8) it is seen that the gradient term in (35) vanishes in an unbounded region and hence that $\partial v_z/\partial t=0$ and v_z is thus constant. From (2), (4) and (8)

$$-\frac{1}{\sigma}\frac{\partial^2\mathbf{H}}{\partial z^2}=-\mu\frac{\partial\mathbf{H}}{\partial t}+\mu\left\{H_{0z}\frac{\partial\mathbf{v}}{\partial z}-v_z\frac{\partial\mathbf{H}}{\partial z}\right\}, \tag{36}$$

where the displacement current has been neglected in deriving (36). Equation (35) now becomes

$$\rho\left(\frac{\partial}{\partial t}+v_z\frac{\partial}{\partial z}-\nu\frac{\partial^2}{\partial z^2}\right)\mathbf{v}=\mu H_{0z}\frac{\partial \mathbf{H}}{\partial z}. \tag{37}$$

Eliminating **H** from (36) and (37) gives

$$\rho\left(\frac{\partial}{dt}+v_z\frac{\partial}{\partial z}-\nu\frac{\partial^2}{\partial z^2}\right)\left(v_z\frac{\partial}{\partial z}+\frac{\partial}{\partial t}-\frac{1}{\sigma\mu}\frac{\partial^2}{\partial z^2}\right)\mathbf{v}=\mu H_{0z}^2\frac{\partial^2\mathbf{v}}{\partial z^2}. \tag{38}$$

Equation (38) is non-linear but the non-linear effects are due to the constant term v_z and thus the equation is amenable to exact solution. For $\nu = 0$ this equation (without the v_z) was obtained by Roberts (1955) by linearizing the equations of motion and employed by him to solve an initial value problem with $v_z = 0$. The above analysis thus shows that Roberts's solution in fact represents an exact solution of the magnetohydrodynamic equations neglecting displacement current.

In the following section the above analysis will be applied to obtain the magnetohydrodynamic analogues of some exact solutions of the Navier–Stokes equations.

4. Viscous flow problems

One of the classical exact solutions of the Navier–Stokes equations is that for the Rayleigh problem. This problem is essentially the solution of the equations of motion for a viscous incompressible fluid outside an infinite flat plate which is suddenly moved parallel to its length with a velocity U. The corresponding problem when the plate is perfectly conducting and there is a uniform magnetic field present perpendicular to the plate has been solved by Ludford (1959) and Chang & Yen (1959). The plate is assumed to occupy the plane $z = 0$ and to be moved parallel to itself with velocity U in the x-direction. Clearly this problem is of the type considered in §3 and v_x will satisfy (12). The solution obtained by the above authors, by using Laplace transformations, is rather complicated but takes on a considerably simpler form for $\nu = (\mu\sigma)^{-1}$. It is also of interest to note that, for a perfectly conducting fluid, the solution may be obtained from that of a completely different type of initial value problem solved by Roberts (1955).

It is of mathematical interest to note that equation (38) may be used to solve the magnetohydrodynamic Rayleigh problem with constant suction on the plate. This problem has been solved in the absence of a magnetic field by Hasimoto (1956).

The Rayleigh problem for a semi-infinite plate may also be reduced to the solution of a simple linear equation. We assume that the plate occupies the region $z = 0, y \geqslant 0$, for all x; it is then easily verified that a solution of the equations of motion is possible with $v_y = v_z = 0$, and v_x, a function of y, z and t, satisfying

$$\left(\frac{\partial}{\partial t}-\nu\nabla^2\right)\left(\frac{\partial}{\partial t}-\eta\nabla^2\right)v_x=V^2\frac{\partial^2 v_x}{\partial z^2}. \tag{39}$$

$\eta = (\mu\sigma)^{-1}$, ∇^2 is the two-dimensional Laplacian operator and V the Alfvén velocity. The only component of $\mathbf{H}$ is H_x and equations (9) and (10) become

$$H_0\left(\nu\nabla^2 - \frac{\partial}{\partial t}\right)v_x + V^2\frac{\partial H_x}{\partial z} = 0, \tag{40}$$

$$\left(\eta\nabla^2 - \frac{\partial}{\partial t}\right)H_x + H_0\frac{\partial v_x}{\partial z} = 0. \tag{41}$$

The electromagnetic boundary conditions are that the tangential components of $\mathbf{E}$ and $\mathbf{H}$ and the normal components of $\mu\mathbf{H}$ are continuous at the plate. It can be shown that the boundary conditions on the plate reduce to $v_x = U$ and $\eta\,\partial H_x/\partial z = 0$. For infinitely conducting fluid the second boundary condition is satisfied identically and in this case the only condition is $v_x = U$. The general boundary-value problem is rather complicated; the Laplace transform method is clearly the appropriate one to employ. The problem is then clearly of the Wiener–Hopf type, the transform variable p will, however, occur in the Wiener–Hopf factorization and the resulting general solution will be extremely complicated. It will, however, be shown that for $\nu = \eta = k_1$, the boundary-value problem reduces to one of a type already solved.

In this case equation (39) becomes

$$\left(k_1\nabla^2 - \frac{\partial}{\partial t} - V\frac{\partial}{\partial z}\right)\left(k_1\nabla^2 - \frac{\partial}{\partial t} + V\frac{\partial}{\partial z}\right)v_x = 0. \tag{42}$$

Thus, from (42), we see that

$$v_x = e^{Vz/2k_1}f(y,z,t) + e^{-Vz/2k_1}g(y,z,t) \tag{43}$$

where f and g are independent solutions of

$$\left(k_1\nabla^2 - \frac{\partial}{\partial t} - \frac{V^2}{4k_1}\right)a = 0.$$

Equation (40) now gives

$$H_x = -\frac{H_0}{V}\{fe^{Vz/2k_1} - ge^{-Vz/2k_1}\}. \tag{44}$$

Equations (43) and (44) show that the boundary conditions on the half-plane become

$$f+g = U \quad \text{and} \quad \frac{\partial}{\partial z}(f-g) + \frac{V}{2k}(f+g) = 0.$$

If ϕ and ψ are defined by

$$\phi = f+g \quad \text{and} \quad \psi = g-f,$$

then the boundary conditions on ϕ and ψ on the half plane are

$$\phi = U \quad \text{and} \quad \partial\psi/\partial z = UV/2k_1.$$

The boundary-value problems for ϕ and ψ are of a well-known type and may be deduced from the solution of the ordinary Rayleigh problem for a half-plane solved by Howarth (1950). The best method of effecting a solution is by means of the Laplace transform. If $\bar{u}(y,z,p)$ denotes the Laplace transform of $u(y,z,t)$, then

$$\bar{u} = \int_0^\infty e^{-pt}u\,dt.$$

We thus require solutions $\overline{\phi}$, $\overline{\psi}$ of

$$\left\{k_1\nabla^2-\left(p+\frac{V^2}{4k_1}\right)\right\}\overline{u}=0, \tag{45}$$

such that $\overline{\phi}=U/p$ and $\partial\overline{\psi}/\partial z=UV/2k_1p$ on the half-plane. For $V=0$ Howarth has obtained a solution $\overline{\phi}_H$ of (45) such that $\overline{\phi}_H=U/p$ on the half plane. This solution is defined by

$$\overline{\phi}_H=\frac{U}{2p}\{2\cosh qz-e^{-qz}\operatorname{erf}q^{\frac{1}{2}}(\eta-\xi)-e^{qz}\operatorname{erf}q^{\frac{1}{2}}(\eta+\xi)\}, \tag{46}$$

where $q^2=p/k_1$ and $y=\xi^2-\eta^2$ and $z=2\xi\eta$.

A solution to the present boundary-value problem for $\overline{\phi}$ is thus

$$\overline{\phi}=\left(p+\frac{V^2}{4k_1}\right)\frac{1}{p}\overline{\phi}_H(y,z,p+V^2/4k_1)$$

and hence

$$\phi=e^{-V^2t/4k_1}\phi_H(y,z,t)+\frac{V^2}{4k_1}\int_0^t e^{-V^2w/4k_1}\phi_H(y,z,w)\,dw. \tag{47}$$

By a method similar to that of Howarth's it is seen that

$$\overline{\psi}=\frac{UV}{4k_1p\beta}\{2\sinh\beta z-e^{\beta z}\operatorname{erf}\beta^{\frac{1}{2}}(\eta+\xi)+e^{-\beta z}\operatorname{erf}\beta^{\frac{1}{2}}(\eta-\xi)\}, \tag{48}$$

where
$$k_1\beta^2=p+V^2/4k_1.$$

The inverses of $\overline{\phi}$ and $\overline{\psi}$ may be expressed in terms of integrals of functions obtained by Howarth, which are themselves infinite integrals involving modified Hankel functions. The actual forms of ϕ and ψ are extremely complicated and will therefore not be considered. It is of some interest to examine the behaviour of the solution for large and small values of t; for these cases it is possible to obtain reasonable simple forms for the solution. A quantity which is of physical interest is the skin friction τ at the wall and we shall consider the limiting forms of τ, keeping y fixed, for large and small t. We have that

$$\tau=\left\{\mu H_0H_x+\rho_0k_1\frac{\partial v_x}{\partial z}\right\}_{\text{wall}}=\rho_0k_1\left\{\frac{\partial\phi}{\partial z}+\frac{V\psi}{2k_1}\right\}_{\text{wall}}.$$

On the wall

$$\frac{\partial\phi}{\partial z}=e^{-V^2t/4k_1}\left(\frac{\partial\phi_H}{\partial z}\right)_{\text{wall}}+\left\{\frac{\partial\overline{\phi}_H}{\partial z}(y,z,V/2k_1)\right\}_{\text{wall}}-\frac{V^2}{4k_1}\int_t^\infty e^{-V^2w/4k_1}\left(\frac{\partial\phi_H}{\partial z}\right)_{\text{wall}}dw \tag{49}$$

For large t,
$$\left(\frac{\partial\phi_H}{\partial z}\right)_{\text{wall}}\sim 0{\cdot}4604U(k_1ty^2)^{-\frac{1}{4}}$$

and thus

$$\frac{1}{U}\left(\frac{\partial\phi_H}{\partial z}\right)_{\text{wall}}\sim 0{\cdot}9208\,(k_1ty^2)^{-\frac{1}{4}}\,e^{-V^2t/4k_1}-\left\{\frac{V}{2k_1}\operatorname{erf}\sqrt{\frac{Vy}{2k_1}}+\sqrt{\frac{V}{2k_1y}}\,e^{-Vy/2k_1}\right\}. \tag{50}$$

One clearly expects that $\partial\phi/\partial z$ will tend to $\partial\phi_H/\partial z$ as $V\to 0$ but equation (50) shows that the asymptotic form of $\partial\phi/\partial z$ is twice that of $\partial\phi_H/\partial z$ in the limiting

case of small V. This apparent discrepancy is due to the fact that for V small the integral in (49) may not be estimated by normal methods and a method developed by Clemmow (1950) must be employed. It can be shown that the appropriate form of the first term in (50) is

$$\frac{0{\cdot}4604}{(k_1 t y^2)^{\frac{1}{4}}}\left\{e^{-V^2t/4k_1}+\left(\frac{V^2t}{4k_1}\right)^{\frac{1}{2}}\int_{V^2t/4k_1}^{\infty}\frac{e^{-w}}{w^{\frac{1}{2}}}dw\right\}. \tag{51}$$

Equation (51) exhibits the appropriate limiting behaviour for $V = 0$ and the integral is an incomplete gamma function. For small t it can be shown that

$$\left(\frac{\partial\phi}{\partial z}\right)_{\text{wall}} \sim \frac{U}{\sqrt{\pi k_1 t}}\left\{1+\frac{V^2t}{4k_1}\right\}.$$

It is easily shown by transform techniques that

$$\psi = -U\,\text{erf}\sqrt{\frac{Vy}{2k_1}}+O(t^{-\frac{3}{4}})$$

for large t, and

$$\psi = -\frac{UVt^{\frac{1}{2}}}{\pi k_1}+O(t)$$

for small t. Thus we finally obtain

$$\left.\begin{aligned}\tau &= -\rho_0 k_1 U\left\{\frac{2V}{k_1}\,\text{erf}\sqrt{\frac{Vy}{2k_1}}+\sqrt{\frac{V}{2k_1 y}}\exp\left(-\frac{Vy}{2k_1}\right)-\frac{0{\cdot}9208}{(y^2k,t)^{\frac{1}{4}}}\exp\left(-\frac{V^2t}{4k_1}\right)\right\} \quad \text{as} \quad t\to\infty;\\ \tau &= \frac{\rho_0 k_1 U}{\sqrt{\pi k_1 t}}\left\{1-\frac{V^2t}{4k_1}\right\} \quad \text{as} \quad t\to 0.\end{aligned}\right\} \tag{52}$$

For small values of t the skin friction is that obtained by Howarth. The first two terms in (52) represent a residual skin friction; there are two contributions, one from the residual magnetic stress and the other from a residual viscous stress. A similar state of affairs occurs in Ludford's work, the only difference being the absence of a residual viscous stress. The third term in (52) is $2\exp(-V^2t/4k_1)$ times the corresponding skin friction obtained by Howarth, and for small V this term should be replaced by equation (51). The difficulties encountered in the expansion of τ for large values of t may be clarified by writing τ as $\rho_0 U(k_1/t)^{\frac{1}{2}}F(R,S)$ where $R^2 = y^2/k_1 t$, $S = V^2t/k_1$. It is now seen that (52) gives the form of τ for small R assuming S large, whilst equation (51) gives the modification necessary for finite values of S, still assuming R large. A similar situation occurs in Ludford's work and since there appears to be a slight discrepancy in his work we shall consider this point very briefly. Ludford obtains

$$\frac{\tau}{\rho U} = V\,\text{erf}\frac{V\sqrt{t}}{\sqrt{\eta}+\sqrt{\nu}}+\sqrt{\frac{\nu}{\pi t}}\exp\left(-\frac{V^2t}{(\sqrt{\eta}+\sqrt{\nu})^2}\right),$$

and thus for large t

$$\frac{\tau}{\rho U} \sim \sqrt{\frac{\nu}{\pi t}}\left\{2+\sqrt{\frac{\eta}{\nu}}\right\}\exp\left(-\frac{V^2t}{(\sqrt{\eta}+\sqrt{\nu})^2}\right).$$

The skin friction is thus

$$\left\{2+\sqrt{\frac{\eta}{\nu}}\right\}\exp - V^2t/(\sqrt{\eta}+\sqrt{\nu})^2$$

times the corresponding result obtained by Rayleigh and again a discrepancy occurs in the limiting case of small V. This discrepancy is due to the fact that for small V it is not possible to expand the error function asymptotically. Ludford has obtained -1 instead of $\{2+\sqrt{\eta/\nu}\}$.

Clearly for η and ν small we can obtain a solution by perturbation methods expanding in powers of $\eta-\nu$. The process will be fairly complicated but it will be shown that a solution neglecting squares of $(\eta-\nu)$ may be obtained immediately from the solution for $\nu=\eta$. If k_1 is now defined by $\frac{1}{2}(\eta+\nu)$ then (39) shows that equation (42) will still hold if terms of order $(\eta-\nu)^2$ are neglected. With this new definition of k_1 we define V_x' by

$$V_x' = e^{-Vz/2k_1}f + e^{-Vz/2k_1}g,$$

where f and g satisfy the same boundary conditions as above. We also have from (4) that

$$V^2\frac{\partial \mathbf{H}}{\partial z}+H_0\left(k_1\nabla^2-\frac{\partial}{\partial t}\right)V_x'+\tfrac{1}{2}H_0(\nu-\eta)\nabla^2V_x'=0. \tag{53}$$

Thus, neglecting terms of order $(\eta-\nu)^2$

$$V^2\frac{\partial H}{\partial z}+\frac{H_0V}{2k_1}(f+g)+H_0\frac{\partial}{\partial z}(f-g)+\tfrac{1}{2}VH_0(\nu-\eta)$$
$$\times\left\{\frac{\partial}{\partial z}(f-g)+\frac{V}{2k_1}(f+g)\right\}+\tfrac{1}{2}H_0(\nu-\eta)\frac{\partial}{\partial t}(f+g)=0.$$

The conditions on f and g show that, to order $(\nu-\eta)^2$, $\partial H/\partial z=0$ on the wall. Thus V_x' represents a solution of the problem neglecting terms of order $(\eta-\nu)^2$.

For $\eta=0$ the solution may be obtained from Howarth's by a suitable variation of the parameters.

Another viscous flow problem capable of exact solutions is that when the plane $z=0$ oscillates parallel to itself. For an insulating wall a solution has been given by Kakutani (1959). The solution for an oscillating half-plane may also be deduced immediately from the Laplace transform of the above solution for impulsive motion.

The author is indebted to a referee for some detailed comments on an earlier form of this paper and for some additional references.

REFERENCES

Baños, A. Jr. 1955*a* *Phys. Rev.* **97**, 1435.

Baños, A. Jr. 1955*b* *Proc. Roy Soc.* A, **233**, 350.

Baños, A. Jr. 1956 *Phys. Rev.* **104**, 300.

Chang, C. C. & Yen, J. T. 1959 *Phys. Fluids*, **2**, 393.

Clemmow, P. C. 1950 *Quart. J. Mech. Appl. Math.* **3**, 241.

Dungey, J. 1958 *Cosmical Electrodynamics.* Cambridge University Press.

Ferraro, V. C. A. 1954 *Astrophys. J.* **119**, 393.
Ferraro, V. C. A. & Plumpton, C. 1958 *Astrophys J.* **127**, 459.
Hasimoto, H. 1956 *Phys. Soc. Japan*, **12**, 68.
Howarth, L. 1950 *Proc. Camb. Phil. Soc.* **46**, 127.
Kakutani, T. 1959 *Phys. Soc. Japan*, **13**, 1504.
Ludford, G. S. S. 1959 *Arch. Rat. Mech.* **3**, 14.
Lundquist, S. 1952 *Arkiv. Fysik.* **5**, 297.
Roberts, P. H. 1955 *Astrophys. J.* **122**, 315.
Williams, W. E. 1960 To appear *Quart. J. Mech. Appl. Math.*

Shock-wave structure in binary mixtures of chemically inert perfect gases

By FREDERICK S. SHERMAN
Division of Aeronautical Sciences, University of California, Berkeley

(Received 13 October 1959 and in revised form 5 February, 1960)

Starting with expressions for viscous stress, heat flux and diffusion flux, we formulate a continuum theory for steady flow of a binary mixture of chemically inert perfect gases through a normal shock of arbitrary strength. For shocks of vanishing strength, a solution by series expansion in Grad's (1952) shock-strength parameter gives a result essentially the same as found previously by Dyakov (1954). For stronger shocks a straightforward numerical integration, quite analogous to that useful in the simpler pure-gas problem, is laid out.

The resulting problem has eight parameters: shock strength, ratio of specific heats, ratio of bulk viscosity to shear viscosity, Prandtl number, Schmidt number, thermal diffusion factor, molecular mass ratio, and initial mixture concentration. A dozen examples were worked out on a simple desk calculator to exhibit the influence of some of these parameters. They involve the gas pairs argon^{40}–argon^{36}, argon–neon, argon–helium, and xenon–helium.

In discussing the results, special attention is paid to the degree of success with which the weak-shock theory may be extrapolated to arbitrary shock strength, and to the question of the accuracy of the Navier–Stokes approximation for a mixture of gases of very different molecular weights.

1. Introduction

A shock wave in a pure gas is broadened into a continuous transition zone by viscosity and thermal conduction, in the view of the continuum theory of gases. From this same viewpoint, a shock in a gas mixture is further broadened by dissipative species-diffusion processes, and a partial separation of the mixture is caused by the gradients within the shock.

Previous theoretical studies of shock waves and sound waves in binary gas mixtures have been made, notably by Cowling (1942), Dyakov (1954), and Kohler (1949), and the essential results for very weak waves have found their way into important reference works by Herzfeld (1955) and Hirschfelder, Curtiss & Bird (1954). Interesting and somewhat related papers on shocks in dusty or ionized gases have recently been contributed by Carrier (1958), Jukes (1957), and Tidman (1958). The present paper is primarily an extension and elaboration of the works of Cowling and Dyakov. Whereas Cowling neglected viscosity, thermal conduction and thermal diffusion in order to gain a preliminary insight into diffusion effects in shocks, and Dyakov limited his treatment to waves of sufficient weakness so that the separation of the mixture could be neglected as a higher order

effect at the first stage of calculation, we make a direct frontal attack by numerical integration, to find the structure of a shock of arbitrary strength in a binary mixture of chemically inert perfect gases, including effects of viscosity, thermal conduction, ordinary-, baro-, and thermal-diffusion.

Of course, even accurate numerical integrations do not make the present theory (based on the Navier–Stokes approximations to viscous stress, heat flux, and diffusion flux) valid for arbitrary shock strength. Indeed one might intuitively expect that the maximum shock strength for which these calculations will give realistic predictions would be reduced as the molecular mass ratio of the mixture increases, due to the difficulty of maintaining thermal equilibrium between the light and the heavy constituents. Thus experiment may prove someday that the more 'interesting' features of the present results, which mostly appear when the mass ratio is fairly large and the shock strength is finite, are not realistic at all. Nevertheless, it has been interesting and instructive to the author to see just what the Navier–Stokes approximation says about this rather complicated problem.

2. Diffusion velocity and conservation of mass

We take as our starting point the results of Chapman and Enskog for the diffusion velocities of a binary mixture of perfect gases, obtained by kinetic theory. Equations 8.4, 7 and 8.3, 7 of Chapman & Cowling (1939) may be combined with the definitions of the total density and mass velocity of the mixture,

$$\rho = \rho_1 + \rho_2, \tag{1}$$

$$\rho u = \rho_1 u_1 + \rho_2 u_2, \tag{2}$$

to give, in our present nomenclature,

$$u_1 - u = \frac{\rho M_1 M_2}{\rho_1 M^2} D_{12}\left\{f(1-f)\left[\frac{M_1 - M_2}{M}\frac{d}{dx}(\ln p) - \alpha \frac{d}{dx}(\ln T)\right] - \frac{df}{dx}\right\}. \tag{3}$$

Subscript 1 refers to the heavier molecular species and f is the mole-fraction of that species

$$f = \rho_1 M/\rho M_1. \tag{4}$$

The mean molecular mass M of the mixture depends on f, being given by

$$M = fM_1 + (1-f)M_2. \tag{5}$$

The binary diffusion coefficient D_{12} and the thermal-diffusion factor α are positive quantities, except in some exceptional gas pairs for which α may be slightly negative.

The qualitative nature of the separation of species within a normal shock can be seen directly from (3). If we view the shock as fixed in space, with steady flow from left to right so that $u > 0$, we then expect $dp/dx > 0$ and $dT/dx > 0$ within the shock (unless the situation varies drastically from that in a pure gas). The driving forces tending to separate the mixture are $d(\ln p)/dx$ and $d(\ln T)/dx$, leading respectively to baro-diffusion and thermal diffusion. From (2) we see that *baro-diffusion speeds up the heavier component*, $M_1 - M_2 > 0$, and slows down the lighter component relative to the mass velocity of the mixture. If $\alpha > 0$, which we would normally expect for M_1 not too close to M_2 (cf. Chapman & Cowling

1952, p. 254), then *thermal diffusion slows down the heavier component* and speeds up the lighter. (This is consistent with the sign convention for α, namely, that it is positive when the heavier molecules seek the colder regions.) Thus under most cirumstances thermal diffusion will partially counteract baro-diffusion within a shock wave. This same conclusion was reached by Dyakov (1954) and, in the related acoustic problem, by Kohler (1949). Of course, once any separation has taken place, ordinary diffusion, with driving potential df/dx, will tend to homogenize the mixture.

In the absence of chemical reactions each component of the mixture is subject to a simple continuity equation,

$$\rho_1 u_1 = m_1 \text{ (constant)}, \tag{6}$$

$$\rho_2 u_2 = m_2 \text{ (constant)}. \tag{7}$$

Equation (2) gives

$$\rho u = m_1 + m_2 = m \text{ (constant)} \tag{8}$$

as the continuity equation of the mixture. These equations make it clear that slowing down a component relative to the mixture velocity increases the concentration of that component relative to its value outside the shock wave. Thus, if baro-diffusion dominates thermal diffusion, the lighter molecules will be concentrated in the shock. This is usually the case. The degree of concentration would be expected to be greatest about where $d(\ln p)/dx$ is maximum. For very weak shocks this proves to be at the centre of the shock, and the concentration profile is symmetric about this point (Dyakov 1954). For stronger shocks, the maximum $d(\ln p)/dx$ will be upstream of the maximum of dp/dx, so we expect a peak concentration of the light species upstream of the centre of the shock. This upstream shift of the separation maximum is reinforced by ordinary diffusion, which accelerates the heavier molecules relative to the mixture when they are upstream of the separation maximum and decelerates them after they pass it.

Note that equations (3), (6) and (8) do not suggest that the relative scarcity of heavy molecules in the upstream portion of the shock is compensated by an equal enrichment of this species at some other position in $-\infty < x < \infty$, unless dp/dx should ever change sign. It does not in any of the examples worked out here. The tempting intuitive notion that conservation of mass prohibits a net deficiency of either species relative to the proportions of the mixture at infinity is not applicable to steady-state analysis, and usually arises when we include in our thinking the essentially transient idea of shock generation in a mixture of initially homogeneous composition.

An accurate analysis of transient shock formation in a mixture is outside our present scope. However, a qualitative description is suggested now in hopes of clarifying the relation between the following strictly steady-state results and the corresponding 'long-time' behaviour of a particular shock-formation problem. Suppose that a piston is impulsively accelerated to constant velocity in a tube containing a mixture initially homogeneous and at rest. The author supposes that in the initial instant (less than a mean molecular collision time) of that piston motion, the light molecules struck by the piston fly away from it more rapidly than their heavy neighbours. In the course of subsequent collisions, which

transmit the impulse of the piston out into the gas, this behaviour is reproduced at the front of the column of gas which has started to move with a mean velocity equal to that of the piston, and becomes a characteristic feature of the structure of this front (the shock wave). After a sufficient number of collisions, the motion and structure of this shock front become locally stationary if viewed by an observer moving with the shock speed.

In the meantime, the heavy molecules which move away slowly from the piston during the initial instant produce a local surplus of this species in the immediate vicinity of the piston. This surplus is embedded in a region of gas which soon has the mean motion of the piston and redistributes itself by ordinary diffusion. The region throughout which this original surplus is subsequently spread thus grows out from the piston face in proportion to $\sqrt{(\text{time})}$, while the shock front moves away from the piston in proportion to time. Between the shock and the region of redistribution of the heavy molecules which are 'left behind' during shock formation, there appears an ever-lengthening column of homogeneous mixture having the velocity of the piston and the composition of the undisturbed gas. In the steady-flow analysis of the shock structure, the properties of this column are those supposed to exist at $x = +\infty$, so that the residual effects of shock formation, including the local enrichment of heavy molecules which compensates for the local depletion in the shock, are specifically excluded from the steady-state theory.

3. Conservation of momentum

The diffusion equation (1) results from the momentum conservation principle applied to the relative motion of the constituents of the mixture. The momentum equation for the mixture moving as a whole is

$$\rho u^2 + p - (\tfrac{4}{3}\mu + \kappa)\frac{du}{dx} = P = \rho_0 u_0^2 + p_0. \tag{9}$$

which differs from that for a pure gas only through the dependence of μ and κ on f in the present case. In fact, virtually nothing is known about the bulk viscosity coefficient κ for gas mixtures, since this additional dissipative mechanism is hard to separate experimentally from ordinary viscosity, heat conduction, and diffusion. We carry the symbol κ in this analysis just to be open-minded, although the subsequent calculation will assume κ/μ to be constant, with no particular physical justification.

4. Conservation of energy

The differential equation of conservation of energy for the mixture may be integrated to give

$$\rho u(h + \tfrac{1}{2}u^2) - u(\tfrac{4}{3}\mu + \kappa)\frac{du}{dx} + q_x = \tfrac{1}{2}Q = m(h_0 + \tfrac{1}{2}u_0^2). \tag{10}$$

The specific enthalpy in (10) is given by the rule for mixtures of chemically inert perfect gases

$$\rho h = \rho_1 h_1 + \rho_2 h_2 = (\rho_1 c_{p1} + \rho_2 c_{p2})T. \tag{11}$$

In (11) explicit use is made of the important assumption that both components of the mixture share the same temperature.

The heat flux q_x in (10) contains two terms in addition to the ordinary Fourier conduction, one a simple convection of partial enthalpies at the diffusion velocity, the other due to the diffusion thermo-effect (Chapman & Cowling 1952, equation 8.41, 3),

$$q_x = -\lambda \frac{dT}{dx} + \rho_1(u_1 - u)\left(h_1 - h_2 + \frac{M^2}{M_1 M_2}\frac{p}{\rho}\alpha\right). \tag{12}$$

When (12) is substituted in (10), it proves convenient to group together all the enthalpy terms. One easily shows that

$$\begin{aligned} \rho u h + \rho_1(u_1 - u)(h_1 - h_2) &= m_1 h_1 + m_2 h_2 \\ &= (m_1 c_{p1} + m_2 c_{p2}) T \\ &\equiv m c_p T, \end{aligned}$$

where c_p denotes not the local and variable specific heat of the mixture, but the specific heat of the mixture outside the shock (hence a constant for any given shock problem). The last step above follows directly from the basic definition of specific heat of an inert perfect gas mixture

$$\rho c_p = \rho_1 c_{p1} + \rho_2 c_{p2}$$

and the observation that outside the shock $u_1 = u_2 = u$.

Equation (10) is thus rewritten as

$$\rho u(\tfrac{1}{2}u^2 + c_p T) - u(\tfrac{4}{3}\mu + \kappa)\frac{du}{dx} - \lambda \frac{dT}{dx} + \frac{\rho_1 M^2}{\rho M_1 M_2}(u_1 - u) p\alpha = \tfrac{1}{2}Q. \tag{13}$$

5. Equation of state

If we define a gas constant for the mixture outside the shock wave by

$$R \equiv p_0/\rho_0 T_0,$$

then inside the shock, where the mean molecular mass is variable, we have

$$p = \frac{M_0}{M}\rho R T. \tag{14}$$

6. Dimensionless variables and boundary conditions

Equations (1) through (7), (9), (13) and (14) give ten independent relations for the ten unknowns ρ, ρ_1, ρ_2, u, u_1, u_2, f, M, p, and T. They can be reduced to three coupled first-order differential equations for u, T and f. These, together with a sufficiency of transport property data and the boundary conditions

$$\frac{du}{dx} = \frac{dT}{dx} = \frac{df}{dx} = 0 \quad \text{at} \quad x = \pm\infty \tag{15}$$

define the problem.

We introduce dimensionless variables and parameters as follows:

$$v = mu/P \text{ (velocity)},$$
$$\tau = m^2RT/P^2 \text{ (temperature)},$$
$$a = mQ/P^2 \text{ (shock strength)},$$
$$\gamma = c_p/(c_p - R) \text{ (specific heats ratio)},$$
$$X = \frac{4}{3} + \frac{\kappa}{\mu},$$
$$\theta = M_1/M_2 \text{ (molecular mass ratio)},$$
$$f_0 = \text{mole fraction of heavy molecules outside the shock},$$

and the reference length $L = \mu/m$.

The three equations for v, τ and f can be arranged as autonomous equations for dv/dx, $d\tau/dx$ and df/dx as follows

$$L\frac{dv}{dx} = \frac{1}{X}\left\{v + \frac{1+(\theta-1)f_0}{1+(\theta-1)f}\frac{\tau}{v} - 1\right\}, \tag{16}$$

$$L\frac{d\tau}{dx} = \frac{\gamma-1}{2\gamma}\left(\frac{\mu c_p}{\lambda}\right)\left\{2v - v^2 - a + 2\tau\left[\frac{\gamma}{\gamma-1} - \frac{1+(\theta-1)f_0}{1+(\theta-1)f} + (f_0 - f)\alpha\right]\right\}, \tag{17}$$

$$L\frac{df}{dx} = -\left(\frac{\mu}{\rho D_{12}}\right)\frac{(f_0-f)[1+(\theta-1)f]^3}{[1+(\theta^2-1)f][1+(\theta-1)f_0]} - L\frac{f(1-f)[1+(\theta-1)f]}{1+(\theta^2-1)f}$$
$$\times\left\{(\theta-1)\frac{d}{dx}(\ln v) - [(\theta-1) - \alpha\{1+(\theta-1)f\}]\frac{d}{dx}(\ln\tau)\right\}. \tag{18}$$

7. Method of solution

The method used to solve (16)–(18) numerically is quite commonplace in the shock-wave literature (e.g. Grad 1952, Gilbarg & Paolucci 1953, or Talbot & Sherman 1959) and will only be described in principle here.*

The independent variable x can be easily eliminated by dividing (17) and (18) by (16). This yields two 'direction field' equations for $d\tau/dv$ and df/dv, for which we seek a particular solution joining the upstream and downstream states of the gas. The co-ordinates of these states (v, τ, f at $x = \pm\infty$) are easily found by setting $dv/dx = d\tau/dx = df/dx = 0$ in (16), (17) and (18).

Since these state points are obviously singular points of the direction-field equations, a preliminary investigation of the direction field in their vicinity must be made to determine the end-slopes of the desired solution curve and the correct point from which to start the numerical integration. This analysis shows in the present case that the downstream singular point is almost invariably a saddle point and the upstream singular point a node, just as they are for the Navier–Stokes equations in a pure gas. The integration must be started from the downstream singular point and this guarantees the existence of a unique solution.

After the solution curve is found in v–τ–f space, the spatial distribution of v is found by a numerical quadrature of (16).

* Readers interested in these details are invited to communicate directly with the author.

8. Concentration dependence of transport properties

The numerical integration of the direction-field equations and the quadrature of (16) require a knowledge of the concentration and temperature dependence of viscosity μ, thermal diffusion factor α, and the ratios μ/λ and $\mu/\rho D_{12}$. Numerical data could of course be used directly, but for the present sample calculations simple analytic approximations were introduced after a study of data for argon–

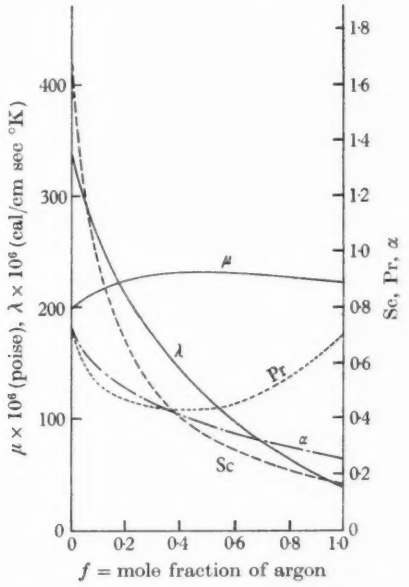

FIGURE 1. Properties of argon–helium mixtures.

helium mixtures (cf. figure 1; Chapman & Cowling 1952, pp. 232, 243, 248; Hirschfelder *et al.* 1954, p. 584). These approximations provide a local fit to the empirical transport property behaviour in the vicinity of the known mixture state ahead of the shock. They are

$$\mu \propto T^{\frac{3}{4}}, \text{ independent of } f,$$

$$\mu/\lambda \propto M, \text{ independent of } T,$$

$$\mu/\rho D_{12} \propto 1/M, \text{ independent of } T,$$

$$\alpha \propto 1/M, \text{ independent of } T.$$

While some of these are certainly inaccurate if applied to large variations of f and T, they are entirely adequate for the purpose at hand, since f actually does not vary widely in a given shock, and the assumed temperature dependence is fairly realistic except in the case of α. Thermal diffusion is fortunately a sufficiently small effect so that sizeable errors in α produce much reduced errors in the shock profiles.

If we introduce the Prandtl number, Schmidt number, and thermal-diffusion factor of the mixture ahead of the shock as basic parameters of the shock-structure problem, the approximations above state that

$$\mu c_p/\lambda = Pr\,(M/M_0) = Pr\,[1+(\theta-1)f]/[1+(\theta-1)f_0]$$

(remember that c_p already refers to the mixture outside the shock),

$$\mu/\rho D_{12} = Sc\,(M_0/M)$$

and

$$\alpha = \alpha_0(M_0/M).$$

9. Series solution for weak shocks

In the limit of vanishing shock strength, $\mathscr{M} \to 1$, a series-expansion solution of (16), (17) and (18) is appropriate, and the first terms have been found by Dyakov (1954), albeit in a nomenclature quite different from ours. We proceed a little differently here, expanding in terms of the shock-strength parameter proposed by Grad (1952) instead of the pressure ratio, Dyakov's choice. One hopes that the former expansion parameter, which remains finite as $\mathscr{M} \to \infty$, would lead to quicker convergence, or at least better approximation by the first term of the series, at moderate Mach numbers. In fact, this seems to be the case.

Grad's parameter ϵ is introduced by

$$v_0 = \frac{1}{2}\left(\frac{\gamma-1}{\gamma+1}\right)\left(\frac{2\gamma}{\gamma-1} \pm \epsilon\right), \tag{19}$$

where the + sign gives $v_0(x=-\infty)$ and the − sign $v_0(x=+\infty)$. It is related to our earlier parameter a by

$$a = \frac{1}{4}\left(\frac{\gamma-1}{\gamma+1}\right)\left[\left(\frac{2\gamma}{\gamma-1}\right)^2 - \epsilon^2\right], \tag{20}$$

and to the shock Mach number by

$$\epsilon = \frac{2\gamma}{\gamma-1}\left(\frac{\mathscr{M}^2-1}{\gamma\mathscr{M}^2+1}\right). \tag{21}$$

Next we define new dimensionless velocity and temperature variables, which vary from -1 to $+1$ through the shock, whatever the value of ϵ. These are w and t, given by

$$v = \frac{1}{2}\left(\frac{\gamma-1}{\gamma+1}\right)\left(\frac{2\gamma}{\gamma-1} + \epsilon w\right), \tag{22}$$

$$\tau = \frac{1}{4}\left(\frac{\gamma-1}{\gamma+1}\right)^2\left\{\frac{4\gamma}{(\gamma-1)^2} + 2\epsilon t - \epsilon^2\right\}. \tag{23}$$

A new concentration variable may be introduced by

$$f_0 - f = \epsilon^2\phi. \tag{24}$$

We now expand w, t and ϕ in ϵ, i.e.,

$$\left.\begin{aligned} w &= w^{(0)} + \epsilon w^{(1)} + \epsilon^2 w^{(2)} + \ldots, \\ t &= t^{(0)} + \epsilon t^{(1)} + \epsilon^2 t^{(2)} + \ldots, \\ \phi &= \phi^{(0)} + \epsilon\phi^{(1)} + \epsilon^2\phi^{(2)} + \ldots, \end{aligned}\right\} \tag{25}$$

and substitute these series into (16), (17) and (18). Grouping terms of like order in ϵ, and solving the resulting simple differential equation for $w^{(0)}$, we get

$$w^{(0)} = -\tanh\left\{\frac{\gamma^2-1}{4\gamma}\frac{\epsilon}{\left[X+\frac{\gamma-1}{Pr}+\frac{\gamma f_0(1-f_0)}{Sc}\left(\frac{M_1-M_2}{M_0}-\frac{\gamma-1}{\gamma}\alpha_0\right)^2\right]}\frac{\rho u x}{\mu}\right\}, \tag{26}$$

$$t^{(0)} = -w^{(0)}, \tag{27}$$

$$\phi^{(0)} = \frac{(\gamma+1)(\gamma-1)^2 f_0(1-f_0)}{8\gamma}\frac{}{Sc} \times\left\{\frac{\frac{M_1-M_2}{M_0}-\frac{\gamma-1}{\gamma}\alpha_0}{\left[X+\frac{\gamma-1}{Pr}+\frac{\gamma f_0(1-f_0)}{Sc}\left(\frac{M_1-M_2}{M_0}-\frac{\gamma-1}{\gamma}\alpha_0\right)^2\right]}\right\}\{(1-(w^{(0)})^2\}, \tag{28}$$

for the lowest-order non-vanishing terms in w, t and ϕ. The corresponding result for shock thickness based on maximum slope,

$$\delta_m = 2/|dw/dx|_{\max}, \tag{29}$$

is

$$\frac{\rho u \delta_m}{\mu} = \frac{8\gamma}{\gamma^2-1}\left(\frac{1}{\epsilon}\right)\left\{X+\frac{\gamma-1}{Pr}+\frac{\gamma f_0(1-f_0)}{Sc}\left(\frac{M_1-M_2}{M_0}-\frac{\gamma-1}{\gamma}\alpha_0\right)^2\right\}. \tag{30}$$

When our nomenclature is brought into agreement with that of Dyakov (1954), these last four results agree perfectly with his. The quantity in braces in (30) is also identical with the corresponding factor in the sound-attenuation coefficient, found by Kohler (1949), and cited by Hirschfelder *et al.* (1954, p. 732, equations 11.4–20). It may be noted in passing that, in Herzfeld (1955, p. 691, equations 18–3), the last term in this brace is cited incorrectly by omission of the factor $f_0(1-f_0)$ which makes that term vanish for a pure gas.

Besides giving a check on the correctness of (16), (17) and (18), equations (28) and (30), when boldly extrapolated to finite shock strengths, give a very useful approximate survey of the results which are obtained more accurately by numerical integrations.

10. Sample numerical calculations

The dozen examples shown here were picked to exhibit the following.

(*a*) The effect of shock strength on the concentration-versus-velocity integrals for a single initial gas mixture (argon–helium, equal parts by moles). The Mach numbers chosen were 1·34 ($\epsilon = 1$), 2·05 ($\epsilon = 2$), 4·84 ($\epsilon = 2{\cdot}8$) and ∞ ($\epsilon = 3$), the last obviously just for fun. These results are shown in figure 2, where they are compared with the approximation given by equations (24) and (28). As might have been expected, the weak-shock approximation is quite accurate at $\epsilon = 1$, and discrepancies between it and the numerical results increase continually with increasing ϵ. The merit of the series solutions in terms of the parameter ϵ, which remains finite as $\mathscr{M} \to \infty$, is seen from the fair approximation given by its first term even at very large shock strengths.

(*b*) The effect of initial mixture ratio on various shock properties, for a particular gas-pair (argon–helium) and shock strength ($\epsilon = 2$). Thus figure 3 shows

concentration-velocity integrals on a semi-logarithmic scale (to emphasize percentage changes in concentration). Note that these are decidedly more symmetrical about the mid-velocity, and thus agree better qualitatively with the weak-shock theory when f_0 is small, than when it is large. This is a coincidence brought about by the superposition of two effects, the first being the general

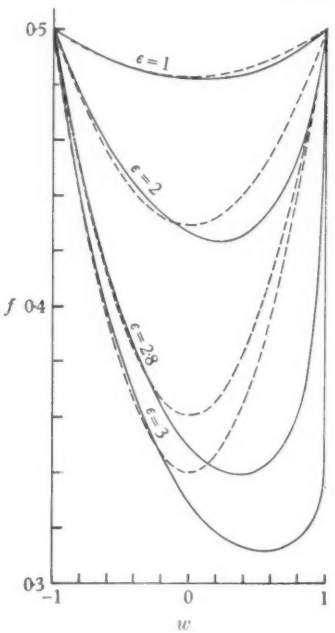

FIGURE 2. Concentration-velocity integrals for various shock strengths; $f_0 = 0{\cdot}5$.

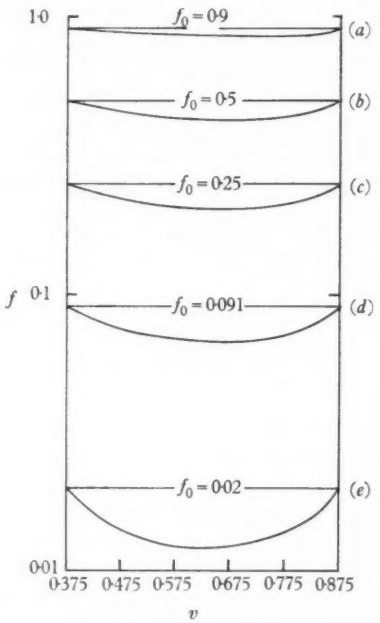

FIGURE 3. Concentration-velocity integrals for various initial mixture ratios; $\epsilon = 2$.

movement of the maximum separation towards the upstream side of the shock (towards the right in figure 3) in response to ordinary diffusion and the fact that the separating potential is $\ln p$ rather than p (as discussed in §2). The second effect is intuitively rather obvious, and well illustrated by figures 4 and 5. When the initial mixture contains just a little of the lighter gas, the separation is brought about by the light molecules of the shocked gas running out ahead of the main shock or mean-velocity transition of the entire mixture. This evidently shifts the maximum separation even farther upstream relative to the main shock and leads to the very asymmetrical f–v curves in figure 3a. When the initial mixture contains just a little heavy gas, the heavier molecules lag behind the main shock, thus shifting the maximum separation downstream and partially cancelling the first effect mentioned above.

If the reader has been distracted from the foregoing argument by the rather odd appearance of the argon velocity profile in figure 5, he is forgiven forthwith. The behaviour of that curve, which indicates that the argon is momentarily

accelerated, rather than slowed down, upon entry into the shock, is the single most intriguing—and perhaps unbelievable—result of the present study. It implies, upon transformation of co-ordinates to a frame at rest in the unshocked gas, that upon arrival of the shock the argon first jumps backwards, then turns and runs fast to catch up with the shock. The same prediction is inherent in Dyakov's weak-shock theory, which incidentally predicts a corresponding undershoot of the helium velocity in figure 4. It is interesting to note that the latter prediction is one

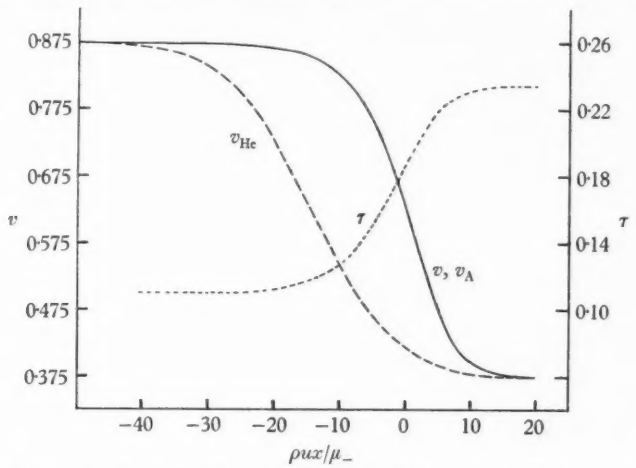

FIGURE 4. Shock profiles with very little light gas; $f_0 = 0{\cdot}9$, $\epsilon = 2$.

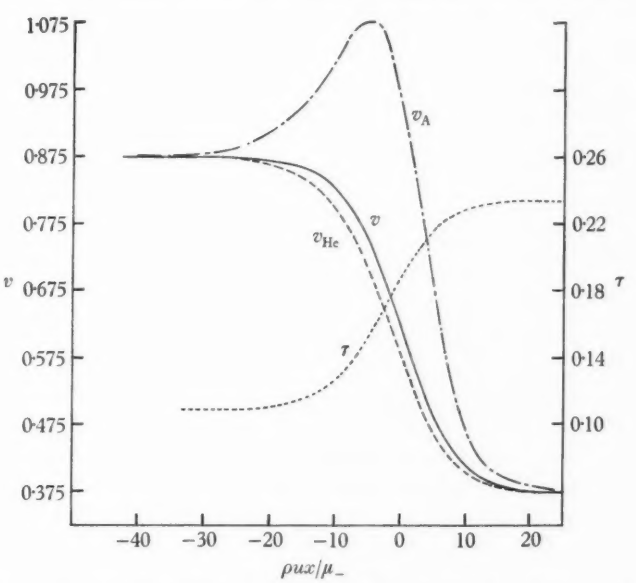

FIGURE 5. Shock profiles with very little heavy gas; $f_0 = 0{\cdot}02$, $\epsilon = 2$.

qualitative implication of the weak-shock theory which is refuted by the accurate numerical integrations. Regarding the physical plausibility of this effect, the author has no very fixed opinion as yet. It is certainly hard to imagine the source of the effect from a molecular viewpoint and no corresponding effect is found in

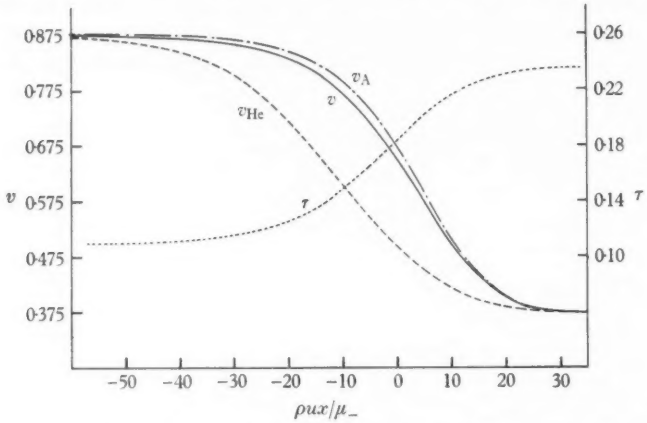

FIGURE 6. Shock profiles with equal initial proportions of light and heavy gases; $f_0 = 0{\cdot}5$, $\epsilon = 2$.

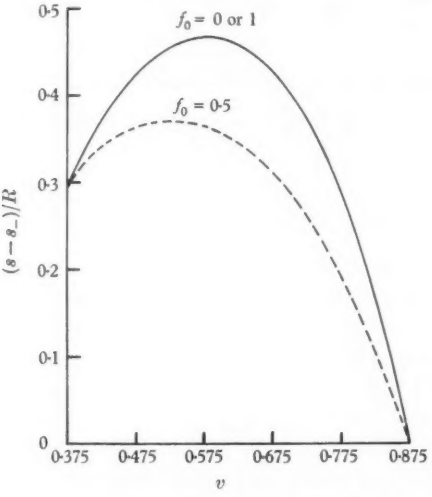

FIGURE 7. Entropy-velocity integrals; $\epsilon = 2$.

Carrier's dusty-gas analysis, if the latter may be considered to give an indication of proper physical behaviour in a limit of very large mass ratio. A mass ratio of 10 (argon–helium) and shock Mach number of 2·05 may simply carry the present analysis beyond the valid range of the Navier–Stokes approximation although that approximation would still be quite accurate for a Mach 2·05 shock in a pure monatomic gas (cf. Talbot & Sherman 1959).

Figures 4, 5 and 6 (the last showing velocity profiles for the intermediate case $f_0 = 0{\cdot}5$) emphasize that a shock wave in a mixture may be quite complicated compared to that in a pure gas, and that it may actually extend over a distance which is quite large compared with the conventionally defined shock thickness (cf. equation (29)). They also suggest that experimentalists interested in this problem should take care to know exactly to what flow properties their instruments respond.

Figure 7 shows the effect of initial mixture ratio on the entropy-velocity relationship within the shock. Actually, the quantity labelled s here is not strictly the entropy of the actual non-equilibrium state of the gas at a point inside the shock, but the entropy of the equilibrium state having the same pressure, temperature and concentration. This is a quantity easy to calculate—in our case from the formula

$$\frac{S-S_-}{R} = f\ln\left[\left(\frac{T}{T_-}\right)^{1/(\gamma_1-1)}\frac{u_1}{u_-}\right] + (1-f)\ln\left[\left(\frac{T}{T_-}\right)^{1/(\gamma_2-1)}\frac{u_2}{u_-}\right]. \tag{31}$$

It is presumably slightly larger than the entropy of the true non-equilibrium state, since a bit of fluid, if isolated in the latter condition, would spontaneously tend to the condition whose entropy we calculate.

Setting aside this rather fine point, we see in figure 7 just what we expect. While the mixture is being separated in the upstream portion of the shock, entropy rises at a rate smaller than in a pure gas shock of the same strength. While remixing is taking place farther downstream, entropy rises faster (or falls more slowly) than in the pure gas.

Figure 8 shows some over-all or extreme properties of the shock transition as functions of f_0. From 8*a* we see both that diffusion effects broaden a shock in A–He quite spectacularly, and that the weak-shock theory, equation (30), gives a very good idea of the dependence of this broadening upon initial mixture ratio. From 8*b* we see that the maximum ratio of diffusion velocity to mixture velocity, $(u_1-u_2)/u$, is smallest when diffusive broadening of the shock is largest, and that the highest diffusion velocities appear when there is only a trace of one gas or the other present. The quantity plotted is simply related to f by use of equations (5), (6) and (7), i.e.

$$\frac{u_1-u_2}{u} = \frac{f_0-f}{f(1-f)}\frac{1+(\theta-1)f}{1+(\theta-1)f_0}. \tag{32}$$

The weak-shock approximation to this result is

$$\frac{u_1-u_2}{u} = \epsilon^2\frac{(\gamma+1)(\gamma-1)^2}{8\gamma Sc}\left\{\frac{\dfrac{M_1-M_2}{M_0}-\dfrac{\gamma-1}{\gamma}\alpha_0}{X+\dfrac{\gamma-1}{Pr}+\dfrac{\gamma f_0(1-f_0)}{Sc}\left(\dfrac{M_1-M_2}{M_0}-\dfrac{\gamma-1}{\gamma}\alpha_0\right)^2}\right\}(1-w^{(0)2}). \tag{33}$$

This equation gives a fairly true image of the numerical results, particularly for small f_0, but is considerably worse at large f_0 for reasons reviewed at the beginning of this subsection.

(*c*) The effect of mass ratios (and accompanying mixture properties) at constant f_0 and shock strength. Instead of making an artificial parameter study by changing θ alone, we deemed it more interesting to treat real mixtures of various

gases, to attain a wide range of θ along with the associated changes in α, Pr, and Sc which nature provides. Thus calculations were made for $f_0 = 0{\cdot}5$ and $\epsilon = 2$ in the mixtures ^{40}A–^{36}A ($\theta = 10/9$), A–Ne ($\theta = 2$), A–He ($\theta = 10$) and Xe–He ($\theta = 32{\cdot}8$). Table 1 shows the variation of shock thickness and maximum diffusion velocity with θ in these mixtures, all of which have $\gamma = 5/3$ and $X = 4/3$.

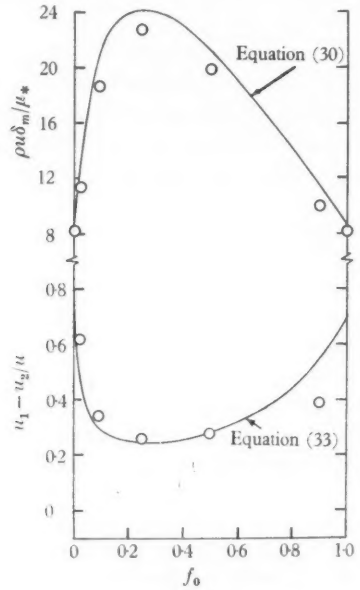

FIGURE 8. Shock thickness and maximum diffusion velocity; $\epsilon = 2$. ○, Numerical results.

Gas pair	θ	$\frac{M_1 - M_2}{M_0}$	α_0	Pr	Sc	$\frac{\rho u\delta_m}{\mu_*}$ Numerical integration	$\frac{\rho u\delta_m}{\mu_*}$ Equation 49	$\left(\frac{u_1-u_2}{u}\right)_{\max}$ Numerical integration	$\left(\frac{u_1-u_2}{u}\right)_{\max}$ Equation 52
Pure argon	1	0	0	0·704	—	8·15	8·55	—	—
^{40}A–^{36}A	10/9	0·10526	0·013	0·704	0·784	8·18	8·58	0·0209	0·0198
A–Ne	2	0·66667	0·17	0·667	0·750	8·99	9·49	0·116	0·112
A–He	10	1·6364	0·37	0·440	0·330	19·84	21·15	0·273	0·284
Xe–He	32·8	1·8817	0·434	0·250	0·200	35·8	37·8	0·276	0·301

TABLE 1. Effect of θ on shock thickness and maximum diffusion velocity. $f_0 = 0{\cdot}5$, $\mathscr{M} = 2{\cdot}05$, $\gamma = 5/3$, $X = 4/3$ for all cases; μ_* = viscosity at point of maximum $\mu\, du/dx$.

We see again that the weak-shock theory is very useful for rough predictions at finite shock strength. Note that quite refined experimentation would be required to detect either the minute separation of the isotopic mixture ^{40}A–^{36}A, or the broadening of the shock due to diffusion in this case. A similar result is found for shocks in atmospheric air, in which the importance of θ is emphasized by the fact that the diffusive shock broadening due to the 0·94 % of argon present is about 80 % as much as that due to the diffusion of the oxygen and nitrogen.

11. Criticism of the theory when θ is large

As mentioned several times above, the present theory seems deficient in the case of large θ, when it insists that both mixture components always share the same temperature. This has led to some intuitively implausible results in the examples worked out here for argon–helium mixtures. For example, figure 4 shows the mean-velocity change of the helium almost half-way accomplished before the random velocity (temperature) of this constituent has been appreciably influenced. One might intuitively expect these two quantities to start changing at about the same time.

To get a better picture of actual events during shock passage through a mixture with large θ, one might try at least two theoretical approaches. The first is to devise some supplementary 'relaxation' equation to account for the difficulty of maintaining thermal equilibrium between light and heavy constituents, and to couple this equation to the present set, modifying the latter somewhat to admit the existence of two different temperatures. An example of this approach is given by Jukes (1957) who discusses shock structure in a mixture of protons and electrons. Jukes's calculation shows a significant difference between electron and ion temperatures throughout a wide zone ahead of the 'velocity shock' but sheds no direct light on the present problem, since diffusive separation of electrons and ions was taken to be negligible in view of the intense electric field which this would produce. Regarding this technique it may be noted pessimistically that the coupling of the ordinary sort of relaxation equation (cf. Jukes 1957) to the Navier–Stokes equations leads to very nasty singular-point behaviour of the resulting equations, which precludes straightforward numerical integration from one side of the shock to the other.

The second possibly profitable approach would be an extension of the method of Mott-Smith (1951) to treat a gas mixture. Again, this approach has been applied to a hydrogen plasma (Tidman 1958), but not to a mixture in which diffusive separation is unrestrained by electric fields.

Finally, of course, one might attempt an experimental determination of the true state of affairs with shocks in, say, A–He mixtures. In fact, some early work along this line, by Professor D. F. Hornig of Brown University (now of Princeton) gave the author his first inclination to study this problem.

REFERENCES

Carrier, G. F. 1958 Shock waves in a dusty gas. *J. Fluid Mech.* **4**, 376.

Chapman, S. & Cowling, T. G. 1939 *Mathematical Theory of Non-uniform Gases.* Cambridge University Press.

Cowling, T. G. 1942 The influence of diffusion on the propagation of shock waves. *Phil. Mag.* **33**, 61.

Dyakov, S. P. 1954 Shock waves in binary mixtures. *Zhur. Eksp. Theor. Fiz.* **27**, 728.

Gilbarg, D. & Paolucci, D. 1953 The structure of shock waves in the continuum theory of fluids. *J. Rational Mech. Anal.* **2**, 617.

Grad, H. 1952 The profile of a steady plane shock wave. *Commun. Pure Appl. Math.* **5**, 257.

HERZFELD, K. F. 1955 Relaxation phenomena in gases, Section H of *Thermodynamics and Physics of Matter*, Vol. 1 of *High Speed Aerodynamics and Jet Propulsion*. Princeton University Press.

HIRSCHFELDER, J. O., CURTISS, C. F. & BIRD, R. B. 1954 *Molecular Theory of Gases and Liquids*. New York: Wiley.

JUKES, J. O. 1957 The structure of a shock wave in a fully ionized gas. *J. Fluid Mech.* **3**, 275.

KOHLER, M. 1949 Schallabsorption in binären gasmischungen. *Zeit. f. Phys.* **127**, 40.

MOTT-SMITH, H. M. 1951 The solution of the Boltzmann equation for a shock wave. *Phys. Rev.* (2) **82**, 885. (See also, Sakurai, A. 1957, A note on Mott-Smith's solution.... *J. Fluid Mech.* **3**, 255.)

TALBOT, L. & SHERMAN, F. S. 1959 Structure of weak shock waves in a monatomic gas. *NASA Memo*, no. 12-14-58W.

TIDMAN, D. A. 1958 Structure of a shock wave in fully ionized hydrogen. *Phys. Rev.* (2) **111**, 1439.

SEVENTH MIDWESTERN CONFERENCE

FLUID MECHANICS AND SOLID MECHANICS

MICHIGAN STATE UNIVERSITY
EAST LANSING, MICHIGAN
6, 7, 8 SEPTEMBER 1961

An attractive and broad program is being prepared for the Seventh Midwestern Conference on Fluid Mechanics and Solid Mechanics. Authors wishing to present papers should send in their abstracts by 1 January 1961.

For further information address inquiries to: Prof. J. E. Lay, Mechanical Engineering Department, Michigan State University, East Lansing, Michigan.

JOURNAL OF FLUID MECHANICS

Volume 8, Part 3 July 1960

CONTENTS

The stability of a stratified flow
by WILLIAM PAUL GRAEBEL *page* 321

Calculations of the motion of non-uniform shock waves
by JAN ROŚCISZEWSKI 337

Velocity and enthalpy distributions in the compressible turbulent boundary layer on a flat plate
by D. A. SPENCE 368

Flow between torsionally oscillating disks
by S. ROSENBLAT 388

An experimental investigation of the effect of ejecting a coolant gas at the nose of a bluff body
by C. H. E. WARREN 400

On Kelvin's ship-wave pattern
by F. URSELL 418

Magnetohydrodynamic flow of a viscous fluid past a sphere
by RICHARD VAN BLERKOM 432

Standing surface waves of finite amplitude
by IRADJ TADJBAKHSH and JOSEPH B. KELLER 442

Exact solutions of the magnetohydrodynamic equations
by W. E. WILLIAMS 452

Shock-wave structure in binary mixtures of chemically inert perfect gases
by FREDERICK S. SHERMAN 465

Printed in Great Britain at the University Press, Cambridge
(Brooke Crutchley, University Printer)